# Seismic Fragility Analysis for Structures, Systems, and Components in Nuclear Power Plants

by

Zhen Cai

A thesis
presented to the University of Waterloo
in fulfilment of the
thesis requirement for the degree of
Doctor of Philosophy
in
Civil Engineering

Waterloo, Ontario, Canada, 2017

© Zhen Cai 2017

# Author's Declaration

I hereby declare that I am the sole author of this thesis. This is a true copy of the thesis, including any required final revisions, as accepted by my examiners.

I understand that my thesis may be made electronically available to the public.

# Abstract

Seismic fragility analysis has been widely used to evaluate seismic capacities of structures, systems, and components (SSCs) in nuclear power plants. In the seismic fragility analysis, a single ground motion parameter (GMP), such as peak ground acceleration (PGA), is chosen to characterize the Review Level Earthquake (RLE) and represent the seismic capacity of an SSC. However, due to the use of a single GMP, problems have been observed in engineering practice.

It is well known, from elastic structural dynamic analyses, structural responses under earthquake excitations depend primarily on spectral accelerations at its dominant natural frequencies. Choosing spectral accelerations at structural dominant natural frequencies as vector-valued GMPs (VGMPs) can more accurately characterize the input RLE and more precisely predict structural responses. The purpose of this study is to develop weighting seismic fragility analysis method that overcomes the problems in current seismic fragility analysis method. The proposed method mainly includes that

1. vector-valued probabilistic seismic hazard analysis (VPSHA) is performed to determine the weights of input ground response spectra (GRS);
2. seismic fragility analysis considering VGMPs method is proposed to calculate seismic fragility based on VGMPs;
3. weights of input GRS and seismic fragility are combined to obtain the weighting seismic fragility of an SSC.

By using VGMPs, the proposed method resolves the problems in current seismic fragility analysis, thus it can obtain more accurate seismic capacities of safety-related SSCs. In addition, weighting seismic fragility curves and High Confidence and Low Probability of Failure (HCLPF) seismic capacities are represented by a single GMP such as PGA, hence they are readily incorporated into Seismic Probabilistic Risk Analysis and Seismic Margin Assessment (SMA).

Based on weighting seismic fragility analysis method, an improved SMA procedure is proposed. The procedure combines the use of weighting and current seismic fragility analysis methods, i.e.,

- weighting seismic fragility analysis is performed to determine HCLPF seismic capacities of "weak link" SSCs, and
- current seismic fragility analysis is conducted to calculate HCLPF seismic capacities of less important SSCs.

This ensures that more accurate plant seismic capacity is obtained, while computational cost is acceptable. The proposed SMA procedure can save redesign cost of "weak link" SSCs.

The proposed weighting seismic fragility analysis method is accurate and applicable, providing more accurate seismic capacity estimates of safety-related SSCs, thus saving redesign cost of "weak link" SSCs that do not satisfy seismic margin requirement.

# Acknowledgement

I would like to express my sincere gratitude and appreciation to my supervisor, Professor Wei-Chau Xie, and co-supervisor, Professor Mahesh D. Pandey, for their expert guidance, continuous encouragement, and selfless support.

I sincerely appreciate Professors Lei Xu, Stan Potapenko, Gordon Savage, and Wenxing Zhou for serving as my thesis examination committee members. Their insightful comments and valuable suggestions are pretty beneficial for my research.

My sincere gratitude goes to Dr. Shun-Hao Ni and Dr. Binh-Le Ly for their brilliant perspectives and suggestions on my research. They also help me better understand seismic design practice of nuclear power plants.

Special thanks go to my research group members and colleagues, including Dr. De-Yi Zhang, Dr. Jian Deng, Dr. Zhao-Liang Wang, Dr. Bo Li, Dr. Wei Jiang, Sen Long, Chao Wu, Si-Gong Zhang, Yi Xiao, Shi-Jun Yang, Yang Zhou, Dr. Dong-Hui Lu, Lan-Lan Yang, Wen-Fu Wang, Xiao-Jun Yu, Qing-Xiang Meng, Dr. Xu-Fang Zhang, and Dr. Xiao-Li Yuan. Their extensive support and successive encouragement help me a lot during my research and life.

The financial support by the Natural Sciences and Engineering Research Council of Canada (NSERC) and the University Network of Excellence in Nuclear Engineering (UNENE) in the form of a Research Assistantship is sincerely appreciated.

I would like to express my deepest gratitude to my beloved family members and relatives, for their endless love and selfless mental support as always.

Last but not least, I deeply appreciate my most beloved girlfriend Shao-Ping (Siwana) Zhou for her successive encouragement and companion. I wouldn't have accomplished this thesis without her unreserved love.

**TO**

*Siwana*

# Table of Contents

*List of Figures* . . . . . xiii

*Nomenclature* . . . . . xviii

1 **Introduction** . . . . . **1**

1.1 Definitions 1

1.2 Research Background 6

1.3 Seismic Fragility Analysis 8

1.3.1 Lognormal Fragility Model 8

1.3.2 Problems in Engineering Applications 9

1.4 Objectives 11

1.5 Thesis Organization 12

2 **Seismic Hazard Analysis** . . . . . **14**

2.1 Probabilistic Seismic Hazard Analysis 14

2.2 Vector-valued Probabilistic Seismic Hazard Analysis 16

2.3 Numerical Example for Darlington NGS Site 21

2.3.1 Logic Tree of PSHA Model 21

2.3.2 Seismic Source Model 23

2.3.3 Magnitude-Recurrence Model 25

2.3.4 Maximum Magnitude Model 26

2.3.5 Ground-Motion Model 28

2.3.6 Development of Seismic Hazard Curves 29

2.3.7 Uniform Hazard Spectra 36

2.3.8 Mean Annual Rate Density Distribution 36

2.4 Summary 41

3 **Seismic Fragility Analysis** . . . . . **42**

3.1 Seismic Fragility Analysis 42

3.1.1 Definition 42

3.1.2 Determination of Seismic Fragility 44

3.2 Numerical Example for Horizontal Heat Exchanger 48

3.2.1 Heat Exchanger Configuration 49

3.2.2 Case Study Objectives 52

3.2.3 Case 1: Influence of Spectral Shape -- NUREG Spectrum is RLE 55

3.2.3.1 Definition of Seismic Input 55

3.2.3.2 Seismic Demand Analysis 55

3.2.3.3 Structural Capacity Analysis 59

3.2.3.4 Median Seismic Capacity 62

3.2.3.5 Logarithmic Standard Deviations 65

3.2.3.6 Seismic Fragility Curves and HCLPF Seismic Capacity 67

3.2.4 Case 1: Influence of Spectral Shape -- Site-specific UHS is RLE 69

3.2.5 Case 2: Influence of Use of GMP -- $\bar{\mathcal{S}}_A$ is GMP 73

3.3 Summary 78

4 **Weighting Seismic Fragility Analysis** . . . . . **79**

4.1 Seismic Probabilistic Risk Analysis considering VGMPs 79

4.2 Methodology of Weighting Seismic Fragility Analysis 82

4.3 Vector-valued Probabilistic Seismic Hazard Analysis 83

4.4 Seismic Fragility Analysis considering VGMPs 86

4.4.1 Definition 86

4.4.2 Determination of Seismic Fragility 88

4.4.2.1 Structural Capacity Analysis 88

4.4.2.2 Seismic Demand Analysis 88
4.4.2.3 Development of Seismic Fragility Surfaces 90
4.4.3 Summary 92
4.5 Development of Weighting Seismic Fragility Curves 92
4.5.1 Weighting Seismic Fragility and HCLPF Seismic Capacity 92
4.5.2 Generalization of Weighting Seismic Fragility Analysis 94
4.5.3 Discussion and Summary 95
4.6 Numerical Example for Horizontal Heat Exchanger 96
4.6.1 Weights of Input GRS 96
4.6.2 Development of Seismic Fragility Surfaces 98
4.6.2.1 Procedure 98
4.6.2.2 Conditional Probability of Failure Given an Input GRS 100
4.6.2.3 Summary 107
4.6.3 Development of Weighting Seismic Fragility Curves 107
4.6.3.1 Procedure 107
4.6.3.2 Weighting Seismic Fragility Curves 109
4.6.3.3 Comparison of Seismic Fragility Curves and HCLPF Seismic Capacities 112
4.6.4 Mean Annual Frequency of Occurrence of Failure of Heat Exchanger 115
4.7 Summary 117

**5 Weighting Seismic Fragility Analysis for Components on Structures . 118**
5.1 Introduction 118
5.2 Methodology 120
5.3 Block Wall and Primary Structure 122
5.3.1 Block Wall Configuration 122
5.3.2 Primary Structure Configuration 125

5.4 Current Seismic Fragility Analysis 125
5.4.1 Review Level Earthquake 125
5.4.2 Seismic Demand Analysis 126
5.4.3 Structural Capacity Analysis 133
5.4.4 Median Seismic Capacity 140
5.4.5 Logarithmic Standard Deviations 142
5.4.5.1 Basic Variables for Seismic Demand 142
5.4.5.2 Basic Variables for Block Wall Capacity 143
5.4.5.3 Variability of Factor of Safety 144
5.4.6 Seismic Fragility Curves 145
5.5 Weighting Seismic Fragility Analysis 145
5.5.1 Generation of Input Ground Response Spectra 146
5.5.2 Weights of Input GRS 149
5.5.3 Development of Seismic Fragility Surfaces 151
5.5.3.1 Procedure 151
5.5.3.2 Conditional Probability of Failure Given an Input GRS 153
5.5.4 Weighting Seismic Fragility Curves 159
5.6 Summary 161

**6 Improved Seismic Margin Assessment . . . . . 162**
6.1 System Analysis 163
6.1.1 Event Tree Analysis 163
6.1.2 Fault Tree Analysis 164
6.2 Numerical Example for Emergency Coolant Injection System 167
6.2.1 Basic Configuration of ECI System 167
6.2.2 Current Seismic Fragility Analysis for Water Tank 171
6.2.2.1 Basic Configuration of Water Tank 171

6.2.2.2 Review Level Earthquake 174
6.2.2.3 Current Seismic Fragility Analysis - NUREG Spectrum is RLE 175
6.2.2.4 Current Seismic Fragility Analysis - UHS is RLE 178
6.2.2.5 Discussion of HCLPF Seismic Capacity 181
6.2.3 Current Seismic Fragility Analysis for Electric Cabinet 182
6.2.3.1 Basic Configuration of Electric Cabinet 182
6.2.3.2 Seismic Demand Analysis 183
6.2.3.3 Structural Capacity Analysis 187
6.2.3.4 Median Seismic Capacity 188
6.2.3.5 Logarithmic Standard Deviations 189
6.2.3.6 Seismic Fragility Curves and HCLPF Seismic Capacity 190
6.2.4 Weighting Seismic Fragility Analysis for Electrical Cabinet 191
6.2.4.1 Weights of Input GRS 191
6.2.4.2 Seismic Fragility Analysis considering VGMPs 192
6.2.4.3 Weighting Seismic Fragility Curves 196
6.2.5 HCLPF Seismic Capacity of ECI System 199
6.3 Summary 200

**7 Conclusions and Future Research . . . . . 201**
7.1 Mean Annual Rate Density Distribution 201
7.2 Investigation of Problems in Seismic Fragility Analysis 202
7.3 Seismic Fragility Analysis considering VGMPs 203
7.4 Weighting Seismic Fragility Analysis 203
7.5 Seismic Probabilistic Risk Analysis considering VGMPs 204
7.6 Improved Seismic Margin Assessment 204
7.7 Future Research 205

**Bibliography** . . . . . **206**

# List of Figures


1.1 The general procedure of seismic probabilistic risk analysis 7

1.2 Spectral shape comparison of two different types of GRS 10

1.3 Region of ground response spectra anchoring to $0.3g$ PGA 11

2.1 Map information around Darlington NGS site 22

2.2 Logic tree of PSHA model for Darlington NGS site 23

2.3 Southeastern Canada H2 seismic source model 24

2.4 Southeastern Canada R2 seismic source model 24

2.5 Median, High, and Low Estimates of $f'_M(m)$ for OBGH seismic source (H2 model) 27

2.6 Median, High, and Low Estimates of Median PGA (i.e. $\mathcal{S}_{\mathrm{A}}(f=50\,\mathrm{Hz})$) versus epicenter distance $r_{\mathrm{epi}}$ 29

2.7 A simplified diagram of gridding an areal source surrounding Darlington NGS site 30

2.8 Seismic hazard curves for PGA (i.e. $\mathcal{S}_{\mathrm{A}}(f_1=50\,\mathrm{Hz})$) from H2 source model 33

2.9 Seismic hazard curves for PGA (i.e. $\mathcal{S}_{\mathrm{A}}(f_1=50\,\mathrm{Hz})$) from HY source model 33

2.10 Seismic hazard curves for PGA (i.e. $\mathcal{S}_{\mathrm{A}}(f_1=50\,\mathrm{Hz})$) from R2 source model 34

2.11 Seismic hazard curves for PGA (i.e. $\mathcal{S}_{\mathrm{A}}(f_1=50\,\mathrm{Hz})$) from all epistemic branches 34

2.12 Empirical CDF of seismic hazard given PGA$=0.1g$ 35

2.13 Seismic hazard curves for PGA at mean and three percentiles 35

2.14 Interpolation of seismic hazard curves regarding representative frequencies at seismic hazard of $1 \times 10^{-2}$ 37

2.15 Mean UHS at four seismic hazard levels at Darlington NGS site 37

2.16 Contour of annual rate density of $\mathcal{S}_{\mathrm{A}}(f)|\mathrm{PGA}$ 38

2.17 Mean annual rate density of $\mathcal{S}_{\mathrm{A}}(f)$ at three PGA values 39

2.18 Interpolation of seismic hazard curves for determining $\mathcal{S}_{\mathrm{A}}(f)$ 40

2.19 Spectral values of $\mathcal{S}_{\mathrm{A}}(f)$ based on PSHA and VPSHA (PGA $= 0.6g$) 40

3.1 An example of family of fragility curves and mean fragility curve 48

3.2 Configuration details of horizontal heat exchanger 50

3.3 NUREG spectrum and site-specific UHS anchoring to PGA at $0.3g$ 53

3.4 Forces due to longitudinal excitation 56

3.5 Forces due to transverse rocking 56

3.6 Forces due to vertical excitation 56

3.7 Anchorage failure modes 60

3.8 Yield line pattern of the base plate 62

3.9 Fillet weld failure 62

3.10 Interaction relationship of tension and shear 64

3.11 Seismic fragility curves of heat exchanger under NUREG spectrum at $0.3g$ PGA 67

3.12 Seismic fragility curves of heat exchanger based on NUREG spectrum and UHS 72

3.13 HCLPF seismic capacity of heat exchanger based on NUREG spectrum and UHS 72

3.14 Seismic fragility curves in terms of $\bar{\mathcal{S}}_A$ under NUREG spectrum 76

4.1 A flow diagram of weighting seismic fragility analysis method 82

4.2 Mean annual rate density of $\mathcal{S}_A(f)$ at three PGA values 84

4.3 Calculation of weights of input GRS with spectral values $s_2$ given PGA$=0.6g$ 86

4.4 An example of GRS Representing Earthquake Response Spectra 87

4.5 An example of PDFs of structural shear strength and force 88

4.6 A flow diagram of development of seismic fragility surfaces 89

4.7 Mean annual rate density of $\mathcal{S}_A(f_L)$ given three PGA values 97

4.8 Mean annual rate density of $\mathcal{S}_A(f_L)$ given PGA$=0.6g$ 97

4.9 Mean seismic hazard curves with respect to $\mathcal{S}_A(f_T)$ and PGA 99

4.10 An example of horizontal input GRS 101

4.11 A family of fragility surfaces of $\mathcal{S}_A(f_L)$ and PGA 105

4.12 Mean fragility surface of $\mathcal{S}_A(f_L)$ and PGA 105

4.13 Sections of mean fragility surface 106

4.14 An example of section of fragility surface and mean annual rate density 108

4.15 Mean seismic hazard curve for $\mathcal{S}_A(f_L)$ 110

4.16 Weights of input GRS 110

4.17 Weighting seismic fragility curves of heat exchanger 113

4.18 Weighting HCLPF seismic capacity of heat exchanger 113

4.19 Seismic fragility curves of heat exchanger based on two methods 114

4.20 HCLPF capacity of heat exchanger based on two methods 114

5.1 Two methods for generating FRS 119

5.2 Geometry information of block wall 123

5.3 Hysteretic loop of centrally-reinforced masonry wall 124

5.4 Finite element model of service building 126

5.5 RLE at Darlington NGS site 128

5.6 Bending of centrally-reinforced unit width uncracked block wall 129

5.7 FRS regarding three sets of damping ratios 131

5.8 Typical force-displacement relationship 135

5.9 The free-body diagram of block wall 139

5.10 FRS of Node 1 in direction 2 of service building 144

5.11 Seismic fragility curves of block wall 147

5.12 Mean seismic hazard curves for PGA and spectral accelerations at three representative frequencies 148

5.13 An example of input GRS 149

5.14 Mean annual rate density of $\mathcal{S}_{\mathrm{A}}(f_1)$ with respect to three PGA values 150

5.15 Mean annual rate density of $\mathcal{S}_{\mathrm{A}}(f_1)$ at PGA$=1.0g$ 150

5.16 Weights of input GRS 152

5.17 An example of horizontal input GRS 154

5.18 FRS at Darlington NGS site given an input GRS 154

5.19 Seismic fragility surfaces of $\mathcal{S}_{\mathrm{A}}(f_1)$ and PGA 158

5.20 Seismic fragility curves of block wall based on two methods 160

5.21 HCLPF seismic capacities of block wall based on two methods 160

6.1 A general procedure of seismic margin assessment 162

6.2 An example of event tree for core damage accident 164

6.3 A simple fault tree 165

6.4 Reduced fault tree 166

6.5 A simplified ECI system 168

6.6 Fault tree of the ECI system 169

6.7 The reduced fault tree of ECI system 171

6.8 Basic configuration of the water tank 172

6.9 NUREG spectrum and site-specific UHS anchoring to PGA at $0.3g$ 175

6.10 The geometry information of electric cabinet 183

6.11 Forces due to earthquake excitations in two horizontal directions 185

6.12 Interaction relationship of tension and shear 188

6.13 Seismic fragility curves of the electric cabinet 192

6.14 Mean derivative of conditional AFE of $\mathcal{S}_{\mathrm{A}}(f_{\mathrm{H}}) \,|\, \mathrm{PGA}$ 193

6.15 Weights of input GRS 193

6.16 An example of horizontal input GRS 194

6.17 Seismic fragility surfaces of $\mathcal{S}_{\mathrm{A}}(f_{\mathrm{H}})$ and PGA 197

6.18 Seismic fragility curves of the electric cabinet based on two methods 198

6.19 HCLPF seismic capacity of the electric cabinet based on two methods 198

# Nomenclature

| | |
|---|---|
| ACI | American Concrete Institute |
| AFE | Annual Frequency of Exceedance |
| ASCE | American Society of Civil Engineering |
| CDF | Cumulative Distribution Function |
| CENA | Central and Eastern North America |
| CSA | Canadian Standard Association |
| ECI | Emergency Coolant Injection |
| ENA | Eastern North America |
| EPRI | Electric Power Research Institute |
| FA | Fragility Analysis |
| FRS | Floor Response Spectrum |
| GMP | Ground-Motion Parameter |
| GMPEs | Ground-Motion Prediction Equations |
| GRS | Ground Response Spectrum |
| HCLPF | High Confidence and Low Probability of Failure |
| MDOF | Multi-Degree-of-Freedom |
| NBCC | National Building Code of Canada |
| NPPs | Nuclear Power Plants |
| NUREG | Nuclear Regulatory |
| PDF | Probability Density Function |
| PGA | Peak Ground Acceleration |
| PSHA | Probabilistic Seismic Hazard Analysis |

| | |
|---|---|
| RLE | Review Level Earthquake |
| $\mathcal{S}_A$ | Spectral Acceleration |
| SDOF | Single Degree-of-Freedom |
| SMA | Seismic Margin Assessment |
| SPRA | Seismic Probabilistic Risk Analysis |
| SRSS | Square Root of Sum of Squares |
| SSCs | Structures, Systems, and Components |
| UHS | Uniform Hazard Spectrum |
| USNRC | U.S. Nuclear Regulatory Commission |
| VGMPs | Vector-valued Ground-Motion Parameters |
| VPSHA | Vector-valued Probabilistic Seismic Hazard Analysis |
| VSFA | Vector-valued Seismic Fragility Analysis |
| WNA | Western North America |

CHAPTER 1

# Introduction

Nuclear facilities are designed in accordance with pertinent codes and specifications. In recent past, beyond Design Basis Earthquake events jeopardized the design concept of redundancy and defense in-depth related to nuclear facilities. Nuclear industry and regulatory commissions frequently face the issue whether modifications of existing nuclear power plants (NPPs) are required. Accurate seismic margin or seismic risk estimates of these NPPs are undoubtedly crucial in the decision-making.

In Section 1.1, definitions of technical terms in seismic analysis and applications are given. In Section 1.2, key elements of Seismic Probabilistic Risk Analysis are introduced. Section 1.3 illustrates seismic fragility analysis method and problems that are observed in engineering practice. To resolve these problems, the objectives of this study are presented in Section 1.4. The organization of this thesis is given in Section 1.5.

## 1.1 Definitions

Definitions of technical terms in seismic analysis and applications are pretty important. In the following, critical definitions are adopted in this study:

- **Earthquake:** the entire phenomenon of fault rupture releasing stored strain in the earth's crust and propagating energy from the source in the form of vibratory waves in all directions (McGuire, 2004).

- **Peak ground acceleration, peak ground velocity, and peak ground displacement:** peak value (acceleration, velocity, and displacement) of an earthquake ground motion.
- **Seismic hazard:** a property of an earthquake that can cause damage and loss. For example, peak ground acceleration (PGA) is greater than a specified value at a specific site. Probabilistic Seismic Hazard Analysis (PSHA) determines the frequency (the number of events per unit time period) with which a seismic hazard will occur. It is common to use "seismic hazard" and "frequency" interchangeably (McGuire, 2004).
- **Frequency:** In the PSHA, "frequency" represents the expected number of events occurring in a time period (e.g., one year). However, in structural dynamic analysis, natural frequency (also called "frequency") is defined as the reciprocal of natural period with respect to a vibration mode of a structure. Therefore, the meaning of "frequency" should be interpreted according to specific context.
- **Seismic hazard curve:** a graphical curve depicting the frequency with which selected values of a seismic hazard are expected to occur (or expected to be exceeded) (McGuire, 2004).
- **Structures, systems, and components:** a technical term that is widely used in nuclear power industry. Structure is the combination of members (e.g., beam, column, and slab) connected together that can satisfy a specific purpose. For example, reactor building container is a typical structure that isolates reactors from outside. Components are affiliated equipments and devices in nuclear facilities. Heat exchanger is an example of component that transfers heat produced by nuclear reaction to drive steam turbines for electricity production. System is a combination of structures or/and components integrated for a specific purpose. For example, emergency coolant injection system is used to cool the heat after reactors shut down abnormally. It needs to make clear that structures, systems, and components (SSCs) are designed to satisfy different functions, thus there is no hierarchy in the definition of SSCs.
- **Structural response:** structural absolute acceleration, relative velocity, and relative displacement varying with time when subjected to a ground motion. Here "relative"

is with respect to ground motion. The structure may be a single degree-of-freedom (SDOF) structure or a multi-degree-of-freedom (MDOF) structure.

- **Spectral acceleration, spectral velocity, and spectral displacement:** peak response (absolute acceleration, relative velocity, and relative displacement) of a SDOF oscillator with a frequency when subjected to a ground motion.
- **Ground response spectrum:** a graphical plot of peak response (absolute acceleration, relative velocity, and relative displacement) of a series of SDOF oscillators with varying frequencies when subjected to the same ground motion. Statistical analyses for historical earthquake records show that ground response spectrum (GRS) approach PGA when frequency exceeds $\sim$33 Hz. In engineering practice, spectral acceleration at 33 Hz is taken as PGA.
- **Uniform hazard spectrum:** a graphical plot of response of a series of SDOF oscillators with varying frequencies. Uniform hazard spectrum (UHS) is obtained from PSHA for a specific site. Given a UHS with respect to a seismic hazard, spectral accelerations at all frequencies of engineering interest are associated with the same seismic hazard. Since UHS is not obtained from realistic earthquake records, PGA is not applicable in a UHS. Engineering practice recognizes that spectral acceleration at a high frequency (e.g. 50 Hz) from a UHS can be approximately taken as PGA.
- **Design Basis Earthquake:** an earthquake represented by a smooth GRS or UHS. In design practice, Design Basis Earthquake (DBE) is defined as seismic input for safety-related nuclear facilities. It is required that, during a DBE event, reactors should safely shut down, while cooling systems remain functional for transferring heat produced by nuclear fuel. Examples of DBE are Regulatory Guide 1.60 design response spectra (USNRC, 2014A) and CSA 289.3-10 design response spectra (CSA, 2010).
- **Review Level Earthquake:** an earthquake represented by a smooth GRS or UHS. It is used in Seismic Margin Assessment and Seismic Probabilistic Risk Analysis, aiming to seek out any "weak links" that limit the plant capacity to safely shut down after a seismic event greater than DBE. An example of Review Level Earthquake (RLE) is NUREG/CR-0098 median response spectra (USNRC, 1978).

- **Ground motion parameter:** a parameter of characterizing an earthquake ground motion or a RLE. For example, PGA, peak ground velocity, or peak ground displacement is usually used to describe an earthquake ground motion, while spectral acceleration at a specified frequency or average spectral acceleration over a frequency range is chosen to represent a RLE. Recall that, from a RLE, spectral acceleration at a sufficient high frequency can be taken as PGA. Therefore, in engineering applications, PGA is also used to represent a RLE.
- **Vector-valued ground motion parameters:** a vector of ground motion parameters of characterizing an earthquake ground motion or a RLE. By using vector-valued ground motion parameters (VGMPs), the inherent variability in earthquake response spectra is more accurately captured in vector-valued PSHA. Ground response spectra in terms of VGMPs are defined as seismic input in seismic fragility analysis, hence seismic fragility can be more precisely described.
- **Screening level:** a ground motion level in terms of a GMP such as PGA. By setting a screening level, a great amount of unnecessary seismic capacity computations are eliminated for SSCs whose High Confidence and Low Probability of Failure (HCLPF) capacities clearly exceed the screening level, so that efforts can be quickly concentrate on those SSCs for which there is a legitimate concern about seismic ruggedness.
- **Aleatory randomness:** the probabilistic uncertainty that is inherent in a random phenomenon and cannot be reduced by acquiring additional data or information (McGuire, 2004).
- **Epistemic uncertainty:** the uncertainty that results from lack of knowledge about some model or parameter. This type of uncertainty can be reduced, at least conceptually, by additional data or improved information (McGuire, 2004).
- **Uncertainty:** a general term for both aleatory *randomness* and epistemic *uncertainty* (McGuire, 2004).
- **Structural capacity:** an intrinsic property of a structure representing its capability to withstand normal stress, shear stress, and bending stress. In design practice, tensile strength, shear strength, and flexural strength are usually used to represent structural

capacity. Due to uncertainty in material strength, structural capacity is a random variable.

- **Response spectrum analysis method:** an approach of determining peak response (e.g. spectral acceleration) of a structure. The seismic input is ground response spectrum (GRS) instead of spectrum-compatible time histories. Peak response of the structure is calculated by combining peak modal responses according to combination rules such as Square-Root-of-Sum-of-Squares (SSRS) rule and 100-40-40 combination rule. Peak modal responses (e.g. spectral accelerations) corresponding to vibration modes (each mode is related to a natural frequency) of the structure are obtained from the input GRS.
- **Seismic demand:** normal stress, shear stress, and bending stress of a structure, which are induced by an input DBE or RLE. In engineering applications, tensile force, shear force, and bending moment are usually used to describe seismic demand. Due to uncertainty in structural response, seismic demand is a random variable.
- **Seismic capacity:** a measure of structural capacity that is characterized by a single GMP. It not only relies on structural intrinsic properties, but also depends on the spectral shape of RLE that is used in seismic fragility analysis. For example, seismic capacity of a heat exchanger will change when it is moved from an NPP in western North America (WNA) to an NPP in eastern North America (ENA), because the typical spectral shape of RLE in the WNA zone is totally different from that in the ENA zone. The uncertainties in structural capacity and response are properly propagated in the determination of seismic capacity, thus seismic capacity is a random variable. It is more convenient to study the capabilities of SSCs to withstand potential earthquake using seismic capacities, because they are represented by the same parameter (e.g. PGA).
- **Seismic fragility:** a property of structure characterizing its vulnerability to withstand a ground motion. It is defined as conditional probability of failure of an SSC given a ground motion level in terms of single GMP such as PGA. Seismic fragility is the cumulative distribution function (CDF) of seismic capacity. It needs to make

clear that seismic fragility is not the CDF of the chosen GMP. Only when structural capacity uncertainty and structural response uncertainty (excluding ground motion) are ignored, seismic fragility is the CDF of the chosen GMP.

- **Seismic fragility curve:** a graphical curve describing the conditional probability of failure of an SSC versus ground motion in terms of a single GMP. Based on seismic fragility curve, a plausible conclusion is that seismic fragility is the CDF of the chosen GMP. However, it is actually the CDF of seismic capacity.
- **Seismic risk:** the probability that some humans will incur loss or that their built environment will be damaged. These probabilities usually represent a level of loss or damage that is equaled or exceeded over some time period. The loss or damage must be quantified; it might be a monetary loss in a defined range, the number of casualties in a region, or the cost to repair a facility as a percentage of replacement cost (McGuire, 2004).

## 1.2 Research Background

Current design practice for nuclear facilities are based on a deterministic perspective. Conservatism is included in each design step to achieve an adequate design related to nuclear facilities. However, it cannot provide sufficient information to estimate actual seismic margin or realistic seismic risk of existing nuclear power plants (NPPs).

An approach termed as Seismic Probabilistic Risk Assessment (SPRA) provides a probabilistic way to quantitatively estimate seismic risk of existing NPPs. The SPRA was firstly proposed in mid 1970s (USNRC, 1975) and has been used to estimate the seismic risk of existing NPPs since late 1970s (Kennedy *et al.*, 1980; Kaplan *et al.*, 1983; Ellingwood, 1994; Huang *et al.*, 2011). The SPRA procedure (EPRI, 2013) mainly includes three key parts, i.e.,

- probabilistic seismic hazard analysis(PSHA),
- seismic fragility analysis (FA), and
- system analysis (also called accident sequence analysis).

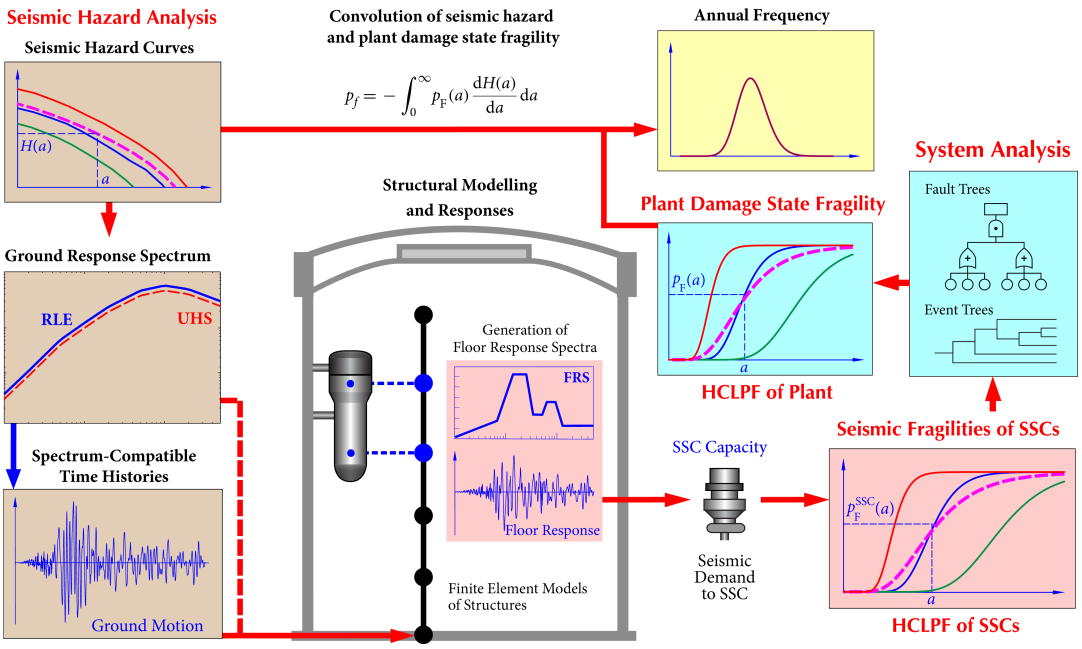


**Figure 1.1** The general procedure of seismic probabilistic risk analysis

As shown in Figure 1.1, PSHA aims to obtain the site-specific seismic hazard represented by seismic hazard curves corresponding to varying frequencies. Another product of PSHA is uniform hazard spectrum (UHS). "Uniform" indicates that spectral accelerations at any frequencies correspond to the same seismic hazard. UHS anchoring to a plant screening level in terms of a ground motion parameter (GMP) is recommended to be chosen as Review Level Earthquake (RLE) in seismic fragility analysis (EPRI, 2013).

Seismic FA aims to determine seismic fragilities of structures, systems, and components (SSCs) in nuclear power plants (NPPs). The results are seismic fragility curves, representing conditional probability of failure of SSCs given ground motions in terms of a single GMP. Seismic fragilities of SSCs are used as input in system analysis.

An NPP consists of a lot of systems that are integrated by a great number of SSCs. In engineering practice, a systematic scheme in terms of event trees and fault trees is developed to properly propagate seismic fragilities of SSCs into plant damage state seismic fragility.

Probability of failure of an NPP due to an earthquake with magnitude above the lower bound (e.g. $m = 4.75$) is determined by total probability formula, i.e.,

$$p = \int_0^\infty p_F(a)\, f_{GMP}(a)\, da, \tag{1.2.1}$$

where $p_{\mathrm{F}}(a)$ is plant damage state seismic fragility, and $f_{\mathrm{GMP}}(a)$ is probability density function of the GMP that is used in PSHA.

Finally, annual frequency that an adverse consequence (e.g. core damage accident) will occur is determined by

$$\gamma = \nu \cdot p = \int_0^\infty p_{\mathrm{F}}(a)\,[\nu\, f_{\mathrm{GMP}}(a)]\,\mathrm{d}a = -\int_0^\infty p_{\mathrm{F}}(a)\,\frac{\mathrm{d}H(a)}{\mathrm{d}a}\,\mathrm{d}a, \tag{1.2.2}$$

where $\nu$ is annual rate of occurrence of earthquake above the lower bound magnitude, and $H(a)$ is seismic hazard at the site of interest, representing annual frequency that spectral value $a$ of the chosen GMP is expected to be exceeded.

In the SPRA, seismic fragility analysis is extremely important, because the failure of an SSC probably triggers an adverse consequence. Overestimate or underestimate of seismic fragilities of SSCs may result in unreliable plant damage state seismic fragility. Therefore, accurate seismic fragility estimates of SSCs are crucial in estimating seismic risk of NPPs.

## 1.3 Seismic Fragility Analysis

### 1.3.1 Lognormal Fragility Model

In nuclear engineering practice, a lognormal model is widely used to determine seismic fragilities of structures, systems, and components (SSCs) (Kennedy *et al.*, 1980; Kennedy and Ravindra, 1984; Pisharady and Basu, 2010; Mandal *et al.*, 2016). Seismic fragility is defined as the conditional probability that seismic capacity $A$ of an SSC is less than a given ground motion level $a$ in terms of a single GMP (e.g. PGA), i.e.,

$$p_{\mathrm{F}}(a) = \mathcal{P}\big\{A < a \,\big|\, \mathrm{GMP} = a\big\}, \qquad A = A_m\,\varepsilon_U\,\varepsilon_R = A_m^U\,\varepsilon_R, \tag{1.3.1}$$

where $A$ is a random variable characterizing seismic capacity in terms of GMP. $A_m$ is the best estimate of *median* seismic capacity, which is a deterministic value. $\varepsilon_R$ and $\varepsilon_U$ are random variables representing aleatory *randomness* and epistemic *uncertainty* about the median value. Both variables are usually taken to be lognormal with unit median (zero logarithmic mean) and logarithmic standard deviations of $\beta_R$ and $\beta_U$, respectively.

Given confidence level $Q=q$, the estimated *median* capacity $A^U_{m,q}$ at the confidence level $Q=q$ can be expressed as

$$A^U_{m,q} = A_m \varepsilon_{U,q} = A_m \mathrm{e}^{-\beta_U \Phi^{-1}(q)}, \qquad \mathcal{P}\{A^U_m > A^U_{m,q}\} = q. \tag{1.3.2}$$

Replacing $A_m \varepsilon_U$ in equation (1.3.1) by $A^U_{m,q}$ obtained in equation (1.3.2) yields the seismic fragility, or the conditional probability of failure given a ground motion level $a$, at confidence level $Q=q$ (Kennedy and Ravindra, 1984)

$$p_{\mathrm{F},q}(a) = \mathcal{P}\{A < a \,|\, \mathrm{GMP} = a,\ Q = q\} = \Phi\left[\frac{\ln(a/A_m) + \beta_U \Phi^{-1}(q)}{\beta_R}\right]. \tag{1.3.3}$$

Based on lognormal fragility model, seismic capacity $A$ is independent on ground motion level $a$. Therefore, it is unnecessary to use a great number of acceleration time histories covering a wide range of ground motion levels in the calculation of seismic demand. In engineering applications, NUREG/CR-0098 median response spectra (USNRC, 1978) or site-specific uniform hazard spectra (UHS), anchoring to a specific plant screening level in terms of a GMP (e.g. $A_{\mathrm{RLE}} = 0.3g$ PGA), is defined as Review Level Earthquake (RLE) in seismic fragility analysis.

### 1.3.2 Problems in Engineering Applications

Lognormal fragility model makes the determination of seismic fragilities of SSCs more convenient and applicable. However, due to the use of a single GMP, problems have been observed in engineering applications (Ni *at al.*, 2015; Cai *at al.*, 2015):

1. **Spectral shape of RLE**

   Suppose that there are two RLE, i.e., NUREG/CR-0098 median rock response spectrum (abbreviated as NUREG spectrum) and eastern North America (ENA) hard-rock response spectrum (abbreviated as ENA spectrum) (Atkinson and Elgohary, 2007), as shown in Figure 1.2, anchoring to PGA at screening level $A_{\mathrm{RLE}} = 0.3g$. PGA is chosen as GMP in seismic fragility analysis. Assume that a structure has three natural frequencies (see Figure 1.2) and is subjected to these two RLE. From elastic structural dynamic analysis, structural response depends primarily on spectral accelerations at its natural frequencies. Since spectral values at frequencies $f_1$ and $f_2$ are totally different

based on two RLE (see Figure 1.2), structural responses would be also different. As a result, seismic demand is inconsistent for the same structure, inevitably leading to inconsistent seismic capacity estimate in terms of PGA.

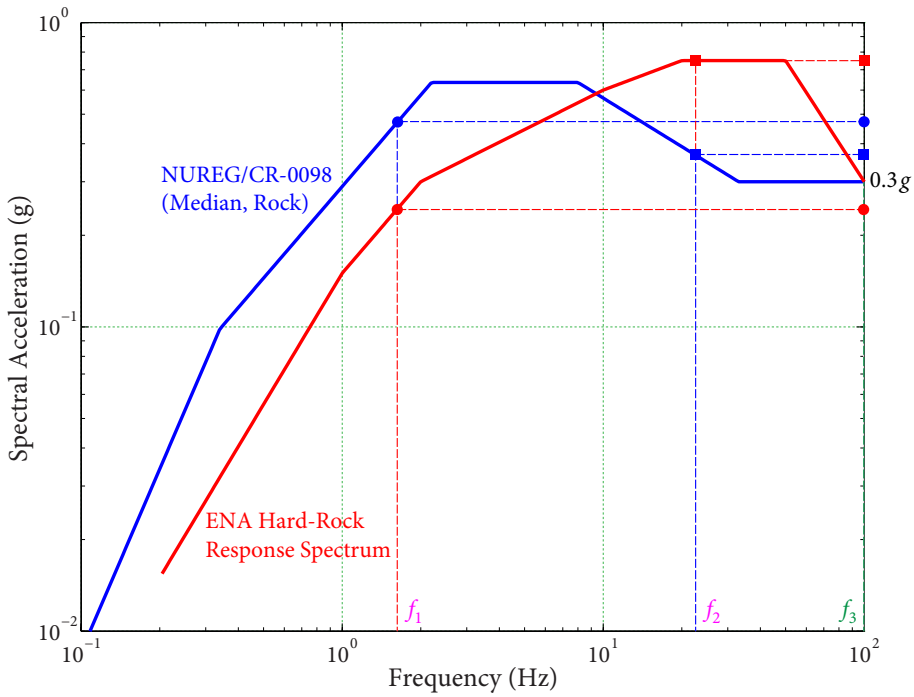


**Figure 1.2** Spectral shape comparison of two different types of GRS

2. **Use of a single GMP**

In engineering applications, PGA is usually used to characterize a RLE and represent seismic capacity of an SSC. However, fundamental frequencies of safety-related structures, systems, and components (SSCs) in nuclear power plants are usually between 2 Hz and 10 Hz, which are much smaller than the frequency ($\sim$50 Hz) where spectral acceleration approach PGA. Figure 1.3 shows the region of ground response spectra from over 200 historical earthquake records, anchoring to PGA at a screening level $A_{\mathrm{RLE}} = 0.3g$. It shows that realistic earthquake response spectra include large variability in spectral accelerations at frequency range between 2 and 10 Hz, indicating that a smooth RLE cannot accurately predict spectral acceleration at the fundamental frequency (e.g. 5 Hz) of a safety-related SSC.

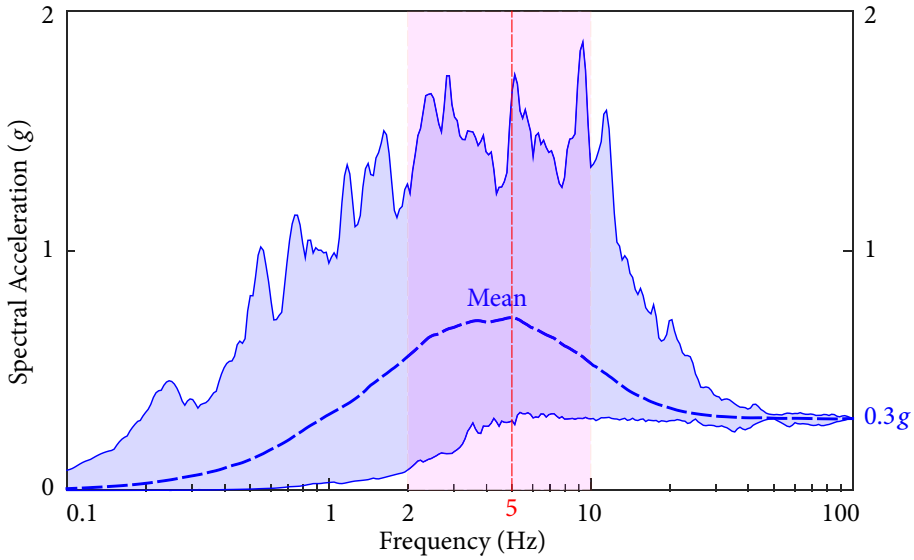


**Figure 1.3** Region of ground response spectra anchoring to 0.3$g$ PGA

3. **Neglect of ground motion intensity effect**

   In current seismic fragility analysis, spectral shape of the chosen RLE is independent on ground motion intensity, which can be scaled downward or upward to meet different ground motion intensities. However, characteristics of ground motions from large earthquakes are different from those from moderate earthquakes, indicating that earthquake response spectra depend on ground motion intensity. Therefore, ground motion intensity effect should be taken into consideration in the determination of seismic fragility.

## 1.4 Objectives

This study aims to develop weighting seismic seismic fragility analysis method based on vector-valued GMPs (VGMPs). The method mainly includes three consecutive parts:

1. vector-valued probabilistic seismic hazard analysis is performed to determine the weights of input ground response spectra (GRS);
2. seismic fragility analysis considering VGMPs method is proposed to calculate seismic fragility based on VGMPs;

3. weights of input GRS and seismic fragility are combined to obtain the weighting seismic fragility of an SSC.

By using VGMPs, the proposed method resolves the problems in current seismic fragility analysis, thus it can more accurately estimate seismic capacities of safety-related SSCs. In addition, weighting seismic fragility curves are in terms of a single GMP; hence they are readily incorporated into Seismic Probabilistic Risk Analysis and Seismic Margin Assessment. Furthermore, the proposed method can save redesign cost of safety-related SSCs that do not satisfy seismic margin requirement.

## 1.5 Thesis Organization

In Chapter 2, scalar PSHA and vector-valued PSHA (VPSHA) are briefly introduced first. Numerical example for Darlington nuclear generating station is then performed. Matlab codes are written by myself to develop seismic hazard curves and uniform hazard spectra (UHS). VPSHA is also performed to predict mean annual rate density distributions. The results show that, by means of VPSHA, aleatory randomness in earthquake response spectra and ground motion intensity effect are taken into consideration. In addition, UHS overestimates the seismic hazard given a spectral value of the chosen GMP. Therefore, vector-valued GMPs (VGMPs) should be introduced to predict seismic hazard.

In Chapter 3, current seismic fragility analysis method is introduced first. To illustrate the procedure and demonstrate the problems of current method, numerical example for a horizontal heat exchanger is performed. The results show that the spectral shape of RLE and the use of GMP have noticeable effect on the determination of seismic fragility. For nuclear power plants in eastern North Amercia, site-specific UHS should be chosen as Review Level Earthquake (RLE) for acquiring more accurate seismic capacity estimates of SSCs. Nevertheless, the problems in current method are not completely resolved.

In Chapter 4, weighting seismic fragility analysis method is proposed based on VGMPs. Numerical example for a horizontal heat exchanger is performed to illustrate the procedure and demonstrate the advantages of the proposed method. The weighting High Confidence Level and Low Probability of Failure (HCLPF) seismic capacity has 26.1% increase comparing to conventional (as opposed to weighting) HCLPF seismic capacity. In addition, mean

annual frequency of the failure of heat exchanger has a remarkable decrease (60.4%). Both results indicate that the proposed method can more accurately estimate HCLPF seismic capacity and annual frequency of occurrence of the failure of heat exchanger.

In Chapter 5, weighting seismic fragility analysis for components mounted on structures is proposed. A direct spectra-to-spectra method is applied to generate floor response spectra (FRS). Given structural information and input RLE, FRS can be directly determined by analytical expressions. Compared to computationally expensive time history analyses, direct spectra-to-spectra method generates FRS with high efficiency and sufficient accuracy. In addition, it would save much computational cost on capturing variabilities of response variables. Numerical example for a block wall located on the second floor of a service building is performed to illustrate the proposed method. The results shows that weighting HCLPF seismic capacity has a remarkable increase (42.5%).

In Chapter 6, an improve SMA procedure is proposed. The procedure combines the use of conventional and weighting HCLPF capacities of SSCs, which ensures that more plant seismic capacity is obtained, while analysis cost is acceptable. To better illustrate the proposed procedure, numerical example for an emergency coolant accident (ECI) system is performed. The results show that the HCLPF capacity of the ECI system based on the proposed procedure meets seismic margin requirement, while HCLPF capacity of ECI system based on conventional procedure cannot satisfy the requirement. By using the proposed procedure, redesign cost for SSCs that do not meet seismic margin requirement are saved.

In Chapter 7, major contributions of the research work and future research are presented to conclude this thesis.

C H A P T E R 2

# Seismic Hazard Analysis

Among a variety of hazards induced by potential seismic sources at the site of interest, ground shaking is the dominant agent of damage to the built environment (Chen and Lui, 2006). To estimate this type of hazard, probabilistic seismic hazard analysis (PSHA) was proposed in late 1960s (Cornell, 1968). It is originated from probabilistic perspective, i.e., model parameters in the prediction of seismic hazard at the site of interest are taken as random variables, thus it properly captures the aleatory randomness of model parameters. In addition, a logic tree is usually developed for capturing epistemic uncertainties in the PSHA model. As a result, PSHA provides a better way to describe the seismic hazard at the site of interest.

In this Chapter, PSHA and vector-valued PSHA (VPSHA) are introduced first. Numerical example for Darlington nuclear generating station site in south Ontario, Canada, is then performed for illustrating the procedure of PSHA and VPSHA. The results indicate that, by means of VPSHA, aleatory randomness in earthquake response spectra and ground motion intensity effect can be properly captured.

## 2.1 Probabilistic Seismic Hazard Analysis

Scalar Probabilistic seismic hazard analysis (PSHA) has been used to predict seismic hazard at nuclear power plant sites since late 1970s. It integrates the uncertainties in seismic source model, magnitude-recurrence model, maximum earthquake magnitude, and

ground-motion model to obtain an explicit expression of seismic hazard, i.e., annual frequency that a threshold value is expected to be exceeded, at the site of interest as (USNRC, 1997; McGuire, 2004; Baker, 2008)

$$\lambda(s_1) = \sum_{i=1}^{N_S} \nu_i \left\{ \int_r \int_m \mathcal{P}\left\{ \mathcal{S}_{\mathrm{A}}(f_1) > s_1 \,\middle|\, m, r \right\} f_M(m)\, f_R(r)\, \mathrm{d}m\, \mathrm{d}r \right\}_i, \tag{2.1.1}$$

where $N_S$ is the number of surrounding seismic sources, $\nu_i$ is the annual rate of occurrence of seismic source $i$. $\mathcal{P}\left\{ \mathcal{S}_{\mathrm{A}}(f_1) > s_1 \,\middle|\, m, r \right\}$ is the complementary cumulative distribution function (CDF) of spectral acceleration $\mathcal{S}_{\mathrm{A}}(f_1)$ given an earthquake with magnitude $m$ and source-to-site distance $r$, representing the conditional probability that $\mathcal{S}_{\mathrm{A}}(f_1)$ exceeds a threshold value $s_1$, given a pair of $m$ and $r$. $f_M(m)$ and $f_R(r)$ are probabilistic density functions (PDFs) of earthquake magnitude $m$ and source-to-site distance $r$, respectively.

Given a pair of $m$ and $r$, $\ln \mathcal{S}_{\mathrm{A}}(f_1)$ is of normal distribution; hence $\mathcal{P}\left\{ \mathcal{S}_{\mathrm{A}}(f_1) > s_1 \,\middle|\, m, r \right\}$ can be determined by

$$\mathcal{P}\left\{ \mathcal{S}_{\mathrm{A}}(f_1) > s_1 \,\middle|\, m, r \right\} = 1 - \mathcal{P}\left\{ \ln \mathcal{S}_{\mathrm{A}}(f_1) \leqslant \ln s_1 \,\middle|\, m, r \right\} = 1 - \Phi\left[ \frac{\ln s_1 - \mu_{\ln \mathcal{S}_{\mathrm{A}}(f_1)|m,r}}{\sigma_{\ln \mathcal{S}_{\mathrm{A}}(f_1)|m,r}} \right], \tag{2.1.2}$$

where $\mu_{\ln \mathcal{S}_{\mathrm{A}}(f_1)|m,r}$ and $\sigma_{\ln \mathcal{S}_{\mathrm{A}}(f_1)|m,r}$ are mean and standard deviation of $\ln \mathcal{S}_{\mathrm{A}}(f_1)$ given a pair of $m$ and $r$, respectively. $\Phi(\cdot)$ denotes the standard normal CDF.

Based on equation (2.1.2), the PDF of $\mathcal{S}_{\mathrm{A}}(f_1)$ given a pair of $m$ and $r$ is calculated by differentiating the CDF with respect to $s_1$,

$$f_{\mathcal{S}_{\mathrm{A}}(f_1)}\left(s_1 \,\middle|\, m, r\right) = \frac{1}{s_1\, \sigma_{\ln \mathcal{S}_{\mathrm{A}}(f_1)|m,r}}\, \phi\left[ \frac{\ln s_1 - \mu_{\ln \mathcal{S}_{\mathrm{A}}(f_1)|m,r}}{\sigma_{\ln \mathcal{S}_{\mathrm{A}}(f_1)|m,r}} \right]. \tag{2.1.3}$$

Integrating $f_{\mathcal{S}_{\mathrm{A}}(f_1)}\left(s_1 \,\middle|\, m, r\right)$ with respect to $m$ and $r$ gives the PDF of $\mathcal{S}_{\mathrm{A}}(f_1)$, i.e.,

$$f_{\mathcal{S}_{\mathrm{A}}(f_1)}(s_1) = \int_r \int_m f_{\mathcal{S}_{\mathrm{A}}(f_1)}\left(s_1 \,\middle|\, m, r\right) f_M(m)\, f_R(r)\, \mathrm{d}m\, \mathrm{d}r. \tag{2.1.4}$$

As in equation (2.1.1), PSHA gives annual frequency (also called annual rate) that a threshold value $s_1$ is expected to be exceeded. Based on equations (2.1.1) and (2.1.4),

annual rate density of $\mathcal{S}_{\mathrm{A}}(f_1)$ is defined as

$$f'_{\mathcal{S}_{\mathrm{A}}(f_1)}(s_1) = \sum_{i=1}^{N_S} \nu_i \left\{ f_{\mathcal{S}_{\mathrm{A}}(f_1)}(s_1) \right\} = \sum_{i=1}^{N_S} \nu_i \left\{ \int_r \int_m f_{\mathcal{S}_{\mathrm{A}}(f_1)}\big(s_1 \,|\, m, r\big) f_M(m) f_R(r) \,\mathrm{d}m \,\mathrm{d}r \right\}. \tag{2.1.5}$$

Therefore, the annual rate of events at the site of interest with $\mathcal{S}_{\mathrm{A}}(f_1)$ between $x_1$ and $x_2$ can be determined by

$$\lambda(x_1 \leqslant s_1 \leqslant x_2) = \int_{x_1}^{x_2} f'_{\mathcal{S}_{\mathrm{A}}(f_1)}(s_1) \,\mathrm{d}s_1 = \sum_{i=1}^{N_S} \nu_i \left\{ \int_{x_1}^{x_2} f_{\mathcal{S}_{\mathrm{A}}(f_1)}(s_1) \,\mathrm{d}s_1 \right\}. \tag{2.1.6}$$

In engineering applications, $\mu_{\ln \mathcal{S}_{\mathrm{A}}(f_1)|m,r}$ and $\sigma_{\ln \mathcal{S}_{\mathrm{A}}(f_1)|m,r}$ are obtained from ground motion models; $f_M(m)$ and $f_R(r)$ are determine from earthquake-recurrence models and seismic source models, respectively. Due to epistemic uncertainties in the PSHA model, the results of PSHA are a set of seismic hazard curves with respect to different percentiles or a mean seismic hazard curve. In addition, annual rate density of $\mathcal{S}_{\mathrm{A}}(f_1)$ can be obtained, which is used in Seismic Probabilistic Risk Analysis (see Section 1.2 of Chapter 1).

## 2.2 Vector-valued Probabilistic Seismic Hazard Analysis

Scalar PSHA provides seismic hazard of a SDOF oscillator at the site of interest, hence it would give accurate seismic hazard information for single-mode dominant structures, systems, and components (SSCs). In nuclear power plants, however, SSCs are usually multi-mode dominant. It indicates that using the joint knowledge of seismic hazard in terms of vector-valued GMPs (VGMPs) would improve the prediction of seismic hazard for SSCs (Bazzurro, 1998). In two-dimensional case, annual frequency that spectral accelerations $\mathcal{S}_{\mathrm{A}}(f_1)$ and $\mathcal{S}_{\mathrm{A}}(f_2)$ (abbreviated as $\boldsymbol{\mathcal{S}}_{\mathrm{A}}(\mathbf{f})$) of an SSC simultaneously exceed threshold values $s_1$ and $s_2$ (abbreviated as $\mathbf{s}$) is given by

$$\lambda(\mathbf{s}) = \sum_{i=1}^{N_S} \nu_i \left\{ \int_r \int_m \mathcal{P}\big\{ \boldsymbol{\mathcal{S}}_{\mathrm{A}}(\mathbf{f}) > \mathbf{s} \,\big|\, m, r \big\} f_M(m) f_R(r) \,\mathrm{d}m \,\mathrm{d}r \right\}_i, \tag{2.2.1}$$

where $\mathcal{P}\big\{ \boldsymbol{\mathcal{S}}_{\mathrm{A}}(\mathbf{f}) > \mathbf{s} \,\big|\, m, r \big\}$ is the conditional probability that $\boldsymbol{\mathcal{S}}_{\mathrm{A}}(\mathbf{f})$ simultaneously exceed $\mathbf{s}$, given an earthquake with magnitude $m$ and source-to-site distance $r$. Statistical tests

have shown that, given a pair of $m$ and $r$, the joint distribution of logarithmic spectral accelerations, i.e., $\ln \boldsymbol{S}_{\mathrm{A}}(\mathbf{f})$, can be well represented by multivariate normal distribution (Jayaram and Baker, 2008). Hence $\mathcal{P}\{\boldsymbol{S}_{\mathrm{A}}(\mathbf{f}) > \mathbf{s} \mid m, r\}$ can be determined by

$$\mathcal{P}\{\boldsymbol{S}_{\mathrm{A}}(\mathbf{f}) > \mathbf{s} \mid m, r\} = 1 - \mathcal{P}\{\boldsymbol{S}_{\mathrm{A}}(\mathbf{f}) \leqslant \mathbf{s} \mid m, r\} = 1 - \mathcal{P}\{\ln \boldsymbol{S}_{\mathrm{A}}(\mathbf{f}) \leqslant \ln \mathbf{s} \mid m, r\}, \quad (2.2.2)$$

where $\mathcal{P}\{\ln \boldsymbol{S}_{\mathrm{A}}(\mathbf{f}) \leqslant \ln \mathbf{s} \mid m, r\}$ is the joint CDF of $\ln \boldsymbol{S}_{\mathrm{A}}(\mathbf{f})$ given a pair of $m$ and $r$.

Based on equation (2.2.2), the joint PDF of $\ln \boldsymbol{S}_{\mathrm{A}}(\mathbf{f})$ given a pair of $m$ and $r$ can be obtained as

$$f_{\ln \boldsymbol{S}_{\mathrm{A}}(\mathbf{f})}(\ln \mathbf{s} \mid m, r) = \frac{1}{\sqrt{(2\pi)^n |\boldsymbol{\Sigma}|}} \exp\left[-\frac{1}{2}(\ln \mathbf{s} - \boldsymbol{\mu})^{\mathrm{T}} \boldsymbol{\Sigma}^{-1} (\ln \mathbf{s} - \boldsymbol{\mu})\right], \quad (2.2.3)$$

where $\boldsymbol{\mu}$ and $\boldsymbol{\Sigma}$ are mean and covariance matrices of $\ln \boldsymbol{S}_{\mathrm{A}}(\mathbf{f})$, i.e.,

$$\boldsymbol{\mu} = \left[\mu_i\right], \quad \boldsymbol{\Sigma} = \left[\rho_{i,j}\sigma_i\sigma_j\right], \quad \rho_{i,i} = 1, \quad i, j = 1, 2, \quad (2.2.4)$$

where $\mu_i$ and $\sigma_i$ are mean and standard deviation of logarithmic spectral acceleration at frequency $f_i$, given a pair of $m$ and $r$. $\rho_{i,j}$ is the correlation coefficient between logarithmic spectral accelerations at two frequencies $f_i$ and $f_j$, which is usually assumed to be independent of $m$ and $r$. $\boldsymbol{\Sigma}$ is a symmetric matrix.

Based on equations (2.2.2) and (2.2.3), the PDF of $\boldsymbol{S}_{\mathrm{A}}(\mathbf{f})$ given a pair of $m$ and $r$ is then calculated by differentiating the joint CDF with respect to $\mathbf{s}$, i.e.,

$$f_{\boldsymbol{S}_{\mathrm{A}}(\mathbf{f})}(\mathbf{s} \mid m, r) = \frac{1}{s_1 \cdot s_2} f_{\ln \boldsymbol{S}_{\mathrm{A}}(\mathbf{f})}(\ln \mathbf{s} \mid m, r). \quad (2.2.5)$$

Therefore, based on equations (2.2.1) and (2.2.5), the annual rate density of $\boldsymbol{S}_{\mathrm{A}}(\mathbf{f})$ can be determined by

$$f'_{\boldsymbol{S}_{\mathrm{A}}(\mathbf{f})}(\mathbf{s}) = \sum_{i=1}^{N_S} \nu_i \left\{ \int_r \int_m f_{\boldsymbol{S}_{\mathrm{A}}(\mathbf{f})}(\mathbf{s} \mid m, r) f_M(m) f_R(r) \mathrm{d}m \, \mathrm{d}r \right\}_i, \quad (2.2.6)$$

$f_{\boldsymbol{S}_{\mathrm{A}}(\mathbf{f})}(\mathbf{s} \mid m, r)$ in equation (2.2.6) can be rewritten in conditional form as

$$f_{\boldsymbol{S}_{\mathrm{A}}(\mathbf{f})}(\mathbf{s} \mid m, r) = f_{\mathcal{S}_{\mathrm{A}}(f_2) \mid \mathcal{S}_{\mathrm{A}}(f_1)}(s_2 \mid s_1, m, r) \cdot f_{\mathcal{S}_{\mathrm{A}}(f_1)}(s_1 \mid m, r), \quad (2.2.7)$$

thus the PDF of $\{\mathcal{S}_{\mathrm{A}}(f_2) \mid \mathcal{S}_{\mathrm{A}}(f_1)\}$ given a pair of $m$ and $r$ is determined by

$$f_{\mathcal{S}_{\mathrm{A}}(f_2) \mid \mathcal{S}_{\mathrm{A}}(f_1)}(s_2 \mid s_1, m, r) = \frac{f_{\boldsymbol{S}_{\mathrm{A}}(\mathbf{f})}(\mathbf{s} \mid m, r)}{f_{\mathcal{S}_{\mathrm{A}}(f_1)}(s_1 \mid m, r)}, \quad (2.2.8)$$

where $f_{\mathcal{S}_A(f_1)}(s_1 \mid m, r)$ is PDF of $\mathcal{S}_A(f_1)$, which can be determined by equation (2.1.4).

Substituting $f_{\mathbf{S}_A(\mathbf{f})}(\mathbf{s} \mid m, r)$ and $f_{\mathcal{S}_A(f_1)}(s_1 \mid m, r)$ into equation (2.2.8) gives

$$f_{\mathcal{S}_A(f_2)|\mathcal{S}_A(f_1)}(s_2 \mid s_1, m, r) = \frac{1}{s_2 \sigma_{\ln \mathcal{S}_A(f_2)|s_1,m,r}} \phi\left[\frac{\ln s_1 - \mu_{\ln \mathcal{S}_A(f_2)|s_1,m,r}}{\sigma_{\ln \mathcal{S}_A(f_2)|s_1,m,r}}\right], \quad (2.2.9)$$

in which

$$\mu_{\ln \mathcal{S}_A(f_2)|s_1,m,r} = \mu_{\ln \mathcal{S}_A(f_2)|m,r} + \rho_{1,2} \frac{\sigma_{\ln \mathcal{S}_A(f_2)|m,r}}{\sigma_{\ln \mathcal{S}_A(f_1)|m,r}} \left[\ln s_1 - \mu_{\ln \mathcal{S}_A(f_1)|m,r}\right], \quad (2.2.10a)$$

$$\sigma_{\ln \mathcal{S}_A(f_2)|s_1,m,r} = \sigma_{\ln \mathcal{S}_A(f_2)|m,r} \sqrt{1 - \rho_{1,2}^2}. \quad (2.2.10b)$$

Equation (2.2.10a) can be simplified as

$$\mu_{\ln \mathcal{S}_A(f_2)|s_1,m,r} = \mu_{\ln \mathcal{S}_A(f_2)|m,r} + \sigma_{\ln \mathcal{S}_A(f_2)|m,r} \rho_{1,2} \varepsilon_{\ln \mathcal{S}_A(f_1)|m,r}(\ln s_1), \quad (2.2.11)$$

in which

$$\varepsilon_{\ln \mathcal{S}_A(f_1)|m,r}(\ln s_1) = \frac{\ln s_1 - \mu_{\ln \mathcal{S}_A(f_1)|m,r}}{\sigma_{\ln \mathcal{S}_A(f_1)|m,r}}. \quad (2.2.12)$$

$\varepsilon_{\ln \mathcal{S}_A(f_1)|m,r}$ is called spectral shape parameter representing the aleatory randomness in estimating $\ln \mathcal{S}_A(f_1)$ given an earthquake with a pair of $m$ and $r$. It yields standard normal distribution.

Based on equation (2.2.11), $\varepsilon_{\ln \mathcal{S}_A(f_2)|s_1,m,r}(\ln s_2)$ is given by

$$\varepsilon_{\ln \mathcal{S}_A(f_2)|s_1,m,r}(\ln s_2) = \rho_{1,2} \varepsilon_{\ln \mathcal{S}_A(f_1)|m,r}(\ln s_1). \quad (2.2.13)$$

Replacing $f_{\mathbf{S}_A(\mathbf{f})}(\mathbf{s} \mid m, r)$ by $f_{\mathcal{S}_A(f_2)|\mathcal{S}_A(f_1)}(s_2 \mid s_1, m, r)$ in the integrand of equation (2.2.6) gives the PDF of $\{\mathcal{S}_A(f_2) \mid \mathcal{S}_A(f_1)\}$

$$f_{\mathcal{S}_A(f_2)|\mathcal{S}_A(f_1)}(s_2 \mid s_1) = \int_r \int_m f_{\mathcal{S}_A(f_2)|\mathcal{S}_A(f_1)}(s_2 \mid s_1, m, r) f_M(m) f_R(r) \mathrm{d}m \, \mathrm{d}r. \quad (2.2.14)$$

Therefore, the annual rate density of $\{\mathcal{S}_A(f_2) \mid \mathcal{S}_A(f_1)\}$ is determined by

$$f'_{\mathcal{S}_A(f_2)|\mathcal{S}_A(f_1)}(s_2 \mid s_1) = \sum_{i=1}^{N_S} \nu_i \left\{f_{\mathcal{S}_A(f_2)|\mathcal{S}_A(f_1)}(s_2 \mid s_1)\right\}. \quad (2.2.15)$$

Given $\mathcal{S}_{\mathrm{A}}(f_1)=s_1$, the annual rate of events at the site of interest with $\mathcal{S}_{\mathrm{A}}(f_2)$ between $y_1$ and $y_2$ is determined by

$$\lambda(y_1 \leqslant s_2 \leqslant y_2 \,|\, s_1) = \int_{y_1}^{y_2} f'_{\mathcal{S}_{\mathrm{A}}(f_2)|\mathcal{S}_{\mathrm{A}}(f_1)}(s_2 \,|\, s_1)\,\mathrm{d}s_2 = \sum_{i=1}^{N_S} \nu_i \left\{ \int_{y_1}^{y_2} f_{\mathcal{S}_{\mathrm{A}}(f_2)|\mathcal{S}_{\mathrm{A}}(f_1)}(s_2 \,|\, s_1)\,\mathrm{d}s_2 \right\}. \tag{2.2.16}$$

In practice, given a pair of $m$ and $r$, $\mu$ and $\sigma$ are obtained from ground-motion models; correlation coefficient $\rho$ is determined based on statistical analyses (Baker and Jayaram, 2008). The mean and covariance matrices are then determined. The annual rate density of $\left\{\mathcal{S}_{\mathrm{A}}(f_2) \,|\, \mathcal{S}_{\mathrm{A}}(f_1)\right\}$ can be easily obtained from equation (2.2.15), which will be used for calculating the weights of ground response spectra in Chapter 4.

### Discussion on Correlation Coefficient

Equations (2.2.11) and (2.2.10b) show that, given an earthquake with a pair of $m$ and $r$, mean and standard deviation of $\ln\mathcal{S}_{\mathrm{A}}(f_2)$ for a given $s_1$ depend on the value of $\rho_{1,2}$:

1. $\rho_{1,2}=0$

   Substituting $\rho_{1,2}=0$ into equations (2.2.11) and (2.2.10b) gives

   $$\mu_{\ln\mathcal{S}_{\mathrm{A}}(f_2)|s_1,m,r} = \mu_{\ln\mathcal{S}_{\mathrm{A}}(2)|m,r}, \quad \sigma_{\ln\mathcal{S}_{\mathrm{A}}(f_2)|s_1,m,r} = \sigma_{\ln\mathcal{S}_{\mathrm{A}}(f_2)|m,r}, \tag{2.2.17}$$

   which indicates that $s_1$ of $\ln\mathcal{S}_{\mathrm{A}}(f_1)$ has no effect on $\ln\mathcal{S}_{\mathrm{A}}(f_2)$.

2. $\rho_{1,2}=1.0$

   $\sigma_{\ln\mathcal{S}_{\mathrm{A}}(f_2)|s_1,m,r}$ in equation (2.2.10b) reduces to zero, indicating that a unique spectral value $s_2$ of $\ln\mathcal{S}_{\mathrm{A}}(f_2)$ is obtained. Based on equation (2.2.13), $\varepsilon_{\ln\mathcal{S}_{\mathrm{A}}(f_2)|s_1,m,r}(\ln s_2)$ is given by

   $$\varepsilon_{\ln\mathcal{S}_{\mathrm{A}}(f_2)|s_1,m,r}(\ln s_2) = \varepsilon_{\ln\mathcal{S}_{\mathrm{A}}(f_1)|m,r}(\ln s_1). \tag{2.2.18}$$

   Recall that in equation (2.1.2), $\mathcal{P}\left\{\mathcal{S}_{\mathrm{A}}(f_1) > s_1 \,|\, m, r\right\}$ is given by

   $$\mathcal{P}\left\{\mathcal{S}_{\mathrm{A}}(f_1) > s_1 \,|\, m, r\right\} = 1 - \Phi\left[\frac{\ln s_1 - \mu_{\ln\mathcal{S}_{\mathrm{A}}(f_1)|m,r}}{\sigma_{\ln\mathcal{S}_{\mathrm{A}}(f_1)|m,r}}\right] = 1 - \Phi\left\{\varepsilon_{\ln\mathcal{S}_{\mathrm{A}}(f_1)|m,r}(\ln s_1)\right\}, \tag{2.2.19}$$

thus

$$\begin{aligned}\mathcal{P}\left\{\mathcal{S}_{\mathrm{A}}(f_2) > s_2 \,\middle|\, s_1, m, r\right\} &= 1 - \Phi\left\{\varepsilon_{\ln\mathcal{S}_{\mathrm{A}}(f_2)|s_1,m,r}(\ln f_2)\right\} \\ &= 1 - \Phi\left\{\varepsilon_{\ln\mathcal{S}_{\mathrm{A}}(f_1)|m,r}(\ln s_1)\right\} = \mathcal{P}\left\{\mathcal{S}_{\mathrm{A}}(f_1) > s_1 \,\middle|\, m, r\right\}.\end{aligned} \tag{2.2.20}$$

Since PDFs of $m$ and $r$ in equation (2.2.1) are the same in scalar PSHA for SDOF oscillators with natural frequencies at $f_1$ and $f_2$, seismic hazard that $s_2$ of $\mathcal{S}_{\mathrm{A}}(f_2)$ is expected to be exceeded for a given $s_1$ is equal to seismic hazard that $s_1$ of $\mathcal{S}_{\mathrm{A}}(f_1)$ is expected to be exceeded.

Recall that for a given uniform hazard spectrum (UHS), spectral accelerations at any frequencies are corresponding to the same seismic hazard. This indicates that, in the generation of UHS, correlation coefficient between any two vibration frequencies is taken as 1.0, i.e., logarithmic spectral accelerations at any two vibration frequencies are assumed to be fully correlated.

3. $0 < \rho_{1,2} < 1.0$

   Based on equation (2.2.13), $\varepsilon_{\ln\mathcal{S}_{\mathrm{A}}(f_2)|s_1,m,r}(\ln s_2)$ is given by

$$\varepsilon_{\ln\mathcal{S}_{\mathrm{A}}(f_2)|s_1,m,r}(\ln s_2) = \rho_{1,2}\,\varepsilon_{\ln\mathcal{S}_{\mathrm{A}}(f_1)|m,r}(\ln s_1) < \varepsilon_{\ln\mathcal{S}_{\mathrm{A}}(f_1)|m,r}(\ln s_1). \tag{2.2.21}$$

   Recall that in the generation of UHS,

$$\varepsilon_{\ln\mathcal{S}_{\mathrm{A}}(f_2)|m,r}(\ln s_2) = \varepsilon_{\ln\mathcal{S}_{\mathrm{A}}(f_1)|m,r}(\ln s_1), \tag{2.2.22}$$

   thus $\mu_{\ln\mathcal{S}_{\mathrm{A}}(f_2)|s_1,m,r}$ in equation (2.2.11) is smaller than $s_2$ obtained from the UHS with respect to seismic hazard that $s_1$ of $\mathcal{S}_{\mathrm{A}}(f_1)$ is expected to be exceeded.

   In addition, standard deviation of $\ln\mathcal{S}_{\mathrm{A}}(f_2)$ is given by

$$\sigma_{\ln\mathcal{S}_{\mathrm{A}}(f_2)|s_1,m,r} = \sigma_{\ln\mathcal{S}_{\mathrm{A}}(f_2)|m,r}\sqrt{1-\rho_{1,2}^2} < \sigma_{\ln\mathcal{S}_{\mathrm{A}}(f_2)|m,r}, \tag{2.2.23}$$

   which indicates that aleatory randomness in estimating $\ln\mathcal{S}_{\mathrm{A}}(f_2)$ is reduced.

### Discussion on Vector-valued GMPs

When $f_1$ is pretty high, e.g., $f_1 = 50$ Hz, $\mathcal{S}_A(f_1)$ can be approximated by PGA (see Section 1.1 of Chapter 1). In current seismic fragility analysis, a generic ground response spectrum (GRS) or uniform hazard spectrum (UHS) is defined as Review Level Earthquake (RLE). The RLE is usually anchored to PGA at a specified screening level $A_{\mathrm{RLE}}$ (e.g. $A_{\mathrm{RLE}} = 0.3g$), indicating that a single spectral shape and ground motion level are considered in the calculation of seismic demand. As a result, the aleatory randomness in earthquake response spectra and ground motion intensity effect cannot be taken into consideration.

In nuclear power industry, dominant frequencies of most safety-related structures, systems, and components (SSCs) are greater than 2 Hz. Based on spectral correlation model developed by Baker and Jayaram(2008), correlation coefficient between logarithmic spectral accelerations at any two frequencies ($>2$ Hz) is between 0.474 and 1.0. To more accurately characterize $\ln\mathcal{S}_A(f_2)$ for a given $s_1$ of $\mathcal{S}_A(f_1 = 50\,\mathrm{Hz})$, correlation coefficient between $\ln\mathcal{S}_A(f_2)$ and $\ln\mathcal{S}_A(f_1)$ should be considered. Taking $f_2$ as the dominant frequency of an SSC, VPSHA can properly capture the aleatory randomness in $\mathcal{S}_A(f_2)$. In addition, by changing spectral values of PGA from lower bound (e.g. $0.05g$) to upper bound (e.g. $5g$), ground motion intensity effect is considered.

## 2.3 Numerical Example for Darlington NGS Site

Darlington nuclear generating station (NGS) (43.53° N, 78.43° W) is located on the north shore of Lake Ontario, Region of Durham in Ontario, Canada. The map information around Darlington NGS site is shown in Figure 2.1.

### 2.3.1 Logic Tree of PSHA Model

Scalar PSHA is performed to determine seismic hazard curves at this site. The PSHA model given in Open File 7576 of 2015 National Building Code of Canada (NBCC) (Halchuk *et al.*, 2014) is used. Four epistemic uncertainties, i.e., seismic source model, maximum earthquake magnitude, magnitude-recurrence model, and ground motion model, are taken into consideration in this PSHA model. To capture these epistemic uncertainties, three-

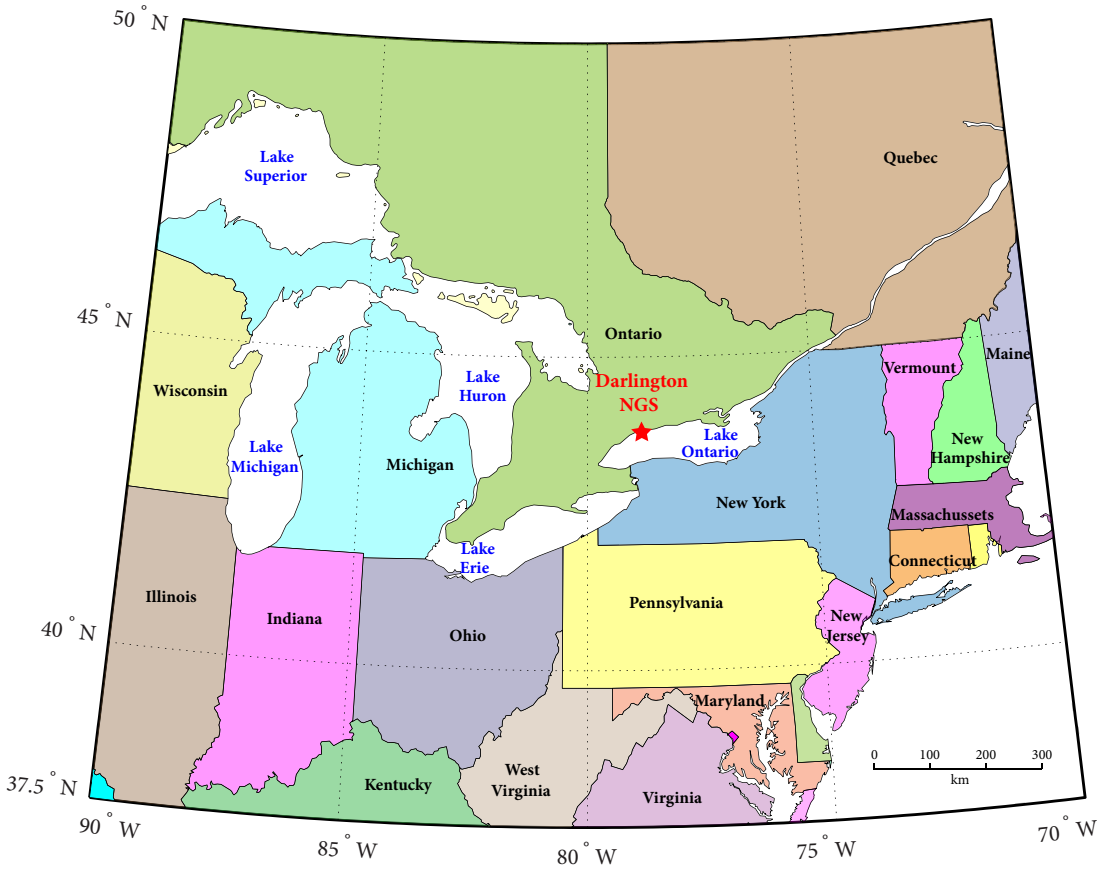


**Figure 2.1** Map information around Darlington NGS site

branch logic tree in Figure 2.2 is developed. Probability of confidence weight for each of the median, high, and low estimates is assigned and shown in Figure 2.2 (Halchuk *et al.*, 2014). Here "median", "high", and "low" are not related to percentiles in statistics.

As shown in Figure 2.2, H2 (H is for historical), HY (HY is for hybrid), and R2 (R is for regional) seismic source models, are used to capture seismic source model uncertainty. For maximum magnitude and magnitude-recurrence model uncertainties, three branches are used to represent median, high, and low estimates of model parameters. For ground motion model, three sets of ground-motion look-up tables are used to predict median, high, and low estimates of median ground motion estimates. For each model, there are three branches, indicating that a total number of $3^4 = 81$ epistemic branches are considered in this PSHA model. Each epistemic branch is related to one possible combination of four epistemic uncertainties. The weight of a epistemic branch is equal to the product of

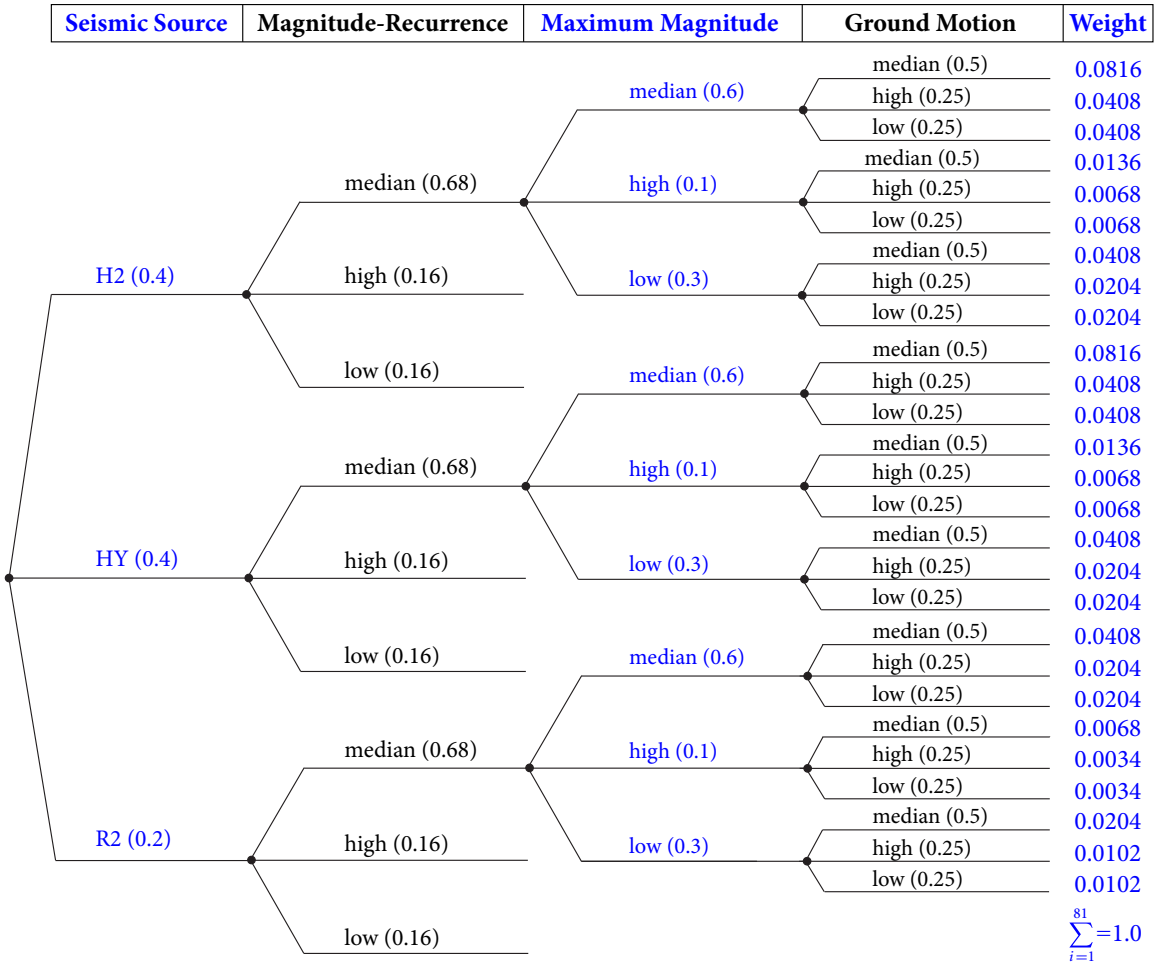


**Figure 2.2** Logic tree of PSHA model for Darlington NGS site

weights of four uncertainties in this branch. For example, as shown in Figure 2.2, weight $0.0816 = 0.4 \times 0.6 \times 0.68 \times 0.5$ is respect to the first epistemic branch. The weights of 27 epistemic branches are shown in Figure 2.2. The summation of weights from 81 epistemic branches should be equal to 1.

## 2.3.2 Seismic Source Model

For sites in southeastern Canada, due to the scarcity of strong historical earthquake records, three seismic source models, i.e., H2, HY, and R2 models are used to take account of seismic source uncertainty. H2 model is mainly based on relatively small historical seismicity

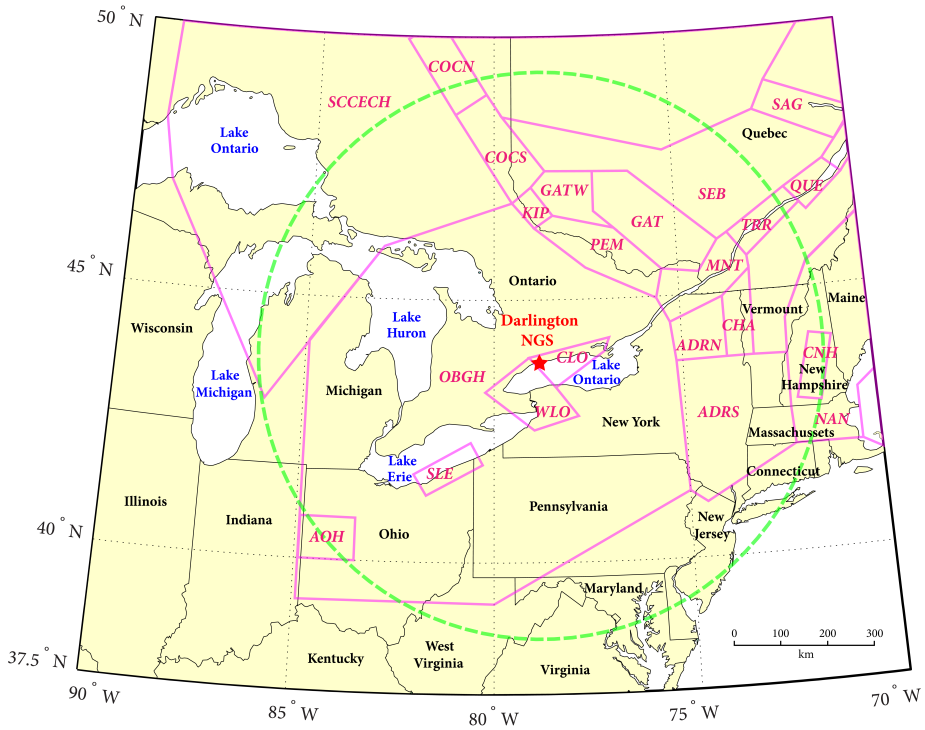


**Figure 2.3** Southeastern Canada H2 seismic source model

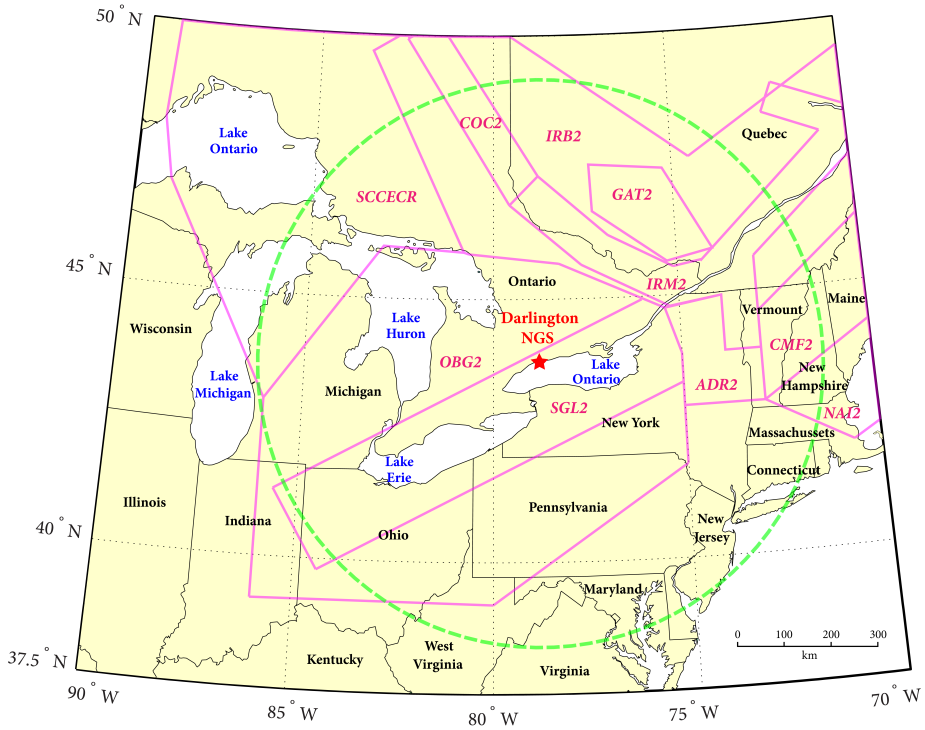


**Figure 2.4** Southeastern Canada R2 seismic source model

clusters in southeastern Canada. R2 model is based on relatively larger regional seismicity zones. HY model is the combination of historical and regional seismicity records, which is a compromise between H2 and R2 models. Figures 2.3 and 2.4 are H2 and R2 source models, respectively. Since several seismic sources are overlapped, HY source model is not graphically illustrated here. All seismic sources around Darlington NGS site are treated as area sources. Based on the geographic coordinates of corner grids of each seismic source, the total area of the seismic source can be calculated based on geodetic coordinate system. In addition, a source depth of 10 km is taken for all seismic sources in the calculation of source-to-site distances, and no uncertainty in the source depth is considered.

### 2.3.3 Magnitude-Recurrence Model

The magnitude-frequency distribution at a site is usually expresses as an exponential form (Richter, 1958)

$$\log_{10}^{N(m)} = a - b\,m, \tag{2.3.1}$$

or

$$N(m) = N_0 \mathrm{e}^{-\beta}, \tag{2.3.2}$$

where $N_0 = 10^a$ is the number of earthquakes per year with magnitude greater than or equal to 0. $\beta = b\ln(10)$ is a constant that depicting the relative number of small-to-large earthquakes.

Due to the uncertainty in magnitude-recurrence model, median, high, and low estimates of $N_0$ and $\beta$ are used. Taking OBGH seismic source of H2 model (see Figure 2.3) as an example, Table 2.1 gives median, high, and low estimates of $N_0$ and $\beta$ (Halchuk *et al.*, 2014).

**Table 2.1** OBGH Seismic Source Magnitude-Recurrence Parameters (H2 Model)

| Seismic source | Magnitude-recurrence parameters | |
|---|---|---|
| **OBGH** | $\beta$ | $N_0$ |
| Median | 2.10 | 155.78 |
| Low | 2.619 | 496.82 |
| High | 1.581 | 49.94 |

### 2.3.4 Maximum Magnitude Model

In engineering applications, it is common to truncate earthquake magnitude at a lower bound $m_{\min}$ and a upper bound $m_{\max}$. The truncated Gutenberg-Richter magnitude-frequency distribution is given by (McGuire, 2004)

$$N(m) = \nu \cdot \bar{F}_M(m) = \nu \frac{\mathrm{e}^{-\beta(m-m_{\min})} - \mathrm{e}^{-\beta(m_{\max}-m_{\min})}}{1-\mathrm{e}^{-\beta(m_{\max}-m_{\min})}}, \quad m_{\min} \leqslant m \leqslant m_{\max}, \tag{2.3.3}$$

where $\nu$ is annual rate of occurrence of earthquake above $m_{\min}$ given by (Atkinson and Goda, 2011)

$$\nu = N_0 \frac{\mathrm{e}^{-\beta m_{\min}} - \mathrm{e}^{-\beta m_{\max}}}{1-\mathrm{e}^{-\beta m_{\max}}}. \tag{2.3.4}$$

$\bar{F}_M(m)$ in equation (2.3.3) is the complementary CDF of magnitude $m$, thus the CDF of magnitude $m$ is easily obtained as

$$F_M(m) = 1 - \bar{F}_M(m) = \frac{1 - \mathrm{e}^{-\beta(m-m_{\min})}}{1-\mathrm{e}^{-\beta(m_{\max}-m_{\min})}}, \quad m_{\min} \leqslant m \leqslant m_{\max}. \tag{2.3.5}$$

The PDF of magnitude $m$ is then calculated by differentiating $F_M(m)$ with respect to $m$,

$$f_M(m) = \frac{\beta \cdot \mathrm{e}^{-\beta(m-m_{\min})}}{1-\mathrm{e}^{-\beta(m_{\max}-m_{\min})}}, \quad m_{\min} \leqslant m \leqslant m_{\max}. \tag{2.3.6}$$

For all seismic sources in southeastern Canada zone, $m_{\min}$ is taken as 4.75. However, there is uncertainty in estimating $m_{\max}$. To capture this uncertainty, median, high, and low estimates of $m_{\max}$ are taken for each seismic source. For example, given OBGH seismic source of H2 model (see Figure 2.3), Table 2.2 shows median, high, and low estimates of $m_{\max}$. $\nu$ regarding median, high, and low estimates of $m_{\max}$ can be determined by equation (2.3.4).

Given a set of magnitude-recurrence parameters in Table 2.1, by taking median, high, and low estimates of $m_{\max}$ in Table 2.2, three estimates of PDFs of magnitude $m$ are obtained. The product of $\nu$ (see Table 2.2) and respective $f_M(m)$ is calculated as

$$f'_M(m) = \nu \cdot f_M(m), \quad m_{\min} \leqslant m \leqslant m_{\max}. \tag{2.3.7}$$

Taking median estimate of magnitude-recurrence parameters in Table 2.1 as an example, three $f'_M(m)$ estimates are determined and shown in Figure 2.5 accounting for maximum

magnitude uncertainty. Here $f'_M(m)$ instead of $f_M(m)$ are compared because in the PSHA, $f'_M(m)$ is used in the calculation of seismic hazard.

**Table 2.2** Maximum Magnitudes and Annual Rate of Occurrence of OBGH Seismic Source (H2 Model)

| Seismic source **OBGH** | Maximum Magnitude ($m_{\max}$) | Annual Rate of Occurrence ($\nu$) |
|---|---|---|
| Median | 7.3 | 0.007 |
| Low | 7.0 | 0.002 |
| High | 7.6 | 0.027 |

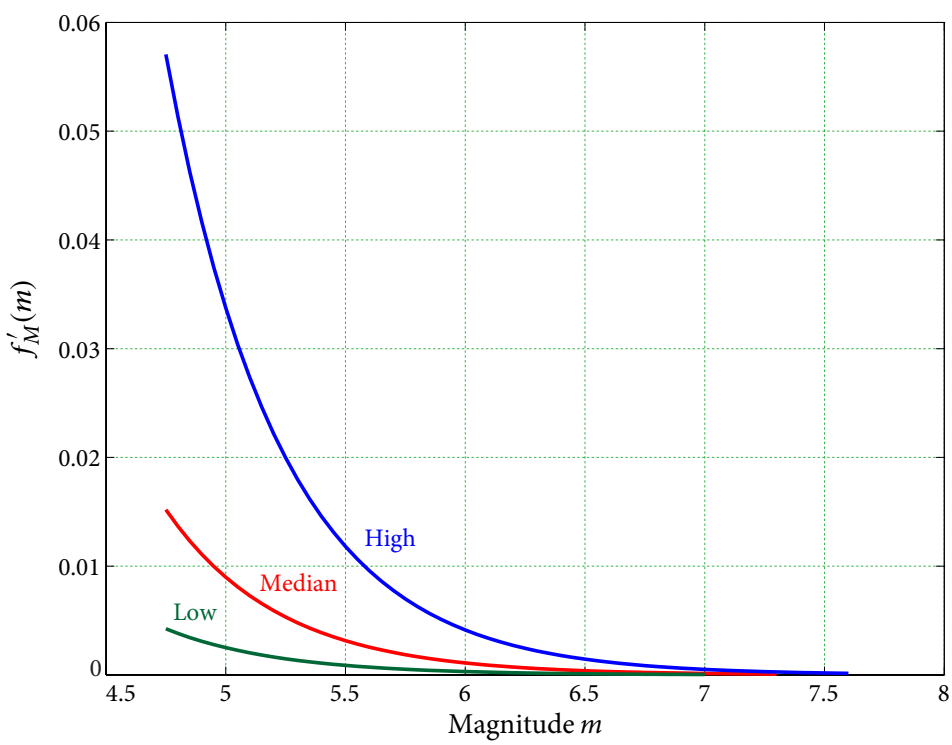


**Figure 2.5** Median, High, and Low Estimates of $f'_M(m)$ for OBGH seismic source (H2 model)

### 2.3.5 Ground-Motion Model

It is known that ground shaking induced by an earthquake attenuates with the increase of source-to-site distance. To predict the ground shaking at the sites in central and eastern North America (CENA), several empirical ground-motion prediction equations (GMPEs) are proposed (Atkinson and Boore, 1995; Silva *et al.*, 2002; Atkinson and Boore, 2006; Boore and Atkinson, 2008; Pezeshk *et al.*, 2011).

In the CENA, a typical expression of GMPEs for logarithmic spectral acceleration $\ln \mathcal{S}_A(f_1)$ at any frequency $f_1$ is given by

$$\ln \mathcal{S}_A(f_1) = f(m, r, f_1) + \sigma(f_1) \cdot \varepsilon, \tag{2.3.8}$$

where $f(m, r, f_1)$ is the mean estimate of $\ln \mathcal{S}_A(f_1)$, which depends on the values of earthquake magnitude $m$, source-to-site distance $r$, and natural frequency $f_1$ of a SDOF oscillator. $\sigma(f_1)$ is the standard deviation of $\ln \mathcal{S}_A(f_1)$, which is assumed to be independent on $m$ and $r$. $\varepsilon$ is a random variable complying with standard normal distribution. Therefore, $\mathcal{S}_A(f_1)$ is lognormally distributed given a pair of $m$ and $r$.

In 2015 NBCC, ground-motion look-up tables are used to predict high, and low estimates of mean logarithmic spectral accelerations (10-base) as functions of $m$ and $r$. In these tables, earthquake magnitudes are uniformly discretized by 0.25 in normal scale between 4.75 and 8.0. Epicenter distance is uniformly discretized in logarithmic scale (10-base) into 30 points between $r_{\text{epi}} = 1.0$ km and $r_{\text{epi}} = 10^{2.9} = 794.3$ km. Given source depth $d = 10$ km, the hypocenter distance $r_{\text{hyp}} = \sqrt{r_{\text{epi}}^2 + d^2}$ can be determined. It is noted that hypocenter distance is taken as source-to-site distance. Ten representative frequencies, i.e., 0.1, 0.2, 0.5, 1, 2, 3.33, 5, 10, 20, and 50 Hz, are considered in these tables.

In order to capture ground-motion model uncertainty, three sets of look-up tables, representing median, high, and low estimates of mean logarithmic spectral values, are presented. Given a natural frequency $f_1$ and a pair of $m$ and $r$, mean estimates of logarithmic spectral acceleration $\ln \mathcal{S}_A(f_1)$ (10-base) can be determined by the interpolating three look-up tables. In 2015 NBCC, spectral acceleration at 50 Hz is taken as peak ground acceleration (PGA). Here one can take $m = 6.5$ as an example, Figure 2.7 shows median, high, and low estimates of median PGA versus epicenter distance $r_{\text{epi}}$.

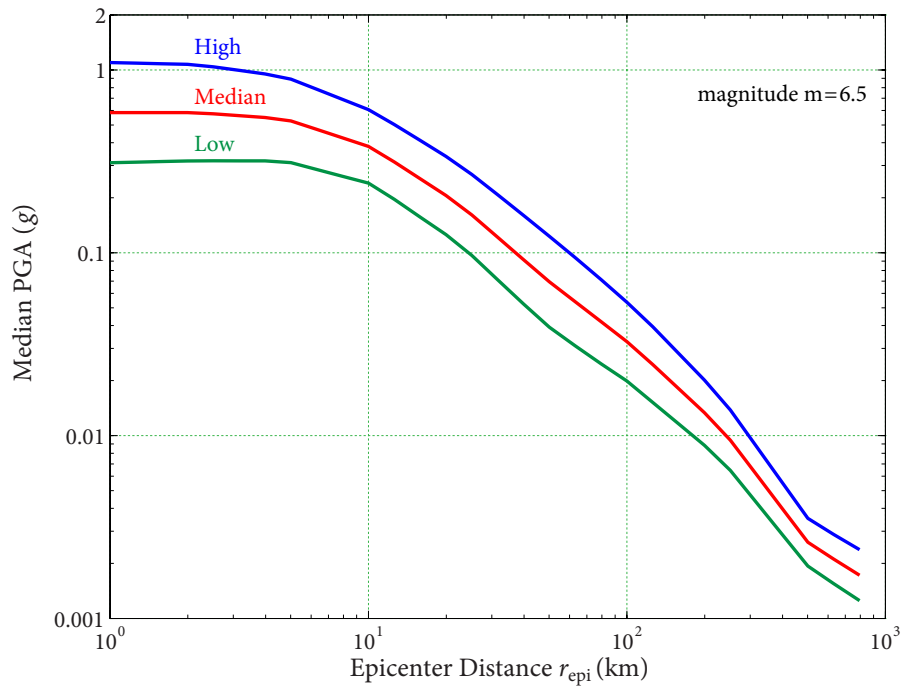


**Figure 2.6** Median, High, and Low Estimates of Median PGA (i.e. $\mathcal{S}_A(f=50\,\text{Hz})$) versus epicenter distance $r_{epi}$

Standard deviations with respect to ten frequencies are also given in look-up tables. Having obtained mean estimates of logarithmic spectral acceleration $f(m, r, f_1)$ and corresponding standard deviation $\sigma(f_1)$, conditional probability that $\mathcal{S}_A(f_1)$ exceeds a threshold value $s_1$, given a pair of $m$ and $r$, can be determined by

$$\mathcal{P}\left\{\mathcal{S}_A(f_1) > s_1 \,\middle|\, m, r\right\} = 1 - \mathcal{P}\left\{\ln\mathcal{S}_A(f_1) \leqslant \ln s_1 \,\middle|\, m, r\right\} = 1 - \Phi\left[\frac{\ln s_1 - f(m, r, f_1)}{\sigma(f_1)}\right]. \tag{2.3.9}$$

## 2.3.6 Development of Seismic Hazard Curves

In this study, seismic sources within a radius of 600 km (dash green line in Figures 2.3 and 2.4) surrounding Darlington NGS site are considered in the PSHA. All seismic sources are gridded by 0.1 degree in longitudinal and attitudinal directions. As a result, the base and height of each gridded source zone are around 10 km. Figure 2.7 gives a simplified diagram of gridded source zones from an areal seismic source.

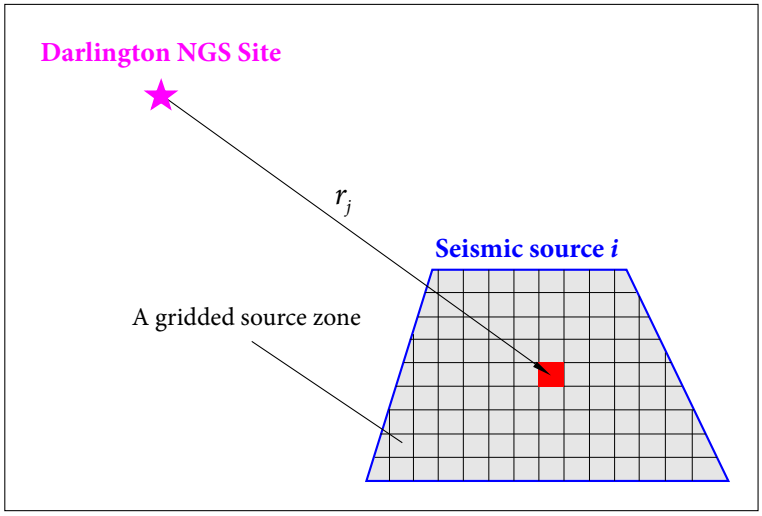


**Figure 2.7** A simplified diagram of gridding an areal source surrounding Darlington NGS site

For each gridded source zone, point-source model is used in the calculation of seismic hazard. The source-to-site distance $r_j$ is taken as a constant (see Figure 2.7) within this relative small zone (hypocenter distance between the center of source zone and Darlington NGS site is taken as source-to-site distance). The annual rate of occurrence $\nu_{i,j}$ in the gridded source $j$ is given by

$$\nu_{i,j} = \nu_i \frac{A_{i,j}}{A_i}, \tag{2.3.10}$$

in which $A_{i,j}$ is the area of source zone $j$, $A_i$ is the total area of seismic source $i$, and $\nu_i$ is annual rate of occurrence in seismic source $i$.

In 2015 NBCC, earthquake magnitude $m$ is uniformly increased by 0.25. The seismic hazard (annual frequency that a specified spectral value $s_1$ is expected to be exceeded) contributed from the grided source zone $j$ is then given by

$$\lambda_i(s_1, r_j) = \nu_{i,j} \sum_{k=1}^{N_k} \mathcal{P}\left\{ \mathcal{S}_{\mathrm{A}}(f_1) > s_1 \,\middle|\, m_k, r_j \right\} f_M(m_k) \Delta m_k, \tag{2.3.11}$$

where $N_k$ is the number of magnitude intervals. $\mathcal{P}\left\{ \mathcal{S}_{\mathrm{A}}(f_1) > s_1 \,\middle|\, m_k, r_j \right\}$ can be determined by equation (2.3.9), and $f_M(m_k)$ is obtained from equation (2.3.6).

Therefore, seismic hazard at Darlington NGS site contributed from seismic source $i$ can be calculated as

$$\lambda_i(s_1) = \sum_{j=1}^{N_j} \lambda_i(s_1, r_j) = \sum_{j=1}^{N_j} \nu_{i,j} \left\{ \sum_{k=1}^{N_k} \mathcal{P}\left\{ \mathcal{S}_{\mathrm{A}}(f_1) > s_1 \,\middle|\, m_k, r_j \right\} f_M(m_k) \Delta m_k \right\}_j, \tag{2.3.12}$$

where $N_j$ is the number of gridded source zones in seismic source $i$.

Finally, seismic hazard from all surrounding sources is calculated as

$$\lambda(s_1) = \sum_{i=1}^{N_i} \lambda_i(s_1), \tag{2.3.13}$$

in which $N_i$ is the number of areal seismic sources surrounding Darlington site.

Matlab codes are written to calculate the seismic hazard at Darlington NGS site. The algorithms are presented as follows:

1. Develop logic tree of the PSHA model (see Figure 2.2)
2. Determine seismic hazard from one epistemic branch of the logic tree
   (a) Discretize area sources into gridded source zones given a seismic source model (H2, HY, or R2 source model)
   (b) Calculate seismic hazard contributed from these gridded source zones using equation (2.3.10) and (2.3.11)
   (c) Calculate seismic hazard from one seismic source by equation (2.3.12)
   (d) Repeat steps (a) to (c) to calculate seismic hazard from other seismic sources
   (e) Calculate seismic hazard from all seismic sources in this epistemic branch by equation (2.3.13)
   (f) Calculate seismic hazard from all the remaining epistemic branches (a total number of 81 epistemic branches)
3. Determine seismic hazard curves at percentiles or mean seismic hazard curve
   (a) Calculate seismic hazard curves at percentiles
   Given a spectral value of $\mathcal{S}_{\mathrm{A}}(f_1)$ (e.g. $f_1 = 50$ Hz), there are 81 seismic hazard values from epistemic branches. It is required to sort these values in ascending

order and then plot the empirical cumulative distribution function (CDF) versus these values. Taking percentile $P=p$, seismic hazard value at this percentile can be determined by interpolating the empirical CDF.

Changing spectral value of $\mathcal{S}_{\mathrm{A}}(f_1)$ from lower bound (e.g. $0.001g$) to upper bound (e.g. $5g$) can obtain seismic hazard values at percentile $P=p$. Afterwards, one can represent the seismic hazard curve at percentile $P=p$ by the numerical distribution of seismic hazard values versus $\mathcal{S}_{\mathrm{A}}(f_1)$.

(b) Calculate mean seismic hazard for $\mathcal{S}_{\mathrm{A}}(f_1)$ by

$$H_{\mathcal{S}_{\mathrm{A}}(f_1)}(s_1) = \sum_{i=1}^{81} w_i \cdot H_{\mathcal{S}_{\mathrm{A}}(f_1),i}(s_1), \tag{2.3.14}$$

where $w_i$ is the weight of epistemic branch $i$, and $H_{\mathcal{S}_{\mathrm{A}}(f_1),i}(s_1)$ is the seismic hazard given a threshold value $s_1$, from epistemic branch $i$.

Changing spectral value of $\mathcal{S}_{\mathrm{A}}(f_1)$ from lower to upper bounds can result in numerical distribution of mean seismic hazard for $\mathcal{S}_{\mathrm{A}}(f_1)$. Afterwards, one can represent mean seismic hazard curve by this numerical distribution.

Seismic hazard at Darlington NGS site is calculated according to above algorithms. The results are seismic hazard curves versus spectral accelerations at frequency range of engineering interest. Taking PGA, i.e., $\mathcal{S}_{\mathrm{A}}(f_1 = 50\,\mathrm{Hz})$, as an example, Figures 2.8 to 2.10 are seismic hazard curves for three seismic source models (for each source model, 27 epistemic branches are developed). Plotting seismic hazard curves from Figures 2.8 to 2.10 together gives Figure 2.11.

Based on seismic hazard curves from all epistemic branches (see Figure 2.11), one can plot empirical cumulative distribution function (CDF) versus seismic hazard for a given PGA value. Figure 2.12 shows the empirical CDF versus seismic hazard, given $\mathrm{PGA} = 0.1g$. Based on this empirical CDF, one can obtain seismic hazard values with three percentiles, e.g., $16^{\mathrm{th}}$, $50^{\mathrm{th}}$, and $84^{\mathrm{th}}$. In addition, one can obtain mean seismic hazard value using equation (2.3.14). Changing PGA values from lower bound of $0.001g$ to upper bound value of $10g$ can result in seismic hazard curves with three percentiles or mean seismic hazard curve (see Figure 2.13), respectively.

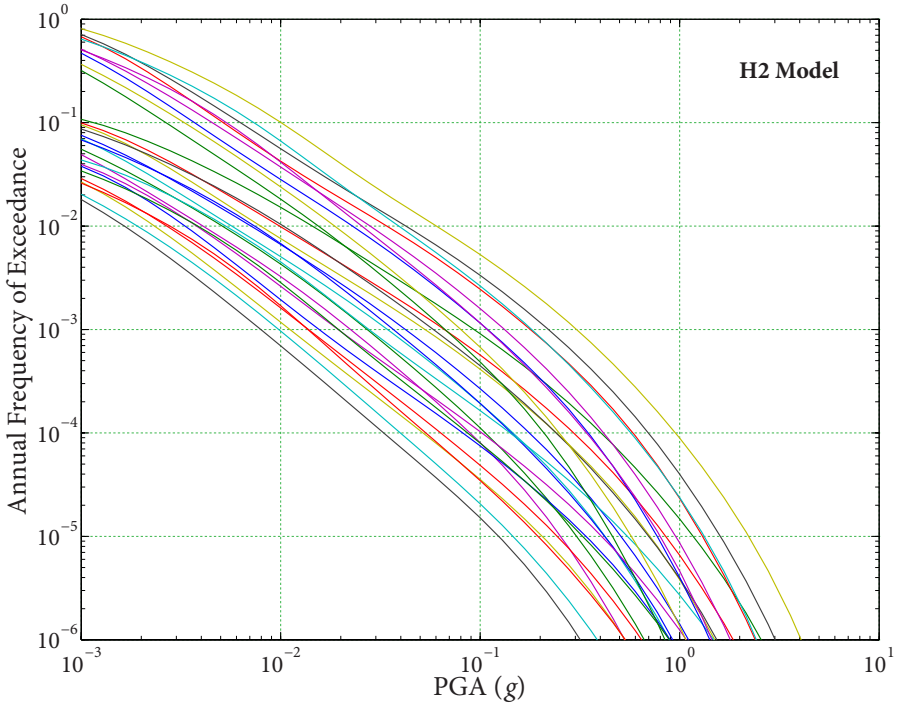


**Figure 2.8** Seismic hazard curves for PGA (i.e. $\mathcal{S}_{\mathrm{A}}(f_1 = 50\,\mathrm{Hz})$) from H2 source model

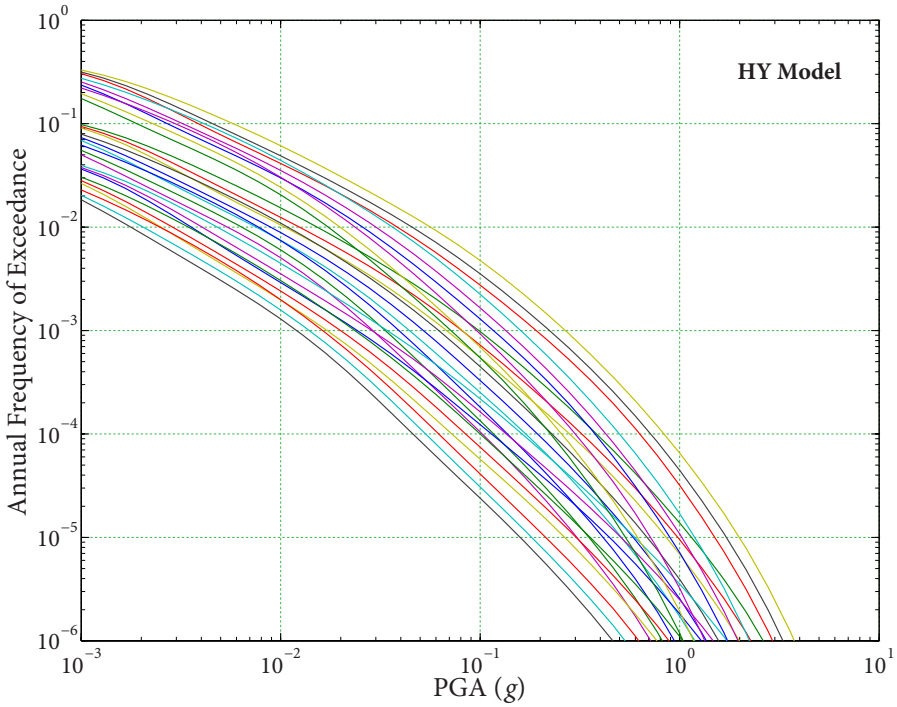


**Figure 2.9** Seismic hazard curves for PGA (i.e. $\mathcal{S}_{\mathrm{A}}(f_1 = 50\,\mathrm{Hz})$) from HY source model

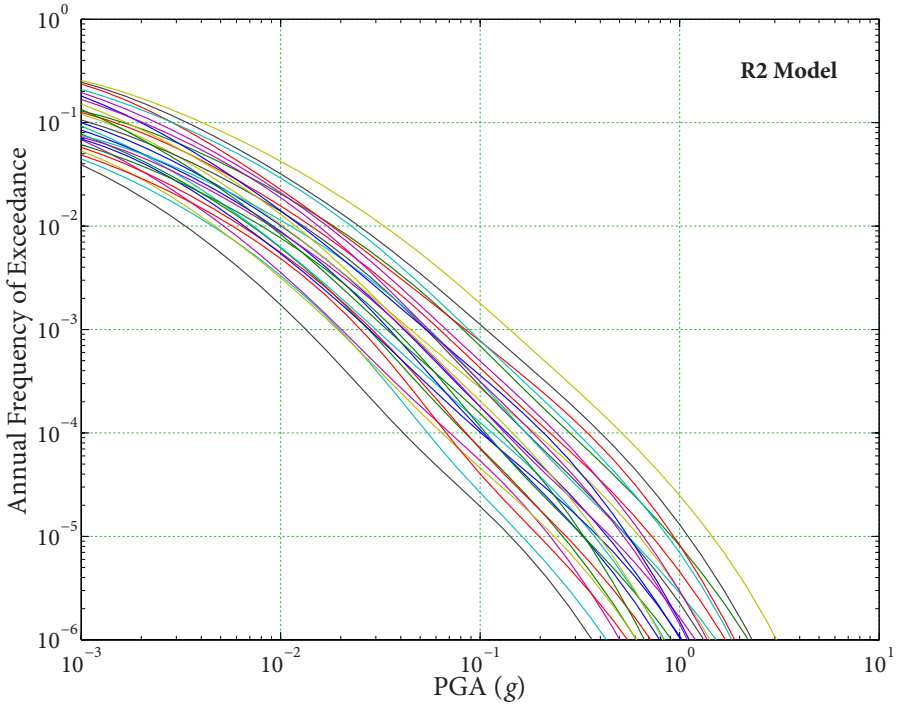


**Figure 2.10** Seismic hazard curves for PGA (i.e. $\mathcal{S}_A(f_1 = 50\,\text{Hz})$) from R2 source model

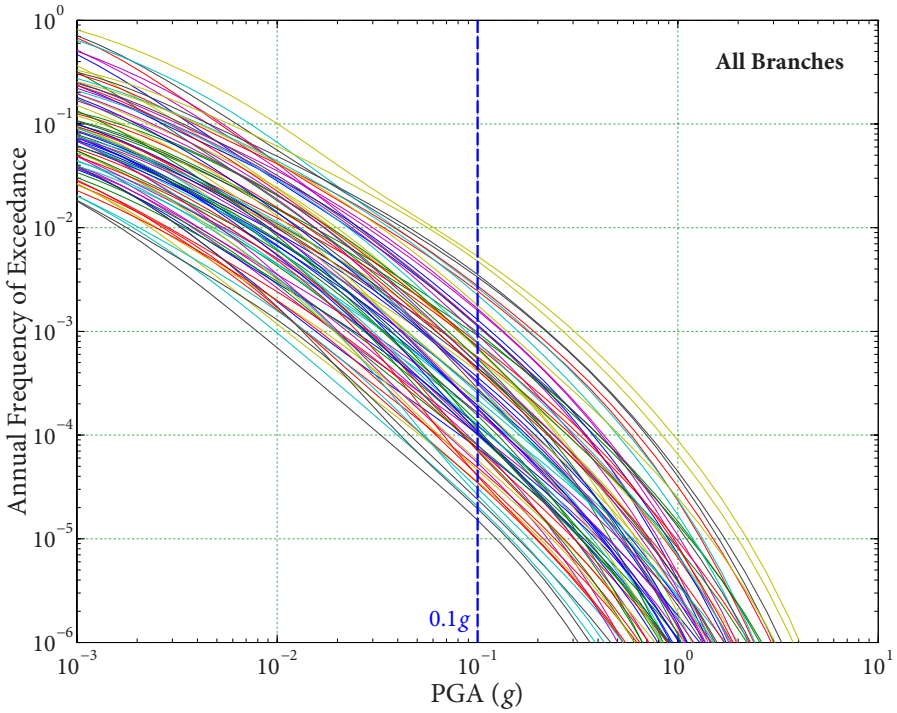


**Figure 2.11** Seismic hazard curves for PGA (i.e. $\mathcal{S}_A(f_1 = 50\,\text{Hz})$) from all epistemic branches

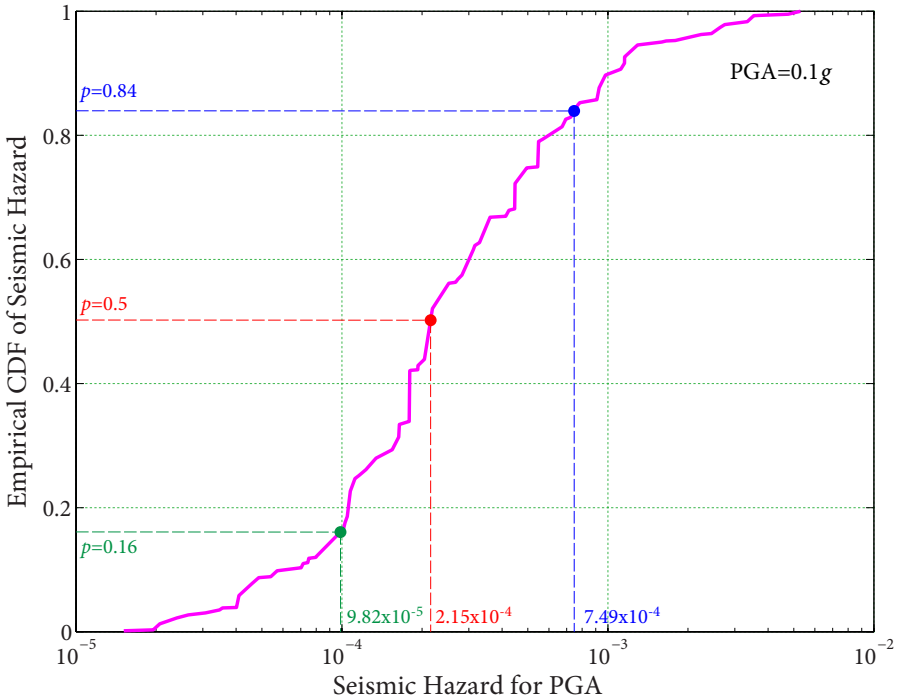


**Figure 2.12** Empirical CDF of seismic hazard given PGA $= 0.1g$

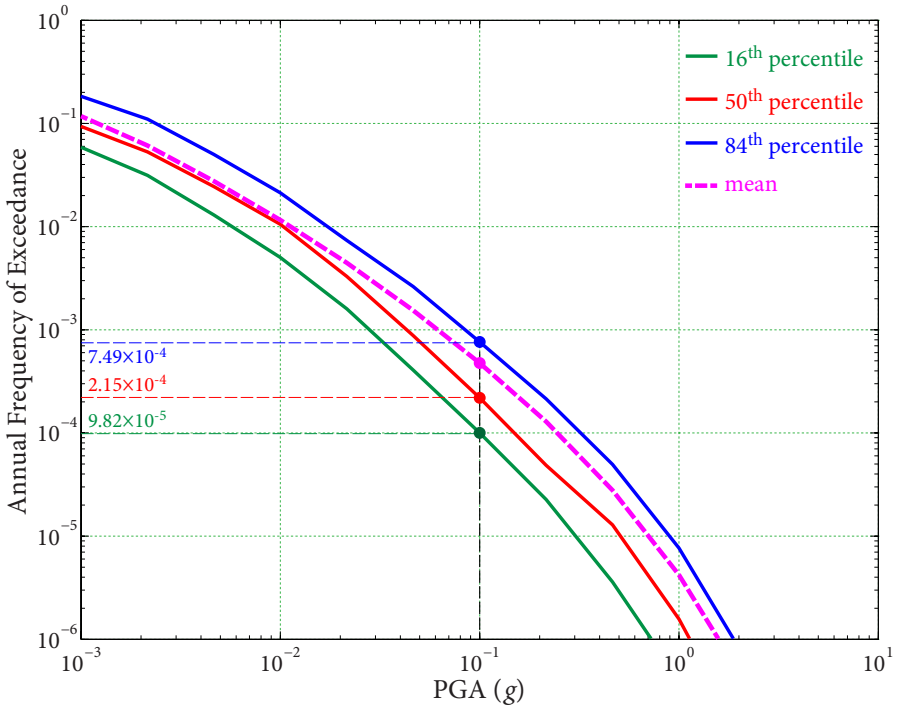


**Figure 2.13** Seismic hazard curves for PGA at mean and three percentiles

### 2.3.7 Uniform Hazard Spectra

Similar to the procedure used in plotting mean seismic hazard curve for PGA (see Figure 2.13), mean seismic hazard curves for spectral accelerations at other frequencies, e.g., 0.2, 0.5, 1, 2, 3.33, 5, 10, 20 Hz, can be obtained and are shown in Figure 2.14. By interpolating these mean seismic hazard curves at a specified seismic hazard such as $1 \times 10^{-2}$ give spectral values regarding these frequencies. Applying linear interpolation in logarithmic scale (10-base) among representative frequencies result in a mean uniform hazard spectrum (UHS) with $1 \times 10^{-2}$ (see Figure 2.15).

Based on Figure 2.14, UHS at any seismic hazard level can be determined. Figure 2.15 gives UHS at four seismic hazard levels, i.e., $1 \times 10^{-2}$, $2.1 \times 10^{-3}$, $1 \times 10^{-3}$, and $4.04 \times 10^{-4}$. In 2015 National Building Code of Canada (NBCC), UHS spectral values at ten representative frequencies are available online (http://www.earthquakescanada.nrcan.gc.ca/hazard-alea/interpolat/index-en.php). Entering the geographic coordinates of Darlington NGS site on the website can obtain UHS spectral values at four mean seismic hazard levels, as shown in Figure 2.15. It can be seen that the calculated UHS agree well with spectral values given in 2015 NBCC. Therefore, the calculated PSHA results would be used in this study.

Figure 2.15 also shows that spectral shapes of mean UHS varies with seismic hazard levels (related to ground motion intensities). It shows that ground motion intensity has effect on response spectra. In current seismic fragility analysis, however, a generic ground response spectrum or a site-specific UHS at a specified seismic hazard level (e.g. $1 \times 10^{-4}$) anchoring to a ground motion parameter (GMP) at a screening level $A_{\mathrm{RLE}}$ (e.g. $A_{\mathrm{RLE}} = 0.3g$), is defined as Review Level Earthquake (RLE), thus ground motion intensity effect is neglected.

### 2.3.8 Mean Annual Rate Density Distribution

In current seismic fragility analysis, PGA, i.e., $\mathcal{S}_{\mathrm{A}}(f_1 = 50\,\mathrm{Hz})$, is usually chosen as GMP. However, the fundamental frequencies of most safety-related structures, systems, and components (SSCs) lie in the frequency range between 2 Hz and 10 Hz. To more accurately characterize the variability in spectral acceleration at the fundamental frequency $f$ of a safety-related SSC, $\mathcal{S}_{\mathrm{A}}(f)$ should be taken as GMP as well. Suppose there is an SSC with

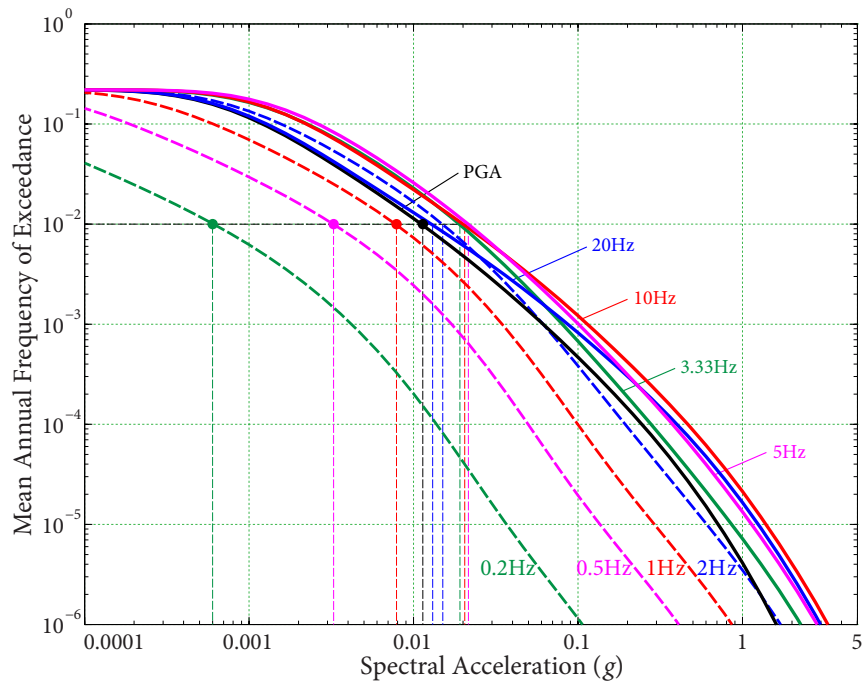


**Figure 2.14** Interpolation of seismic hazard curves regarding representative frequencies at seismic hazard of $1 \times 10^{-2}$

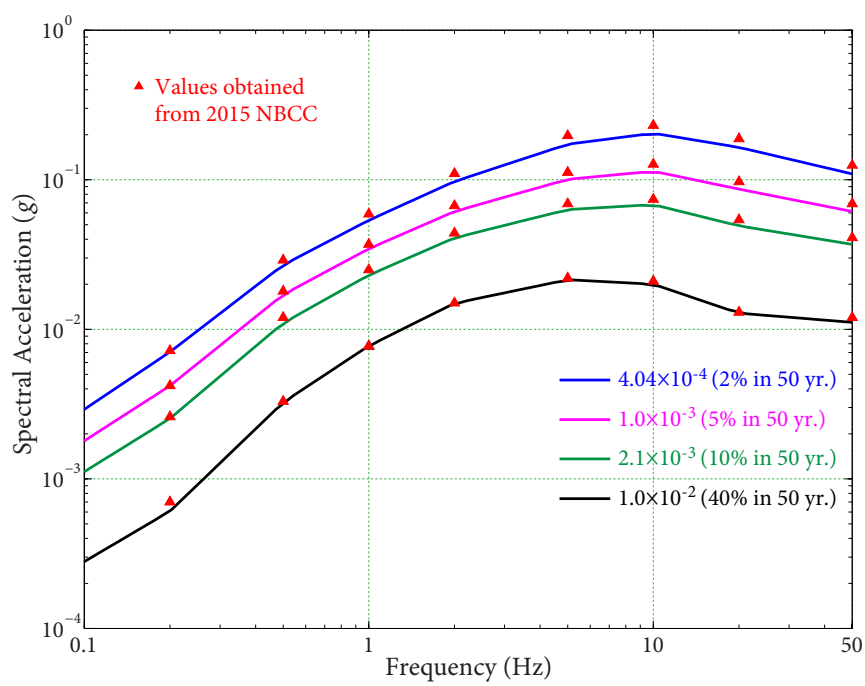


**Figure 2.15** Mean UHS at four seismic hazard levels at Darlington NGS site

the fundamental frequency of $f = 5$ Hz (between 2 Hz and 10 Hz). $\mathcal{S}_A(f = 5\,\text{Hz})$ and PGA are chosen as vector-valued GMPs (VGMPs). Vector-valued Probabilistic Seismic Hazard Analysis (VPSHA) is performed to determine mean annual rate density of $\left\{\mathcal{S}_A(f) \,\middle|\, \text{PGA}\right\}$, as defined in equation (2.2.15), for this SSC.

Based on spectral correlation model by Baker and Jayaram (2008), the correlation coefficient $\rho$ between $\ln \mathcal{S}_A(f)$ and $\ln \text{PGA}$ is equal to 0.875. Due to the use of VGMPs, given a PGA value, spectral value of $\mathcal{S}_A(f)$ yields a distribution. Therefore, mean annual rate density of $\left\{\mathcal{S}_A(f) \,\middle|\, \text{PGA}\right\}$ is a two-dimensional distribution. Figure 2.16 gives the contour of the distribution. It can be seen that high density values are clustered in a diagonal region, indicating earthquakes with spectral accelerations $\mathcal{S}_A(f)$ and PGA in the diagonal region are more likely to occur.

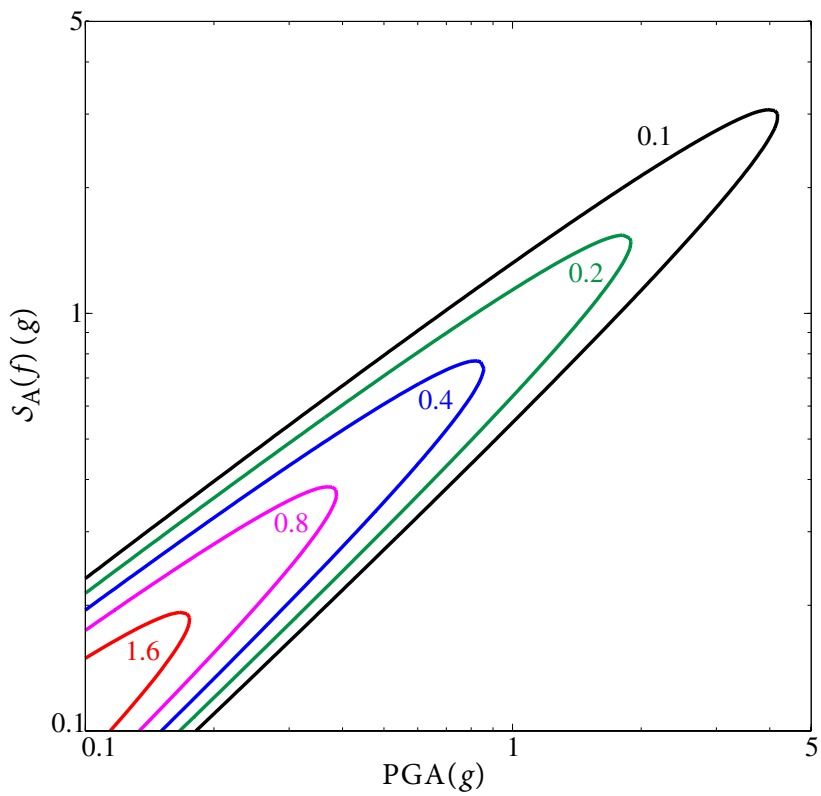


**Figure 2.16** Contour of annual rate density of $\mathcal{S}_A(f)$|PGA

Taking a number of spectral values of PGA, such as $0.3g$, $0.6g$, and $0.9g$, a set of curves of $\mathcal{S}_A(f)$ are obtained (see Figure 2.17), indicating VPSHA can take ground motion intensity effect into consideration. In addition, the variability of $\mathcal{S}_A(f)$ in earthquake response spectra is also considered for a given PGA value.

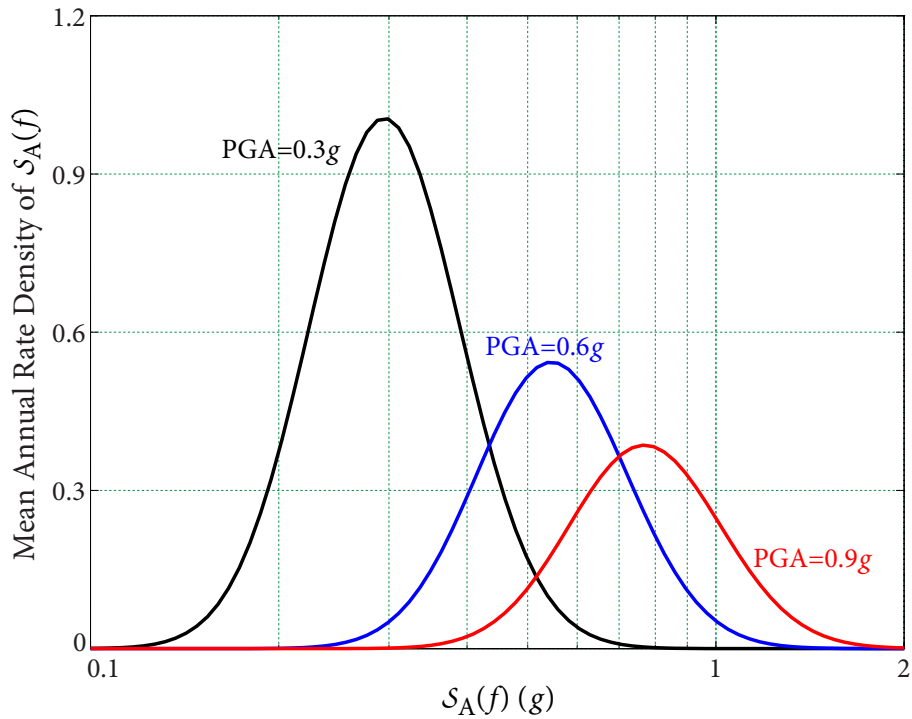


**Figure 2.17** Mean annual rate density of $\mathcal{S}_A(f)$ at three PGA values

Based on seismic hazard curves in Figure 2.18, given PGA $=0.6g$, one can determine spectral value of $\mathcal{S}_A(f)=0.95g$ by interpolating two seismic hazard curves at the same seismic hazard. Figure 2.19 gives spectral values of $\mathcal{S}_A(f)$ given PGA $=0.6g$ based on PSHA and VPSHA. Integrating annual rate density in Figure 2.18 from lower bound $0.1g$ to $\mathcal{S}_A(f)=0.95g$, and then divided by the value integrating from $0.1g$ to upper bound $5g$ (see Figure 2.16), gives 96th percentile at $\mathcal{S}_A(f)=0.95g$. It indicates that UHS is more likely to overestimate spectral value of $\mathcal{S}_A(f)$. Therefore, VGMPs should be introduced in the determination of ground response spectra for seismic fragility analysis.

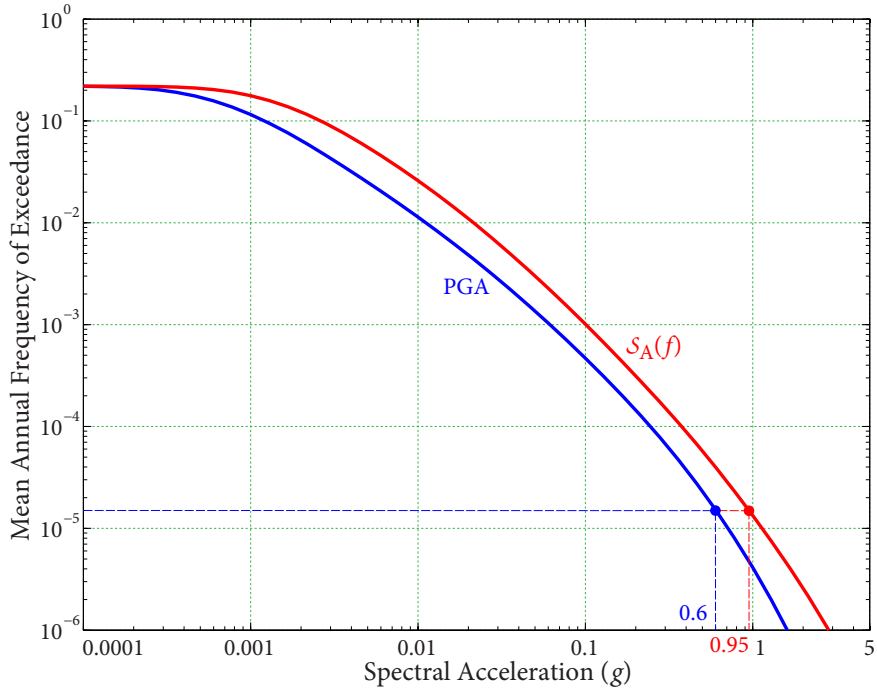


**Figure 2.18** Interpolation of seismic hazard curves for determining $\mathcal{S}_A(f)$

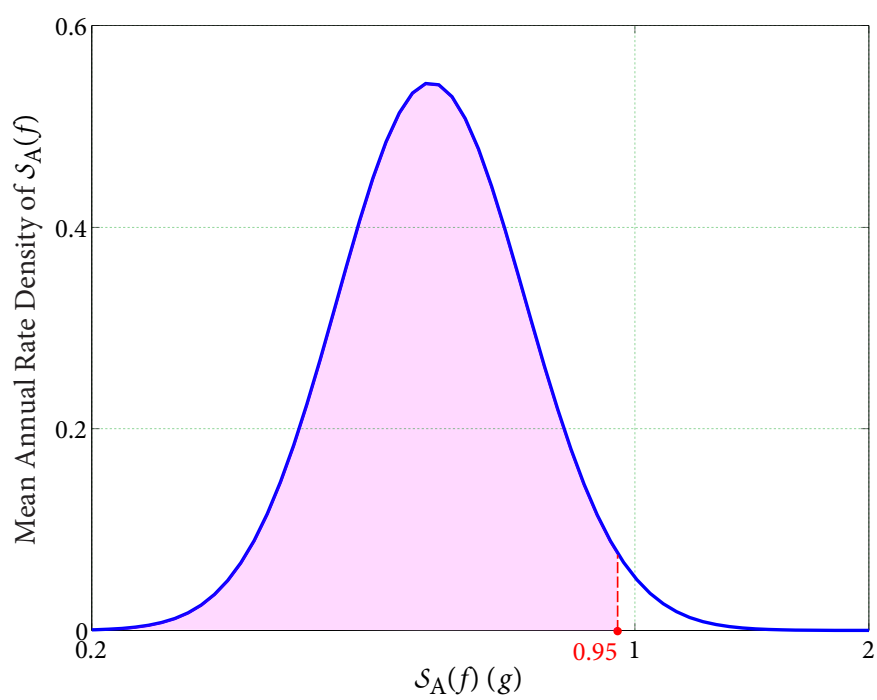


**Figure 2.19** Spectral values of $\mathcal{S}_A(f)$ based on PSHA and VPSHA (PGA $= 0.6g$)

## 2.4 Summary

In this Chapter, Probabilistic Seismic Hazard Analysis (PSHA) and vector-valued PSHA (VPSHA) are introduced first. To better illustrate the procedure of PSHA, numerical example for Darlington nuclear generating station (NGS) is performed:

- a logic tree consisting 81 epistemic branches is developed to capture the uncertainties in seismic source model, magnitude-recurrence model, maximum earthquake magnitude, and ground-motion model;
- Matlab codes are written by myself to calculate seismic hazard curves from epistemic branches;
- seismic hazard curves at mean and percentiles are determined based on seismic hazard curves from epistemic branches;
- mean uniform hazard spectra (UHS) are obtained from interpolating mean seismic hazard curves at ten representative frequencies.

Spectral values from calculated UHS match well with those values from 2015 National Building Code of Canada.

VPSHA is then performed for a safety-related component in Darlington NGS. Spectral acceleration $\mathcal{S}_{\mathrm{A}}(f=5\,\mathrm{Hz})$ at structural fundamental frequency and PGA, i.e. $\mathcal{S}_{\mathrm{A}}(f=50\,\mathrm{Hz})$, are chosen as vector-valued GMPs (VGMPs). Mean annual rate density of $\left\{\mathcal{S}_{\mathrm{A}}(f)\,\middle|\,\mathrm{PGA}\right\}$ is determined. The results show that

- aleatory randomness in earthquake response spectra is properly captured;
- ground motion intensity effect is taken into consideration;
- UHS overestimates $\mathcal{S}_{\mathrm{A}}(f)$ for a given PGA value.

For safety-related structures, systems, and components (SSCs), VGMPs should be introduced to characterize earthquake response spectra at the site of interest.

C H A P T E R 3

# Seismic Fragility Analysis

Seismic fragility analysis has been widely used to evaluate seismic capacities of systems, structures, and components (SSCs) in nuclear power plants. The seismic capacity of an SSC from the seismic fragility analysis, in terms of seismic fragility curve or High Confidence and Low Probability of Failure seismic capacity, is used as an input to Seismic Probabilistic Risk Analysis or Seismic Margin Assessment. Therefore, accurate seismic capacity estimate is extremely important.

In Section 3.1, current seismic fragility analysis method is briefly reviewed. Section 3.2 performs case studies for quantitatively evaluating the influences of spectral shape and use of ground motion parameter (GMP) in current method. Section 3.3 provides several recommendations and summarizes this Chapter.

## 3.1 Seismic Fragility Analysis

### 3.1.1 Definition

Seismic fragility of an SSC is defined as the conditional probability that seismic capacity $A$ of an SSC is less than a given ground motion level $a$ in terms of GMP, i.e.,

$$p_{\mathrm{F}}(a) = \mathcal{P}\left\{A < a \,\middle|\, \mathrm{GMP} = a\right\}. \tag{3.1.1}$$

Seismic capacity $A$ of an SSC is often expressed as the product of three variables

$$A = A_m \, \varepsilon_R \, \varepsilon_U, \tag{3.1.2}$$

where $A_m$ is the best estimate of *median* seismic capacity, which is a deterministic value. $\varepsilon_R$ is the random variable representing aleatory *randomness* about the median value, and $\varepsilon_U$ is the random variable representing the epistemic *uncertainty* in estimating the median value due to lack of knowledge. The random variables $\varepsilon_R$ and $\varepsilon_U$ are usually taken to be lognormal with unit median (zero logarithmic mean) and logarithmic standard deviations of $\beta_R$ and $\beta_U$, respectively.

Let $A_m^U = A_m \varepsilon_U$ be the estimated *median* value when epistemic uncertainty is considered. Since $\varepsilon_U \sim \mathcal{LN}(0, \beta_U^2)$, then $A_m^U$ is lognormally distributed with $A_m^U \sim \mathcal{LN}(\ln A_m, \beta_U^2)$, in which $\ln A_m$ and $\beta_U$ are corresponding logarithmic mean and standard deviation.

For a random variable $X$, the confidence level $Q$ is defines as

$$\mathcal{P}\{X > X_Q\} = 1 - \mathcal{P}\{X \leqslant X_Q\} = Q. \tag{3.1.3}$$

Replacing $X$ by $\varepsilon_U$ and substituting $Q = q$ into equation (3.1.3) results in

$$1 - \mathcal{P}\{\varepsilon_U \leqslant \varepsilon_{U,q}\} = q. \tag{3.1.4}$$

Recalling that $\varepsilon_U \sim \mathcal{LN}(0, \beta_U^2)$, hence $\varepsilon_{U,q}$ can be determined by solving equation (3.1.4),

$$1 - \Phi\left[\frac{\ln \varepsilon_{U,q} - 0}{\beta_U}\right] = q \implies \varepsilon_{U,q} = \mathrm{e}^{-\beta_U \Phi^{-1}(q)}. \tag{3.1.5}$$

Therefore, the estimated *median* capacity $A_{m,q}^U$ at the confidence level $Q = q$ can be expressed as

$$A_{m,q}^U = A_m \varepsilon_{U,q} = A_m \mathrm{e}^{-\beta_U \Phi^{-1}(q)}, \qquad \mathcal{P}\{A_m^U > A_{m,q}^U\} = q. \tag{3.1.6}$$

Replacing $A_m \varepsilon_U$ in equation (3.1.2) by $A_{m,q}^U$ obtained in equation (3.1.4) yields the seismic fragility, or the conditional probability of failure given a ground motion level $a$, at confidence level $Q = q$ (Kennedy and Ravindra, 1984)

$$p_{\mathrm{F},q}(a) = \mathcal{P}\{A < a \,|\, \mathrm{GMP} = a,\ Q = q\} = \Phi\left[\frac{\ln(a/A_m) + \beta_U \Phi^{-1}(q)}{\beta_R}\right]. \tag{3.1.7}$$

The confidence level $Q$ is continuous between 0 and 1. In applications, it is usually taken as discrete values, such as 5%, 50%, and 95%.

When composite variability $\varepsilon_C = \varepsilon_R \varepsilon_U$ is used, $p_{F,C}$ can be determined by (EPRI, 1994)

$$p_{F,C}(a) = \mathcal{P}\{A < a \mid \text{GMP} = a\} = \Phi\left[\frac{\ln(a/A_m)}{\beta_C}\right], \qquad \beta_C = \sqrt{\beta_R^2 + \beta_U^2}. \tag{3.1.8}$$

where $\beta_C$ is logarithmic standard deviation of composite variability $\varepsilon_C$.

### 3.1.2 Determination of Seismic Fragility

Let $A_{RLE}$ be plant screening level in terms of a single GMP (e.g. PGA) from Review Level Earthquake (RLE). In estimating the fragility parameters, it is more convenient to work with an intermediate random variable $F$, called the *factor of safety*. $F$ describes the level that the seismic capacity $A$ of an individual SSC is above the reference seismic capacity $A_{RLE}$, and is defined as (Kennedy and Ravindra, 1984)

$$A = F \cdot A_{RLE}, \tag{3.1.9}$$

$$\begin{aligned} F &= \frac{\text{Actual structural capacity of SSC}}{\text{Actual seismic demand due to RLE}} \\ &= \frac{\text{Actual structural capacity of SSC}}{\text{Calculated seismic demand due to RLE}} \times \frac{\text{Calculated seismic demand due to RLE}}{\text{Actual seismic demand due to RLE}} \\ &= F_C \cdot F_{RS}, \end{aligned} \tag{3.1.10}$$

in which the actual structural capacity and actual seismic demand due to RLE are both random variables; whereas the calculated seismic demand due to RLE is a deterministic value because response variabilities are not included in the calculation. As a result, capacity factor $F_C$ and response factor $F_{RS}$ are both random variables.

#### Capacity Factor

In equation (3.1.10), $F_C$ can be determined by

$$F_C = F_\mu \cdot F_S, \tag{3.1.11}$$

where $F_\mu$ is the inelastic energy absorption factor, considering the fact that an earthquake is a limited energy source and many structures, systems, and components (SSCs) are capable of absorbing energy beyond yield without loss-of-function. For safety-related SSCs, $F_\mu$ is not

needed to be considered, because they are designed to behaviour elastically during strong ground motions. $F_S$ is the strength factor, representing the ratio of structural capacity to the calculated seismic demand due to the reference earthquake, which can be determined by

$$F_S = \frac{C - D_{NS}}{D_S + \Delta C_S}, \tag{3.1.12}$$

where $C$ is a random variable representing the structural capacity for a specific failure mode. $\Delta C_S$ is the reduction in structural capacity due to concurrent seismic loadings. $D_S$ is the calculated elastic seismic demand, $D_{NS}$ is the concurrent non-seismic demand or normal operating load (such as dead load and operating temperature load). $\Delta C_S$, $D_S$, and $D_{NS}$ are all deterministic values.

In nuclear engineering practice, $F_C$ is usually taken as lognormal random variable.

### Response Factor

$F_{RS}$ in equation (3.1.10) is a random variable due to uncertainties in ground motion and dynamic properties of SSCs. For structures, $F_{RS}$ is usually modelled as a product of several factors that contribute to the response variability, i.e.,

$$F_{RS} = \prod_i F_{RS_i}, \tag{3.1.13}$$

where $F_{RS_i}$ denotes the $i$th response factor. Some basic response factors that influence structural response are

- Ground Motion (earthquake response spectrum shape, horizontal direction peak response, vertical component response)
- Damping
- Modelling (modal frequency, modal shape, torsional coupling)
- Modal Combination
- Time History Simulation
- Foundation-Structure Interaction (ground motion incoherence, vertical spatial variation of ground motion, soil-structure interaction)
- Earthquake Component Combination

For equipments and other components, the *factor of safety* $F$ in equation (3.1.10) includes one more factor $F_{\mathrm{RE}}$ accounting for variabilities in equipment response. $F_{\mathrm{RE}}$ is usually expressed as the product of several variables, i.e.,

$$F_{\mathrm{RE}} = \prod_i F_{\mathrm{RE}_i}, \tag{3.1.14}$$

Some basic variables that influence equipment response factor $F_{\mathrm{RE}}$ are

- Qualification Method
- Damping
- Modelling (modal frequency, modal shape)
- Modal Combination
- Earthquake Component Combination

In engineering applications, variables in damping, modelling, modal combination, and earthquake component combination are usually assumed to be lognormal with unit median (zero logarithmic mean) values. When response spectrum analysis method is used to calculate structural response, there is no time history simulation variability and qualification method variability.

### Factor of Safety

*Factor of safety* $F$ is also lognormally distributed from multiplication of basic variables. Equation (3.1.10) can be rewritten as

$$F = F_m\, \varepsilon_R\, \varepsilon_U, \quad F_m = F_{\mu,m} \cdot F_{\mathrm{S},m} \cdot F_{\mathrm{RS},m}, \tag{3.1.15}$$

where $\varepsilon_R$ and $\varepsilon_U$ represent aleatory *randomness* and epistemic *uncertainty* in estimating $F$, respectively. $\varepsilon_R$ and $\varepsilon_U$ are both lognormally distributed with unit median (zero logarithmic mean) and logarithmic standard deviations $\beta_R$ and $\beta_U$, respectively.

When ground motion variability is unit median, foundation-structure interaction is not considered, and response spectrum analysis method is used to calculate structural response, $F_{\mathrm{RS}}$ is lognormal with unit median values, i.e., $F_{\mathrm{RS},m} = 1.0$. $F_m$ is thus given by

$$F_m = F_{\mu,m} \cdot F_{\mathrm{S},m}. \tag{3.1.16}$$

### Median Seismic Capacity

Combining equations (3.1.2), (3.1.9), and (3.1.15) gives

$$A = A_m \, \varepsilon_R \, \varepsilon_U = (F_m \cdot A_{\mathrm{RLE}}) \, \varepsilon_R \, \varepsilon_U. \tag{3.1.17}$$

Therefore, *median* seismic capacity $A_m$ is given by

$$A_m = F_m \cdot A_{\mathrm{RLE}}. \tag{3.1.18}$$

$\varepsilon_R$ and $\varepsilon_U$ in equations (3.1.2) and (3.1.15) are essentially the same, because they are dimensionless random variables. In engineering practice, logarithmic standard deviations of $F$ instead of $A$ are calculated.

### Logarithmic Standard Deviations

EPRI-TR-103959 (EPRI, 1994) proposes three available methods to determine propagated logarithmic standard deviations of capacity and response variables: approximate second moment procedure, second moment procedure, and Monte Carlo simulation. In applications, *approximate second-moment procedure* is usually used to determine total logarithmic standard deviations of aleatory *randomness* $\beta_R$ and epistemic *uncertainty* $\beta_U$, i.e.,

$$\beta = \sqrt{\sum_j \beta_j^2}. \tag{3.1.19}$$

In equation (3.1.15), $\beta$ represents either $\beta_R$ or $\beta_U$, and $\beta_i$ is the part of the final $\beta$-value due to the effect of variation in the $i$th underlying basic variable, which can be determined by

$$\beta_i = \frac{1}{|\phi|} \ln \frac{F_{\phi\sigma_i}}{F_m}, \tag{3.1.20}$$

in which $F_{\phi\sigma_i}$ is the value of $F$ where the $i$th variable is set at $\phi$ standard deviation ($\sigma_i$) level, and all other basic variables are kept at their median levels. $\phi$ is usually set to be either 1 or $-1$. It is recommend that demand variables be increased (evaluated at $+\sigma_i$ level) and that capacity variables be decreased (evaluated at $-\sigma_i$ level).

### Seismic Fragility Curves

Having obtained $A_m$, $\beta_R$ and $\beta_U$, seismic fragility of the SSC can be determined by equation (3.1.7). Figure 3.1 shows an example of family of fragility curves at three confidence levels. In addition, when composite variability is used, a composite (also called mean) fragility curve can be obtained and is also shown in Figure 3.1.

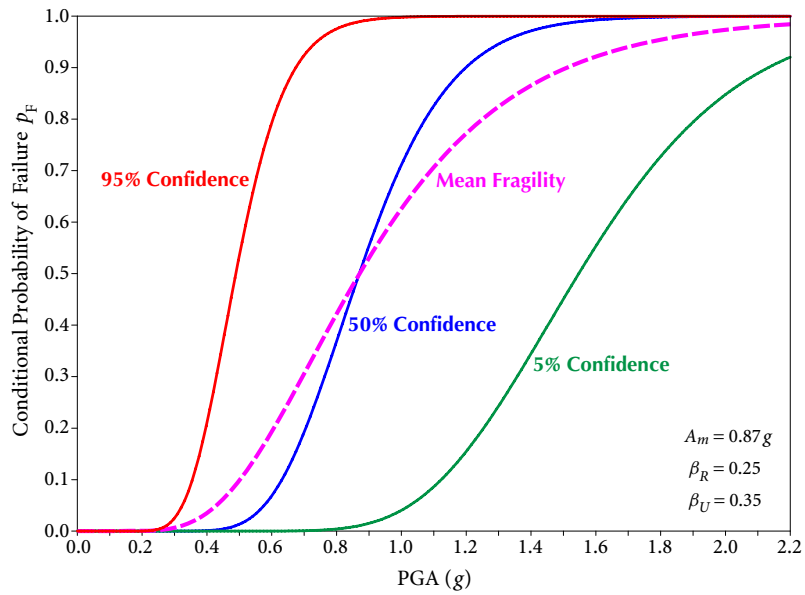


**Figure 3.1** An example of family of fragility curves and mean fragility curve

### HCLPF Seismic Capacity

Taking conditional probability of failure $p_{F,q} = 5\%$ at confidence level $Q = 95\%$, and solving for $a$ in equation (3.1.7), a High Confidence and Low Probability of Failure (HCLPF) seismic capacity in terms of the chosen GMP can be obtained as (EPRI, 1994)

$$C_{\text{HCLPF}} = A_m \, e^{(\beta_R + \beta_U)\,\Phi^{-1}(0.05)} = A_m \, e^{-1.6449\,(\beta_R + \beta_U)}. \tag{3.1.21}$$

## 3.2 Numerical Example for Horizontal Heat Exchanger

The problems in current seismic fragility analysis have been discussed in Chapter 1. To illustrate the procedure of current seismic fragility analysis method and demonstrate its problems, numerical example for a horizontal heat exchanger is performed.

### 3.2.1 Heat Exchanger Configuration

In NPPs, heat exchanger is used to transfer heat produced by nuclear reaction to drive steam turbines for electricity production. The anchorage of heat exchanger has been identified as one of the governing components for overall plant risk (EPRI-1000895, EPRI, 2000). Section 8 of EPRI-TR-103959 (EPRI, 1994) presents an example of horizontal heat exchanger.

#### Basic Information

Details of the horizontal heat exchanger is shown in Figure 3.2 and properties are listed in Table 3.1. It has a diameter of 8 ft = 96 in, length of 30 ft = 360 in, and is supported by three equally spaced saddles. Each saddle is secured to the concrete floor by three sets of 2 cast-in-place anchor bolts. Two of the saddle base plates (Support $S_1$) have slotted holes, which allow thermal expansion of the tank in the longitudinal direction. Therefore, when the heat exchanger is subjected to longitudinal earthquake excitation, only one saddle withstands the shear force due to the longitudinal translation of water tank. Each saddle has four stiffener plates to increase the rigidity of the heat exchanger in the longitudinal direction. A total weight of $W = 110$ kips is estimated for the exchanger. The connecting piping is relatively light, and its weight is included in $W = 110$ kips.

#### Potential Failure Modes

The basic material strength properties are listed in Table 3.2. It is assumed that the heat exchanger itself was designed to be seismically robust. The capacity of the connection of the saddles to the heat exchanger is relatively high and this potential failure mode is not considered. Only the following failure modes regarding the anchorage and support are considered:

- anchorage failure,
- bending failure of the support base plate,
- weld connection failure between base plate and saddle plate.

In the following, median static capacities based on these potential failure modes are calculated in accordance with pertinent codes.

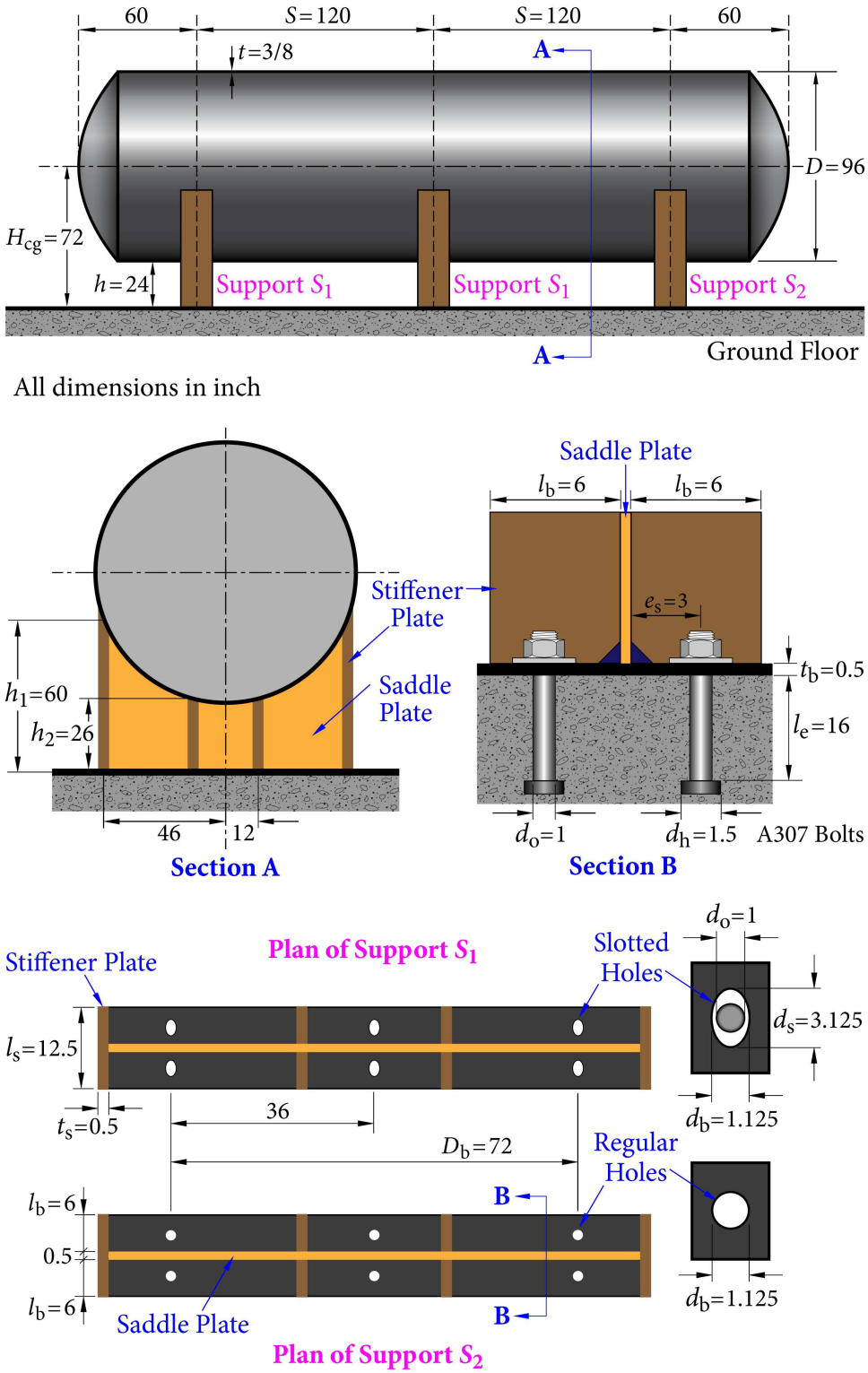


**Figure 3.2** Configuration details of horizontal heat exchanger

**Table 3.1** Deterministic Properties of Horizontal Heat Exchanger

| Property | Parameter | Value |
|---|---|---|
| **Heat Exchanger Tank** | | |
| Diameter | $D$ | 96 in |
| Length | $L$ | 360 in |
| Floor to bottom tank | $h$ | 24 in |
| Height to center of gravity | $H_{cg}$ | 72 in |
| Shell thickness | $t$ | 3/8 in |
| Weight | $W$ | 110 kip |
| **Saddle Supports (ASTM A36)** | | |
| Base plate thickness | $t_b$ | 0.5 in |
| Anchor bolt hole diameter | $d_b$ | 1-1/8 in |
| Slotted anchor hole dimension | $d_s$ | 3-1/8 in |
| Saddle plate to edge of base plate | $l_b$ | 6 in |
| Distance between outside bolts in saddle base plate | $D_b$ | 72 in |
| Weld length | $l_w$ | 6 in |
| Weld leg dimension | $t_w$ | 1/4 in |
| Stiffener width | $l_s$ | 12-1/2 in |
| Stiffener height (outside pair) | $h_1$ | 60 in |
| Stiffener height (inside pair) | $h_2$ | 26 in |
| Stiffener thickness | $t_s$ | 0.5 in |
| Number of supports | NS | 3 |
| **Anchor Bolts (ASTM A307)** | | |
| Area through bolt | $A_{gross}$ | 0.7854 in$^2$ |
| Area through threads | $A_{net}$ | 0.6057 in$^2$ |
| Embedment length | $l_e$ | 16 in |
| Bolt diameter | $d_o$ | 1 in |
| Head diameter | $d_h$ | 1-1/2 in |
| Eccentricity from anchor bolt centerline to saddle plate | $e_s$ | 3 in |
| Number of anchor bolt locations at each saddle | NL | 3 |
| Number of anchor bolts at each location | NB | 2 |

**Table 3.2** Material Strength Properties

| Property | Variable | Median | $\beta_U$ |
|---|---|---|---|
| **Steel (ASTM A36, A307)** | | | |
| Yield strength | $\sigma_y$ | 44 ksi | 0.12 |
| Ultimate strength | $\sigma_u$ | 64 ksi | 0.06 |
| **Concrete** | | | |
| Compressive strength | $f_c'$ | 6120 psi | 0.12 |
| **Weld** | | | |
| Tensile strength of electrode ($F_{EXX} = 60$ ksi) | $F_{EXX}$ | $1.1\,F_{EXX}$ | 0.05 |
| **Anchor Bolt** | | | |
| Tension | $N_{tension}$ | $0.9\,A_{net}\,\sigma_u$ | 0.13 |
| Shear | $V_{shear}$ | $0.62\,A_{net}\,\sigma_u$ | 0.10 |
| Coefficient of friction | | | |
| for shear friction capacity of concrete | $\mu$ | 1.0 | 0.24 |

### 3.2.2 Case Study Objectives

Assume the heat exchanger is located on ground floor of a reactor building in Darlington nuclear generating station (NGS), Ontario, Canada (see Chapter 2), and is subjected to earthquake excitations from three directions. Therefore, the fundamental frequency of the heat exchanger in each of three earthquake directions need to be determined. Since this component is relatively simple, the heat exchanger responds primarily in the first mode in each earthquake direction. Structural analysis shows that fundamental frequencies in longitudinal and transverse directions are $f_L = 8.15$ Hz and $f_T = 25.4$ Hz, respectively. Since the heat exchanger is seismically robust in vertical direction, fundamental frequency in this direction is taken as $f_V = 50$ Hz, where spectral acceleration returns to PGA.

In current seismic fragility analysis, a generic ground response spectrum (GRS) such as NUREG/CR-0098 median response spectrum (abbreviated as NUREG spectrum) or uniform hazard spectrum (UHS) at Darlington NGS site, can be defined as Review Level Earthquake (RLE). The RLE is then anchored to a screening level in terms of a ground

motion parameter (GMP). In engineering applications, average spectral acceleration $\bar{S}_A$ between 5 and 10 Hz or PGA can be chosen as GMP.

As in Chapter 1, for a given structure, spectral shape of RLE and the use of GMP affect its seismic fragility estimate. Case studies are conducted herein to evaluate these influences.

### Case 1: Influence of Spectral Shape of RLE

NUREG spectrum and mean UHS at $1 \times 10^{-4}$ (Darlington nuclear generating station site) are anchored to PGA at screening level $A_{RLE} = 0.3g$. Spectral shapes of these two response spectra are shown in Figure 3.3. Site-specific UHS is much lower in low to intermediate frequencies while a little higher in high frequencies.

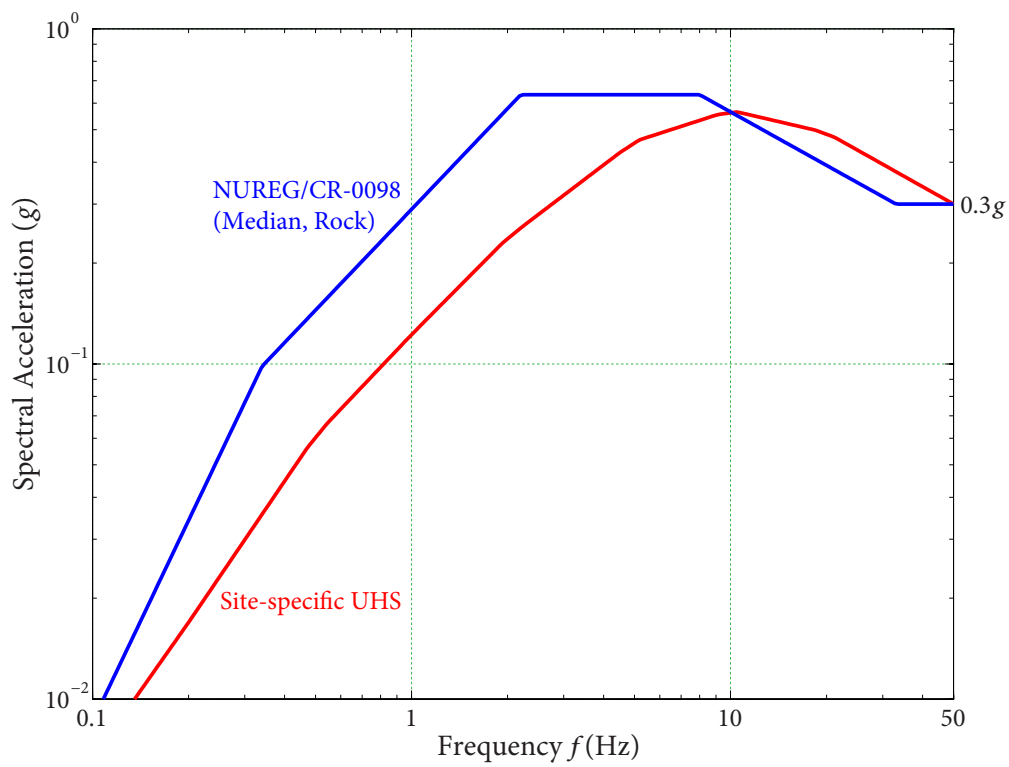


**Figure 3.3** NUREG spectrum and site-specific UHS anchoring to PGA at $0.3g$

NUREG spectrum is chosen as RLE first and then site-specific UHS is chosen as RLE. Seismic fragility results are compared to illustrate the influence of spectral shape of RLE.

### Case 2: Influence of Use of GMP

A generic GRS is generally different from a site-specific response spectrum, thus response spectrum shape variability needs to be considered. In this case study, NUREG spectrum is defined as RLE, Table 3.3 gives logarithmic standard deviations ($\beta_R$ for aleatory *randomness* and $\beta_U$ for epistemic *uncertainty*) of response spectrum shape variability (Table 3-2, EPRI, 1994). It shows that response spectrum shape variability depends the chosen GMP where RLE is anchored.

**Table 3.3** Earthquake Response Spectrum Shape Variability (NUREG Spectrum)

| Earthquake response spectrum shape variability | Logarithmic standard deviation | |
|---|---|---|
| | $\beta_R$ | $\beta_U$ |
| RLE anchored to PGA | | |
| 1 Hz | 0.18 to 0.22 | 0.32 |
| 5 Hz | 0.18 to 0.22 | 0.24 |
| 10 Hz | 0.18 to 0.22 | 0.16 |
| 16 Hz | 0.15 to 0.19 | 0.12 |
| 33 Hz | 0.12 to 0.15 | 0 |
| RLE anchored to $\bar{\mathcal{S}}_{\mathrm{A}}$ | | |
| 1 Hz | 0.18 to 0.22 | 0.20 |
| 5 Hz | 0.18 to 0.22 | 0 |
| 10 Hz | 0.18 to 0.22 | 0 |
| 16 Hz | 0.15 to 0.18 | 0.10 |
| 33 Hz | 0.12 to 0.15 | 0.13 |

As in Figure 3.3, site-specific UHS is linear in natural log (ln) scale between 5 and 10 Hz, thus the average spectral acceleration $\bar{\mathcal{S}}_{\mathrm{A}}$ between 5 and 10 Hz is given by

$$\bar{\mathcal{S}}_{\mathrm{A}} = \mathrm{e}^{[\ln \mathcal{S}_{\mathrm{A}}(f=5\,\mathrm{Hz}) + \ln \mathcal{S}_{\mathrm{A}}(f=10\,\mathrm{Hz})]/2} = \mathrm{e}^{[\ln(0.45) + \ln(0.56)]/2} = 0.5g. \tag{3.2.1}$$

Recall that the dominant frequency $f_{\mathrm{L}}$ of heat exchanger is equal to 8.15 Hz. When RLE is anchored to PGA at $0.3g$, $\beta_U = 0.19$ by interpolating $\beta_U$ between 5 and 10 Hz. However, when RLE is anchored to $\bar{\mathcal{S}}_{\mathrm{A}}$, there is no epistemic *uncertainty* at spectral acceleration at $f_{\mathrm{L}}$.

To quantitatively study the effect of use of GMP in seismic capacity estimate, RLE is anchored to PGA first and then anchored to $\bar{\mathcal{S}}_A$. Seismic fragility results are compared to illustrate the influence of GMP.

### 3.2.3 Case 1: Influence of Spectral Shape – NUREG Spectrum is RLE

In this Section, seismic fragility analysis for the heat exchanger is presented in detail.

#### 3.2.3.1 Definition of Seismic Input

NUREG spectrum anchoring to PGA at screening level $0.3g$ is defined as RLE. The vertical GRS is assumed to be $2/3$ of the horizontal input over the entire frequency range. The heat exchanger is subjected to earthquake excitations in three directions.

#### 3.2.3.2 Seismic Demand Analysis

Response spectrum analysis method is used to calculate peak equipment response in three directions. For the heat exchanger, only the fundamental mode in each direction needs to be considered (see Section 3.2.1). Therefore, peak equipment response from each direction is equal to the peak modal response in that direction. Peak modal responses (spectral accelerations) of fundamental modes in three directions are obtained from horizontal and vertical seismic inputs and are presented in Table 3.4.

**Table 3.4** Spectral Values at Frequencies in Three Directions

| **Direction** | **Frequency (Hz)** | $\mathcal{S}_A\,(g)$ |
|---|---|---|
| Longitudinal | 8.15 | 0.63 |
| Transverse | 25.4 | 0.345 |
| Vertical | 50 | $\frac{2}{3} \times 0.30 = 0.20$ |

Peak equipment responses in three directions, i.e., spectral accelerations in three directions, are used to calculate seismic demand, i.e., tension and shear forces, of the anchorage of heat exchanger in three directions.

## Median Seismic Demand in Longitudinal Direction

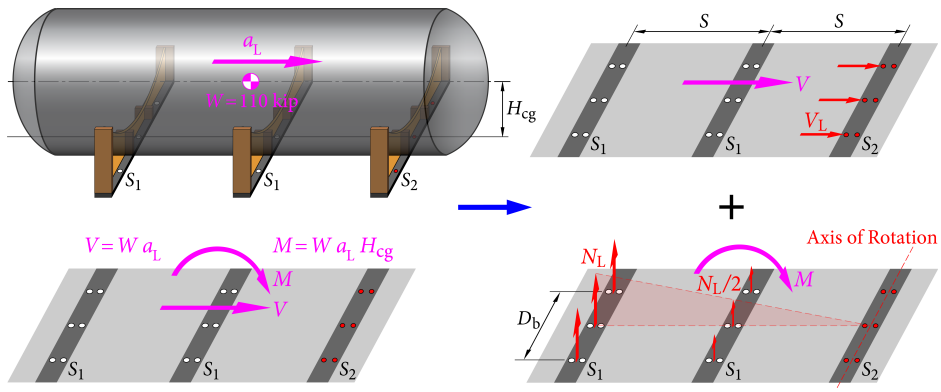


**Figure 3.4** Forces due to longitudinal excitation

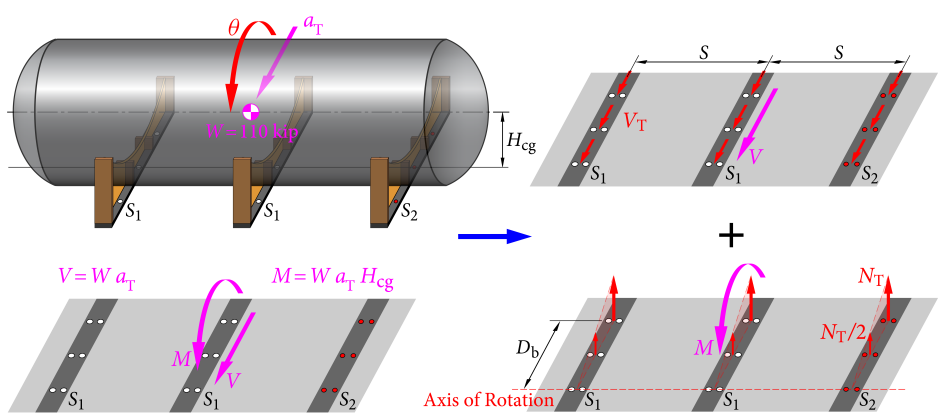


**Figure 3.5** Forces due to transverse rocking

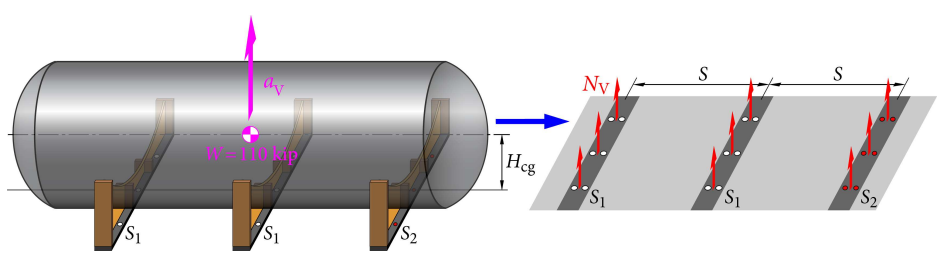


**Figure 3.6** Forces due to vertical excitation

In the longitudinal direction, under seismic excitation, the tank is subjected to an inertia force equal to the product of its weight $W$ and the spectral acceleration $a_L = 0.63g$, as shown in Figure 3.4. The inertia force is then transferred to the supports, exerting tension

and shear force on anchors bolts. Assume that all anchor bolts are in elastic tension and shear during earthquake excitations. The geometric information of the heat exchanger is given in Table 3.1.

Since Supports $S_1$ have slotted holes to allow for longitudinal movement, the shear force are evenly distributed in the anchor bolts of Support 2 only. The shear force in a single bolt is given by

$$V_{\mathrm{L}} = \frac{W \cdot a_{\mathrm{L}}}{\mathrm{NL} \cdot \mathrm{NB}} = \frac{110 \times 0.63}{3 \times 2} = 11.55 \text{ kips.} \tag{3.2.2}$$

Tension forces in the two Supports 1 are due to the moment $W \cdot a_{\mathrm{L}} \cdot H_{\mathrm{cg}}$, as shown in Figure 3.4. For the critical anchor bolts, the tension force is given by

$$N_{\mathrm{L}} = \frac{W \cdot a_{\mathrm{L}} \cdot H_{\mathrm{cg}}}{\mathrm{NL} \cdot \mathrm{NB} \cdot \left(2S + \frac{1}{2}S\right)} = \frac{110 \times 0.63 \times 72}{3 \times 2 \times \frac{5}{2} \times 120} = 2.77 \text{ kips.} \tag{3.2.3}$$

### Median Seismic Demand in Transverse Direction

In the transverse direction, under seismic excitation, the seismic loading due to transverse excitation is also transferred to the supports, exerting tension and shear forces in the anchor bolts, as shown in Figure 3.5. Shear force is induced in all the anchor bolts in all the supports evenly. For a single bolt, the shear force is

$$V_{\mathrm{T}} = \frac{W \cdot a_{\mathrm{T}}}{\mathrm{NL} \cdot \mathrm{NB} \cdot \mathrm{NS}} = \frac{110 \times 0.345}{3 \times 2 \times 3} = 2.11 \text{ kips.} \tag{3.2.4}$$

The moment induces tension forces in the anchor bolts at 2 locations in all 3 supports, as shown in Figure 3.5. For the critical anchor bolts, the tension is

$$N_{\mathrm{T}} = \frac{W \cdot a_{\mathrm{T}} \cdot H_{\mathrm{cg}}}{\mathrm{NB} \cdot \mathrm{NS} \cdot \left(D_{\mathrm{b}} + \frac{1}{4}D_{\mathrm{b}}\right)} = \frac{110 \times 0.345 \times 72}{2 \times 3 \times \frac{5}{4} \times 72} = 5.06 \text{ kips.} \tag{3.2.5}$$

### Median Demand in Vertical Direction

In the vertical direction, under seismic excitation, the inertial force of the tank due to seismic vertical acceleration is transferred to the support as pure tension force, without shear force, as shown in Figure 3.6. All anchor bolts share the seismic load evenly so that the tension force is

$$N_{\mathrm{V}} = \frac{W \cdot a_{\mathrm{V}}}{\mathrm{NL} \cdot \mathrm{NB} \cdot \mathrm{NS}} = \frac{110 \times 0.2}{3 \times 2 \times 3} = 1.22 \text{ kips.} \tag{3.2.6}$$

When the bolts are in tension, the dead load of the heat exchanger also exerts forces in the anchor bolts. All the bolts share the dead load evenly as

$$N_{\mathrm{DL}} = \frac{-W}{\mathrm{NL} \cdot \mathrm{NB} \cdot \mathrm{NS}} = \frac{-110}{3 \times 2 \times 3} = -6.11 \text{ kips.} \tag{3.2.7}$$

### Combination of Seismic Demand from Three Directions

When the response spectrum analysis method is used, the maximum earthquake-induced response of interest in an SSC should be obtained by the SRSS combination or the 100-40-40 percent combination of the maximum responses from the three earthquake components calculated separately (USNRC, 2006).

To combine the effect of the three earthquake components on the critical anchor bolt, first assuming that the longitudinal direction controls and then assuming that the transverse direction controls. It is obvious that the vertical direction will not control; thus this case is not considered further.

1. **Longitudinal direction controls**

   - Tension force in the critical anchor bolt is

$$\begin{aligned} N_{\mathrm{Long}} &= N_{\mathrm{L}} + 0.4\,N_{\mathrm{T}} + 0.4\,N_{\mathrm{V}} \\ &= 1.0 \times 2.77 + 0.4 \times 5.06 + 0.4 \times 1.22 = 5.28 \text{ kips.} \end{aligned} \tag{3.2.8}$$

   - Shear force in the critical anchor bolt is

$$V_{\mathrm{Long}} = \sqrt{(V_{\mathrm{L}})^2 + (0.4\,V_{\mathrm{T}})^2} = \sqrt{11.55^2 + (0.4 \times 2.11)^2} = 11.58 \text{ kips.} \tag{3.2.9}$$

2. **Transverse direction controls**

   - Tension force in the critical anchor bolt is

$$\begin{aligned} N_{\mathrm{Tran}} &= N_{\mathrm{T}} + 0.4\,N_{\mathrm{L}} + 0.4\,N_{\mathrm{V}} \\ &= 1.0 \times 5.06 + 0.4 \times 2.77 + 0.4 \times 1.22 = 6.65 \text{ kips.} \end{aligned} \tag{3.2.10}$$

   - Shear force in the critical anchor bolt is

$$V_{\mathrm{Tran}} = \sqrt{(V_{\mathrm{T}})^2 + (0.4\,V_{\mathrm{L}})^2} = \sqrt{2.11^2 + (0.4 \times 11.55)^2} = 5.08 \text{ kips.} \tag{3.2.11}$$

The tension and shear demand of the heat exchanger are summarized in Table 3.5. It is easily to find that longitudinal direction is controlling direction.

**Table 3.5** Median Tension and Shear Demand of Heat Exchanger under NUREG Spectrum at $0.3g$ PGA

| Controlling Direction | Shear Force (kips) | Tension Force (kips) |
|---|---|---|
| **Longitudinal** | **11.58** | **5.28** |
| Transverse | 5.08 | 6.65 |

### 3.2.3.3 Structural Capacity Analysis

#### Median Capacity of Anchorage

Typical failure mechanisms of anchorage are illustrated in Figure 3.7. Median capacities for these types of failure are calculated in accordance with ACI 349-06 (ACI, 2007).

The median tensile strength of a single anchor is given by

$$N_{\text{tension},m} = \phi A_{\text{net}} \sigma_{\text{u}} = 0.90 \times 0.6057 \times 64 = 34.89 \text{ kips}, \tag{3.2.12}$$

where $\phi = 0.9$ is the reduction factor accounting for the notch effects of threads and slight eccentricities in loading.

The median shear strength of a single cast-in headed bolt is given by

$$V_{\text{shear},m} = 0.6 A_{\text{net}} \sigma_{\text{u}} = 0.60 \times 0.6057 \times 64 = 23.26 \text{ kips}. \tag{3.2.13}$$

For a cast-in headed bolt with bolt diameter $d_{\text{o}} = 1$ in and head diameter $d_{\text{h}} = 1.5$ in, the median pullout strength in tension is

$$\begin{aligned} A_{\text{bearing}} &= \frac{\pi}{4}(d_{\text{h}}^2 - d_{\text{o}}^2) = \frac{\pi}{4}(1.5^2 - 1.0^2) = 0.9817 \text{ in}^2, \\ N_{\text{pullout},m} &= 8\,\psi_{\text{c,P}} A_{\text{bearing}} f_{\text{c}}' = 1.0 \times 8 \times 0.9817 \times 6.12 = 48.06 \text{ kips}, \end{aligned} \tag{3.2.14}$$

where $\psi_{\text{c,P}} = 1.0$ is taken for cracked concrete.

The median concrete breakout strength of a single anchor in tension is determined by

$$N_{\text{b}} = k_{\text{c}} \sqrt{f_{\text{c}}'}\, h_{\text{ef}}^{1.5} = 24 \times \sqrt{6120} \times 16^{1.5} = 120.0 \text{ kips},$$

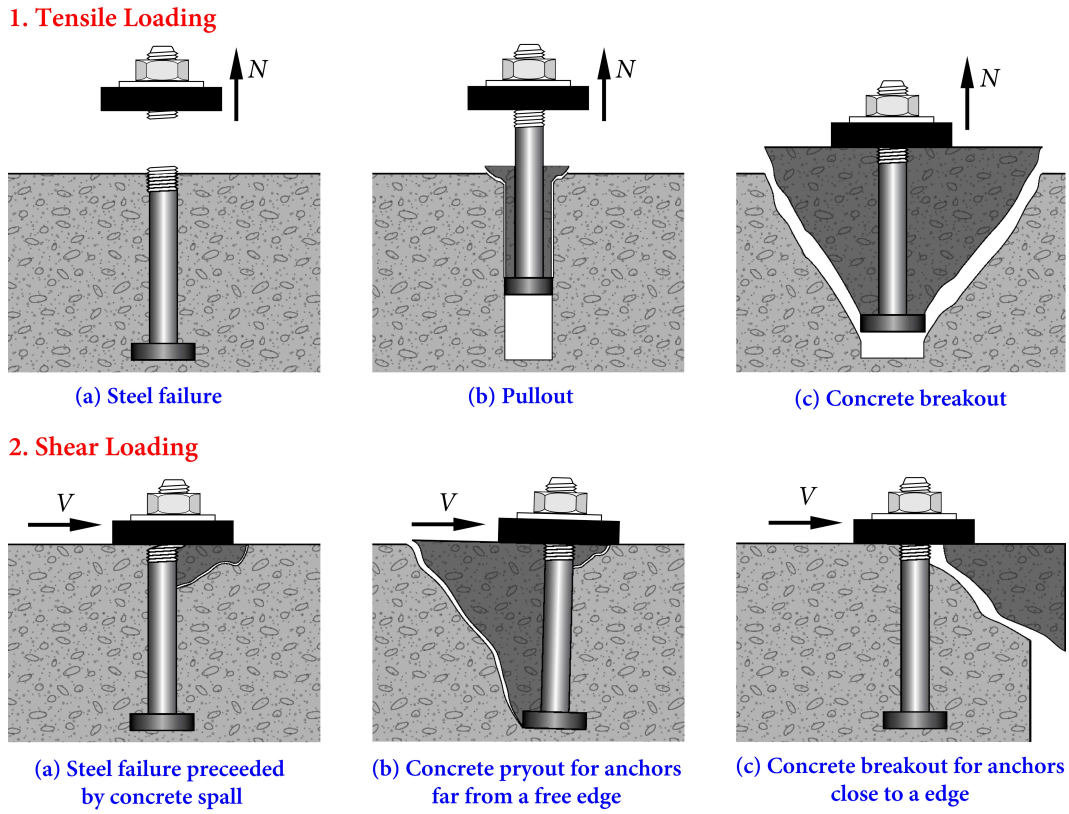


**Figure 3.7** Anchorage failure modes

$$N_{\text{breakout},m} = \frac{A_{\text{Nc}}}{A_{\text{Nc0}}}\,\psi_{\text{ed,N}}\,\psi_{\text{c,N}}\,\psi_{\text{cp,N}}\,N_{\text{b}}$$
$$= 1.0\times1.0\times1.0\times1.0\times120.0 = 120.0 \text{ kips}, \tag{3.2.15}$$

where

- for cast-in headed stud, $k_{\text{c}} = 24$ and $h_{\text{ef}} = 16$ in is the embedment length,
- for a single stud away from edge $\dfrac{A_{\text{Nc}}}{A_{\text{Nc0}}} = 1.0$,
- $\psi_{\text{ed,N}} = 1.0$ is the modification factor for edge,
- $\psi_{\text{c,N}} = 1.0$ is the modification factor for concrete cracking,
- $\psi_{\text{cp,N}}$ is the modification factor for splitting control applicable to post-installed anchors only, $\psi_{\text{cp,N}} = 1.0$ is taken for cast-in anchors.

For anchor bolts, the median concrete pryout strength of a single anchor in shear is given by

$$V_{\text{pryout},m} = k_{\text{cp}}\, N_{\text{breakout},m} = 2.0 \times 120.0 = 240.0 \text{ kips}, \tag{3.2.16}$$

where $k_{\text{cp}} = 2.0$, since the effective embedment depth $h_{\text{ef}} \geqslant 2.5$ in.

The median shear-friction strength in terms of the ultimate stress can be determined by

$$V_{\text{shear-friction},m} = 0.9\,\mu\, A_{\text{net}}\,\sigma_{\text{u}} = 0.9 \times 1.0 \times 0.6057 \times 64 = 34.89 \text{ kips}, \tag{3.2.17}$$

where $\mu$ is coefficient of friction given in Table 3.2.

### Median Bending Capacity of Support Base Plate

Due to earthquake excitation in vertical direction, the heat exchanger might move upwards from the floor. In the meanwhile, anchor bolts would resist its vertical movement. Therefore, the base plate will be in bending due to reactions from anchor bolts. In this example, the connection between saddle plate and base plate, and the connection between stiffness plate and base plate, are both assumed to be rigid. Therefore, the base plate surrounded by one saddle plate and two stiffness plates (see Figure 3.2) can be treated as a plate with three fixed ends and one free end.

The base plate bending capacity is realistically estimated using yield line theory. A postulated yield line pattern for the steel base plate is shown in Figure 3.8. Based on yield line theory, the median bending capacity of the base plate can be obtained as

$$\begin{aligned} N_{\text{pb},m} &= \frac{l_{\text{b}}\, t_{\text{b}}^2\, \sigma_{\text{y}}}{2 e_{\text{s}}}\left(\frac{2 l_{\text{b}} - d_{\text{s}}}{x} + \frac{x}{l_{\text{b}}}\right) = \sqrt{2 - \frac{d_{\text{s}}}{l_{\text{b}}}} \cdot \frac{l_{\text{b}}\, t_{\text{b}}^2}{e_{\text{s}}}\sigma_{\text{y}}, \quad x = l_{\text{b}}\sqrt{2 - \frac{d_{\text{s}}}{l_{\text{b}}}}, \\ &= \sqrt{2 - \frac{3.125}{6}} \times \frac{6 \times 0.5^2}{3} \times 44 = 26.76 \text{ kips}. \end{aligned} \tag{3.2.18}$$

### Median Weld Connection Capacity between Base Plate and Saddle Plate

Fillet welds are commonly used in structural connections. The weld area $A_{\text{w}}$ resisting the applied loads is given by an effective length $l_{\text{w}}$ times the effective throat thickness, which is equals to $t_{\text{w}}/\sqrt{2} = 0.707\, t_{\text{w}}$, where $t_{\text{w}}$ is the weld leg size, as shown in Figure 3.9; hence $A_{\text{w}} = 0.707\, l_{\text{w}}\, t_{\text{w}}$.

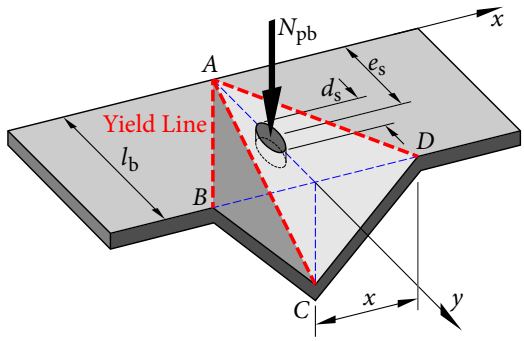


**Figure 3.8** Yield line pattern of the base plate

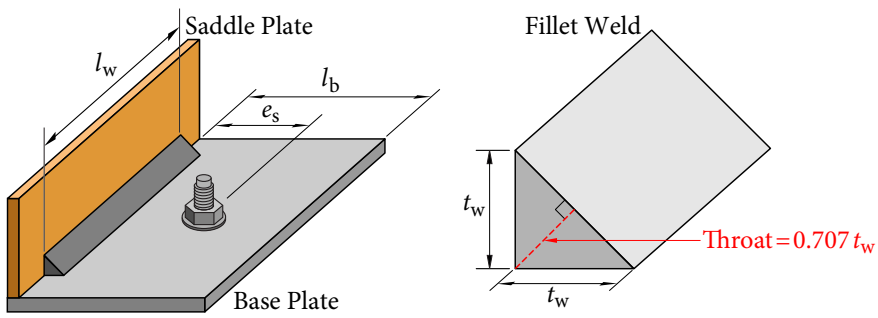


**Figure 3.9** Fillet weld failure

For the heat exchanger, the median weld connection capacity between the base plate and saddle plate in the transverse direction is given by

$$A_w = 0.707\, l_w\, t_w = 0.707 \times 6 \times 0.25 = 1.0605 \text{ in}^2,$$

$$P_{\text{weld},m} = 1.26\, A_w\, F_{\text{EXX},m} = 1.26 \times 1.0605 \times (1.1 \times 60) = 88.19 \text{ kips}. \tag{3.2.19}$$

Table 3.6 summarizes median capacities from potential failure modes. It can be seen that the minimum shear and tensile capacities are 23.26 kips and 26.76 kips, respectively. In addition, anchor bolts are simultaneously subjected to tensile and shear forces. Therefore, the tension-shear interaction relationship shall be used in the evaluation of seismic capacity of the heat exchanger.

### 3.2.3.4 Median Seismic Capacity

Recall that *median* seismic capacity $A_m$ is determined by

$$A_m = F_m \cdot A_{\text{RLE}}. \tag{3.2.20}$$

**Table 3.6** Median Capacities of Heat Exchanger from Potential Failure Modes

| Failure Mode | Median Capacities (kips) | |
|---|---|---|
| | **Shear** | **Tension** |
| **Anchorage failure** | | |
| anchor bolt steel | 23.26 | 34.89 |
| pullout | | 48.06 |
| concrete breakout and pryout | 240.0 | 120.0 |
| shear friction | 34.89 | |
| **Support base plate bending failure** | | 26.76 |
| **Fillet weld failure between base plate and saddle plate** | | 88.19 |

In this example, $A_{\mathrm{RLE}}$ is taken as $0.3g$ PGA. *Median factor of safety* $F_m$ is given by

$$F_m = F_{\mathrm{C},m} \cdot F_{\mathrm{RS},m} = F_\mu \cdot F_{\mathrm{S},m} \cdot F_{\mathrm{RS},m}. \tag{3.2.21}$$

Neglecting inelastic energy absorption effects, i.e., $F_\mu = 1.0$.

For the anchor bolts, horizontal peak response is unit median (Table 3-3, EPRI TR-103959, EPRI, 1994), foundation-soil interaction is not considered, and response spectrum analysis method is used to calculate peak response of heat exchanger, hence $F_{\mathrm{RS},m} = 1.0$ (see Section 3.1.2). Finally, equation (3.2.21) can be simplified as

$$F_m = F_{\mathrm{S},m} \cdot F_{\mathrm{RS},m} = F_{\mathrm{S},m}. \tag{3.2.22}$$

### Median Strength Factor

Since anchor bolts are subjected to tension and shear simultaneously, a tension-shear interaction relationship is required. Based on a large number of shear-tension test data, EPRI-NP-5228-SL (EPRI, 1991B) recommends a shear-tension-interaction formulation for expansion bolts and cast-in bolts. The results are plotted in terms of $N/N_m$ and $V/V_m$ in a bilinear form as shown in Figure 3.10, where $N_m$ and $V_m$ are the bolt tension and shear capacities in the absence of combined loading:

$$\frac{N}{N_m} = 1.0, \qquad \frac{V}{V_m} \leqslant 0.3, \tag{3.2.23a}$$

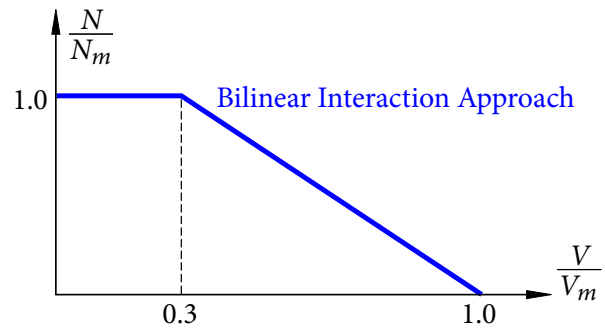


**Figure 3.10** Interaction relationship of tension and shear

$$0.7\,\frac{N}{N_m} + \frac{V}{V_m} = 1.0, \qquad 0.3 < \frac{V}{V_m} \leqslant 1.0. \tag{3.2.23b}$$

To determine the *median* strength factor $F_{S,m}$, two regions in Figure 3.10, i.e., pure tension region and shear/tension region are considered.

- Pure tension region

  The median strength factor is determined by equation (3.2.23a)

$$F_{S1,m} = \frac{C - D_{NS}}{D_S + \Delta C_S} = \frac{N_{min} - N_{DL}}{N_{Long}} = \frac{26.76 - (-6.11)}{5.28} = 6.22. \tag{3.2.24}$$

- Shear/Tension region

  The median strength factor is determined by equation (3.2.23b)

$$F_{S2,m} = \frac{C - D_{NS}}{D_S + \Delta C_S} = \frac{V_{ST} - 0.7\,\dfrac{V_{ST}}{N_{ST}}\,N_{DL}}{V_{Long} + 0.7\,\dfrac{V_{ST}}{N_{ST}}\,N_{Long}} = \frac{23.26 - 0.7 \times \frac{23.26}{34.89} \times (-6.11)}{11.58 + 0.7 \times \frac{23.26}{34.89} \times 5.28} = 1.86. \tag{3.2.25}$$

Since $F_{S2,m} < F_{S1,m}$, the controlling failure mode is shear-tension interaction failure of anchor bolts in longitudinal direction. Therefore, $F_{S,m} = F_{S2,m} = 1.86$.

### Median Seismic Capacity

Since $F_{S,m} = 1.86$, *median factor of safety* $F_m = F_{S,m} = 1.86$. Finally, *median* seismic capacity of heat exchanger is given by

$$A_m = F_m \cdot A_{RLE} = 1.86 \times 0.30g \text{ PGA} = 0.558\,g \text{ PGA}. \tag{3.2.26}$$

#### 3.2.3.5 Logarithmic Standard Deviations

Logarithmic standard deviations for basic response variables are taken in accordance EPRI-TR-103959 (EPRI, 1994). Logarithmic standard deviations of capacity variables are obtained from Table 3.2. It is noted that damping and frequency uncertainties need to be converted to be uncertainties on spectral accelerations at three frequencies.

- **Damping**

  Assume the median damping for horizontal heat exchanger is 5% and the damping at the $-1\sigma$ level is 3%. The uncertainty $\beta_U$ in ground response spectrum due to uncertainty in damping is obtained from the ground response spectra with $\zeta = 5\%$ and 3% damping values.

  - In longitudinal direction:

$$\beta_U = \frac{1}{|-1|} \ln \frac{\mathcal{S}_A(f = 8.15 \text{ Hz}, \zeta = 3\%)}{\mathcal{S}_A(f = 8.15 \text{ Hz}, \zeta = 5\%)} = \ln \frac{0.730g}{0.630g} = 0.15. \quad (3.2.27)$$

  - In transverse direction:

$$\beta_U = \frac{1}{|-1|} \ln \frac{\mathcal{S}_A(f = 25.4 \text{ Hz}, \zeta = 3\%)}{\mathcal{S}_A(f = 25.4 \text{ Hz}, \zeta = 5\%)} = \ln \frac{0.354g}{0.345g} = 0.03. \quad (3.2.28)$$

  - In vertical direction:

    Since $\mathcal{S}_A(f_V)$ returns to PGA, damping uncertainty in vertical direction has no effects on the response spectral acceleration value.

- **Frequency**

  - In longitudinal direction:

    The fundamental frequency of the heat exchanger in the longitudinal direction is $f_L = 8.15$ Hz, which is close to the plateau region of NUREG spectrum (see Figure 3.3). Therefore, the effect of variation of frequency on the response spectral acceleration value is negligible.

  - In transverse direction:

    Since $f_T = 25.4$ Hz in the transverse direction, the uncertainty $\beta_U$ in modal frequency is 0.10 for simple equipment models, according to EPRI-TR-103959 (EPRI, 1994). Around 25.4 Hz, spectral acceleration increases when frequency

decreases. Hence, at the $-1\sigma$ level, the frequency is $25.4 \cdot e^{-0.10} = 22.98$ Hz. Therefore, the uncertainty $\beta_U$ in spectral acceleration in the transverse direction due to modal frequency variation is

$$\beta_U = \frac{1}{|-1|} \ln \frac{\mathcal{S}_A(f = 22.98 \text{ Hz}, \zeta = 5\%)}{\mathcal{S}_A(f = 25.4 \text{ Hz}, \zeta = 5\%)} = \ln \frac{0.363g}{0.344g} = 0.05. \quad (3.2.29)$$

- In vertical direction:
  Since spectral acceleration around $f_V = 50$ Hz returns to PGA, frequency uncertainty in vertical direction has no effects on $\mathcal{S}_A(f_V)$.

Table 3.7 (the third and fourth columns) enumerates the logarithmic standard deviations for all basic variables. The *approximate second-moment procedure* (see Section 1.2) is applied to calculate variability of $F$ due to basic variables. The variability of $F$ due to damping uncertainty is taken as an example. Spectral accelerations in the longitudinal and transverse directions become

$$a_L = S_a(f_L)\, e^{0.15} = 0.630g \times e^{0.15} = 0.730g,$$
$$a_T = S_a(f_T)\, e^{0.03} = 0.345g \times e^{0.02} = 0.354g.$$

Spectral acceleration in the vertical direction is kept at $0.2g$. Afterwards, seismic demand analysis is performed (see Section 3.2.3.2). The combined seismic demand in longitudinal direction (controlling direction) is given by

$$N_{\text{Long}} = 5.78 \text{ kips}, \qquad V_{\text{Long}} = 13.42 \text{ kips}. \quad (3.2.30)$$

The median strength factor is then given by

$$F_{S,m} = \frac{C - D_{NS}}{D_S + \Delta C_S} = \frac{V_{ST} - 0.7 \dfrac{V_{ST}}{N_{ST}} N_{DL}}{V_{\text{Long}} + 0.7 \dfrac{V_{ST}}{N_{ST}} N_{\text{Long}}} = \frac{23.26 - 0.7 \times \frac{23.26}{34.89} \times (-6.11)}{13.42 + 0.7 \times \frac{23.26}{34.89} \times 5.78} = 1.62. \quad (3.2.31)$$

Therefore, *factor of safety* $F_{1\sigma}$ can be determined by

$$F_{1\sigma} = F_\mu \cdot F_{RS,m} \cdot F_{S,m} = 1.0 \times 1.0 \times 1.62 = 1.62. \quad (3.2.32)$$

Finally, the variability of $F$ due to damping uncertainty is calculated by

$$\beta = \frac{1}{|+1|} \ln\left(\frac{F_m}{F_{1\sigma}}\right) = \ln\frac{1.86}{1.62} = 0.14. \tag{3.2.33}$$

One can repeat above procedure to calculate the variability of $F$ due to all other basic variables, as shown in Table 3.7 (the sixth and seventh columns). Square-root-of-sum-of-squares (SRSS) rule is used to calculate $\beta_R$ of total *randomness* and $\beta_U$ of total *uncertainty* from basic variables. $\beta_C$ of composite variability is then determined by

$$\beta_C = \sqrt{\beta_R^2 + \beta_U^2}. \tag{3.2.34}$$

### 3.2.3.6 Seismic Fragility Curves and HCLPF Seismic Capacity

Having obtained *median* seismic capacity $A_m$ and its variability, seismic fragility can be determined by equation (3.1.7). When composite (mean) seismic fragility is required, equation (3.1.8) would be used. Seismic fragility curves of the heat exchanger are shown in Figure 3.11.

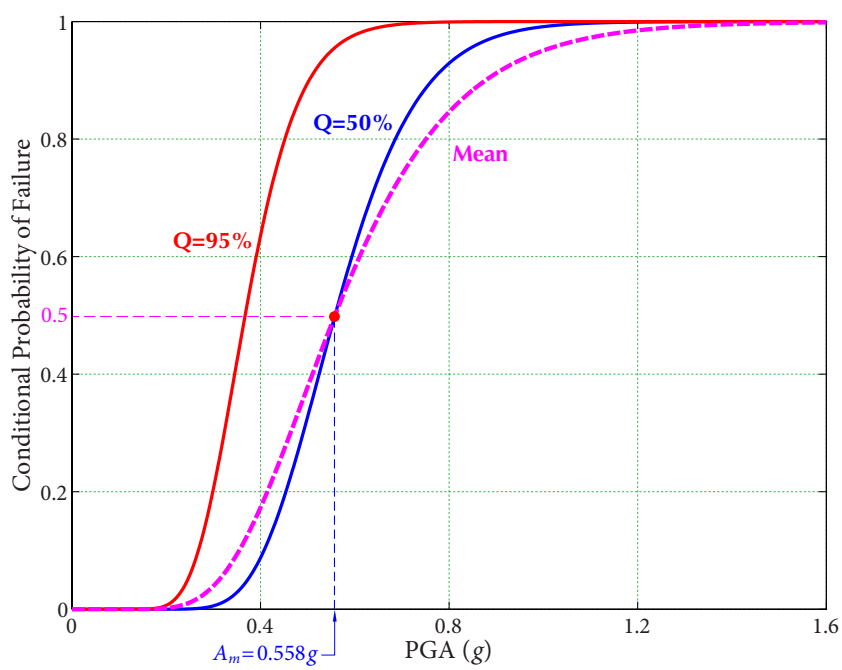


**Figure 3.11** Seismic fragility curves of heat exchanger under NUREG spectrum at 0.3$g$ PGA

**Table 3.7** The Variability of $F$ from Response and Capacity Variables

| Case | **Variable** | *Randomness* | *Uncertainty* | $F$ | $\beta$ | |
|---|---|---|---|---|---|---|
| 0 | **Base Case** | Variable at median | | 1.86 | | |
| | **Response Variables** | Variable at median plus $1\sigma$ | | $F_{1\sigma}$ | $\beta_R$ | $\beta_U$ |
| 1 | Earthquake response spectrum shape anchored to PGA | $\mathcal{S}_A(f_L)\,e^{0.20}$<br>$\mathcal{S}_A(f_T)\,e^{0.20}$ | $\mathcal{S}_A(f_L)\,e^{0.19}$<br>$\mathcal{S}_A(f_T)\,e^{0.19}$ | 1.53 | 0.20 | 0.19 |
| 2 | Horizontal direction peak response | $\mathcal{S}_A(f_L)\,e^{0.13}$<br>$\mathcal{S}_A(f_T)\,e^{-0.13}$ | | 1.66 | 0.11 | |
| 3 | Vertical component response | $\mathcal{S}_A(f_V)\,e^{0.34}$ | | 1.85 | 0.01 | |
| 4 | Damping | | $\mathcal{S}_A(f_L)\,e^{0.15}$<br>$\mathcal{S}_A(f_T)\,e^{0.03}$ | 1.62 | | 0.14 |
| 5 | Frequency | $\mathcal{S}_A(f_T)\,e^{0.05}$ | | 1.85 | 0.0 | |
| 6 | Modal shape | | $\mathcal{S}_A(f_L)\,e^{0.05}$<br>$\mathcal{S}_A(f_T)\,e^{0.05}$ | 1.77 | | 0.05 |
| 7 | Modal combination | | $\mathcal{S}_A(f_L)\,e^{0.05}$<br>$\mathcal{S}_A(f_T)\,e^{0.05}$ | 1.77 | | 0.05 |
| 8 | Earthquake component combination | Abs. Sum at $2.3\sigma$ | | 1.72 | 0.08 | |
| | **Capacity Variable** | Variable at median minus $1\sigma$ | | $F_{-1\sigma}$ | $\beta_R$ | $\beta_U$ |
| 9 | Anchor bolts | | $V_{ST}\,e^{-0.10}$<br>$N_{ST}\,e^{-0.13}$ | 1.70 | | 0.09 |
| | **SRSS Combination** | | | | $\beta_R$ | $\beta_U$ |
| | | | | | 0.245 | 0.254 |
| | | | | $\beta_C$ | 0.353 | |

In addition, one can obtain HCLPF seismic capacity of the heat exchanger as

$$C_{\text{HCLPF}} = A_m\, e^{(\beta_R+\beta_U)\,\Phi^{-1}(0.05)} = 0.558 \times e^{-1.6449\,(0.245+0.254)} = 0.245g\ \text{PGA}. \quad (3.2.35)$$

### 3.2.4 Case 1: Influence of Spectral Shape – Site-specific UHS is RLE

#### Median Seismic Demand

Site-specific UHS anchoring to $0.3g$ PGA is chosen as RLE and defined as horizontal input ground response spectra (GRS). The vertical input GRS can be obtained using V/H ratios given in Table 3.8 (AMEC, 2009). Given $f_V = 50$ Hz, one can obtain $V/H = 0.865$ by linear interpolation in logarithmic scale between 40 Hz and 62.5 Hz; hence spectral acceleration in vertical direction $\mathcal{S}_A(f_V) = 0.3 \times 0.865 = 0.259g$. Table 3.9 summarizes spectral accelerations at three frequencies of the heat exchanger.

**Table 3.8** V/H Ratios at Frequency Range of Engineering Interest

| Frequency (Hz) | 0.25 | 1 | 2.5 | 10 | 25 | 40 | 62.5 | 100 |
|---|---|---|---|---|---|---|---|---|
| V/H Ratio | 0.68 | 0.67 | 0.67 | 0.67 | 0.76 | 0.85 | 0.88 | 0.78 |

**Table 3.9** Spectral Values at Three Frequencies from UHS

| **Direction** | **Frequency (Hz)** | $\mathcal{S}_A\ (g)$ |
|---|---|---|
| Longitudinal | 8.15 | 0.530 |
| Transverse | 25.4 | 0.426 |
| Vertical | 50 | $0.865 \times 0.30 = 0.259$ |

The tension and shear demand of the heat exchanger are summarized in Table 3.10.

**Table 3.10** Median Tension and Shear Demand of Heat Exchanger under Site-specific UHS at $0.3g$ PGA

| **Controlling Direction** | **Shear Force (kips)** | **Tension Force (kips)** |
|---|---|---|
| Longitudinal | 9.77 | 5.47 |
| Transverse | 4.68 | 7.82 |

### Median Seismic Capacity

It is found that shear-tension interaction failure of anchor bolts in longitudinal direction is the controlling failure mode. *Median* strength factor $F_{S,m}$ is then given by

$$F_{S,m} = \frac{C - D_{NS}}{D_S + \Delta C_S} = \frac{V_{ST} - 0.7\,\dfrac{V_{ST}}{N_{ST}}\,N_{DL}}{V_{Long} + 0.7\,\dfrac{V_{ST}}{N_{ST}}\,N_{Long}} = \frac{23.26 - 0.7 \times \frac{23.26}{34.89} \times (-6.11)}{9.77 + 0.7 \times \frac{23.26}{34.89} \times 5.47} = 2.12. \tag{3.2.36}$$

Therefore, *median factor of safety* $F_m = F_{S,m} = 2.12$.

*Median* seismic capacity of the heat exchanger is then given by

$$A_m = F_m \cdot A_{RLE} = 2.12 \times 0.30g \text{ PGA} = 0.636g \text{ PGA}. \tag{3.2.37}$$

Compared to $A_m$ of $0.558g$ PGA using NUREG spectrum as RLE, $A_m$ using UHS as RLE has 13.9% increase.

### Logarithmic Standard Deviations

The procedure is almost the same as that in Section 3.2.3.5. Since site-specific UHS is chosen as RLE, there is not earthquake response spectrum shape variability. The logarithmic standard deviations in *factor of safety F* contributed from basic variables are presented in Table 3.11.

### Seismic Fragility Curves

Having obtained $A_m$, $\beta_R$, and $\beta_U$, seismic fragility curves in terms of PGA are determined and shown in Figures 3.7 and 3.8.

In addition, HCLPF seismic capacity of the heat exchanger is determined by

$$C_{HCLPF} = A_m\, e^{(\beta_R + \beta_U)\,\Phi^{-1}(0.05)} = 0.636 \times e^{-1.6449\,(0.158 + 0.204)} = 0.349g \text{ PGA}. \tag{3.2.38}$$

Compared to $C_{HCLPF}$ of $0.245g$ PGA using NUREG spectrum as RLE, $C_{HCLPF}$ using UHS as RLE has 41.9% increase.

**Table 3.11** The Variability of $F$ from Response and Capacity Variables

| Case | **Variable** | *Randomness* | *Uncertainty* | $F$ | $\beta$ | |
|---|---|---|---|---|---|---|
| 0 | **Base Case** | Variable at median | | 2.12 | | |
| | **Response Variables** | Variable at median plus $1\sigma$ | | $F_{1\sigma}$ | $\beta_R$ | $\beta_U$ |
| 1 | Horizontal direction peak response | $\mathcal{S}_A(f_L)\,e^{0.13}$<br>$\mathcal{S}_A(f_T)\,e^{-0.13}$ | | 1.91 | 0.10 | |
| 2 | Vertical component response | $\mathcal{S}_A(f_V)\,e^{0.34}$ | | 2.10 | 0.01 | |
| 3 | Damping | | $\mathcal{S}_A(f_L)\,e^{0.17}$<br>$\mathcal{S}_A(f_T)\,e^{0.16}$ | 1.79 | | 0.17 |
| 4 | Frequency | | $\mathcal{S}_A(f_L)\,e^{0.05}$<br>$\mathcal{S}_A(f_T)\,e^{0.05}$ | 2.02 | | 0.05 |
| 5 | Modal shape | | $\mathcal{S}_A(f_L)\,e^{0.05}$<br>$\mathcal{S}_A(f_T)\,e^{0.05}$ | 2.02 | | 0.05 |
| 6 | Modal combination | | $\mathcal{S}_A(f_L)\,e^{0.05}$<br>$\mathcal{S}_A(f_T)\,e^{0.05}$ | 2.02 | | 0.05 |
| 7 | Earthquake component combination | Abs. Sum<br>at $2.3\sigma$ | | 1.90 | 0.11 | |
| | **Capacity Variable** | Variable at median minus $1\sigma$ | | $F_{-1\sigma}$ | $\beta_R$ | $\beta_U$ |
| 8 | Anchor bolts | | $V_{ST}\,e^{-0.10}$<br>$N_{ST}\,e^{-0.13}$ | 1.93 | | 0.09 |
| | **SRSS Combination** | | | | $\beta_R$ | $\beta_U$ |
| | | | | | 0.158 | 0.204 |
| | | | | $\beta_C$ | 0.258 | |

## Comparison of NUREG spectrum and Site-specific UHS

Seismic fragility curves based on NUREG spectrum are also plotted in Figures 3.7 and 3.8. The results show that spectral shape of RLE has significant influence on HCLPF seismic capacity estimate of the heat exchanger.

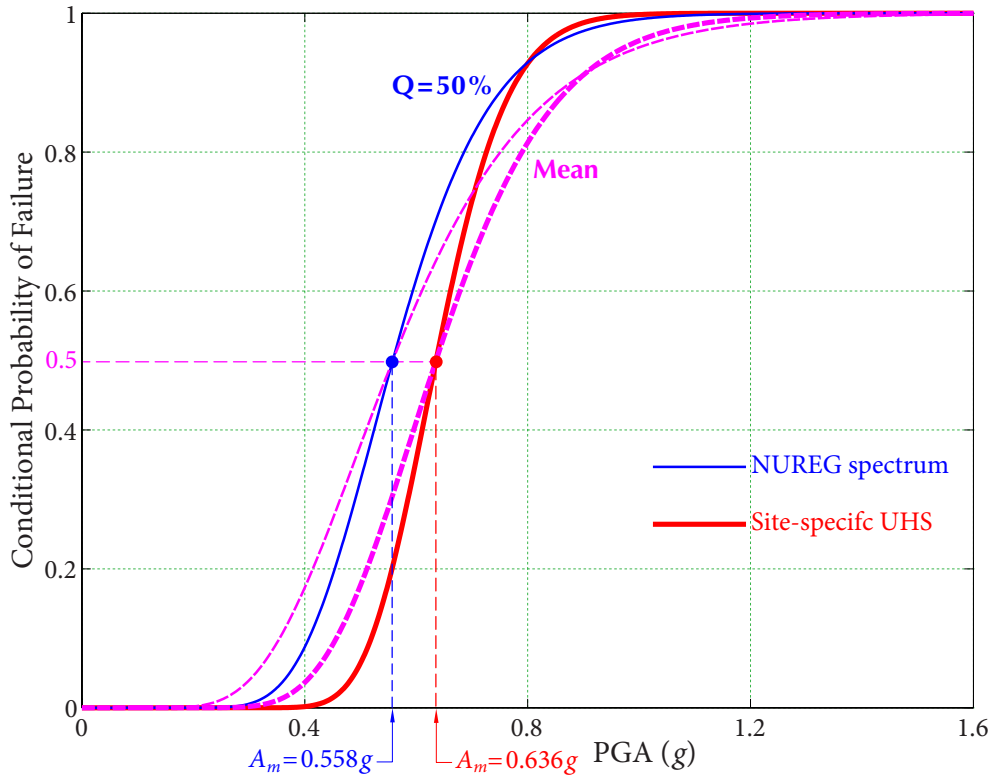


**Figure 3.12** Seismic fragility curves of heat exchanger based on NUREG spectrum and UHS

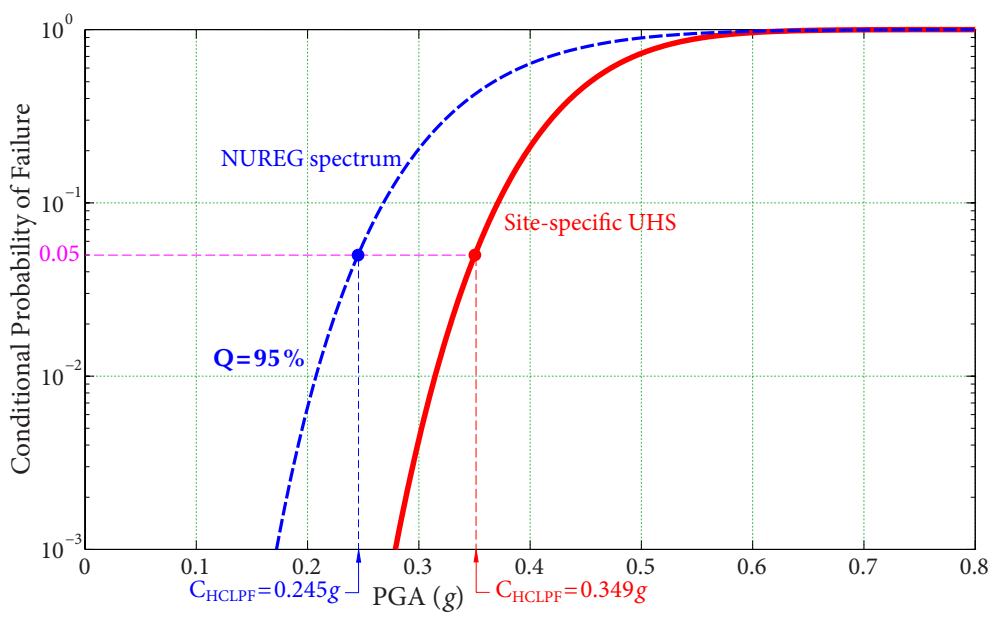


**Figure 3.13** HCLPF seismic capacity of heat exchanger based on NUREG spectrum and UHS

Two sources contribute to the significant increase in $C_{\text{HCLPF}}$:

1. NUREG spectrum is much higher in low and intermediate frequencies, i.e., $f \leqslant 10$ Hz. Since $f_{\text{L}} = 8.15$ Hz lies in this range, it leads to overestimation of *median* seismic demand thus underestimation of $A_m$, i.e., $0.558g$ PGA (obtained from NUREG spectrum) compared to $0.636g$ PGA (based on UHS).
2. Earthquake response spectrum shape variability of NUREG spectrum is given by (Table 3.7)

$$\beta = \sqrt{\beta_R^2 + \beta_U^2} = \sqrt{0.2^2 + 0.19^2} = 0.28. \tag{3.2.39}$$

However, there is no response spectrum shape variability in site-specific UHS.
As a result, $\beta_{\text{C}}$ of composite variability is significantly reduced, i.e., 0.258 (obtained from UHS) compared to 0.35 (based on NUREG spectrum).

In nuclear power industry, HCLPF seismic capacities are usually used to represent seismic capacities of safety-related structures, systems, and components (SSCs). Therefore, accurate HCLPF seismic capacity estimates of safety-related SSCs are important in evaluating plant HCLPF seismic capacity. Spectral shapes of UHS at the sites in eastern North America (ENA) are similar to that of UHS at Darlington nuclear generating station (NGS). Based on seismic fragility results in this case study, using NUREG spectrum as RLE would not give accurate HCLPF seismic capacities of safety-related SSCs in this region. Therefore, for nuclear power plants (NPPs) in the ENA, site-specific UHS should be defined as RLE.

### 3.2.5 Case 2: Influence of Use of GMP – $\bar{\mathcal{S}}_{\text{A}}$ is GMP

PGA and average spectral acceleration $\bar{\mathcal{S}}_{\text{A}}$ between 5 and 10 Hz are taken as GMPs separately to study the influence of use of GMP on seismic capacity estimate of the heat exchanger. In Section 3.2.3, NUREG spectrum anchoring to PGA at $0.3g$ is taken as RLE. In this Section, NUREG spectrum anchoring to $\bar{\mathcal{S}}_{\text{A}}$ at $0.5g$ is taken as RLE.

#### Median Seismic Demand

Recall that in equation (3.2.1), $\bar{\mathcal{S}}_{\text{A}} = 0.5g$ is obtained from site-specific UHS. NUREG spectrum has a plateau between 2.2 and 8 Hz, thus NUREG spectrum with the plateau

anchoring to $\bar{\mathcal{S}}_A$ is defined as horizontal seismic input. The vertical seismic input is assumed to be 2/3 of the horizontal input over the entire frequency range.

Based on horizontal and vertical seismic inputs, spectral accelerations are determined and presented in Table 3.12.

**Table 3.12** Spectral Values at Frequencies in Three Directions under NUREG Spectrum at $0.5g\ \bar{\mathcal{S}}_A$

| **Direction** | **Frequency (Hz)** | $\mathcal{S}_A\ (g)$ |
|---|---|---|
| Longitudinal | 8.15 | 0.5 |
| Transverse | 25.4 | 0.271 |
| Vertical | 50 | $\frac{2}{3} \times 0.236 = 0.157$ |

The tension and shear demand of the heat exchanger are summarized in Table 3.13.

**Table 3.13** Median Tension and Shear Demand of Heat Exchanger under NUREG Spectrum at $0.5g\ \bar{\mathcal{S}}_A$

| **Controlling Direction** | **Shear Force (kips)** | **Tension Force (kips)** |
|---|---|---|
| Longitudinal | 9.19 | 4.17 |
| Transverse | 4.02 | 5.24 |

## Median Seismic Capacity

*Median* strength factor $F_{S,m}$ from the controlling failure mode, i.e., shear-tension interaction failure in longitudinal direction, is calculated as

$$F_{S,m} = \frac{C - D_{NS}}{D_S + \Delta C_S} = \frac{V_{ST} - 0.7\,\dfrac{V_{ST}}{N_{ST}}\,N_{DL}}{V_{Long} + 0.7\,\dfrac{V_{ST}}{N_{ST}}\,N_{Long}} = \frac{23.26 - 0.7 \times \frac{23.26}{34.89} \times (-6.11)}{9.19 + 0.7 \times \frac{23.26}{34.89} \times 4.17} = 2.366. \tag{3.2.40}$$

Therefore, *median factor of safety* $F_m = F_{S,m} = 2.366$.

*Median* seismic capacity of the heat exchanger is then given by

$$A_m = F_m \cdot A_{RLE} = 2.366 \times 0.5g\ \bar{\mathcal{S}}_A = 1.183g\ \bar{\mathcal{S}}_A. \tag{3.2.41}$$

## Logarithmic Standard Deviations

Since $\bar{\mathcal{S}}_A$ is chosen as GMP, earthquake response spectrum variability is reduced. Table 3.14 enumerates logarithmic standard deviations in $F$ contributed from basic variables.

**Table 3.14** The Variability of $F$ from Response and Capacity Variables

| Case | **Variable** | *Randomness* | *Uncertainty* | $F$ | $\beta$ | |
|---|---|---|---|---|---|---|
| 0 | **Base Case** | Variable at median | | 2.37 | | |
| | **Response Variables** | Variable at median plus $1\sigma$ | | $F_{1\sigma}$ | $\beta_R$ | $\beta_U$ |
| 1 | Earthquake response spectrum shape anchored to $\bar{\mathcal{S}}_A$ | $\mathcal{S}_A(f_L)\,e^{0.20}$<br>$\mathcal{S}_A(f_T)\,e^{0.20}$ | $\mathcal{S}_A(f_L)\,e^{0.0}$<br>$\mathcal{S}_A(f_T)\,e^{0.12}$ | 1.94 | 0.20 | 0.01 |
| 2 | Horizontal direction peak response | $\mathcal{S}_A(f_L)\,e^{0.13}$<br>$\mathcal{S}_A(f_T)\,e^{-0.13}$ | | 2.12 | 0.11 | |
| 3 | Vertical component response | $\mathcal{S}_A(f_V)\,e^{0.34}$ | | 2.35 | 0.01 | |
| 4 | Damping | | $\mathcal{S}_A(f_L)\,e^{0.15}$<br>$\mathcal{S}_A(f_T)\,e^{0.03}$ | 2.06 | | 0.14 |
| 5 | Frequency | $\mathcal{S}_A(f_T)\,e^{0.05}$ | | 2.36 | 0.0 | |
| 6 | Modal shape | | $\mathcal{S}_A(f_L)\,e^{0.05}$<br>$\mathcal{S}_A(f_T)\,e^{0.05}$ | 2.25 | | 0.05 |
| 7 | Modal combination | | $\mathcal{S}_A(f_L)\,e^{0.05}$<br>$\mathcal{S}_A(f_T)\,e^{0.05}$ | 2.25 | | 0.05 |
| 8 | Earthquake component combination | Abs. Sum at $2.3\sigma$ | | 2.18 | 0.08 | |
| | **Capacity Variable** | Variable at median minus $1\sigma$ | | $F_{-1\sigma}$ | $\beta_R$ | $\beta_U$ |
| 9 | Anchor bolts | | $V_{ST}\,e^{-0.10}$<br>$N_{ST}\,e^{-0.13}$ | 2.16 | | 0.09 |
| | **SRSS Combination** | | | | $\beta_R$ | $\beta_U$ |
| | | | | | 0.245 | 0.172 |
| | | | | $\beta_C$ | 0.30 | |

### Seismic Fragility Curves

Having obtained *median* seismic capacity $A_m$ and logarithmic standard deviations $\beta_R$ and $\beta_U$, seismic fragility curves in terms of $\bar{\mathcal{S}}_{\mathrm{A}}$ are plotted in Figure 3.14.

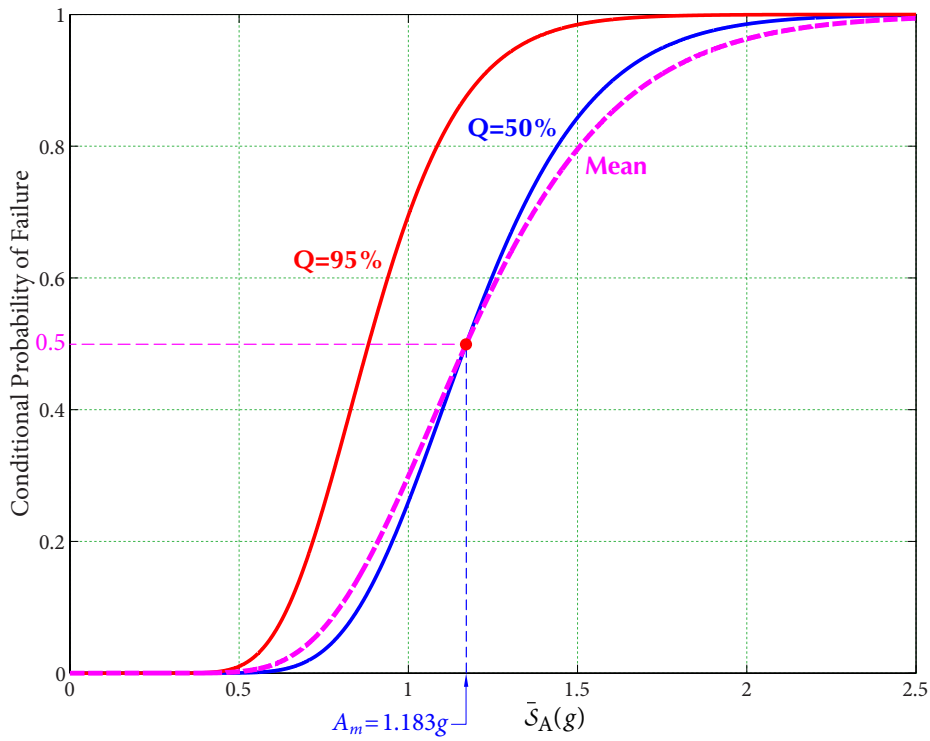


**Figure 3.14** Seismic fragility curves in terms of $\bar{\mathcal{S}}_{\mathrm{A}}$ under NUREG spectrum

In addition, HCLPF seismic capacity in terms of $\bar{\mathcal{S}}_{\mathrm{A}}$ is obtained as

$$C_{\mathrm{HCLPF}} = A_m\, \mathrm{e}^{(\beta_R+\beta_U)\,\Phi^{-1}(0.05)} = 1.183 \times \mathrm{e}^{-1.6449\,(0.245+0.172)} = 0.595\,g\,\bar{\mathcal{S}}_{\mathrm{A}}. \tag{3.2.42}$$

Recalling that the ratio of spectral acceleration at the plateau to PGA is 2.12 from NUREG spectrum, indicating that equivalent HCLPF seismic capacity in terms of PGA is given by

$$C_{\mathrm{HCLPF}} = \frac{0.595}{2.12}\,g\,\mathrm{PGA} = 0.281\,g\,\mathrm{PGA}. \tag{3.2.43}$$

Compared to HCLPF seismic capacity of $0.245g$ using PGA as GMP, choosing $\bar{\mathcal{S}}_{\mathrm{A}}$ as GMP has a 14.6% increase.

### Comparison of NUREG Spectrum Anchoring to PGA and $\bar{\mathcal{S}}_{\mathrm{A}}$

The seismic fragility results show that use of GMP has noticeable effect on HCLPF seismic capacity estimate of the heat exchanger. This is mainly because earthquake response spectrum shape uncertainty in $\mathcal{S}_{\mathrm{A}}(f_{\mathrm{L}})$ is removed when $\bar{\mathcal{S}}_{\mathrm{A}}$ is taken as GMP (see Table 3.14). As a result, $\beta_U$ of total epistemic *uncertainty* in $F$ has a remarkable reduction, i.e., 0.172 ($\bar{\mathcal{S}}_{\mathrm{A}}$ is GMP) compared to 0.254 (PGA is GMP).

In nuclear power plants, fundamental frequencies of most of safety-related structures, systems, and components (SSCs) are located in frequency range between 2 and 10 Hz. Choosing PGA as GMP will introduce large earthquake response spectrum shape uncertainty. Therefore, to reduce this uncertainty, average spectral acceleration $\bar{\mathcal{S}}_{\mathrm{A}}$ should be chosen as GMP. Here $\bar{\mathcal{S}}_{\mathrm{A}}$ instead of spectral accelerations at the fundamental frequencies of SSCs is chosen as GMP, because in Seismic Probabilistic Risk Analysis and Seismic Margin Assessment, a single GMP is used. Choosing $\bar{\mathcal{S}}_{\mathrm{A}}$ as GMP ensures that GMP is consistent in seismic fragility analysis for different safety-related SSCs.

## 3.3 Summary

In this Chapter, current seismic fragility analysis method is introduced first. Numerical example for a horizontal heat exchanger is performed to investigate the influences of spectral shape of Review Level Earthquake (RLE) and use of ground motion parameter (GMP). The results show that both spectral shape and GMP have remarkable effect in estimating High Confidence and Low Probability of Failure seismic capacity of the heat exchanger.

Based on current seismic fragility analysis method, in order to obtain more accurate HCLPF seismic capacities of safety-related structures, systems, and components, two recommendations are presented:

- for nuclear power plants in eastern North America, site-specific uniform hazard spectrum should be defined as RLE;
- when a generic ground response spectrum is chosen as RLE, average spectral acceleration $\bar{S}_A$ between 5 and 10 Hz should be taken as GMP.

Nevertheless, the recommendations cannot completely resolves the problems in current method. Due to inherent variability in earthquake motions, a single GMP is not sufficient to characterize earthquake response spectra. In addition, ground motion intensity effect cannot be incorporated into current method. To resolve these problems, vector-valued GMPs (VGMPs) should be introduced to quantify seismic capacities of safety-related structures, systems, and components.

C H A P T E R 4

# Weighting Seismic Fragility Analysis

In this Chapter, weighting seismic fragility analysis method is firstly proposed. Vector-valued ground motion parameters (VGMPs) are used to characterize earthquake response spectra, aiming to obtain more accurate seismic capacities of safety-related structures, systems, and components. Weighting seismic fragility curves and High Confidence and Low Probability of Failure seismic capacities are represented by a single GMP such as PGA, hence they are readily incorporated into Seismic Probabilistic Risk Analysis and Seismic Margin Assessment. Therefore, the proposed method is beneficial and applicable for determining more reliable plant seismic capacity.

To illustrate the procedure of the proposed method and demonstrate its advantages, numerical example for a horizontal heat exchanger in Darlington nuclear generating station is performed. The results show that the proposed method can provide more reliable seismic capacity estimate and more accurate mean annual frequency of occurrence of failure estimate.

## 4.1 Seismic Probabilistic Risk Analysis considering VGMPs

In current seismic fragility analysis, Review Level Earthquake anchoring to a single ground motion parameter (GMP) at a specified screening level is defined as seismic input. The consequential problems are demonstrated in Chapter 3.

In nuclear power industry, seismic capacities are usually used to represent structural capabilities withstanding potential earthquakes at the site of interest. The uncertainties in seismic capacity estimates of safety-related structures, systems, and components (SSCs) are contributed from two sources, i.e., structural capacity and structural response. Engineering practice has recognized that, ground motion uncertainty contributes significantly to structural response uncertainty. Comparing to structural capacity uncertainty and other basic response uncertainties, ground motion uncertainty is more likely to be reduced.

It is well known, from elastic structural dynamic analyses, structural responses under earthquake excitations primarily depend on spectral accelerations at its dominant frequencies. In existing nuclear power plants, dominant frequencies of most safety-related SSCs lie in the frequency range between 2 and 10 Hz. By choosing spectral accelerations at dominant frequencies and commonly used PGA as vector-valued GMPs (VGMPs), ground motion uncertainty is effectively reduced.

In two-dimensional case, spectral acceleration at the first dominant frequency of a safety-related SSC and PGA are chosen as VGMPs. In this study, $\mathcal{S}_{\mathrm{A}}(f_1 = 50\,\mathrm{Hz})$ is taken as PGA. The probability of failure of the SSC due to an earthquake with magnitude above the lower bound (e.g. $m = 4.75$) is determined by total probability formula, i.e.,

$$p = \int_0^\infty \int_0^\infty p_{\mathrm{F}}(s_1, s_2) \cdot f_{\mathcal{S}_{\mathrm{A}}(f_1), \mathcal{S}_{\mathrm{A}}(f_2)}\left(s_1, s_2\right) \mathrm{d}s_1 \mathrm{d}s_2, \tag{4.1.1}$$

where $p_{\mathrm{F}}(s_1, s_2)$ is the seismic fragility in terms of VGMPs. This thesis firstly proposes seismic fragility analysis considering VGMPs method to calculate $p_{\mathrm{F}}(s_1, s_2)$. $f_{\mathcal{S}_{\mathrm{A}}(f_1), \mathcal{S}_{\mathrm{A}}(f_2)}\left(s_1, s_2\right)$ is the joint probability density function of VGMPs, which is determined by vector-valued Probabilistic Seismic Hazard Analysis (VPSHA) (see Chapter 2).

$f_{\mathcal{S}_{\mathrm{A}}(f_1), \mathcal{S}_{\mathrm{A}}(f_2)}\left(s_1, s_2\right)$ can be rewritten in conditional form as

$$f_{\mathcal{S}_{\mathrm{A}}(f_1), \mathcal{S}_{\mathrm{A}}(f_2)}\left(s_1, s_2\right) = f_{\mathcal{S}_{\mathrm{A}}(f_2) | \mathcal{S}_{\mathrm{A}}(f_1)}\left(s_2 \,|\, s_1\right) \cdot f_{\mathcal{S}_{\mathrm{A}}(f_1)}\left(s_1\right). \tag{4.1.2}$$

Combining equations (4.1.1) and (4.1.2) gives probability of failure:

$$\begin{aligned} p &= \int_0^\infty \int_0^\infty p_{\mathrm{F}}(s_1, s_2) \cdot \left[ f_{\mathcal{S}_{\mathrm{A}}(f_2) | \mathcal{S}_{\mathrm{A}}(f_1)}\left(s_2 \,|\, s_1\right) \cdot f_{\mathcal{S}_{\mathrm{A}}(f_1)}\left(s_1\right) \right] \mathrm{d}s_1 \mathrm{d}s_2 \\ &= \int_0^\infty \left\{ \int_0^\infty p_{\mathrm{F}}(s_1, s_2) \cdot f_{\mathcal{S}_{\mathrm{A}}(f_2) | \mathcal{S}_{\mathrm{A}}(f_1)}\left(s_2 \,|\, s_1\right) \mathrm{d}s_2 \right\} f_{\mathcal{S}_{\mathrm{A}}(f_1)}\left(s_1\right) \mathrm{d}s_1. \end{aligned} \tag{4.1.3}$$

The integral in the big parentheses of equation (4.1.3) is defined as weighting seismic fragility:

$$\bar{p}_{\mathrm{F}}(s_1) = \int_0^{\infty} p_{\mathrm{F}}(s_1, s_2) \cdot f_{\mathcal{S}_{\mathrm{A}}(f_2)|\mathcal{S}_{\mathrm{A}}(f_1)}\left(s_2 \,\middle|\, s_1\right) \mathrm{d}s_2. \tag{4.1.4}$$

"Weighting" indicates that seismic fragilities given input ground response spectra with spectral values $s_2$ at $\mathcal{S}_{\mathrm{A}}(f_1) = s_1$ are weighted according to their probability of occurrences. $f_{\mathcal{S}_{\mathrm{A}}(f_2)|\mathcal{S}_{\mathrm{A}}(f_1)}\left(s_2 \,\middle|\, s_1\right)$ is probability density function of $\left\{\mathcal{S}_{\mathrm{A}}(f_2) \,\middle|\, \mathcal{S}_{\mathrm{A}}(f_1)\right\}$, which is determined by VPSHA.

Therefore, annual frequency of occurrence of the failure of the SSC is determined by

$$\gamma = \nu \cdot p = \int_0^{\infty} \bar{p}_{\mathrm{F}}(s_1) \left[\nu \cdot f_{\mathcal{S}_{\mathrm{A}}(f_1)}(s_1)\right] \mathrm{d}s_1 = -\int_0^{\infty} \bar{p}_{\mathrm{F}}(s_1) \frac{\mathrm{d}H(s_1)}{\mathrm{d}s_1} \mathrm{d}s_1, \tag{4.1.5}$$

where $\nu$ is annual rate of occurrence of earthquake above the lower bound magnitude, and $H(s_1)$ is seismic hazard at the site of interest. $H(s_1)$ is obtained from PSHA.

To determine annual rate of occurrence of an adverse consequence (e.g. core damage accident), $\bar{p}_{\mathrm{F}}(s_1)$ of SSCs need to be propagated to plant damage state seismic fragility by means of system analysis (see Chapter 1).

### Discussions and Recommendations

It needs to make clear that the number of VGMPs can be extended to higher dimensions. However, in engineering applications, computational cost and accuracy should be balanced. When an SSC is first several mode dominant, two GMPs, i.e., spectral acceleration at the first dominant mode and PGA, can be chosen as VGMPs. Since weighting seismic fragility is represented by PGA, thus it is readily incorporated into Seismic Probabilistic Risk Analysis while preserves the benefits of the use of VGMPs.

Engineering practice has recognized that, "weak link" SSCs contribute significantly to plant seismic capacity and seismic risk estimates. Therefore, in engineering applications, weighting seismic fragility analysis method can be performed to calculate seismic capacities of "weak link" components, while current seismic fragility analysis method is conducted to determined seismic capacities of less important SSCs. This ensures that plant seismic capacity and seismic risk estimates are more accurate, while computational cost is acceptable.

## 4.2 Methodology of Weighting Seismic Fragility Analysis

In two-dimensional case, weighting seismic fragility with respect to $\mathcal{S}_A(f_1)$ is obtained as

$$\bar{p}_F(s_1) = \int_0^{\infty} p_F(s_1, s_2) \cdot f_{\mathcal{S}_A(f_2)|\mathcal{S}_A(f_1)}(s_2 \,|\, s_1)\, \mathrm{d}s_2. \tag{4.2.1}$$

In applications, $\mathcal{S}_A(f_1)$ and $\mathcal{S}_A(f_2)$ are usually truncated at lower bounds (e.g. $0.05g$) and upper bounds (e.g. $5g$). Numerical method is applied to calculate the integral in equation (4.2.1) by

$$\bar{p}_F(s_1) = \sum_{i_2=1}^{N_2} \left[ p_F\left(s_1, s_2^{(i_2)}\right) \cdot w\left(s_2^{(i_2)} \leqslant s_2 < s_2^{(i_2+1)} \,\middle|\, s_1\right) \right], \tag{4.2.2}$$

where $N_2$ is the number of intervals of $\mathcal{S}_A(f_2)$ and $w\left(s_2^{(i_2)} \leqslant s_2 < s_2^{(i_2+1)} \,\middle|\, s_1\right)$ is the weight of input ground response spectrum (GRS) with spectral value $s_2^{(i_2)}$ at $\mathcal{S}_A(f_1) = s_1$.

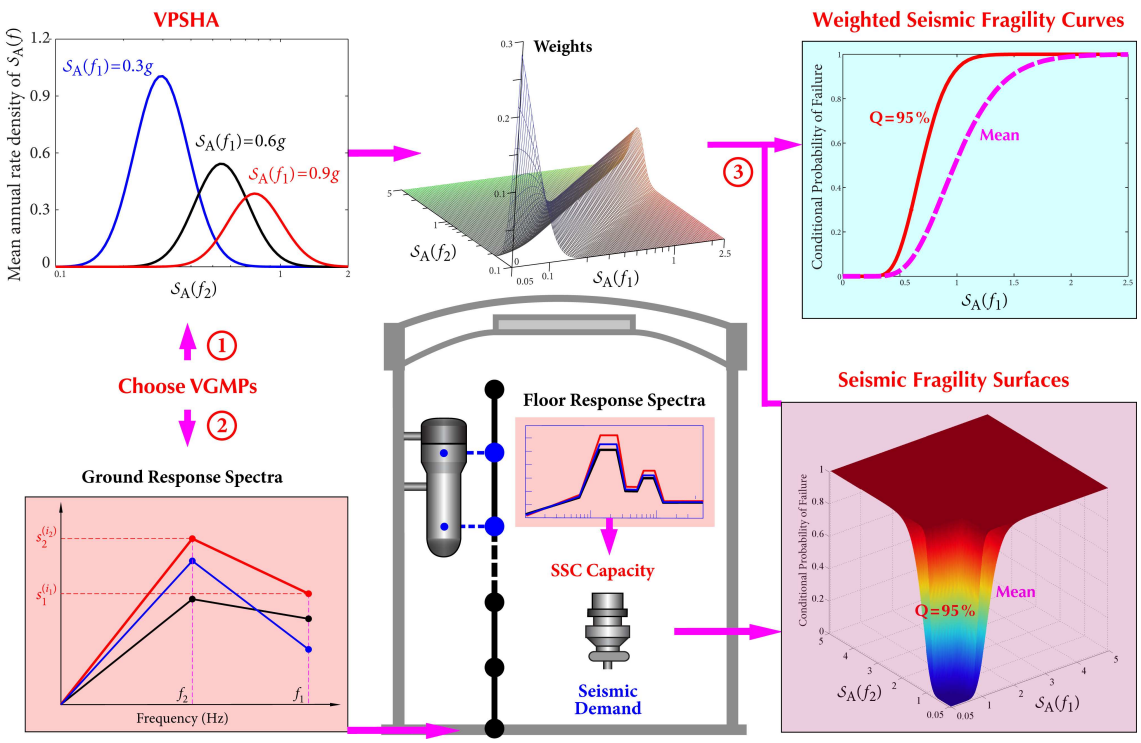


**Figure 4.1** A flow diagram of weighting seismic fragility analysis method

Figure 4.1 shows a flow diagram for developing weighting seismic fragility curves. The procedure mainly includes three parts:

1. vector-valued PSHA is performed to determine the weights of input GRS;
2. seismic fragility analysis considering vector-valued GMPs (VGMPs) method is conducted to determine seismic fragility based on VGMPs;
3. weights of input GRS and seismic fragility are combined to obtain the weighting seismic fragility of an SSC.

By using VGMPs, problems in current seismic fragility analysis are resolved. To better illustrate the proposed method, three consecutive parts are presented in the following.

## 4.3 Vector-valued Probabilistic Seismic Hazard Analysis

### Annual Rate Density

As in Chapter 2, in two-dimensional case, the annual rate density of $\left\{\mathcal{S}_{\mathrm{A}}(f_2) \,\middle|\, \mathcal{S}_{\mathrm{A}}(f_1)\right\}$ is given by

$$f'_{\mathcal{S}_{\mathrm{A}}(f_2)|\mathcal{S}_{\mathrm{A}}(f_1)}\left(s_2 \,\middle|\, s_1\right) = \sum_{i=1}^{N_S} \nu_i \left\{ f_{\mathcal{S}_{\mathrm{A}}(f_2)|\mathcal{S}_{\mathrm{A}}(f_1)}\left(s_2 \,\middle|\, s_1\right)\right\}. \tag{4.3.1}$$

where $f_{\mathcal{S}_{\mathrm{A}}(f_2)|\mathcal{S}_{\mathrm{A}}(f_1)}\left(s_2 \,\middle|\, s_1\right)$ is probability density function (PDF) of $\left\{\mathcal{S}_{\mathrm{A}}(f_2) \,\middle|\, \mathcal{S}_{\mathrm{A}}(f_1)\right\}$.

The results of VPSHA are a set of curves representing annual rate density of $\mathcal{S}_{\mathrm{A}}(f_2)$ with respect to a set of spectral values of $\mathcal{S}_{\mathrm{A}}(f_1)$. Take a safety-related SSC with its first dominant frequency $f = 5$ Hz for example. $\mathcal{S}_{\mathrm{A}}(f = 5\,\mathrm{Hz})$ and PGA (i.e. $\mathcal{S}_{\mathrm{A}}(f_1 = 50\,\mathrm{Hz})$) are chosen as VGMPs. Assume the SSC is located in Darlington nuclear generating station. By performing VPSHA (see Chapter 2), mean annual rate density of $\mathcal{S}_{\mathrm{A}}(f_2)$ at three PGA values are shown in Figure 4.2.

Given a PGA value, the inherent variability in earthquake response spectra at $\mathcal{S}_{\mathrm{A}}(f)$ can be captured by its distribution (see Figure 4.2 for example). In addition, ground motion intensity effect considered by taking a lot of PGA values in equation (4.3.1).

### Weights of Input GRS

Taking lower and upper bounds as $\mathbf{s}_{\mathrm{L}} = \left\{s_{\mathrm{L},1}, s_{\mathrm{L},2}\right\}$ and $\mathbf{s}_{\mathrm{U}} = \left\{s_{\mathrm{U},1}, s_{\mathrm{U},2}\right\}$, the domain $\mathbf{s} = \left\{s_1, s_2\right\}$ is discretized into intervals $s_{\mathrm{L},1} = s_1^{(0)} < s_1^{(1)} < \cdots < s_1^{(N_1)} = s_{\mathrm{U},1}$, $s_{\mathrm{L},2} = s_2^{(0)} < s_2^{(1)} < \cdots < s_2^{(N_2)} = s_{\mathrm{U},2}$. For example, as shown in Figure 4.3, given $\mathcal{S}_{\mathrm{A}}(f_1) = s_1 = 0.6g$,

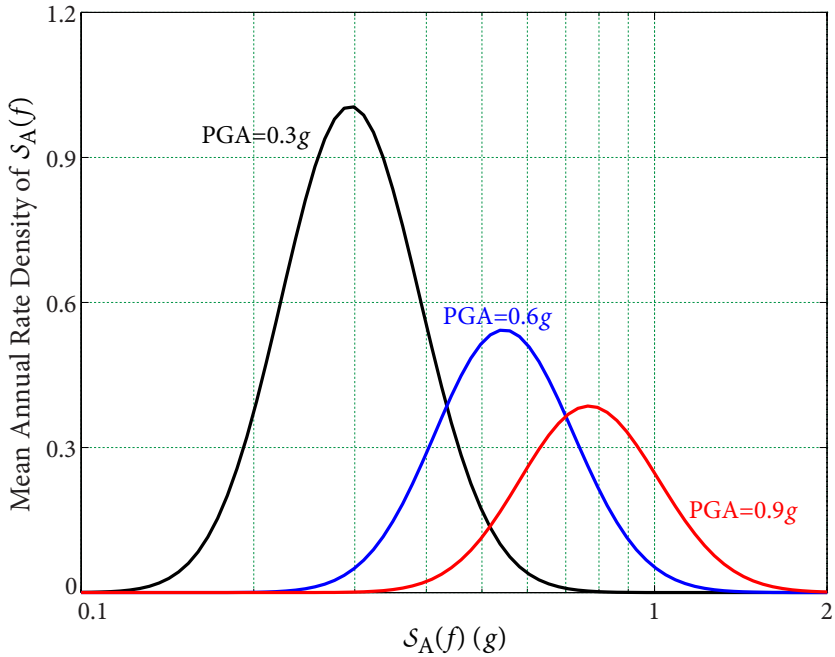


**Figure 4.2** Mean annual rate density of $\mathcal{S}_A(f)$ at three PGA values

numerical method is applied to calculate the annual rate of occurrence of $s_2$ in the interval between $s_2^{(i_2)}$ and $s_2^{(i_2+1)}$ by

$$\lambda\left(s_2^{(i_2)} \leqslant s_2 < s_2^{(i_2+1)} \,\middle|\, s_1 = 0.6g\right) = \int_{s_2^{(i_2)}}^{s_2^{(i_2+1)}} f'_{\mathcal{S}_A(f_2)|\mathcal{S}_A(f_1)}\left(s_2 \,\middle|\, s_1 = 0.6g\right) \mathrm{d}s_2$$
$$\approx \sum_{i=1}^{N_S} \nu_i \left\{ f_{\mathcal{S}_A(f_2)|\mathcal{S}_A(f_1)}\left(s_2 \,\middle|\, s_1 = 0.6g\right) \Delta s_2^{(i_2)} \right\}. \tag{4.3.2}$$

Given $\mathcal{S}_A(f_1) = 0.6g$, annual rate of occurrences of $s_2$ in the entire spectral domain of $\mathcal{S}_A(f_2)$ is given by

$$\lambda\left(s_{L,2} \leqslant s_2 < s_{U,2} \,\middle|\, s_1 = 0.6g\right) = \int_{s_{L,2}}^{s_{U,2}} f'_{\mathcal{S}_A(f_2)|\mathcal{S}_A(f_1)}\left(s_2 \,\middle|\, s_1 = 0.6g\right) \mathrm{d}s_2$$
$$\approx \sum_{i=1}^{N_S} \nu_i \left\{ \sum_{i_2=1}^{N_2} \left[ f_{\mathcal{S}_A(s_2)|\mathcal{S}_A(f_1)}\left(s_2^{(i_2)} \,\middle|\, s_1 = 0.6g\right) \Delta s_2^{(i_2)} \right]_{i_2} \right\}. \tag{4.3.3}$$

The normalizing constant $N_f$ of function $f'_{\mathcal{S}_A(f_2)|\mathcal{S}_A(f_1)}\left(s_2 \,|\, s_1 = 0.6g\right)$ is defined as

$$N_f = \frac{1}{\lambda\left(s_{L,2} \leqslant s_2 < s_{U,2} \,|\, s_1 = 0.6g\right)} = \frac{1}{k \cdot \sum_{i=1}^{N_S} \nu_i}, \tag{4.3.4}$$

where $k$ is the probability that $s_2$ in the entire spectral domain of $\mathcal{S}_A(f_2)$, i.e.,

$$k = \sum_{i_2=1}^{N_2} \left[ f_{\mathcal{S}_A(s_2)|\mathcal{S}_A(f_1)}\left(s_2^{(i_2)} \,|\, s_1 = 0.6g\right) \Delta s_2^{(i_2)} \right]_{i_2}. \tag{4.3.5}$$

Due to the truncation of spectral domain, $k$ is always smaller than 1.

Therefore, the weight of input ground response spectrum with with spectral value of $\mathcal{S}_A(f_2)$ in the interval between $s_2^{(i_2)}$ and $s_2^{(i_2+1)}$, representing the probability that $s_2$ in this interval, is calculated by

$$w\left(s_2^{(i_2)} \leqslant s_2 < s_2^{(i_2+1)} \,|\, s_1\right) = N_f \cdot f'_{\mathcal{S}_A(f_2)|\mathcal{S}_A(f_1)}\left(s_2^{(i_2)} \,|\, s_1 = 0.6g\right) \Delta s_2^{(i_2)} \tag{4.3.6a}$$

$$= \frac{\sum_{i=1}^{N_S} \nu_i \left\{ f_{\mathcal{S}_A(f_2)|\mathcal{S}_A(f_1)}\left(s_2^{(i_2)} \,|\, s_1 = 0.6g\right) \Delta s_2^{(i_2)} \right\}}{k \cdot \sum_{i=1}^{N_S} \nu_i} \tag{4.3.6b}$$

$$= \frac{1}{k} \cdot \left\{ f_{\mathcal{S}_A(f_2)|\mathcal{S}_A(f_1)}\left(s_2^{(i_2)} \,|\, s_1 = 0.6g\right) \Delta s_2^{(i_2)} \right\}. \tag{4.3.6c}$$

In the calculation of weights, equation (4.3.6a) is usually used, because the output of VPSHA is annual rate density function instead of probability density function.

As shown in Figure 4.3, for example, given $\mathcal{S}_A(f_1) = 0.6g$, the weight of $s_2$ in the interval between $0.8g$ and $0.82g$ is given by

$$\begin{aligned} w\left(0.8g \leqslant s_2 < 0.82g \,|\, s_1 = 0.6g\right) &= N_f \cdot f'_{\mathcal{S}_A(f_2)|\mathcal{S}_A(f_1)}\left(s_2 \,|\, s_1 = 0.6g\right) \Delta s_2^{(i_2)} \\ &= \frac{f'_{\mathcal{S}_A(f_2)|\mathcal{S}_A(f_1)}\left(s_2 = 0.8g \,|\, s_1 = 0.6g\right) \cdot 0.2g}{\lambda\left(0.2g \leqslant s_2 < 2.0g \,|\, s_1 = 0.6g\right)}. \end{aligned} \tag{4.3.7}$$

The red column area in Figure 4.3 is the numerator in equation (4.3.7), while the entire area below the curve is the denominator in equation (4.3.7).

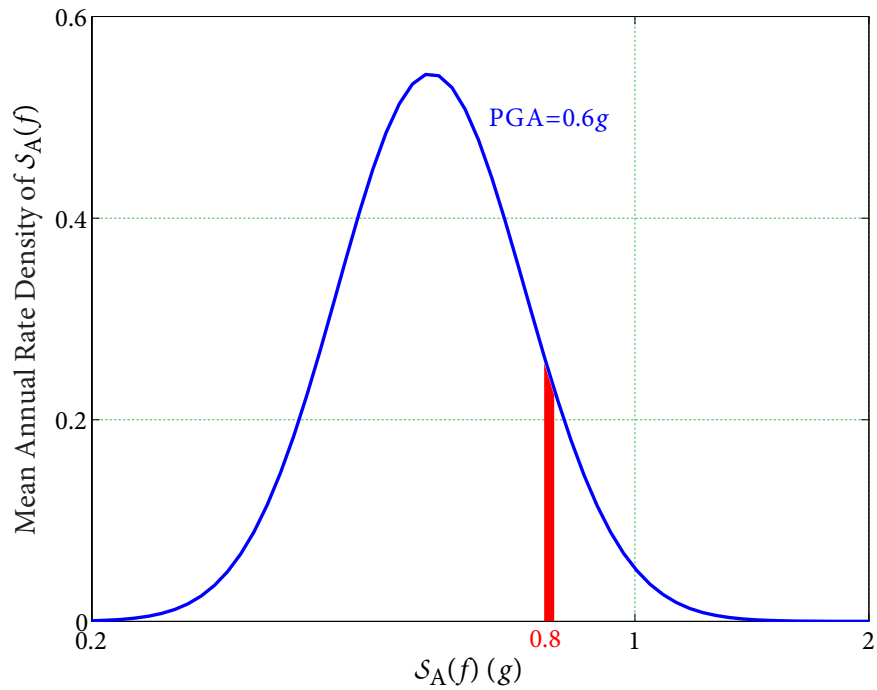


**Figure 4.3** Calculation of weights of input GRS with spectral values $s_2$ given PGA$=0.6g$

## 4.4 Seismic Fragility Analysis considering VGMPs

### 4.4.1 Definition

Suppose a structure having two natural frequencies $f_1$ and $f_2$. The seismic fragility of this structure is expressed as the conditional probability that structural seismic demand exceeds its capacity, given a ground motion level in terms of $\mathcal{S}_A(f_1)$ and $\mathcal{S}_A(f_2)$, i.e.,

$$p_F(s_1, s_2) = \mathcal{P}\left\{ C < D(s_1, s_2) \,\middle|\, \mathcal{S}_A(f_1) = s_1, \mathcal{S}_A(f_2) = s_2 \right\}, \tag{4.4.1}$$

where $C$ is the structural capacity, and $D$ is the seismic demand. $f_1$ and $f_2$ are natural frequencies of the structure. $s_1$ and $s_2$ are spectral values of VGMPs from an earthquake response spectrum at the site of interest.

In nuclear power industry, safety-related structures, systems, and components (SSC) are designed to behaviour elastically during earthquake ground motions. Therefore, in this thesis, response spectrum analysis method is used to calculate structural responses of these SSCs. Recall that in response spectrum analysis method, only spectral accelerations

at structural natural frequencies are needed. When VGMPs are used, a smooth ground response spectrum (GRS) with spectral values $s_1$ and $s_2$ can be used to represent the earthquake response spectrum at the site of interest.

As opposed to a single Review Level Earthquake in current seismic fragility analysis, given a spectral value $s_1$ of $\mathcal{S}_A(f_1)$, a great number of GRS with different spectral values of $\mathcal{S}_A(f_2)$ are defined as seismic input, accounting for aleatory randomness in estimating $\mathcal{S}_A(f_2)$. By changing spectral values of $\mathcal{S}_A(f_1)$, ground motion intensity effect is taken into consideration. Three examples of GRS are shown in Figure 4.4, in which $s_1^{(i_1)}$ and $s_2^{(i_2)}$ are from one combination of spectral values of VGMPs.

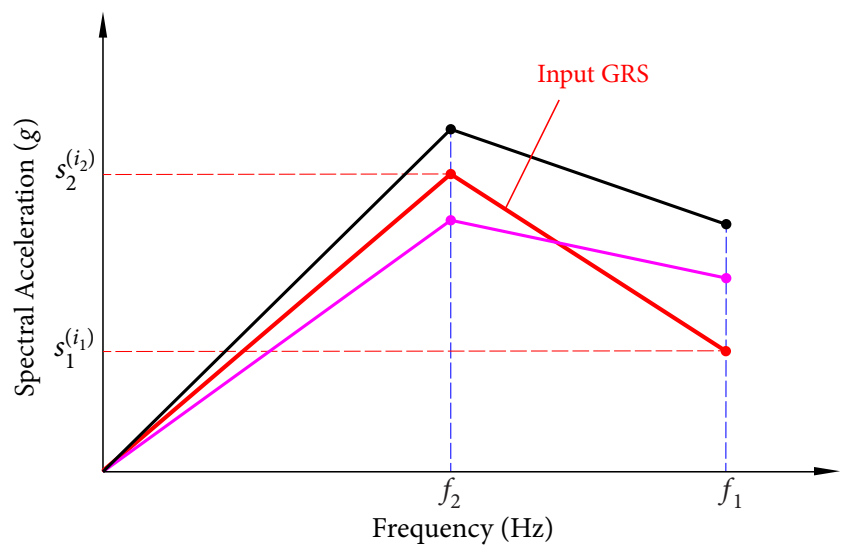


**Figure 4.4** An example of GRS Representing Earthquake Response Spectra

Given an input GRS, $D$ and $C$ are univariate random variables due to response uncertainty and structural capacity uncertainty, respectively. Figure 4.5 shows an example of probability density functions (PDFs) of structural shear strength $C$ and shear force $D$ given an input GRS. It needs to make clear that $p_F(s_1, s_2)$ is not cumulative distribution function of VGMPs, but the conditional probability of failure on VGMPs.

For simplicity of presentation, the condition of given "$\mathcal{S}_A(f_1) = s_1$, $\mathcal{S}_A(f_2) = s_2$" (abbreviated as $\boldsymbol{\mathcal{S}}_A(\mathbf{f}) = \mathbf{s}$) is usually dropped. Hence, equation (4.4.1) can be rewritten as

$$p_F(\mathbf{s}) = \mathcal{P}\left\{C < D(\mathbf{s}) \,\middle|\, \boldsymbol{\mathcal{S}}_A(\mathbf{f}) = \mathbf{s}\right\} = \mathcal{P}\left\{C < D(\mathbf{s})\right\}. \tag{4.4.2}$$

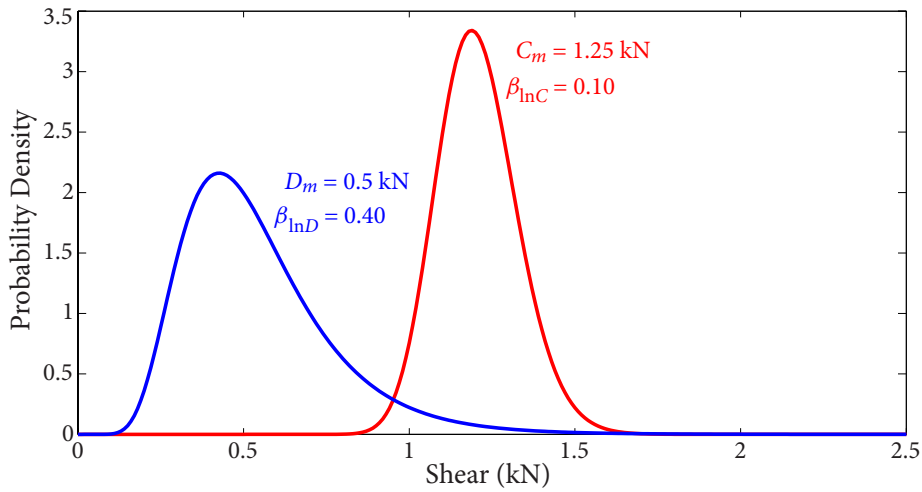


**Figure 4.5** An example of PDFs of structural shear strength and force

### 4.4.2 Determination of Seismic Fragility

As shown in Figure 4.6, the procedure to determine two-dimensional conditional probability of failure distributions, i.e., seismic fragility surfaces, mainly consists of three key steps: structural capacity analysis, seismic demand analysis, and development of seismic fragility surfaces.

#### 4.4.2.1 Structural Capacity Analysis

For an SSC, a variety of failure modes may result in its failure. Therefore, potential failure modes should be identified prior to conducting structural capacity analysis. Identification of potential failure modes is mainly based on experience and judgement (EPRI TR-103959, EPRI, 1994).

After identifying potential failure modes, structural capacity analysis is performed. Median material strengths should be used in capacity formulas given in design codes or textbooks to remove conservatism in the determination of structural capacity.

#### 4.4.2.2 Seismic Demand Analysis

It is recognized that spectral values from realistic ground motions are impossible to approach infinity; hence it is reasonable to truncate the domain of spectral accelerations $\mathbf{s}$ at a reasonable large value $s_U$, such as $5g$, in each dimension. In addition,

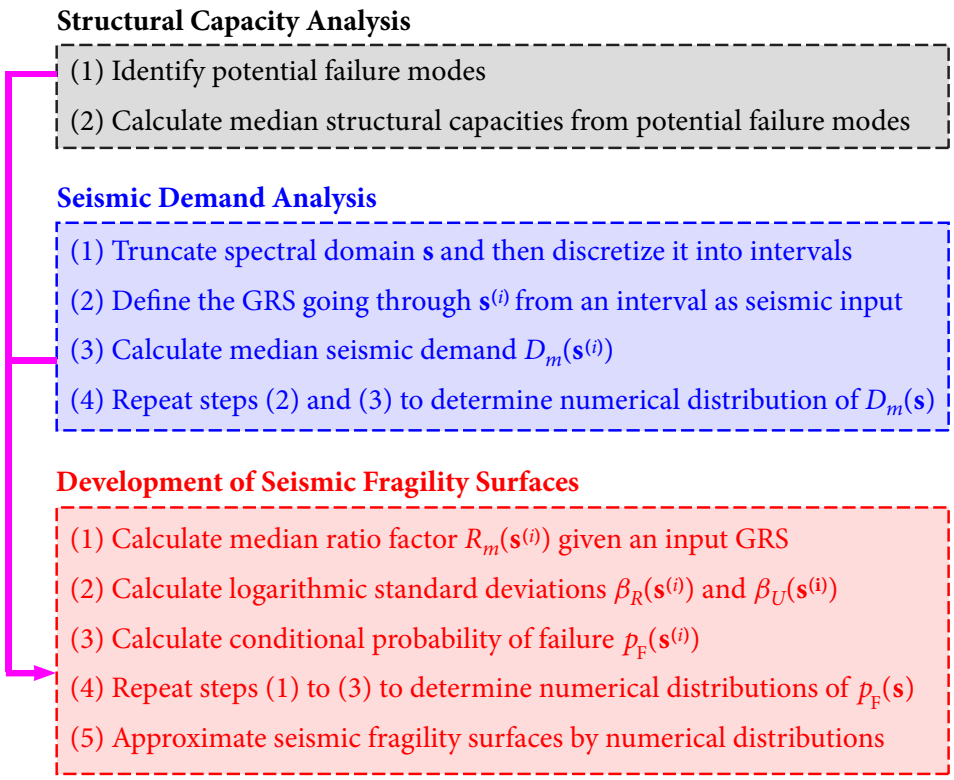


**Figure 4.6** A flow diagram of development of seismic fragility surfaces

spectral values over the entire frequency range of engineering interest are always positive during an earthquake; hence one can truncate $\mathbf{s}$ at a reasonable small value $s_{\mathrm{L}}$, such as $0.01g$, in each dimension. Subsequently, discretize truncated $\mathbf{s}$ into intervals $s_{\mathrm{L},1} = s_1^{(0)} < s_1^{(1)} < \cdots < s_1^{(N_1)} = s_{\mathrm{U},1}$, $s_{\mathrm{L},2} = s_2^{(0)} < s_2^{(1)} < \cdots < s_2^{(N_2)} = s_{\mathrm{U},2}$, in which there are $N_1 \times N_2$ intervals generated.

Defining a GRS simultaneously going through spectral values $s_1^{(i_1)}, s_2^{(i_2)}$ (abbreviated as $\mathbf{s}^{(i)}$) from an interval as seismic input, $D_m(\mathbf{s}^{(i)})$ can be determined as follows:

- **For structures located on the ground:** Response spectrum analysis method is used to calculate $D_m(\mathbf{s}^{(i)})$. Spectral values $\mathbf{s}^{(i)}$ in the calculation are directly obtained from the input GRS.
- **For equipments mounted on structures:** Given an input GRS with spectral values $\mathbf{s}^{(i)}$, a direct spectra-to-spectra method is used to calculate the floor response spectra (FRS) where equipments are located (Jiang *et al.*, 2015; Li *et al.*, 2015). Define the FRS as seismic

input, response spectrum analysis method is then applied to calculate $D_m(\mathbf{s}^{(i)})$. Spectral values at natural frequencies of equipments are obtained from the input FRS.

Applying input GRS with spectral values of GMPs in other intervals as seismic input and repeating this procedure yield median seismic demand in all intervals. Finally integrating these values results in two-dimensional numerical distribution of median seismic demand $D_m(\mathbf{s})$.

#### 4.4.2.3 Development of Seismic Fragility Surfaces

**Median Ratio Factor**

In seismic FA, an intermediate random variable, called *factor of safety F*, is usually used to estimate fragility parameters (see Chapter 3). Similarly, in the proposed method, an intermediate random variable, termed as *ratio factor R*, is defined as the ratio of structural capacity to its seismic demand. Given an input GRS with spectral values $\mathbf{s}^{(i)}$, $R(\mathbf{s}^{(i)})$ can be determined by

$$R(\mathbf{s}^{(i)}) = \frac{C}{D(\mathbf{s}^{(i)})} = F_{\mathrm{C}}\, F_{\mathrm{RS}}(\mathbf{s}^{(i)}) = R_m(\mathbf{s}^{(i)})\, \varepsilon_R(\mathbf{s}^{(i)})\, \varepsilon_U(\mathbf{s}^{(i)}), \tag{4.4.3}$$

where $R_m(\mathbf{s}^{(i)})$ is *median ratio factor*. The random variables $\varepsilon_R(\mathbf{s}^{(i)})$ and $\varepsilon_U(\mathbf{s}^{(i)})$ are lognormally distributed with unit median (zero logarithmic mean) and logarithmic standard deviations of $\beta_R(\mathbf{s}^{(i)})$ and $\beta_U(\mathbf{s}^{(i)})$, respectively. Since structure response uncertainty depends on the input GRS, $\beta_R(\mathbf{s}^{(i)})$ and $\beta_U(\mathbf{s}^{(i)})$ depend on the input GRS, i.e., $\mathbf{s}^{(i)}$.

For structures located on the ground, *median ratio factor* $R_m(\mathbf{s}^{(i)})$ is given by

$$R_m(\mathbf{s}^{(i)}) = F_{\mathrm{C},m}\, F_{\mathrm{RS},m}(\mathbf{s}^{(i)}), \tag{4.4.4}$$

where $F_{\mathrm{C},m}$ and $F_{\mathrm{RS},m}(\mathbf{s}^{(i)})$ are *median* capacity and response factors (see Chapter 3).

For equipments mounted on structures, $R_m(\mathbf{s}^{(i)})$ consists of three variables, i.e.,

$$R_m(\mathbf{s}^{(i)}) = F_{\mathrm{C},m}\, F_{\mathrm{RS},m}(\mathbf{s}^{(i)})\, F_{\mathrm{RE},m}(\mathbf{s}^{(i)}), \tag{4.4.5}$$

where $F_{\mathrm{RE},m}(\mathbf{s}^{(i)})$ is *median* equipment response factor (see Chapter 3).

### Logarithmic Standard Deviations

The variability of $R$ due to capacity and response variables is determined according to the methods in Chapter 3. Recall that in the proposed method, a large number of input GRS (see Figure 4.4), rather than a generic GRS (e.g. NUREG/CR-0098 median rock response spectrum), are used to calculate structural seismic demand; the procedure for determining logarithmic standard deviations in structural response due to damping variability is slightly different from that given in seismic fragility analysis guides (EPRI, 1994; EPRI, 2009).

Generally, design response spectra are defined for structures with 5% damping ratio. In practice, however, many types of structures have smaller damping ratios (such as steel structures) or larger damping ratios (such as piping systems). For generic GRS, empirical damping modification factors (DMFs) are used to adjust response spectral values with 5% damping ratio to other damping ratios (CSA N289.3-10, CSA, 2010; NUREG-CR-0098, USNRC, 1978; R.G. 1.60, USNRC, 2014A). For site-specific GRS, many studies are performed to obtain empirical DMFs incorporating site conditions and ground motion characteristics (Cameron and Green, 2007; Rezaeian *et al.*, 2012; SRP 3.7.1, USNRC, 2014B). In the proposed method, the input GRS are input site-specific response spectra; hence DMFs given in Appendix C of SRP 3.7.1 (USNRC, 2014B) may be used to estimate spectral values at damping levels other than 5% damping ratio.

### Conditional Probability of Failure given an Input GRS

In terms of the ratio factor, conditional probability of failure of an SSC given an input GRS simultaneously going through $\mathbf{s}^{(i)}$ can be rewritten as

$$p_{\mathrm{F}}(\mathbf{s}^{(i)}) = \mathcal{P}\big\{C < D(\mathbf{s}^{(i)})\big\} = \mathcal{P}\left\{\frac{C}{D(\mathbf{s}^{(i)})} < 1\right\} = \mathcal{P}\big\{R(\mathbf{s}^{(i)}) < 1\big\}. \tag{4.4.6}$$

Note that $R(\mathbf{s}^{(i)})$ is lognormally distributed from equation (4.4.3). Due to lack of knowledge, the estimated *median* ratio factor $R_m^U(\mathbf{s}^{(i)}) = R_m(\mathbf{s}^{(i)})\varepsilon_U(\mathbf{s}^{(i)})$ is lognormally distributed with $R_m^U(\mathbf{s}^{(i)}) \sim \mathcal{LN}\big(\ln R_m(\mathbf{s}^{(i)}),\ \beta_U^2(\mathbf{s}^{(i)})\big)$. Hence, $R_{m,q}^U(\mathbf{s}^{(i)})$ at the confidence level $Q = q$, can be expressed as

$$R_{m,q}^U(\mathbf{s}^{(i)}) = R_m(\mathbf{s}^{(i)})\,\varepsilon_{U,q}(\mathbf{s}^{(i)}) = R_m(\mathbf{s}^{(i)})\,\mathrm{e}^{-\beta_U(\mathbf{s}^{(i)})\,\Phi^{-1}(q)}. \tag{4.4.7}$$

Finally, seismic fragility, or the conditional probability of failure of the SSC given $\mathbf{s}^{(i)}$, at confidence level $Q=q$, is given by

$$p_{\mathrm{F},q}(\mathbf{s}^{(i)}) = \mathcal{P}\left\{R(\mathbf{s}^{(i)}) < 1\right\} = \Phi\left\{\frac{\ln[1/R_m(\mathbf{s}^{(i)})] + \beta_U(\mathbf{s}^{(i)})\,\Phi^{-1}(q)}{\beta_R(\mathbf{s}^{(i)})}\right\}. \tag{4.4.8}$$

When composite variability is used,

$$p_{\mathrm{F}}(\mathbf{s}^{(i)}) = \Phi\left\{\frac{\ln[1/R_m(\mathbf{s}^{(i)})]}{\beta_{\mathrm{C}}(\mathbf{s}^{(i)})}\right\}, \qquad \beta_{\mathrm{C}}(\mathbf{s}^{(i)}) = \sqrt{\beta_R^2(\mathbf{s}^{(i)}) + \beta_U^2(\mathbf{s}^{(i)})}. \tag{4.4.9}$$

**Development of Fragility Surface**

Employing GRS from other intervals as seismic input, and repeating the procedure give conditional probabilities of failure from all intervals of spectral domain $\mathbf{s}$. The outcome of seismic fragility analysis considering VGMPs is a family of numerical two-dimensional conditional probability of failure distributions. When composite variability is used, it is a mean numerical conditional probability of failure distribution. As long as the spectral increment is reasonable small, e.g., $0.01g$, seismic fragility surfaces can be approximated by numerical distributions of conditional probability of failure.

### 4.4.3 Summary

In this Section, seismic fragility analysis considering vector-valued GMPs (VGMPs) method is presented. Spectral accelerations at structural natural frequencies, i.e., $\mathcal{S}_{\mathrm{A}}(f_1)$ and $\mathcal{S}_{\mathrm{A}}(f_2)$, are chosen as VGMPs. By using VGMPs, the aleatory randomness in earthquake response spectra and ground motion intensity effect are taken into account. Since response spectrum analysis method is used to calculate structural response, the determination of seismic fragility surfaces is time efficient even although a great number of input GRS are defined as seismic input.

## 4.5 Development of Weighting Seismic Fragility Curves

### 4.5.1 Weighting Seismic Fragility and HCLPF Seismic Capacity

Let $\mathbf{s}^{(i)} = \left\{s_1, s_2^{(i_2)}\right\}$, seismic fragility or the conditional probability of failure at confidence level $Q=q$, given input GRS going through $\mathbf{s}^{(i)}$, is given by equation (4.4.8). Therefore, the

weighting seismic fragility given $\mathcal{S}_{\mathrm{A}}(f_1)=s_1$ can be determined by equation (4.2.2), i.e.,

$$\bar{p}_{\mathrm{F},q}(s_1) = \sum_{i_2=1}^{N_2} \Big[ p_{\mathrm{F},q}(\mathbf{s}^{(i)}) \cdot w\big(s_2^{(i_2)} \leqslant s_2 < s_2^{(i_2+1)} \,\big|\, s_1\big) \Big], \tag{4.5.1}$$

where $w\big(s_2^{(i_2)} \leqslant s_2 < s_2^{(i_2+1)} \,\big|\, s_1\big)$ is the weight of input GRS with spectral values $\mathbf{s}^{(i)}$.

Changing value $s_1$ of $\mathcal{S}_{\mathrm{A}}(f_1)$ from lower bound value of $0.05g$ to upper bound value of $5g$, and repeating above procedure give a numerical distribution of weighting seismic fragility at confidence level $Q=q$. Since the sizes of intervals are very small, the weighting seismic fragility curve of an SSC can be well represented by this numerical distribution.

In practice, confidence level $Q$ is usually taken as discrete values, such as 5%, 50%, and 95%. Therefore, seismic capacity of an SSC can be characterized by a family of weighting seismic fragility curves.

When composite variability is used,

$$p_{\mathrm{F,C}}(\mathbf{s}^{(i)}) = \Phi\left\{ \frac{\ln[1/R_m(\mathbf{s}^{(i)})]}{\beta_{\mathrm{C}}(\mathbf{s}^{(i)})} \right\}, \qquad \beta_{\mathrm{C}}(\mathbf{s}^{(i)}) = \sqrt{\beta_R^2(\mathbf{s}^{(i)}) + \beta_U^2(\mathbf{s}^{(i)})}. \tag{4.5.2}$$

Hence, the weighting composite seismic fragility given $\mathcal{S}_{\mathrm{A}}(f_1) = s_1$ can be determined by

$$\bar{p}_{\mathrm{F,C}}(s_1) = \sum_{i_2=1}^{N_2} \Big[ p_{\mathrm{F,C}}(\mathbf{s}^{(i)}) \cdot w\big(s_2^{(i_2)} \leqslant s_2 < s_2^{(i_2+1)} \,\big|\, s_1\big) \Big]. \tag{4.5.3}$$

Instead of a family of weighting seismic fragility curves, a weighting composite (mean) seismic fragility curve could be used to represent seismic capacity of an SSC.

In current SMA, HCLPF seismic capacity is used to represent structural seismic capacity. To determine the weighting HCLPF seismic capacity, weighting seismic fragility curve at confidence level $Q=95\%$ is used. Taking seismic fragility $\bar{p}_{\mathrm{F},q}=5\%$, one can easily find weighting HCLPF seismic capacity ($\bar{\mathscr{C}}_{\mathrm{HCLPF}}$) from this curve, in which $\bar{\mathscr{C}}$ denotes weighting capacity.

When composite variability is used, weighting mean seismic fragility curve is taken to determine the weighting HCLPF seismic capacity. Seismic capacity ($\bar{\mathscr{C}}_{1\%}^{\mathrm{C}}$, where the superscript "C" stands for "composite") can be easily determined from this curve using seismic fragility $\bar{p}_{\mathrm{F,C}}=1\%$. In applications, $\bar{\mathscr{C}}_{\mathrm{HCLPF}}$ can be approximated by $\bar{\mathscr{C}}_{1\%}^{\mathrm{C}}$.

### 4.5.2 Generalization of Weighting Seismic Fragility Analysis

The number of VGMPs can be extended to $n$-dimension. Spectral accelerations $\mathcal{S}_{\mathrm{A}}(f_1), \ldots, \mathcal{S}_{\mathrm{A}}(f_n)$ (abbreviated as $\boldsymbol{\mathcal{S}}_{\mathrm{A}}(\mathbf{f})$) are chosen as VGMPs. Seismic fragility with respect to $\mathcal{S}_{\mathrm{A}}(f_k)$ is determined by

$$\bar{p}_{\mathrm{F}}(s_k) = \underbrace{\int_0^{\infty} \cdots \int_0^{\infty}}_{(n-1)} p_{\mathrm{F}}(\mathbf{s}) \cdot f_{\boldsymbol{\mathcal{S}}_{\mathrm{A}}(\mathbf{f}'_k)|\mathcal{S}_{\mathrm{A}}(f_k)}\left(\mathbf{s}'_k \,\middle|\, s_k\right) \underbrace{\mathrm{d}s_1 \cdots \mathrm{d}s_n}_{(n-1)\text{ without } s_k}, \tag{4.5.4}$$

where $p_{\mathrm{F}}(\mathbf{s})$ is the seismic fragility which can be determined by seismic fragility analysis considering VGMPs method. $f_{\boldsymbol{\mathcal{S}}_{\mathrm{A}}(\mathbf{f}'_k)|\mathcal{S}_{\mathrm{A}}(f_k)}\left(\mathbf{s}'_k \,\middle|\, s_k\right)$ is probability density function (PDF) of $\left\{\boldsymbol{\mathcal{S}}_{\mathrm{A}}(\mathbf{f}'_k) \,\middle|\, \mathcal{S}_{\mathrm{A}}(f_k)\right\}$ which can be calculated by VPSHA. $\boldsymbol{\mathcal{S}}_{\mathrm{A}}(\mathbf{f}'_k)$ stands for $\boldsymbol{\mathcal{S}}_{\mathrm{A}}(\mathbf{f})$ without $\mathcal{S}_{\mathrm{A}}(f_k)$, and $\mathbf{s}'_k$ represents $\mathbf{s}$ without $s_k$.

Numerical method is applied to calculate the integral in equation (4.5.4) by

$$\bar{p}_{\mathrm{F}}(s_k) = \underbrace{\sum_{i_1=1}^{N_1} \cdots \sum_{i_n=1}^{N_n}}_{(n-1)\text{ without } i_k} \left[p_{\mathrm{F}}(\mathbf{s}^{(i)}) \cdot w\left(\mathbf{s}'^{(i)} \leqslant \mathbf{s}'_k < \mathbf{s}'^{(i+1)} \,\middle|\, s_k\right)\right], \tag{4.5.5}$$

Taking lower and upper bounds as $\mathbf{s}_{\mathrm{L}} = \left\{s_{\mathrm{L},1}, \ldots, s_{\mathrm{L},n}\right\}$ and $\mathbf{s}_{\mathrm{U}} = \left\{s_{\mathrm{U},1}, \ldots, s_{\mathrm{U},n}\right\}$, the domain $\mathbf{s}$ is discretized into intervals $s_{\mathrm{L},1} = s_1^{(0)} < s_1^{(1)} < \cdots < s_1^{(N_1)} = s_{\mathrm{U},1}, \ \ldots, \ s_{\mathrm{L},n} = s_n^{(0)} < s_n^{(1)} < \cdots < s_n^{(N_n)} = s_{\mathrm{U},n}$.

Given $\mathcal{S}_{\mathrm{A}}(f_k) = s_k$, the annual rate of occurrence of $\mathbf{s}'_k$ in the interval between $\mathbf{s}'^{(i)}$ and $\mathbf{s}'^{(i+1)}$ can be determined by the VPSHA, i.e.,

$$\lambda\left(\mathbf{s}'^{(i)} \leqslant \mathbf{s}'_k < \mathbf{s}'^{(i+1)} \,\middle|\, s_k\right) = \underbrace{\int_{s_1^{(i_1)}}^{s_1^{(i_1+1)}} \cdots \int_{s_n^{(i_n)}}^{s_n^{(i_n+1)}}}_{(n-1)\text{ without } s_k^{(i_k)} \text{ to } s_k^{(i_k+1)}} f'_{\boldsymbol{\mathcal{S}}_{\mathrm{A}}(\mathbf{f}'_k)|\mathcal{S}_{\mathrm{A}}(f_k)}\left(\mathbf{s}'_k \,\middle|\, s_k\right) \underbrace{\mathrm{d}s_1 \cdots \mathrm{d}s_n}_{(n-1)\text{ without } s_k}, \tag{4.5.6}$$

where $f'_{\boldsymbol{\mathcal{S}}_{\mathrm{A}}(\mathbf{f}'_k)|\mathcal{S}_{\mathrm{A}}(f_k)}\left(\mathbf{s}'_k \,\middle|\, s_k\right)$ is mean annual rate density of $\left\{\boldsymbol{\mathcal{S}}_{\mathrm{A}}(\mathbf{f}'_k) \,\middle|\, \mathcal{S}_{\mathrm{A}}(f_k)\right\}$.

Let $\mathbf{s}'_{\mathrm{L}} = \left\{s_{\mathrm{L},1}, \ldots, s_{\mathrm{L},k-1}, s_{\mathrm{L},k+1}, \ldots, s_{\mathrm{L},n}\right\}$ and $\mathbf{s}'_{\mathrm{U}} = \left\{s_{\mathrm{U},1}, \ldots, s_{\mathrm{U},k-1}, s_{\mathrm{U},k+1}, \ldots, s_{\mathrm{U},n}\right\}$. Given $\mathcal{S}_{\mathrm{A}}(f_k) = s_k$, the annual rate of occurrence of $\mathbf{s}'_k$ in interval between $\mathbf{s}'_{\mathrm{L}}$ and $\mathbf{s}'_{\mathrm{U}}$ is then

given by

$$\lambda\big(\mathbf{s}'_{\mathrm{L}} \leqslant \mathbf{s}'_k \leqslant \mathbf{s}'_{\mathrm{U}} \,\big|\, s_k\big) = \underbrace{\int_{s_{\mathrm{L},1}}^{s_{\mathrm{U},1}} \cdots \int_{s_{\mathrm{L},n}}^{s_{\mathrm{U},n}}}_{(n-1)\text{ without } s_{\mathrm{L},k} \text{ to } s_{\mathrm{U},k}} f'_{\mathcal{S}_{\mathrm{A}}(\mathbf{f}'_k)|\mathcal{S}_{\mathrm{A}}(f_k)}\big(\mathbf{s}'_k \,\big|\, s_k\big) \underbrace{\mathrm{d}s_1 \cdots \mathrm{d}s_n}_{(n-1)\text{ without } s_k}$$

$$\approx \underbrace{\sum_{i_1=1}^{N_1} \cdots \sum_{i_n=1}^{N_n}}_{(n-1)\text{ without } i_k} \Big[ f'_{\mathcal{S}_{\mathrm{A}}(\mathbf{f}'_k)|\mathcal{S}_{\mathrm{A}}(f_k)}\big(\mathbf{s}'^{(i)} \,\big|\, s_k\big) \underbrace{\Delta s_1^{(i_1)} \cdots \Delta s_n^{(i_n)}}_{(n-1)\text{ without } \Delta s_k^{(i_k)}} \Big]. \tag{4.5.7}$$

Given $\mathcal{S}_{\mathrm{A}}(f_k) = s_k$, combining equations (4.5.6) and (4.5.7) gives the weight of input GRS with spectral values of remaining $(n-1)$ GMPs in interval between $\mathbf{s}'^{(i)}$ and $\mathbf{s}'^{(i+1)}$, i.e.,

$$w\big(\mathbf{s}'^{(i)} \leqslant \mathbf{s}'_k < \mathbf{s}'^{(i+1)} \,\big|\, s_k\big) = \frac{\lambda\big(\mathbf{s}'^{(i)} \leqslant \mathbf{s}'_k < \mathbf{s}'^{(i+1)} \,\big|\, s_k\big)}{\lambda\big(\mathbf{s}'_{\mathrm{L}} \leqslant \mathbf{s}'_k \leqslant \mathbf{s}'_{\mathrm{U}} \,\big|\, s_k\big)}. \tag{4.5.8}$$

### 4.5.3 Discussion and Summary

For most safety-related SSCs, the first a few modes contribute most to the total structural response. It is therefore reasonable to choose the spectral accelerations at a few natural frequencies as VGMPs. The correlations among spectral accelerations at remaining natural frequencies and a chosen GMP can be taken as 1.0, i.e., spectral accelerations at remaining natural frequencies are fully correlated with one of VGMPs. This technique can ensure that more accurate seismic capacities of safety-related SSCs are obtained while computational cost is acceptable.

In this Section, the weighting seismic fragility is determined based on the VPSHA and seismic fragility analysis considering VGMPs method. It is noted that, since a great number of input GRS are used to determine the weighting seismic fragility, structural seismic capacity probably no longer follows lognormal distribution. By using VGMPs, weighting seismic fragility analysis method resolves the problems in current method. Furthermore, weighting seismic fragility curves or HCLPF seismic capacity are in terms of a single GMP; hence it can be readily incorporated into Seismic Probabilistic Risk Analysis and Seismic Margin Assessment.

## 4.6 Numerical Example for Horizontal Heat Exchanger

To demonstrate the benefits of weighting seismic fragility analysis method, weighting seismic fragility curves and HCLPF seismic capacities in terms of PGA are determined for a heat exchanger in Darlington nuclear generating station.

### 4.6.1 Weights of Input GRS

As in Chapter 3, the heat exchanger has three natural frequencies corresponding to three directions. Since the natural frequency in transverse direction $f_{\mathrm{T}} = 25.4$ Hz is quite high, the correlation ($\rho = 0.982$) between $\ln \mathcal{S}_{\mathrm{A}}(f_{\mathrm{T}})$ and $\ln(\mathrm{PGA})$ is close to 1.0. To illustrate mean annual rate density distribution, the correlation between $\ln \mathcal{S}_{\mathrm{A}}(f_{\mathrm{T}})$ and $\ln(\mathrm{PGA})$ is taken as 1.0; two GMPs, i.e., spectral acceleration at the natural frequency in the longitudinal direction $\mathcal{S}_{\mathrm{A}}(f_{\mathrm{L}})$ and PGA, are used. The correlation coefficient between $\ln \mathcal{S}_{\mathrm{A}}(f_{\mathrm{L}})$ and $\ln(\mathrm{PGA})$ is equal to 0.905 (Baker and Jayaram, 2008).

#### Mean Annual Rate Density

VPSHA is performed to calculate mean annual rate density of $\mathcal{S}_{\mathrm{A}}(f_{\mathrm{L}}) \,|\, \mathrm{PGA}$ as

$$f'_{\mathcal{S}_{\mathrm{A}}(f_{\mathrm{L}})|\mathrm{PGA}}\left(s_2 \,|\, s_1\right) = \sum_{i=1}^{N_S} \nu_i \left\{ f_{\mathcal{S}_{\mathrm{A}}(f_{\mathrm{L}})|\mathrm{PGA}}\left(s_2 \,|\, s_1\right) \right\}, \tag{4.6.1}$$

where $f_{\mathcal{S}_{\mathrm{A}}(f_{\mathrm{L}})|\mathrm{PGA}}\left(s_2 \,|\, s_1\right)$ is PDF of $\mathcal{S}_{\mathrm{A}}(f_{\mathrm{L}}) \,|\, \mathrm{PGA}$.

The results of VPSHA are a set of curves representing aleatory randomness in estimating $\mathcal{S}_{\mathrm{A}}(f_{\mathrm{L}})$ given a set of PGA values. Figure 4.7 shows three curves given three PGA values.

#### Weights of input GRS

Given a PGA value, the weights of input GRS with spectral values of $\mathcal{S}_{\mathrm{A}}(f_{\mathrm{L}})$ can be determined by equation (4.3.6a). Taking $s_1 = 0.6g$ as an example (see Figure 4.8), the red curve denotes mean annual rate density of $\mathcal{S}_{\mathrm{A}}(f_{\mathrm{L}})$ given $\mathrm{PGA} = 0.6g$. The annual rate of occurrence $\lambda\left(0.1g \leqslant s_2 \leqslant 5g \,|\, s_1 = 0.6g\right) = 0.215$ is the area under the blue curve. In addition, one can calculate the annual rate of occurrence $\lambda\left(0.8g \leqslant s_2 \leqslant 0.825g \,|\, s_1 = 0.6g\right) = 0.009$ (red column in Figure 4.8). The weight of input GRS in the interval between $0.8g$ and

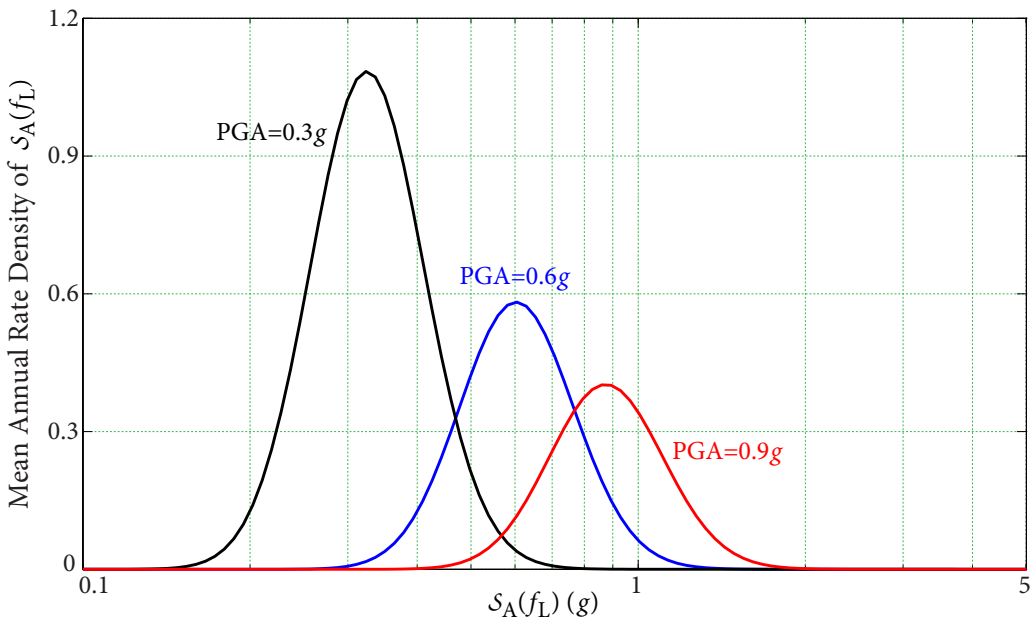


**Figure 4.7** Mean annual rate density of $\mathcal{S}_A(f_L)$ given three PGA values

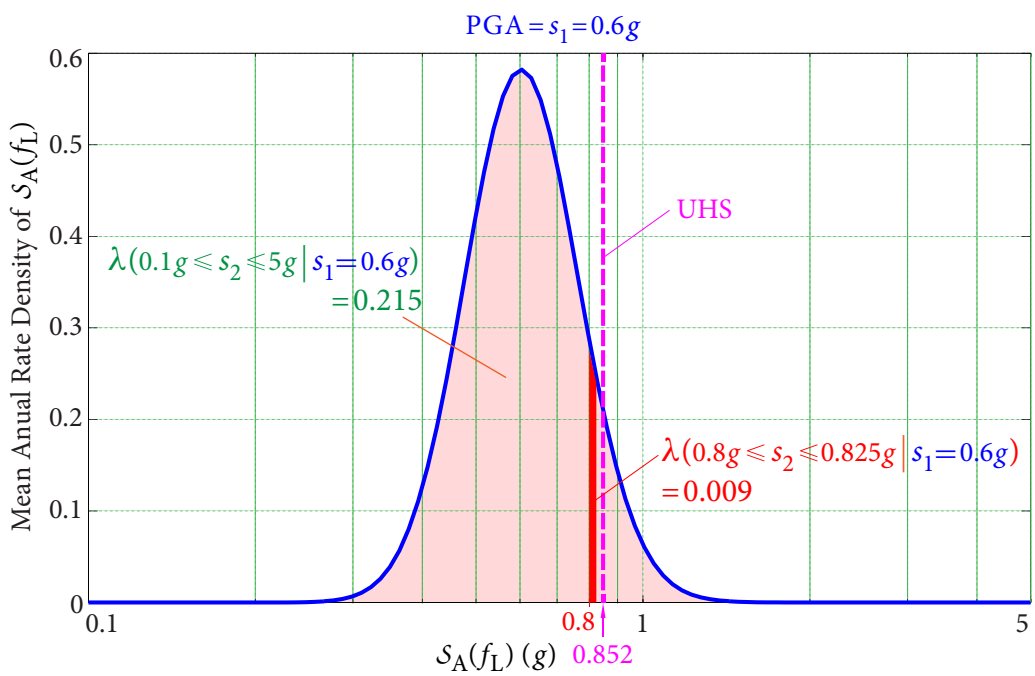


**Figure 4.8** Mean annual rate density of $\mathcal{S}_A(f_L)$ given PGA $= 0.6g$

$0.825g$ is determined by

$$w\big(0.8g \leqslant s_2 \leqslant 0.825g \,\big|\, s_1 = 0.6g\big) = \frac{\lambda\big(0.8g \leqslant s_2 \leqslant 0.825g \,\big|\, s_1 = 0.6g\big)}{\lambda\big(0.1g \leqslant s_2 \leqslant 5g \,\big|\, s_1 = 0.6g\big)} = \frac{0.009}{0.215} = 0.042. \tag{4.6.2}$$

Changing the spectral value of $\mathcal{S}_{\mathrm{A}}(f_{\mathrm{L}})$ from $0.1g$ to $5g$, the weights for all input GRS intervals can be obtained.

In current seismic fragility analysis, site-specific UHS is recommended to be chosen as RLE (see Chapter 3). In the generation of UHS, $\ln\mathcal{S}_{\mathrm{A}}(f_{\mathrm{L}})$ and $\ln\mathrm{PGA}$ are assumed to be fully correlated. Given $\mathrm{PGA} = s_1 = 0.6g$, a unique spectral value $\mathcal{S}_{\mathrm{A}}(f_{\mathrm{L}}) = 0.852g$ is obtained from the UHS (see Figure 4.8). Compared to $\mathcal{S}_{\mathrm{A}}(f_{\mathrm{L}})$ based on VPSHA (see the curve in Figure 4.8), UHS is more likely to overestimate the spectral value of $\mathcal{S}_{\mathrm{A}}(f_{\mathrm{L}})$.

## 4.6.2 Development of Seismic Fragility Surfaces

The correlation between $\ln\mathcal{S}_{\mathrm{A}}(f_{\mathrm{T}})$ and $\ln(\mathrm{PGA})$ is taken as 1.0. Given a PGA value, seismic hazard that spectral value of $\mathcal{S}_{\mathrm{A}}(f_{\mathrm{T}})$ is expected to be exceeded is equal to seismic hazard that the given PGA value is expected to be exceeded (see Discussion of Section 2.2 in Chapter 2). Therefore, as shown in Figure 4.9, given a value of PGA, one can easily find seismic hazard, i.e., mean annual frequency of exceedance (AFE), with respect to this PGA value from mean seismic hazard curve for PGA. Based on this mean AFE value, spectral acceleration $\mathcal{S}_{\mathrm{A}}(f_{\mathrm{T}})$ can be obtained from mean seismic hazard curve for $\mathcal{S}_{\mathrm{A}}(f_{\mathrm{T}})$. Take $\mathrm{PGA} = 0.1g$ as an example. Given $\mathrm{PGA} = 0.1g$, it is easily to obtain mean AFE value of $4.677 \times 10^{-4}$. Based on this mean AFE value, one can find $\mathcal{S}_{\mathrm{A}}(f_{\mathrm{T}}) = 0.134g$ from seismic hazard curve for $\mathcal{S}_{\mathrm{A}}(f_{\mathrm{T}})$. Changing PGA values from $0.05g$ to $2.5g$, one can determine the corresponding spectral values of $\mathcal{S}_{\mathrm{A}}(f_{\mathrm{T}})$ accordingly. Therefore, only two GMPs, i.e., $\mathcal{S}_{\mathrm{A}}(f_{\mathrm{L}})$ and PGA are needed in the generation of input GRS and then in the subsequent development of seismic fragility surfaces.

### 4.6.2.1 Procedure

To account for aleatory randomness in earthquake response spectra, a great number of input GRS corresponding to various combinations of $\mathcal{S}_{\mathrm{A}}(f_{\mathrm{T}})$ and PGA are defined as

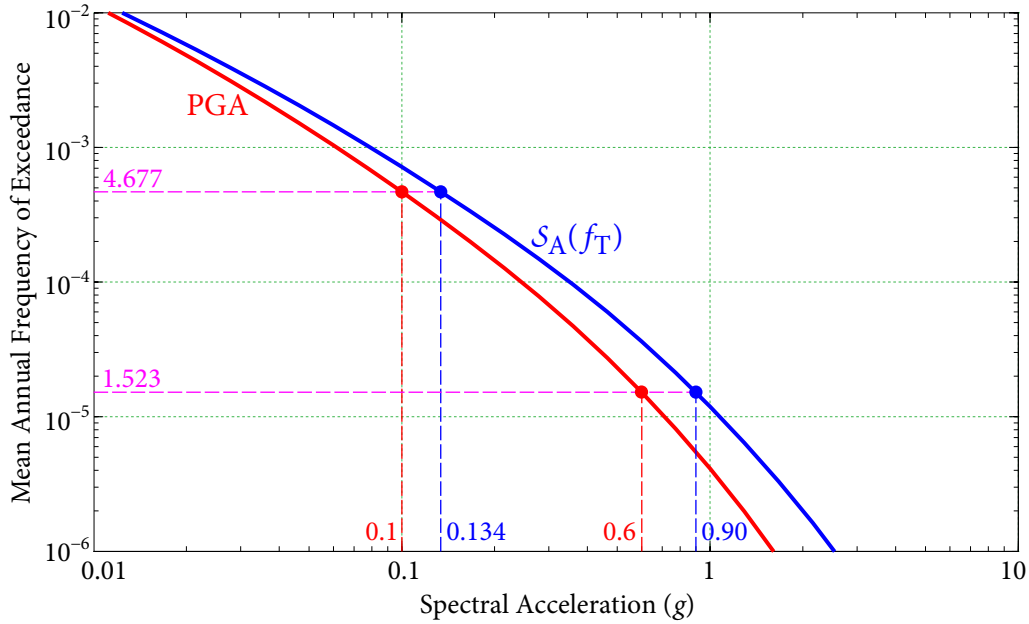


**Figure 4.9** Mean seismic hazard curves with respect to $\mathcal{S}_A(f_T)$ and PGA

seismic input for developing seismic fragility surfaces of the heat exchanger. The procedure for developing seismic fragility surfaces is given briefly as follows:

**1.** Calculate median capacities of the heat exchanger from potential failure modes.

**2.** Discretize spectral domain of $\mathcal{S}_A(f_L)$ and PGA into suitable intervals:

(1) Truncate spectral domain at a reasonably small value $(0.05g)$ and at a reasonably large value $(5g)$.

(2) Uniformly discretize spectral domain in logarithmic scale into $200 \times 200$ intervals.

**3.** Calculate median seismic demand of the heat exchanger:

(1) Define the GRS with spectral acceleration values from an interval as seismic input.

(2) Calculate median seismic demand of the heat exchanger given the input GRS.

(3) Repeat Steps (1) and (2) to determine median seismic demand given input GRS with spectral acceleration values from all intervals.

**4.** Determine numerical distributions of seismic fragility for the heat exchanger:

(1) Calculate *median* ratio factor $R_m$ given an input GRS.

(2) Calculate logarithmic standard deviations $\beta_R$ and $\beta_U$ given the input GRS.

(3) Determine conditional probability of failure value given the input GRS.

(4) Repeat Steps (1) to (3) to calculate conditional probability of failure values for all input GRS.

(5) Integrate conditional probability of failure values to obtain numerical conditional probability of failure distributions.

As long as the intervals are reasonably small, seismic fragility surfaces can be well represented by numerical conditional probability of failure distributions.

#### 4.6.2.2 Conditional Probability of Failure Given an Input GRS

To illustrate the procedure presented in Section 4.6.2.1, conditional probability of failure given an input GRS is calculated. Median capacities of the heat exchanger have been obtained in Chapter 3, hence structural capacity analysis is not performed here.

**Seismic Demand Analysis**

Response spectrum analysis method is used to calculate median seismic demand of the heat exchanger. Prior to performing seismic demand analysis, input GRS needs to be defined (see Figure 4.10). Herein, the input GRS with spectral values $\mathcal{S}_{\mathrm{A}}(f_{\mathrm{L}}) = 0.8g$ and $\mathrm{PGA} = 0.6g$ is taken for example. Recall that $\mathcal{S}_{\mathrm{A}}(f_{\mathrm{T}})$ is proportional to PGA. As shown in Figure 4.9, when $\mathrm{PGA} = 0.6g$, mean AFE value is equal to $1.523 \times 10^{-5}$ from seismic hazard curve for PGA; hence one can obtain spectral value $\mathcal{S}_{\mathrm{A}}(f_{\mathrm{T}}) = 0.9g$ from seismic hazard curve at $f_{\mathrm{T}} = 25.4$ Hz. Therefore, an input GRS going through these three spectral acceleration values, as shown in Figure 4.10, can be defined as horizontal input GRS. Since response spectrum analysis method is used, only spectral values at these three frequencies are needed in the calculation of median seismic demand.

Having defined horizontal input GRS, the vertical input GRS can be obtained using V/H ratios given in Table 3.8 (AMEC, 2009). Given $f_{\mathrm{V}} = 50$ Hz, one can obtain $\mathrm{V/H} = 0.865$ by linear interpolation in logarithmic scale between 40 Hz and 62.5 Hz; hence spectral acceleration in vertical direction $\mathcal{S}_{\mathrm{A}}(f_{\mathrm{V}}) = 0.6 \times 0.865 = 0.52g$. Table 4.1 summarizes spectral accelerations in three directions. Assuming that seismic inputs in longitudinal and trans-

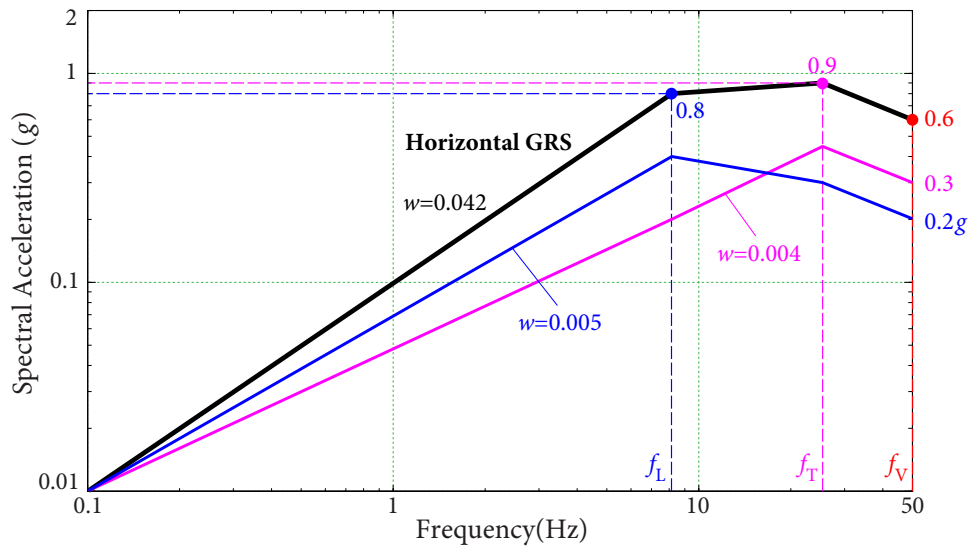


**Figure 4.10** An example of horizontal input GRS

verse directions are equal in magnitude, seismic inputs in three directions can be applied simultaneously to calculate median seismic demand of the heat exchanger.

**Table 4.1** Spectral Values at Three Frequencies

| **Direction** | **Frequency (Hz)** | $\mathcal{S}_A\,(g)$ |
|---|---|---|
| Longitudinal | 8.15 | 0.8 |
| Transverse | 25.4 | 0.9 |
| Vertical | 50 | $0.865 \times 0.6 = 0.52$ |

**Table 4.2** Tension and Shear Demand of Heat Exchanger

| **Controlling Direction** | **Shear Force (kips)** | **Tension Force (kips)** |
|---|---|---|
| Longitudinal | 14.83 | 10.07 |
| Transverse | 15.88 | 8.04 |

Having obtained spectral accelerations in three directions, median tension and shear demand of the heat exchanger can be determined according to the procedure in Chapter 3, and are summarized in Table 4.2.

### Median Ratio Factor

Since anchor bolts are subjected to tension and shear simultaneously, a tension-shear interaction relationship (see Chapter 3) is applied. To determine the *median* strength factor, two regions, i.e., pure tension region and shear/tension region are considered.

**1. Longitudinal direction controls**

- Pure tension region

  The *median* strength factor is given by

$$F_{S1,m} = \frac{C - D_{NS}}{D_S + \Delta C_S} = \frac{N_{min} - N_{DL}}{N_{Long}} = \frac{26.76 - (-6.11)}{10.07} = 3.26. \tag{4.6.3}$$

- Shear/Tension region

  The *median* strength factor is given by

$$F_{S2,m} = \frac{C - D_{NS}}{D_S + \Delta C_S} = \frac{V_{ST} - 0.7\,\frac{V_{ST}}{N_{ST}}\,N_{DL}}{V_{Long} + 0.7\,\frac{V_{ST}}{N_{ST}}\,N_{Long}} = \frac{23.26 - 0.7 \times \frac{23.26}{34.89} \times (-6.11)}{14.83 + 0.7 \times \frac{23.26}{34.89} \times 10.07} = 1.34. \tag{4.6.4}$$

**2. Transverse direction controls**

- Pure tension region

  The *median* strength factor is given by

$$F_{S3,m} = \frac{C - D_{NS}}{D_S + \Delta C_S} = \frac{N_{min} - N_{DL}}{N_{Tran}} = \frac{26.76 - (-6.11)}{15.88} = 2.07. \tag{4.6.5}$$

- Shear/Tension region

  The *median* strength factor is given by

$$F_{S4,m} = \frac{C - D_{NS}}{D_S + \Delta C_S} = \frac{V_{ST} - 0.7\,\frac{V_{ST}}{N_{ST}}\,N_{DL}}{V_{Tran} + 0.7\,\frac{V_{ST}}{N_{ST}}\,N_{Tran}} = \frac{23.26 - 0.7 \times \frac{23.26}{34.89} \times (-6.11)}{8.04 + 0.7 \times \frac{23.26}{34.89} \times 15.88} = 1.69. \tag{4.6.6}$$

Therefore, the controlling failure mode is shear-tension interaction failure of anchor bolts in longitudinal direction. Having obtained *median* strength factor $F_{S,m} = 1.34$, neglecting

inelastic energy absorption effects, i.e., $F_\mu = 1.0$, *median* ratio factor $R_m$ can be determined by

$$R_m = F_\mu \cdot F_{\mathrm{RS},m} \cdot F_{\mathrm{S},m} = 1.0 \times 1.0 \times 1.34 = 1.34. \tag{4.6.7}$$

### Logarithmic Standard Deviations

The *approximate second-moment procedure* is applied to calculate the variability of ratio factor $R$ due to basic capacity and response variables. Table 4.3 enumerates the logarithmic standard deviations for all basic variables. SRSS rule is used to calculate $\beta_R$ of total *randomness* and $\beta_U$ of total *uncertainty* from basic variables. $\beta_{\mathrm{C}}$ of composite variability is then determined by

$$\beta_{\mathrm{C}} = \sqrt{\beta_R^2 + \beta_U^2}. \tag{4.6.8}$$

### Determination of Seismic Fragility

Having obtained *median* ratio factor $R_m$ and logarithmic standard deviations $\beta_R$ and $\beta_U$, given the input GRS, conditional probability of failure $p_{\mathrm{F},q}\big(0.6, 0.8\big)$, at confidence level $Q = q$, can be determined by

$$p_{\mathrm{F},q}\big(0.6, 0.8 \,\big|\, Q = q\big) = \Phi\left\{\frac{\ln\big(1/R_m\big) + \beta_U \Phi^{-1}(q)}{\beta_R}\right\}. \tag{4.6.9}$$

In applications, confidence level $Q$ is usually taken as discrete values. Taking confidence level $Q = 95\%$ for example, $p_{\mathrm{F},q}\big(0.6, 0.8 \,\big|\, Q = 0.95\big)$ is given by

$$p_{\mathrm{F},q}\big(0.6, 0.8 \,\big|\, Q = 0.95\big) = \Phi\left\{\frac{\ln(1/1.34) + 0.20 \times \Phi^{-1}(0.95)}{0.18}\right\} = 0.601. \tag{4.6.10}$$

When composite variability is used, composite (mean) seismic fragility is calculated as

$$p_{\mathrm{F,C}}\big(0.6, 0.8\big) = \Phi\left\{\frac{\ln\big(1/R_m\big)}{\beta_{\mathrm{C}}}\right\} = \Phi\left\{\frac{\ln(1/1.34)}{0.27}\right\} = 0.140. \tag{4.6.11}$$

### Development of Seismic Fragility Surfaces

Defining input GRS with spectral acceleration values at three frequencies from all other intervals of spectral domain, and repeating the procedure for calculating conditional probability of failure values result in a family of numerical conditional probability of failure

**Table 4.3** The Variability of $R$ from Response and Capacity Variables

| Case | **Variable** | *Randomness* | *Uncertainty* | $R$ | $\beta_i$ | |
|---|---|---|---|---|---|---|
| 0 | **Base Case** | Variable at median | | 1.34 | | |
| | **Response Variables** | Variable at median plus $1\sigma$ | | $R_{1\sigma}$ | $\beta_R$ | $\beta_U$ |
| 1 | Horizontal direction peak response | $\mathcal{S}_a(f_{\mathrm{L}})\,\mathrm{e}^{0.13}$<br>$\mathcal{S}_a(f_{\mathrm{T}})\,\mathrm{e}^{-0.13}$ | | 1.21 | 0.10 | |
| 2 | Vertical component response | $\mathcal{S}_a(f_{\mathrm{V}})\,\mathrm{e}^{0.34}$ | | 1.32 | 0.01 | |
| 3 | Damping | | $\mathcal{S}_a(f_{\mathrm{L}})\,\mathrm{e}^{0.17}$<br>$\mathcal{S}_a(f_{\mathrm{T}})\,\mathrm{e}^{0.16}$ | 1.13 | | 0.17 |
| 4 | Frequency | | $\mathcal{S}_a(f_{\mathrm{L}})\,\mathrm{e}^{0.05}$<br>$\mathcal{S}_a(f_{\mathrm{T}})\,\mathrm{e}^{0.05}$ | 1.27 | | 0.05 |
| 5 | Modal shape | | $\mathcal{S}_a(f_{\mathrm{L}})\,\mathrm{e}^{0.05}$<br>$\mathcal{S}_a(f_{\mathrm{T}})\,\mathrm{e}^{0.05}$ | 1.27 | | 0.05 |
| 6 | Modal combination | | $\mathcal{S}_a(f_{\mathrm{L}})\,\mathrm{e}^{0.05}$<br>$\mathcal{S}_a(f_{\mathrm{T}})\,\mathrm{e}^{0.05}$ | 1.27 | | 0.05 |
| 7 | Earthquake component combination | Abs. Sum<br>at $3.0\sigma$ | | 1.17 | 0.14 | |
| | **Capacity Variable** | Variable at median minus $1\sigma$ | | $R_{-1\sigma}$ | $\beta_R$ | $\beta_U$ |
| 8 | Anchor bolts | | $V_{\mathrm{ST}}\,\mathrm{e}^{-0.10}$<br>$N_{\mathrm{ST}}\,\mathrm{e}^{-0.13}$ | 1.22 | | 0.09 |
| | **SRSS Combination** | | | | $\beta_R$ | $\beta_U$ |
| | | | | | 0.18 | 0.20 |
| | | | | $\beta_{\mathrm{C}}$ | 0.27 | |

distributions, as shown in Figure 4.11. Since the size of intervals are reasonable small, a family of seismic fragility surfaces can be approximated by the numerical distributions. Figure 4.12 gives the composite (mean) seismic fragility surface of the heat exchanger.

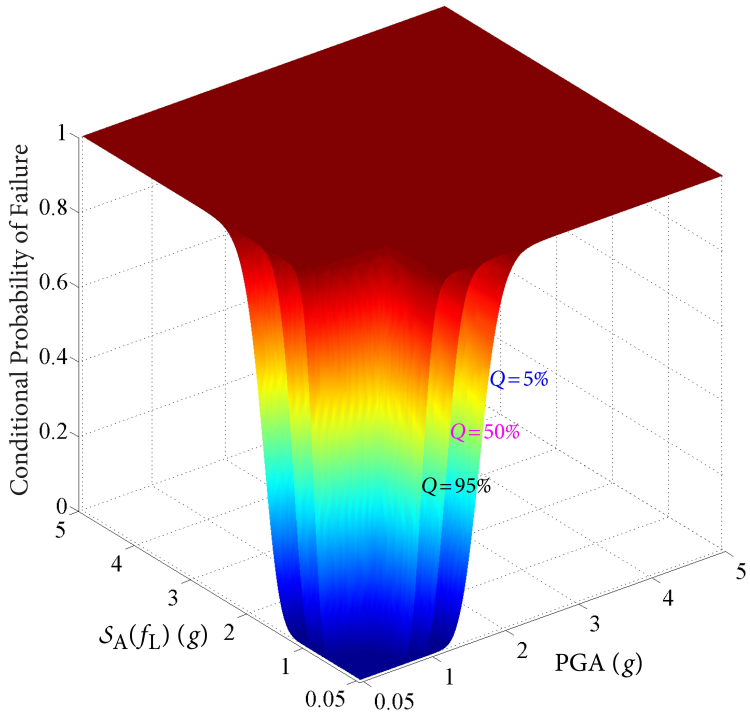


**Figure 4.11** A family of fragility surfaces of $\mathcal{S}_A(f_L)$ and PGA

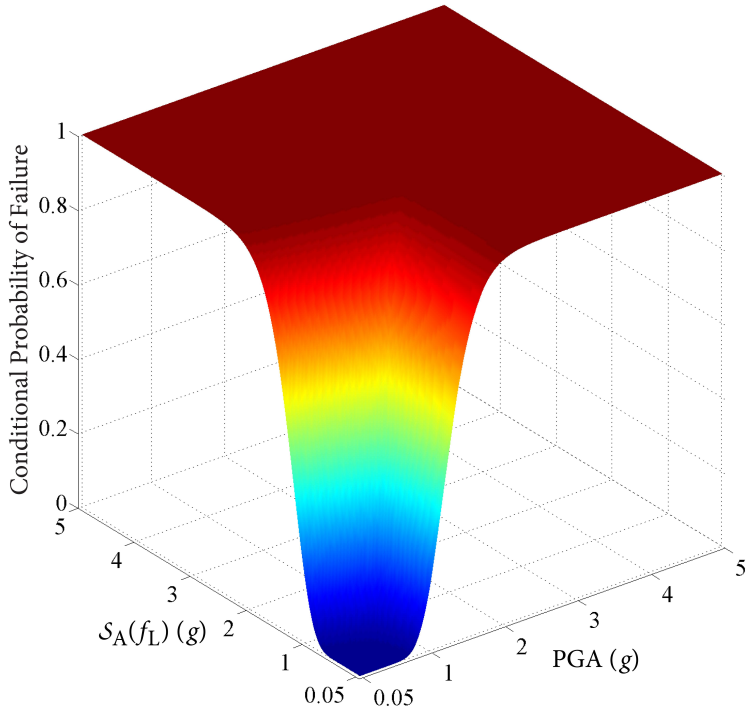


**Figure 4.12** Mean fragility surface of $\mathcal{S}_A(f_L)$ and PGA

Compared to conventional fragility curve in current seismic fragility analysis, features of fragility surface are summarized as follows:

- Aleatory randomness in earthquake response spectra is properly captured

  In the UHS, logarithmic spectral accelerations at any two frequencies are assumed to be fully correlated. In seismic fragility analysis considering VGMPs, since the correlation between $\ln \mathcal{S}_A(f_L)$ and $\ln \mathrm{PGA}$ is addressed, the aleatory randomness in earthquake response spectra is properly captured. As shown Figure 4.13, given a PGA value, $\mathcal{S}_A(f_L)$ can take a great number of values. Therefore, it would better predict structural response of the heat exchanger induced by seismic hazard at Darlington NGS site.

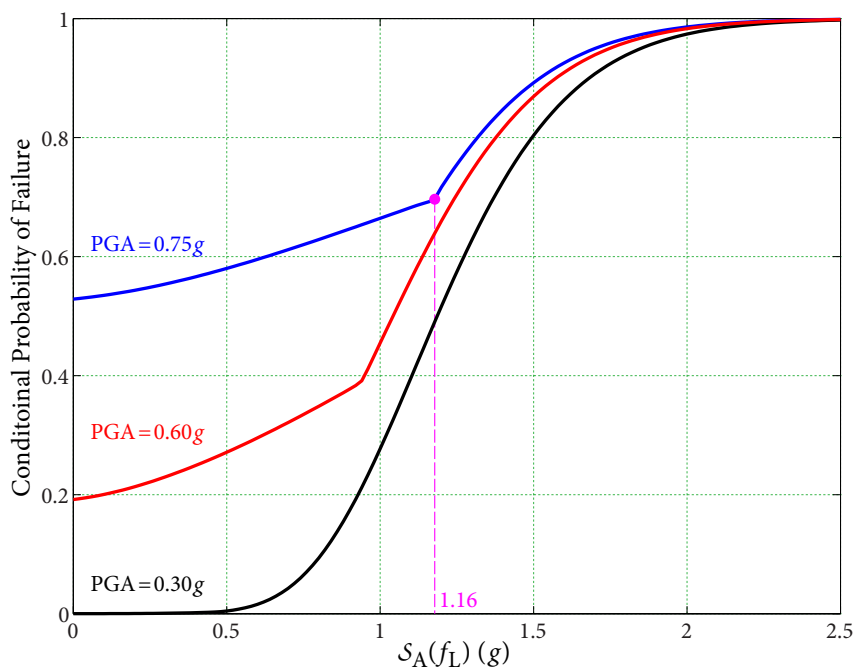


**Figure 4.13** Sections of mean fragility surface

- There exist multiple controlling failure modes

  In current seismic fragility analysis, only a single controlling failure mode is considered in the analysis. In reality, however, multiple failure modes probably become the controlling failure mode, induced by different earthquake excitations. In seismic fragility analysis considering VGMPs, a great number of input GRS are defined as

seismic input, covering a wide range of earthquake excitations. Therefore, it can take account of multiple potential controlling failure modes in the analysis. For example, as shown in Figure 4.13, given $\mathrm{PGA} = 0.75g$, conditional probability of failure increases slowly when $\mathcal{S}_{\mathrm{A}}(f_{\mathrm{L}}) < 1.16g$, while increases dramatically after $\mathcal{S}_{\mathrm{A}}(f_{\mathrm{L}})$ exceeds $1.16g$. It implies there are more than one controlling failure mode occurring.

#### 4.6.2.3 Summary

In this Section, two GMPs $\mathcal{S}_{\mathrm{A}}(f_{\mathrm{L}})$ and PGA are used in the development of seismic fragility surfaces of the heat exchanger. Due to the use of a great number of input GRS, the aleatory randomness in earthquake response spectra is properly captured In addition, since response spectrum analysis method is used in seismic demand analysis, the development of seismic fragility surfaces is time efficient even though a great number of input GRS are used.

### 4.6.3 Development of Weighting Seismic Fragility Curves

#### 4.6.3.1 Procedure

Figure 4.14 shows the section of seismic fragility surface with $Q = 95\%$ at $\mathrm{PGA} = 0.6g$ (thick black curve). It can be seen that, given $\mathrm{PGA} = 0.6g$, $\mathcal{S}_{\mathrm{A}}(f_{\mathrm{L}})$ can take different spectral values from $0.05g$ to $5g$ to account for its aleatory variability. Given $\mathrm{PGA} = 0.6g$, for input GRS going through a spectral value of $\mathcal{S}_{\mathrm{A}}(f_{\mathrm{L}})$, one can determine the conditional probability of failure from the thick black curve. The blue curve in the horizontal plane describes mean annual rate density of $\mathcal{S}_{\mathrm{A}}(f_{\mathrm{L}})$. Given $\mathrm{PGA} = 0.6g$, based on mean annual rate density, one can obtain the weights of input GRS corresponding to different spectral acceleration values of $\mathcal{S}_{\mathrm{A}}(f_{\mathrm{L}})$. To illustrate, take the input GRS in Section 4.6.2.2 as an example. For this input GRS, $\mathcal{S}_{\mathrm{A}}(f_{\mathrm{L}}) = 0.8g$ and $\mathrm{PGA} = 0.6g$, the conditional probability of failure is obtained as 0.601 (see thick black curve). From mean annual rate density given $\mathrm{PGA} = 0.6g$ (blue curve in horizontal plane), the annual rate of occurrence of input GRS (magenta column under blue curve) is obtained as 0.009. The weight of the input GRS is determined using equation (4.6.2). For input GRS with other spectral values of $\mathcal{S}_{\mathrm{A}}(f_{\mathrm{L}})$, the weights can be determined using an equation similar to (4.6.2). Similarly, changing PGA values gives the weights of input GRS with different spectral values of $\mathcal{S}_{\mathrm{A}}(f_{\mathrm{L}})$.

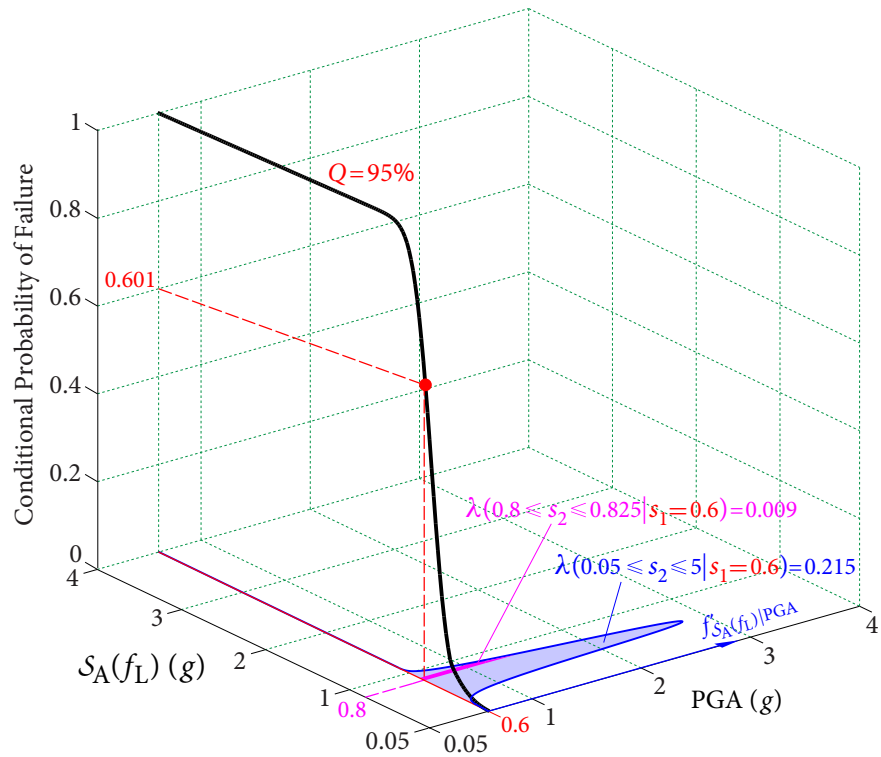


**Figure 4.14** An example of section of fragility surface and mean annual rate density

In this example, weighting seismic fragility curves in terms of PGA are determined. The procedure to determine weighting curves is briefly summarized as follows:

1. Discretize spectral domain of $\mathcal{S}_{\mathrm{A}}(f_{\mathrm{L}})$ and PGA into intervals:
   (a) Truncate two-dimensional spectral domain at lower and upper bound values.
   (b) Uniformly discretize spectral domain in logarithmic scale into intervals.

2. Determine numerical distribution of weighting seismic fragility:
   (a) Calculate the weights of input GRS given a PGA value.
   (b) Determine seismic fragility given the input GRS.
   (c) Combine the weights and seismic fragility to obtain weighting seismic fragility given the PGA value.
   (d) Repeat Steps (a) to (c) to determine weighting seismic fragility given other PGA values.

(e) Integrate weighting seismic fragility values to determine numerical distribution of weighting seismic fragility curves.

As long as the intervals of spectral domain are sufficiently small, the weighting seismic fragility curves can be well represented by the numerical distributions.

#### 4.6.3.2 Weighting Seismic Fragility Curves

##### Discretization of Spectral Domain

In nuclear engineering practice, the GMP selected is usually truncated at lower and upper bound values. As in EPRI-1022995 (EPRI, 2011), for severe core damage frequency (SCDF) ranging from $p_{f,\mathrm{L}} = 1 \times 10^{-5}$ to $p_{f,\mathrm{H}} = 5 \times 10^{-5}$ ($f$ stands for frequency, and L and H stand for "Low" and "High"), mean seismic hazard range of GMP is determined by

$$\begin{aligned} p_{\mathrm{h,L}} &= 0.1 \times p_{f,\mathrm{L}} = 0.1 \times 1 \times 10^{-5} = 1 \times 10^{-6}, \\ p_{\mathrm{h,H}} &= 20 \times p_{f,\mathrm{H}} = 20 \times 5 \times 10^{-5} = 1 \times 10^{-3}, \end{aligned} \tag{4.6.12}$$

where h stands for "hazard".

Having obtained $p_{\mathrm{h,L}}$ and $p_{\mathrm{h,H}}$, lower and upper bound values of GMP can be obtained from interpolating mean seismic hazard curve with respect to $p_{\mathrm{h,L}}$ and $p_{\mathrm{h,H}}$. Take mean seismic hazard curve for $\mathcal{S}_{\mathrm{A}}(f_{\mathrm{L}})$ (Figure 4.15) as an example. Taking $p_{\mathrm{h,L}}$ and $p_{\mathrm{h,H}}$ in equations (4.6.12), one can easily find recommended lower and upper bound values $s_{\mathrm{L}} = 0.11g$ and $s_{\mathrm{U}} = 3.16g$. In addition, one can also find $s_{\mathrm{L}} = 0.06g$ and $s_{\mathrm{U}} = 1.60g$ for PGA. In this example, $\mathcal{S}_{\mathrm{A}}(f_{\mathrm{L}})$ is uniformly discretized in logarithmic scale into 100 intervals between $\left[0.10g, 5g\right]$, and PGA is uniformly discretized in logarithmic scale into 100 intervals between $\left[0.05g, 2.5g\right]$. Having discretized the spectral domain, the GRS with different combination of spectral values of VGMPs are defined as seismic input.

##### Weights of Input GRS

Given a PGA value, weights of input GRS with different spectral values of $\mathcal{S}_{\mathrm{A}}(f_{\mathrm{L}})$ can be calculated based on mean annual rate density of $\mathcal{S}_{\mathrm{A}}(f_{\mathrm{L}}) \,|\, \mathrm{PGA}$. Based on Figure 4.8, taking $\mathrm{PGA} = 0.6g$ for example, the annual rate of occurrence of $\mathcal{S}_{\mathrm{A}}(f_{\mathrm{L}})$ in interval $\left[0.10g, 5g\right]$ is

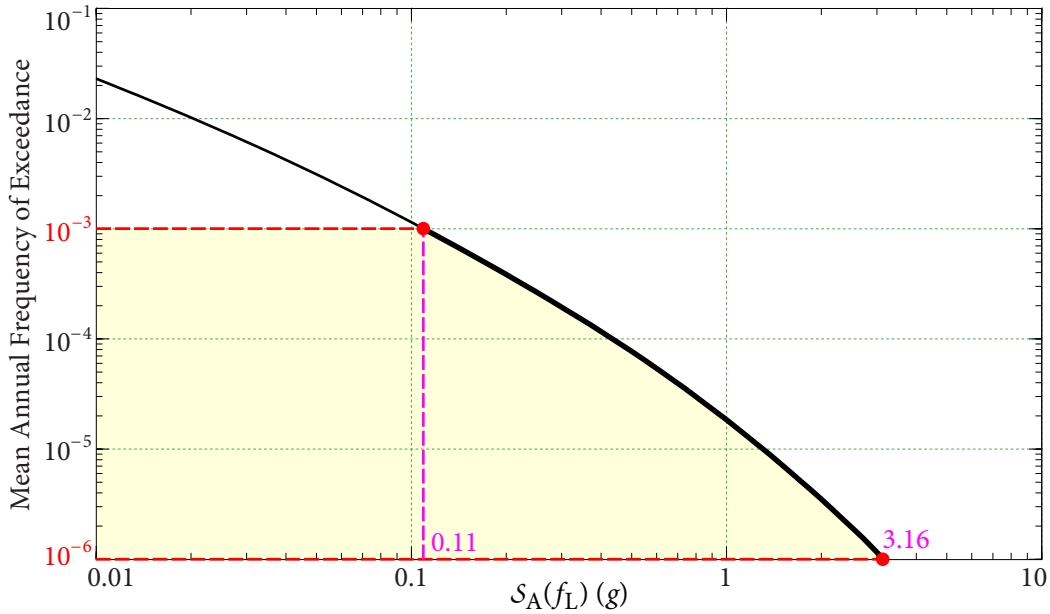


**Figure 4.15** Mean seismic hazard curve for $\mathcal{S}_A(f_L)$

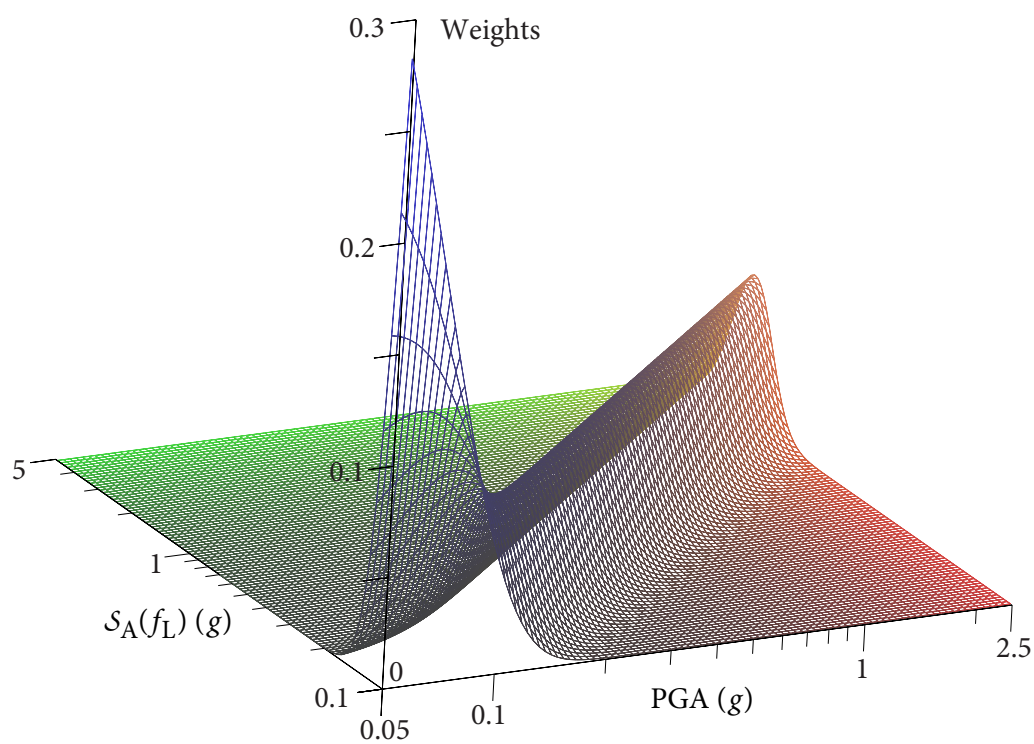


**Figure 4.16** Weights of input GRS

given by

$$\lambda\left(s_{\mathrm{L}} \leqslant s_2 \leqslant s_{\mathrm{U}} \,\middle|\, s_1\right) \approx \sum_{i_2=1}^{100} \left[ f'_{\mathcal{S}_{\mathrm{A}}(f_{\mathrm{L}})|\mathrm{PGA}}\left(s_2^{(i_2)} \,\middle|\, s_1 = 0.6g\right) \Delta s_2^{(i_2)} \right] = 0.215. \tag{4.6.13}$$

Therefore, given $s_1 = 0.6g$, the weight of input GRS with spectral value $\mathcal{S}_{\mathrm{A}}(f_{\mathrm{L}}) = s_2^{(i_2)}$ can be determined by

$$w\left(s_2^{(i_2)} \leqslant s_2 < s_2^{(i_2+1)} \,\middle|\, s_1\right) = \frac{\lambda\left(s_2^{(i_2)} \leqslant s_2 \leqslant s_2^{(i_2+1)} \,\middle|\, s_1\right)}{\lambda\left(s_{\mathrm{L}} \leqslant s_2 \leqslant s_{\mathrm{U}} \,\middle|\, s_1\right)} \approx \frac{f'_{\mathcal{S}_{\mathrm{A}}(f_{\mathrm{L}})|\mathrm{PGA}}\left(s_2^{(i_2)} \,\middle|\, s_1 = 0.6g\right) \Delta s_2^{(i_2)}}{0.215}. \tag{4.6.14}$$

For example, given $\mathcal{S}_{\mathrm{A}}(f_{\mathrm{L}}) = 0.8g$ and $\mathrm{PGA} = 0.6g$, the weight of the input GRS going through these two spectral values is given by $w\left(0.8g \leqslant s_2 \leqslant 0.825g \,\middle|\, s_1 = 0.6g\right) = 0.042$. Repeating for all PGA values gives the numerical distribution of weights of input GRS, as shown in Figure 4.16.

### Weighting Seismic Fragility

As in Section 4.6.2.2, given input GRS with spectral values $\mathcal{S}_{\mathrm{A}}(f_{\mathrm{L}}) = s_2^{(i_2)}$ and $s_1 = 0.6g$, seismic fragility at confidence level $Q = q$, is given by

$$p_{\mathrm{F},q}\left(s_2^{(i_2)}, s_1 = 0.6g\right) = \Phi\left\{ \frac{\ln\left[1/R_m(s_2^{(i_2)}, s_1)\right] + \beta_U(s_2^{(i_2)}, s_1)\,\Phi^{-1}(q)}{\beta_R(s_2^{(i_2)}, s_1)} \right\}, \tag{4.6.15}$$

where $R_m\left(s_2^{(i_2)}, s_1\right)$ is *median* ratio factor for the input GRS. $\beta_R(s_2^{(i_2)}, s_1)$ and $\beta_U(s_2^{(i_2)}, s_1)$ are total logarithmic standard deviations of aleatory *randomness* and epistemic *uncertainty*, respectively, for the input GRS.

Therefore, the weighting seismic fragility in terms of PGA, at $s_1 = 0.6g$, is determined by

$$\bar{p}_{\mathrm{F},q}(s_1 = 0.6g) = \sum_{i_2=1}^{100} \left[ p_{\mathrm{F},q}\left(s_2^{(i_2)}, s_1 = 0.6g\right) \cdot w\left(s_2^{(i_2)} \leqslant s_2 < s_2^{(i_2+1)} \,\middle|\, s_1\right) \right]. \tag{4.6.16}$$

For example, given $Q = 95\%$, the weighting seismic fragility at $s_1 = 0.6g$ is given by

$$\bar{p}_{\mathrm{F},q}(s_1 = 0.6g) = \sum_{i_2=1}^{100} \left[ p_{\mathrm{F},q}\left(s_2^{(i_2)}, s_1 = 0.6g\right) \cdot w\left(s_2^{(i_2)} \leqslant s_2 \leqslant s_2^{(i_2+1)} \,\middle|\, s_1 = 0.6g\right) \right] = 0.302, \tag{4.6.17}$$

where $p_{\mathrm{F},q}\left(s_2^{(i_2)}, s_1 = 0.6g\right)$ can be determined from the section of fragility surface as shown in Figure 4.14 (the thick black curve with $Q = 95\%$).

Changing PGA value from lower bound $0.05g$ to upper bound $2.5g$, and repeating above procedure gives a set of numerical distributions of weighting seismic fragility, as shown in Figure 4.17. When mean fragility surface is used, a mean weighting fragility curve can be obtained and is shown in Figure 4.17.

Furthermore, HCLPF seismic capacity can be determined based on its definition and is shown in Figure 4.18. It is noted that conditional probability of failure is plotted in logarithmic scale. One can see that $\bar{\mathscr{C}}_{1\%}^{\mathrm{C}}$ is very close to HCLPF seismic capacity ($\bar{\mathscr{C}}_{\mathrm{HCLPF}}$). It implies that, in the proposed method, $\bar{\mathscr{C}}_{1\%}^{\mathrm{C}}$ also can be used to approximate $\bar{\mathscr{C}}_{\mathrm{HCLPF}}$ in applications.

#### 4.6.3.3 Comparison of Seismic Fragility Curves and HCLPF Seismic Capacities

In this Section, seismic fragility curves of the heat exchanger are determined based on two methods, i.e., current and weighting seismic fragility analysis methods. Both sets of fragility curves are shown in Figure 4.19. Conventional seismic fragility curves of the heat exchanger are obtained in Chapter 3.

Figure 4.19 shows that the weighting *median* seismic capacity of the heat exchanger has 53.9% increase (from $0.636g$ PGA to $0.979g$ PGA). The HCLPF seismic capacities based on two methods are calculated from 95% confidence seismic fragility curves, and are shown in Figure 4.20. It can be seen that the weighting HCLPF seismic capacity has 26.1% increase (from $0.349g$ PGA to $0.440g$ PGA). Both results indicate that current seismic fragility analysis includes considerable conservatism in estimating *median* and HCLPF seismic capacity. The conservatism primarily stems from the absence of correlation between logarithmic spectral acceleration at longitudinal direction $\mathcal{S}_{\mathrm{A}}(f_{\mathrm{L}})$ and PGA. For

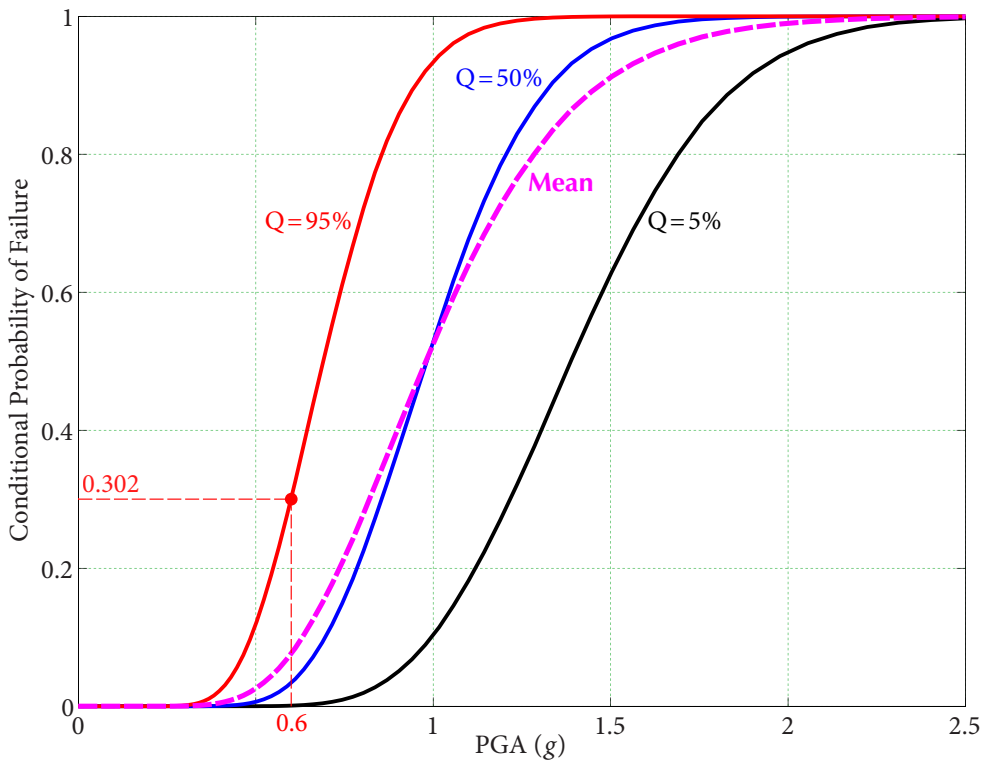


**Figure 4.17** Weighting seismic fragility curves of heat exchanger

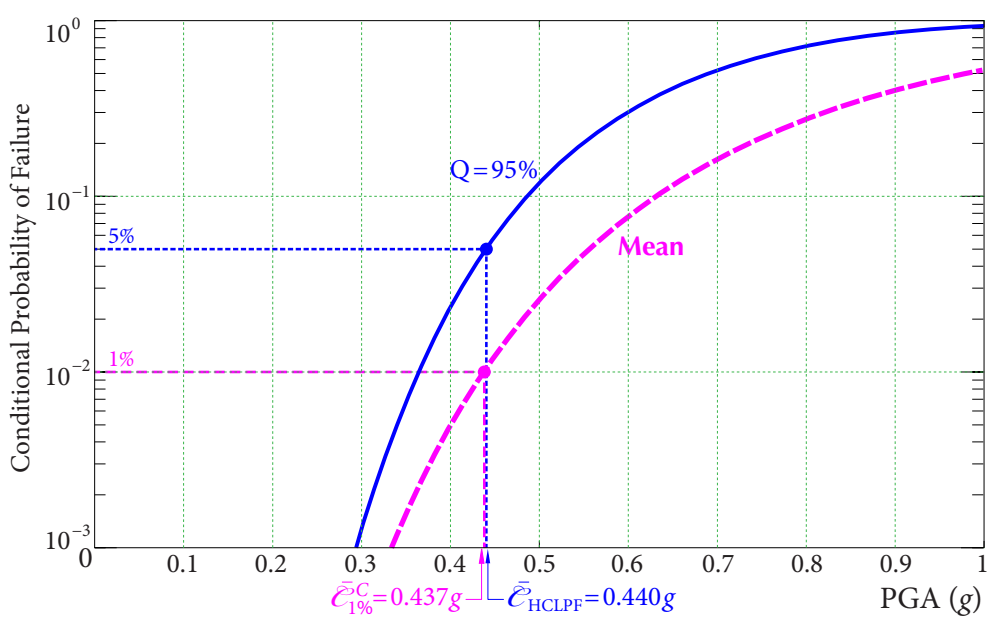


**Figure 4.18** Weighting HCLPF seismic capacity of heat exchanger

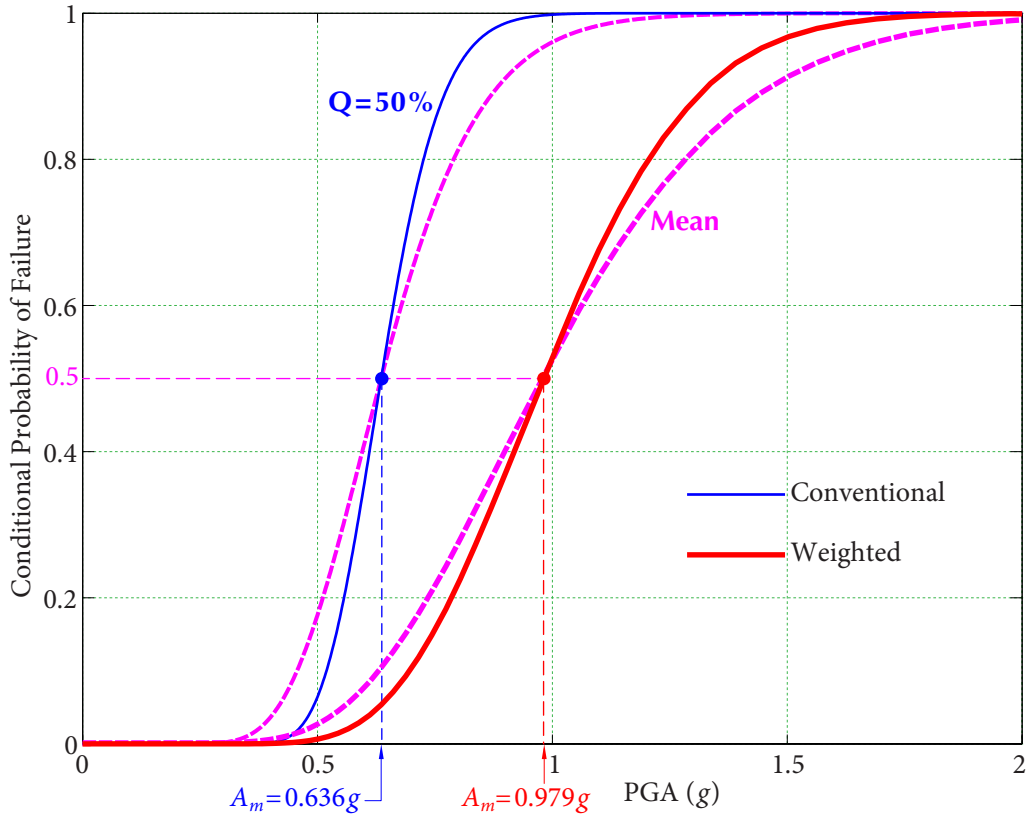


**Figure 4.19** Seismic fragility curves of heat exchanger based on two methods

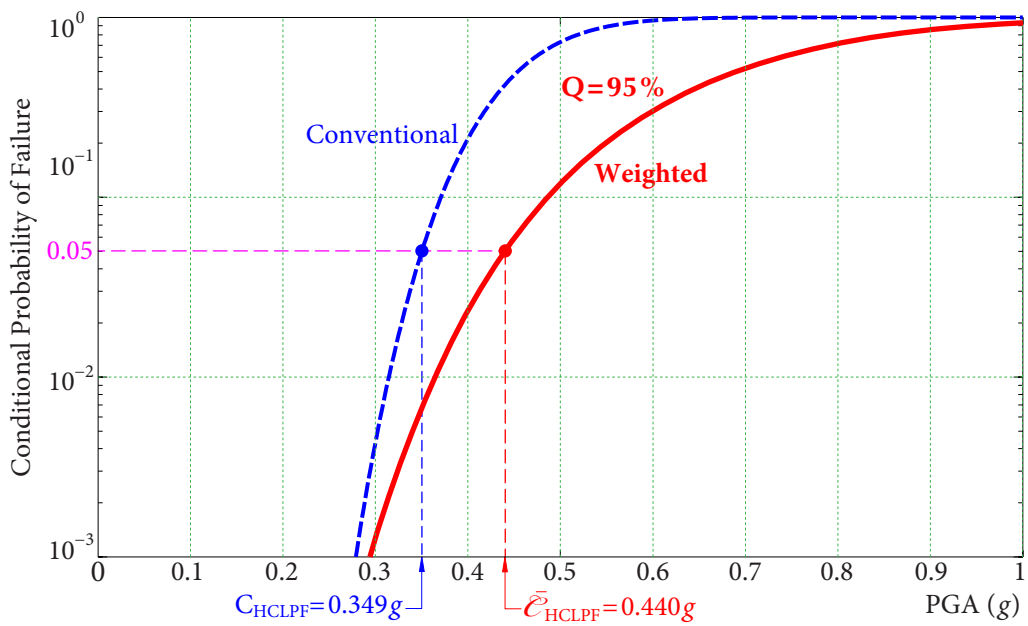


**Figure 4.20** HCLPF capacity of heat exchanger based on two methods

safety-related SSCs, incorporating correlations among logarithmic spectral accelerations can more accurately estimate their HCLPF seismic capacities.

### 4.6.4 Mean Annual Frequency of Occurrence of Failure of Heat Exchanger

In nuclear power plants, the failure of heat exchanger probably triggers an adverse consequence such as core damage accident. Mean annual frequency of occurrence of the failure of heat exchanger is calculated by equation (4.1.5), i.e.,

$$\gamma = -\int_0^{\infty} \bar{p}_{\mathrm{F,C}}(s_1)\frac{\mathrm{d}H(s_1)}{\mathrm{d}s_1}\mathrm{d}s_1. \tag{4.6.18}$$

Numerical method is usually applied to quantify the integral in equation (4.6.18) as

$$\gamma = -\sum_{i=1}^{N_1} \bar{p}_{\mathrm{F,C}}(s^{(i)})\Delta H(s^{(i)}), \tag{4.6.19}$$

where $N_1$ is the number of intervals of $\mathcal{S}_{\mathrm{A}}(f_1)$.

Recall that in Chapter 1, mean annual frequency of occurrence of the failure of heat exchanger is given by

$$\gamma = -\int_0^{\infty} p_{\mathrm{F,C}}(s_1)\frac{\mathrm{d}H(s_1)}{\mathrm{d}s_1}\mathrm{d}s_1 = -\sum_{i=1}^{N_1} p_{\mathrm{F,C}}(s^{(i)})\Delta H(s^{(i)}). \tag{4.6.20}$$

In this example, mean annual frequency of occurrence of the failure of heat exchanger is calculated separately by equations (4.6.19) and (4.6.20). Site-specific UHS is defined as RLE in the development of conventional (as opposed to weighting) mean seismic fragility curve:

- **Conventional mean fragility curve is used**

  Mean annual frequency of occurrence of the failure of heat exchanger is given by

  $$\gamma = -\sum_{i=1}^{N_1} p_{\mathrm{F,C}}(s^{(i)})\Delta H(s^{(i)}) = 1.534\times 10^{-5}, \tag{4.6.21}$$

  where $N_1 = 100$ is the number of intervals of PGA between lower bound $0.05g$ and upper bound $2.5g$. $H(s^{(i)})$ is mean seismic hazard with respect to spectral value $s^{(i)}$ of PGA.

- **Weighting mean fragility curve is used**

  Weighting mean annual frequency of occurrence of the failure of heat exchanger is given by

$$\bar{\gamma} = -\sum_{i=1}^{N_1} \bar{p}_{\mathrm{F,C}}(s^{(i)})\Delta H(s^{(i)}) = 6.074 \times 10^{-6}, \tag{4.6.22}$$

  where $N_1 = 100$ is the number of intervals of PGA.

It can be seen that the weighting mean annual frequency has 60.4% decrease compared to that based on conventional mean fragility curve.

## 4.7 Summary

In this Chapter, weighting seismic fragility analysis method is firstly proposed for developing weighting seismic fragility curves and HCLPF seismic capacities of safety-related structures, systems, and components (SSCs):

1. vector-valued Probabilistic Seismic Hazard Analysis (VPSHA) is performed for capturing aleatory randomness in earthquake response spectra and considering ground motion intensity effect;
2. seismic fragility analysis considering vector-valued GMPs (VGMPs) method is proposed for calculating seismic fragility in terms of VGMPs;
3. weighting process is conducted for determining weighting seismic fragility and HCLPF seismic capacity in terms of a single GMP such as PGA, based on Steps 1 and 2.

By using VGMPS, more accurate seismic capacities of safety-related SSCs are obtained. They are also readily incorporated into Seismic Probabilistic Risk Analysis and Seismic Margin Assessment.

To better illustrate the procedure and demonstrate the advantages of weighting seismic fragility analysis method, numerical example for a horizontal heat exchanger is performed:

- weighting HCLPF seismic capacity has 26.1% increase, comparing to conventional HCLPF seismic capacity;
- weighting mean annual frequency of occurrence of the failure of heat exchanger has a 60.4% decrease, comparing to conventional mean annual frequency of occurrence.

The results show that the weighting seismic fragility analysis method can more accurately estimate seismic capacity and mean annual frequency of the failure of heat exchanger.

Weighting seismic fragility analysis method should be performed for safety-related SSCs so that more accurate seismic capacity estimates are achieved.

C H A P T E R 5

# Weighting Seismic Fragility Analysis for Components on Structures

For components mounted on primary structures, floor response spectra (FRS) are defined as seismic input for calculating structural responses of components. Time history analyses are widely used to calculate structural responses. To achieve accurate structural responses, a number of sets of acceleration time histories spectrum-compatible with ground response spectra are needed for generating FRS. As a result, time history analyses are computationally expensive.

In this Chapter, weighting seismic fragility analysis for components on structures is presented. A direct spectra-to-spectra method instead of time history analyses is applied to generate FRS for components, aiming to improve the efficiency in developing seismic fragility surfaces. To illustrate the procedure of the proposed method, weighting seismic fragility curves and High Confidence and Low Probability of Failure (HCLPF) seismic capacities of a block wall on a service building are determined. The results show that weighting *median* and HCLPF seismic capacities of the block wall have significant increase.

## 5.1 Introduction

ASCE 4-98 (ASCE, 1998) requires that FRS be generated by either time history analyses or a direct spectra-to-spectra method, as illustrated in Figure 5.1.

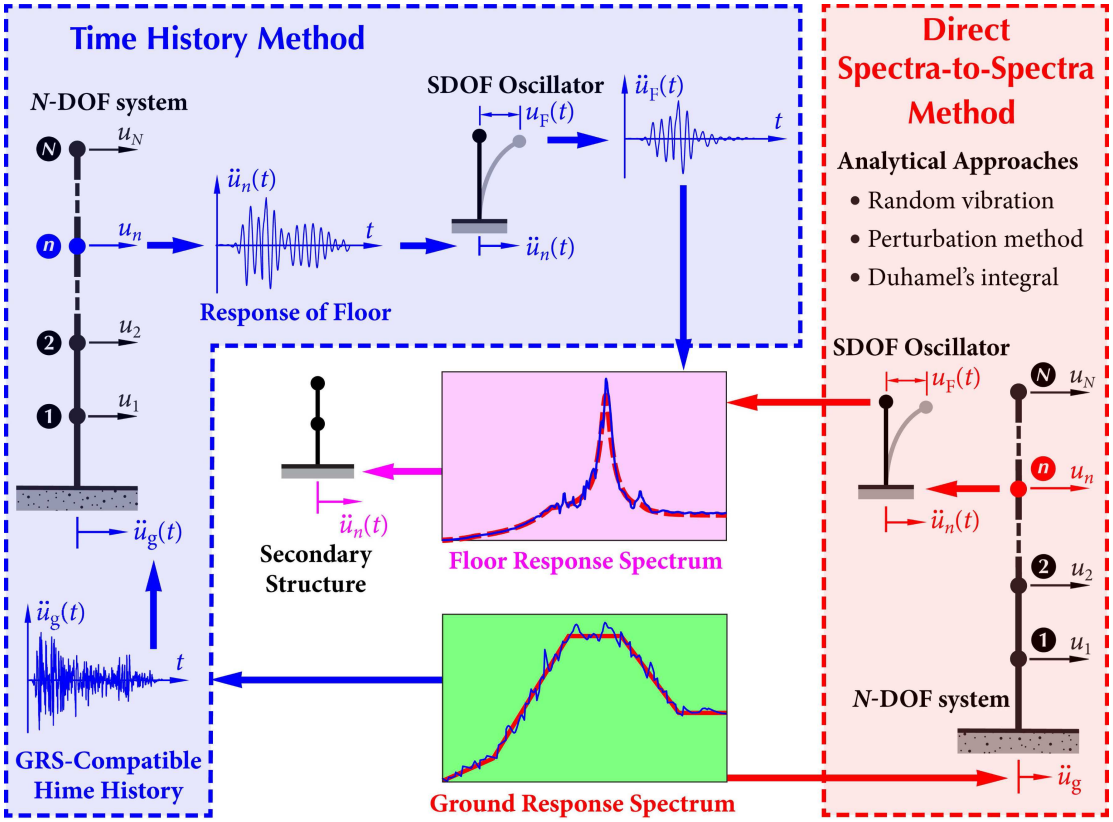


**Figure 5.1** Two methods for generating FRS

Time history analyses have been widely used to generate FRS. The procedure of generating FRS includes three steps:

1. **Generation of time histories spectrum-compatible with ground response spectra**
   - Define the input ground response spectra (GRS) at the site of interest.
   - Generate tri-directional time histories spectrum-compatible with the input GRS.
2. **Structural dynamic analyses**
   - Employ finite element software to establish finite element model of the structure.
   - Define tri-directional spectrum-compatible time histories as seismic input.
   - Perform structural dynamic analyses to calculate structural responses.
3. **Generation of FRS**
   - Define structural responses as seismic input where components are mounted.

- Calculate spectral responses for a single degree-of-freedom (SDOF) oscillator mounted on certain floor of the structure.
- Change natural frequency of the SDOF oscillator from 0.1 Hz to 100 Hz and repeat dynamic analyses for the oscillator to obtain a raw FRS.
- Smooth and broaden the raw FRS to obtain FRS.

Engineers have recognized that the generation of spectrum-compatible time histories is time-consuming. In addition, FRS generated by a single set of spectrum-compatible time histories has large variability, thus a number of sets of time histories are required in structural dynamic analyses. This makes the generation of FRS computationally expensive.

Spectra-to-spectra method does not need to generate spectrum-compatible time histories and to repeatedly perform structural dynamic analyses (see Figure 5.1); hence it can efficiently generate FRS. However, the accuracy of FRS is a main concern in past decades. In addition, spectra-to-spectra method only works when structures undergo elastic deformation. As a result, spectra-to-spectra method is not widely used in engineering practice.

## 5.2 Methodology

### Generation of Floor Response Spectra

Recently, Jiang *et al.* (2015) proposed a new direct spectra-to-spectra method for generating FRS. It is concluded that, compared to time history analyses, this direct spectra-to-spectra method would generate FRS with high efficiency and sufficient accuracy. The mathematical expressions of generating FRS are presented below:

**If components are mounted on SDOF structures**

- For non-tuning case

  The FRS of a SDOF oscillator of frequency $f_0$ and damping ratio $\zeta_0$ mounted on a SDOF structure of frequency $f$ and damping ratio $\zeta$ is given by

$$\mathcal{S}_{\mathrm{F}}(f_0, \zeta_0) = \sqrt{\mathcal{AF}_0^2 \cdot \mathcal{S}_{\mathrm{A}}^2(f_0, \zeta_0) + \mathcal{AF}^2 \cdot \mathcal{S}_{\mathrm{A}}^2(f, \zeta)}, \tag{5.2.1}$$

  in which $\mathcal{S}_{\mathrm{A}}(f_0, \zeta_0)$ and $\mathcal{S}_{\mathrm{A}}(f, \zeta)$ are obtained from the input GRS. $\mathcal{AF}$ and $\mathcal{AF}_0$ are amplification factors due to ground and structural motions, respectively.

- For perfect-tuning case

  The FRS of a SDOF oscillator of frequency $f_0$ and damping ratio $\zeta_0$ mounted on a SDOF structure of frequency $f_0$ and damping ratio $\zeta_0$ is given by

$$\mathcal{S}_{\mathrm{F}}(f_0, \zeta_0) = \mathcal{S}_{\mathrm{A}}^{\mathrm{t}}(f_0, \zeta_0), \tag{5.2.2}$$

  where $\mathcal{S}_{\mathrm{A}}^{\mathrm{t}}(f_0, \zeta_0)$ is the t-response spectrum (Li *et al.*, 2015).

**If components are mounted on multi-degree-of-freedom (MDOF) structures**

- For non-tuning case

  The FRS of the $n$th node in direction $j$ under tri-directional earthquake excitations is obtained from

$$\mathcal{S}_{n,j}(f_0, \zeta_0) = \sqrt{\sum_{i=1}^{3} [\mathcal{S}_{n,j}^{i}(f_0, \zeta_0)]^2}, \tag{5.2.3}$$

  where $\mathcal{S}_{n,j}^{i}(f_0, \zeta_0)$ is the FRS of the $n$th node in direction $j$ subjected to earthquake excitation in direction $i$ given by

$$\mathcal{S}_{n,j}^{i}(f_0, \zeta_0) = \sqrt{\sum_{k=0}^{6N} \sum_{\mathcal{K}=0}^{6N} \rho_{k\mathcal{K}} R_{n,j;k}^{i} R_{n,j;\mathcal{K}}^{i}}, \tag{5.2.4}$$

  where $\rho_{k\mathcal{K}}$ is the correlation coefficient between the contributions to the response under an earthquake excitation in direction $i$ by the $k$th and $\mathcal{K}$th modes, and $R_{n,j;k}^{i}$ is the maximum absolute acceleration contributed by the $k$th mode given by

$$R_{n,j;k}^{i} = \phi_{n,j;k} \Gamma_k^i \sqrt{\mathcal{AF}_{0,k}^2 \cdot \left[\mathcal{S}_{\mathrm{A}}^{i}(f_0, \zeta_0)\right]^2 + \mathcal{AF}_k^2 \cdot \left[\mathcal{S}_{\mathrm{A}}^{i}(f_k, \zeta_k)\right]^2}, \tag{5.2.5}$$

  where $\phi_{n,j;k}$ and $\Gamma_k^i$ are modal information obtained from modal analysis.

- For perfect-tuning case

  The maximum absolute acceleration contributed by the $k$th mode is given by

$$R_{n,j;k}^{i} = \phi_{n,j;k} \Gamma_k^i \mathcal{S}_{\mathrm{A}}^{\mathrm{t},i}(f_0, \zeta_0). \tag{5.2.6}$$

  Having obtained $R_{n,j;k}^{i}$, FRS can be determined by equations (5.2.3) and (5.2.4).

It can be seen that, given structural modal information and input GRS, FRS can be directly obtained by analytical expressions. Safety-related structures in nuclear power

plants are designed to behave elastically under earthquake excitations; hence direct spectra-to-spectra method is applicable in nuclear engineering practice.

#### Determination of Weighting Seismic Fragility

In seismic fragility analysis, the variability in seismic capacity due to response uncertainties needs to be evaluated. By applying spectra-to-spectra method, one only needs to take different values of pertinent response variables to generate FRS for capturing these variabilities. It would significantly improve the efficiency for generating FRS while ensure the accuracy.

Defining FRS where components are mounted as seismic input, weighing seismic fragility analysis in Chapter 4 is performed to determine weighting seismic fragility curves and HCLPF seismic capacities of the components.

In the following, numerical example for a block wall on the second floor of a service building is performed to illustrate the procedure and benefits of the proposed method.

## 5.3 Block Wall and Primary Structure

Assume the service building is located in Darlington nuclear generating station. Seismic fragility curves and HCLPF seismic capacities of the block wall are developed based on current and weighting seismic fragility analysis methods.

### 5.3.1 Block Wall Configuration

In NPPs, lightly reinforced non-load-bearing masonry block walls are often used as partition or fire-barrier walls. The seismic capacity of such walls is generally governed by out-of-plane bending.

#### Construction Details

Details of the block wall are shown in Figure 5.2 and the properties are listed in Table 5.1 (EPRI, 1991A). It is a lightly reinforced non-load-bearing masonry block wall constructed using 8-inch masonry concrete units. The wall is assumed to be simply supported between the floor and the ceiling level, so that it can be analyzed as an element simply supported at top and bottom. This is a common assumption in design, because supporting elements do

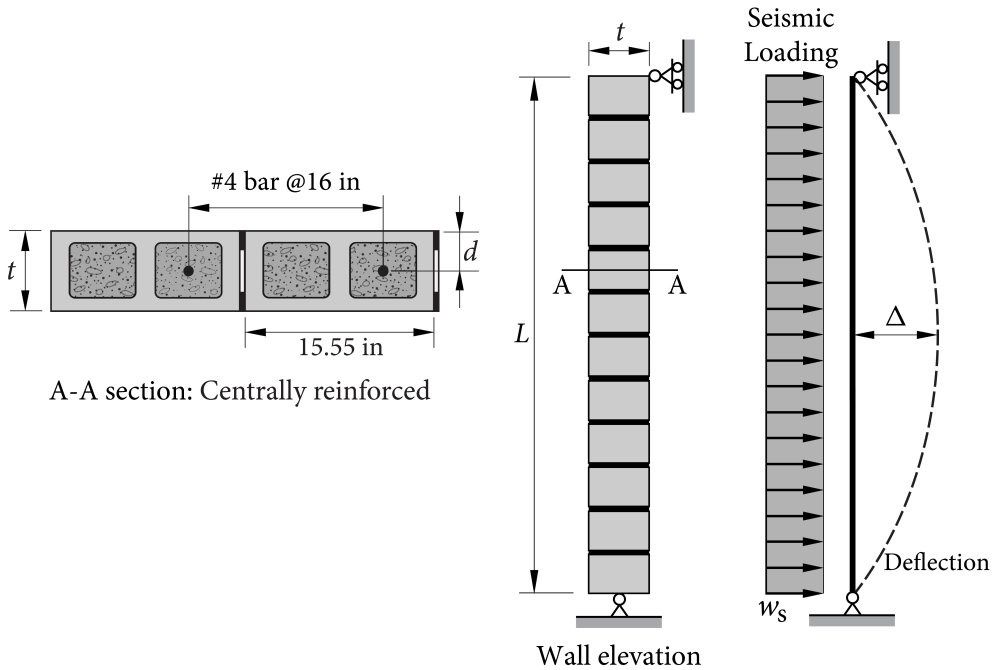


**Figure 5.2** Geometry information of block wall

not usually possess sufficient stiffness to transfer the wall moments to the supports. The wall is fully-grouted and has a height $L$ of 11 feet and a nominal depth of 8 inch (wall thickness $t$ is actually equal to 7.625 inch), with #4 bars at 16 inch spacing located at mid-depth of the wall. The wall weight $W$ is estimated to be 83.5 pounds per square foot (psf or lb/ft$^2$) of the wall surface.

**Table 5.1** Deterministic Properties of Block Wall

| Property | Value |
|---|---|
| **Block wall** | |
| Wall height $L$ | 11 ft |
| Wall thickness $t$ | 7.625 in |
| Slenderness ratio | 17.3 |
| Extent of grouting | fully-grouted |
| Wall weight $W$ | 83.5 psf of wall surface |
| Reinforce steel | #4 bars at 16 in spacing |

### Dynamic Behaviour

Since the primary loads imposed on the block wall are due to seismic ground motions, the seismic capacity of such block walls is usually governed by the out-of-plane bending failure mode. The maximum deformation or drift limit and structural integrity of the wall should be ensured so that the operability of safety-related systems is not compromised.

Previous test results showed that these walls exhibit substantial nonlinear drift capability under cyclic loading and that the effective frequency of the wall will be lowered due to the drift (Hamid *et al.*, 1989). However, severe pinching phenomenon of the hysteretic loop of this type of centrally-reinforced walls was observed under cyclic loading (see Figure 5.3); as a result, negligible inelastic energy absorption capability can be assumed, i.e., $F_\mu = 1.0$.

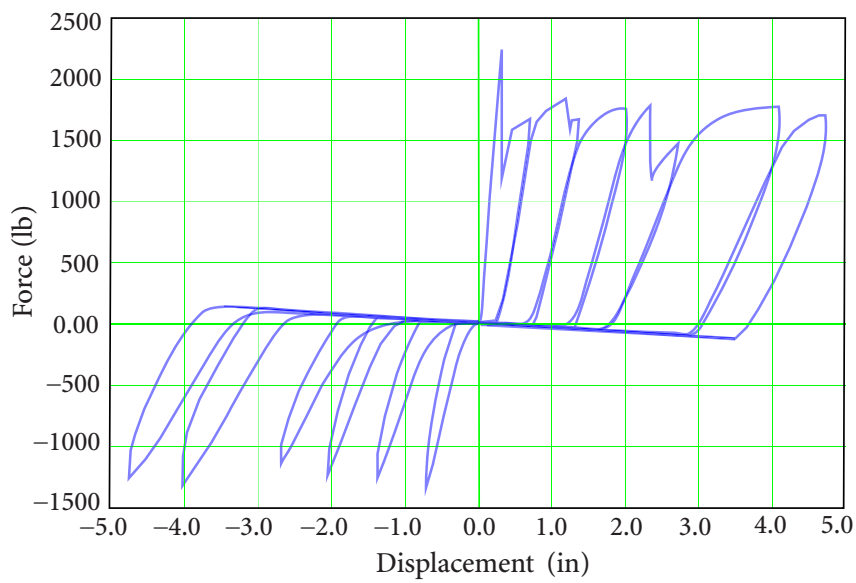


**Figure 5.3** Hysteretic loop of centrally-reinforced masonry wall

### Strength Variables

The basic variables for structural capacity analysis of the block wall are given in Table 5.2. The nominal compressive strength of the masonry and the nominal yield strength of the reinforce steel are given in Appendix R of EPRI-NP-6041-SL (1991A). It is noted that these two values are not defined at the 95% confidence level, but taken as the minimum strength.

**Table 5.2** Material Capacity Properties

| Property | Nominal | Median | $\beta_U$ |
|---|---|---|---|
| **Masonry concrete** | | | |
| Compressive strength | 1950 psi | 2678 psi | 0.05 |
| Tensile strength | 163 psi | | |
| **Reinforce steel** | | | |
| Yield strength | 40 ksi | 55.65 ksi | 0.08 |

### 5.3.2 Primary Structure Configuration

A service building as shown in Figure 5.4 is taken as the primary structure. Commercial finite element analysis software STARDYNE is used to establish the three-dimensional finite element model of the building. The superstructure of the building consists of steel frames and concrete floor slabs, and the basement is constructed using concrete. The elevation of each floor and the dimensions of the building are shown in Figure 5.4. Some information of the finite element model is listed in Table 5.3. A modal analysis is performed to obtain modal frequencies, modal participation factors, and modal shapes of the model.

Assume the block wall is located at the second floor of the building, as shown in Figure 5.4. Table 5.4 enumerates modal information of the significant modes where the block wall is located (Node 1). The participation factors and modal shapes in Table 5.4 are for direction 2 shown in Figure 5.4.

## 5.4 Current Seismic Fragility Analysis

In this section, current seismic fragility analysis is applied to determine conventional seismic fragility curves and HCLPF seismic capacity of the block wall.

### 5.4.1 Review Level Earthquake

Assume the service building is located at Darlington nuclear generating station (NGS). Figure 5.5 gives UHS with mean annual frequency of exceedance of $1 \times 10^{-4}$ for this site.

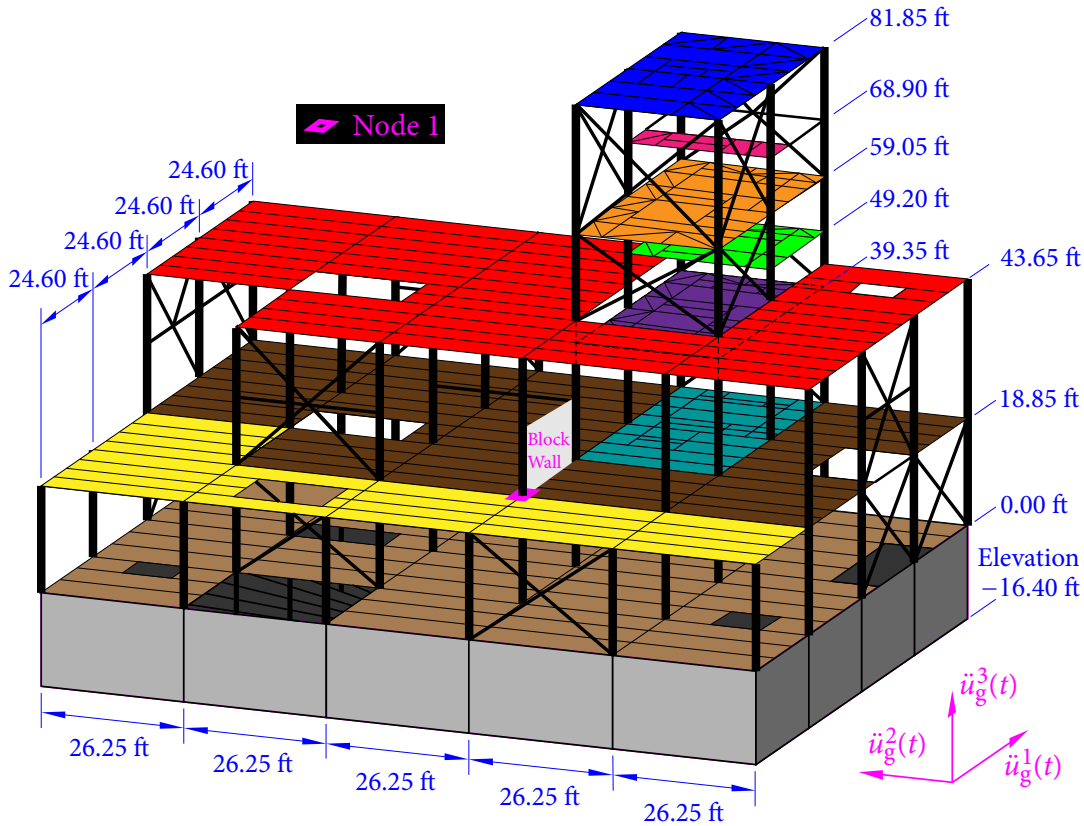


**Figure 5.4** Finite element model of service building

Spectral acceleration at $f = 50$ Hz is taken as PGA. Since Darlington NGS is located in eastern North America, the plant screening level can be taken as $0.3g$ PGA. Scale the UHS to meet the screening level and then define the scaled UHS as Review Level Earthquake (RLE). Take this RLE as input GRS in two horizontal directions. The input GRS in vertical direction can be determined using V/H ratios (AMEC, 2009). The service building is subjected to tri-directional excitations simultaneously.

## 5.4.2 Seismic Demand Analysis

### Elastic Frequency

Prior to reaching the code-specified nominal moment strength, the wall will behave approximately as an elastic structure under applied seismic loading. For simplicity, the wall is treated as a simply supported uniform beam with span $L$. Free vibration analysis gives the

**Table 5.3** Information of Finite Element Model

| | Node | Lumped Mass | Beam | | Shell | |
|---|---|---|---|---|---|---|
| | | | Element | Section | Element | Section |
| **Number** | 1351 | 120 | 1740 | 31 | 830 | 8 |

**Table 5.4** Mode Information at Node 1

| Mode | Frequency (Hz) | Participation factor | Modal Shape | Contribution factor |
|---|---|---|---|---|
| 2 | 2.676 | -7.143 | -0.05082 | 0.38 |
| 20 | 5.838 | -2.945 | -0.02603 | 0.08 |
| 21 | 5.918 | 2.943 | 0.06409 | 0.19 |
| 31 | 7.212 | -8.883 | -0.01942 | 0.17 |
| 103 | 22.95 | -100.8 | -0.00088 | -0.09 |
| 106 | 23.96 | -337.3 | 0.00024 | -0.08 |

fundamental frequency of the beam by

$$f = \frac{1}{2\pi} \cdot \frac{\pi^2}{L^2} \sqrt{\frac{E_{\mathrm{m}} I_{\mathrm{e}}}{\bar{m}}} = \frac{\pi}{2L^2} \sqrt{\frac{E_{\mathrm{m}} I_{\mathrm{e}} g}{W}}. \tag{5.4.1}$$

According to Clause 1.8.2.2.1 of TMS 402-11/ACI 530-11/ASCE 5-11 (2011), the elastic modulus $E_{\mathrm{m}}$ of concrete masonry unit is determined by

$$E_{\mathrm{m}} = 900\, f'_{\mathrm{m}} = 900 \times 1950 = 1.755 \times 10^6 \text{ psi}. \tag{5.4.2}$$

Denote the applied out-of-plane moment as $M_a$ and the cracking moment as $M_{\mathrm{cr}}$. For walls with $M_a > M_{\mathrm{cr}}$, the moment of inertia should be represented by the effective moment of inertia $I_{\mathrm{e}}$. Equation (1-1) in Clause 1.13.1.4.2 of TMS 402-11/ACI 530-11/ASCE 5-11 (2011) determines $I_{\mathrm{e}}$ as

$$I_{\mathrm{e}} = I_{\mathrm{n}} \left(\frac{M_{\mathrm{cr}}}{M_a}\right)^3 + I_{\mathrm{cr}} \left[1 - \left(\frac{M_{\mathrm{cr}}}{M_a}\right)^3\right] \leqslant I_{\mathrm{n}}, \tag{5.4.3}$$

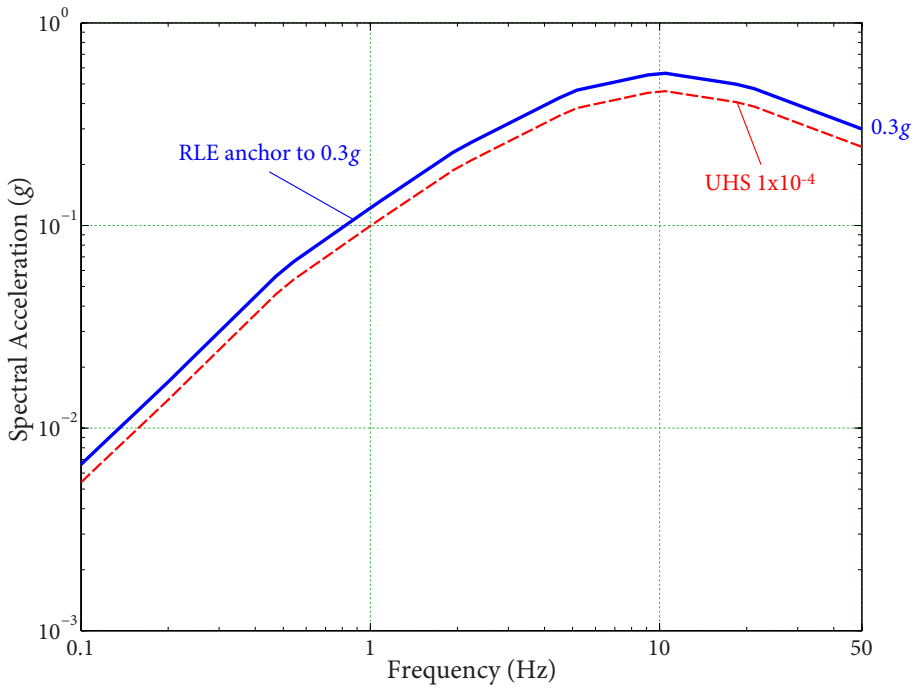


**Figure 5.5** RLE at Darlington NGS site

where $I_n$ is the net moment of inertia of the cross section, and $I_{cr}$ is the moment of inertia of cracked cross section ($I_{cr}$ is conservatively assumed to apply over the entire height of the wall).

Equation (9-9) in Clause 9.5.2.3 of ACI 318-08 (2008) determines the cracking moment as

$$M_{cr} = \frac{f_t I_g}{y_t}, \tag{5.4.4}$$

where $f_t$ is the maximum tensile strength of the concrete, and $y_t$ is the distance from the neutral axis to the extreme face of the prismatic member.

For this case, the neutral axis is in the middle of the transverse section and $y_t = t/2$, as shown in the Figure 5.6. Since the reinforcements are located in the middle of the transverse section of the block wall or on the neutral axis, the reinforcements do not withstand tensile stress when the concrete is uncracked.

The gross moment of inertia $I_g$ about the neutral axis of unit wall section is given by

$$I_g = \frac{bt^3}{12} = \frac{1.0 \times 7.625^3}{12} = 36.94\,\frac{\text{in}^4}{\text{in}}. \tag{5.4.5}$$

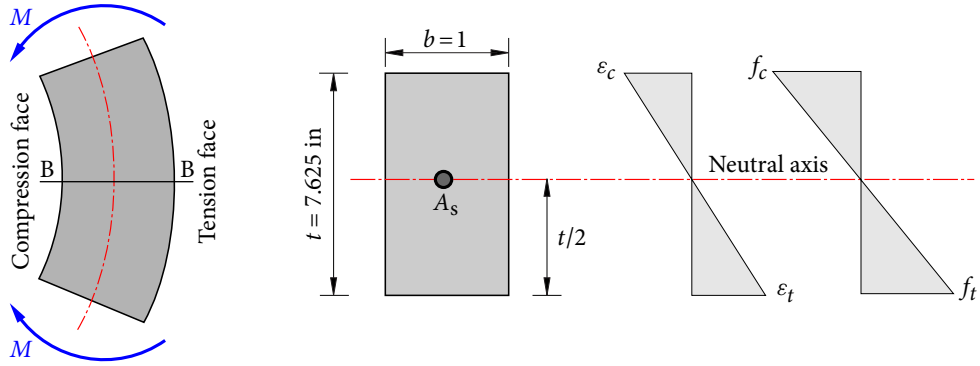


(a) Deformed shape at mid-span of uncracked block wall (b) B-B section of block wall of unit width (c) Strain and stress distribution of B-B section

**Figure 5.6** Bending of centrally-reinforced unit width uncracked block wall

Hence the cracking moment $M_{cr}$ is

$$M_{cr} = \frac{f_t I_g}{t/2} = \frac{0.163 \times 36.94}{3.812} = 1.58 \frac{\text{kip} \cdot \text{in}}{\text{in}}. \tag{5.4.6}$$

For fully-grouted 8-in masonry unit with grout spacing of 16 in, Table 3a of TEK 14-01B (2007) gives the value of the net moment of inertia of the cross section

$$I_n = 378.6 \frac{\text{in}^4}{\text{ft}} = 31.55 \frac{\text{in}^4}{\text{in}}. \tag{5.4.7}$$

Clause 3.3.5.5 of TMS 402-11/ACI 530-11/ASCE 5-11 (2011) gives simplified formulas for determining $I_{cr}$ for non-load-bearing fully-grouted wall sections.

Since the #4 rebars with 0.5-in diameter are placed at 16-in spacing, the steel area per unit width is

$$A_s = \frac{1}{16} \cdot \pi \left(\frac{1}{2} d_s\right)^2 = \frac{1}{16} \times 3.14 \times \left(\frac{1}{2} \times 0.5\right)^2 = 0.0123 \frac{\text{in}^2}{\text{in}}. \tag{5.4.8}$$

The modulus ratio $n$ of steel and masonry is

$$n = \frac{E_s}{E_m} = \frac{29.0 \times 10^6}{1.755 \times 10^6} = 16.52, \tag{5.4.9}$$

in which $E_s = 29.0 \times 10^6$ psi is the elastic modulus of steel, $E_m = 1.755 \times 10^6$ psi is the elastic modulus of concrete masonry given by equation (5.4.2). Since the block wall is non-load-bearing, i.e., $P_u = 0$, the depth $c$ of compressive fiber in section is given by equation (3-32)

of TMS 402-11/ACI 530-11/ASCE 5-11 (2011)

$$c = \frac{A_s f_y}{0.64\, f'_m\, b} = \frac{0.0123 \times 40}{0.64 \times 1.95 \times 1} = 0.39\,\text{in}, \tag{5.4.10}$$

where $f_y = 40$ ksi is the nominal yield strength of the reinforce steel, $f'_m = 1.95$ ksi is the nominal compressive strength of the grouted masonry concrete. $I_{cr}$ is the moment of inertia of cracked cross section given by equation (3-31) of TMS 402-11/ACI 530-11/ASCE 5-11 (2011)

$$\begin{aligned} I_{cr} &= n\, A_s (d-c)^2 + \frac{bc^3}{3} \\ &= 16.52 \times 0.0123 \times (3.812 - 0.39)^2 + \frac{1 \times 0.39^3}{3} = 2.40\, \frac{\text{in}^4}{\text{in}}, \end{aligned} \tag{5.4.11}$$

in which $d = t/2 = 7.625/2 = 3.812$ in is the depth from the compressive surface to the centerline of steel.

Commentary 3.3.5.4 of TMS 402-11/ACI 530-11/ASCE 5-11 (2011) gives the depth $a$ and the moment strength $M_u$ of an equivalent compression stress block as

$$a = \frac{A_s f_y + \frac{1}{\phi} P_u}{0.80\, f'_m\, b}, \qquad M_u = \left(\frac{1}{\phi} P_u + A_s f_y\right)\left(d - \frac{1}{2} a\right). \tag{5.4.12}$$

Since $P_u = 0$, the strength reduction factor $\phi = 0.9$ is not used in determining the moment strength. These equations reduce to

$$a = \frac{A_s f_y}{0.80\, f'_m\, b}, \tag{5.4.13}$$

$$M_u = A_s f_y \left(d - \frac{1}{2} a\right). \tag{5.4.14}$$

Hence,

$$a = \frac{0.0123 \times 40}{0.80 \times 1.95 \times 1} = 0.315\,\text{in}, \tag{5.4.15}$$

$$M_a = M_u = 0.0123 \times 40 \times \left(3.812 - \frac{0.315}{2}\right) = 1.798\, \frac{\text{kip-in}}{\text{in}}. \tag{5.4.16}$$

The effective moment of inertia $I_e$ is determined using equation (5.4.3)

$$I_e = I_n \left(\frac{M_{cr}}{M_a}\right)^3 + I_{cr}\left[1 - \left(\frac{M_{cr}}{M_a}\right)^3\right]$$

$$= 31.55\left(\frac{1.58}{1.798}\right)^3 + 2.40\left[1 - \left(\frac{1.58}{1.798}\right)^3\right] = 22.15 \leqslant 31.55\,\frac{\text{in}^4}{\text{in}}. \tag{5.4.17}$$

The elastic frequency $f$ is then given by equation (5.4.1)

$$f = \frac{\pi}{2L^2}\sqrt{\frac{E_m I_e g}{W}} = \frac{3.14}{2\times 11^2\times 12}\sqrt{\frac{1.755\times 10^6\times 22.15\times 386.4}{83.5}} = 14.51\ \text{Hz}. \tag{5.4.18}$$

### Floor Response Spectra

The direct seismic input to this block wall is in terms of the FRS in one of the horizontal directions. For the block wall, the median damping is 6% and the one-minus-standard-deviation ($-1\sigma$) damping is 4%. For the service building, the median damping is 5% and $-1\sigma$ damping is 3%. In order to capture damping variabilities of the block wall and service building, the direct spectra-to-spectra method is used to generate three FRS, as shown in Figure 5.7.

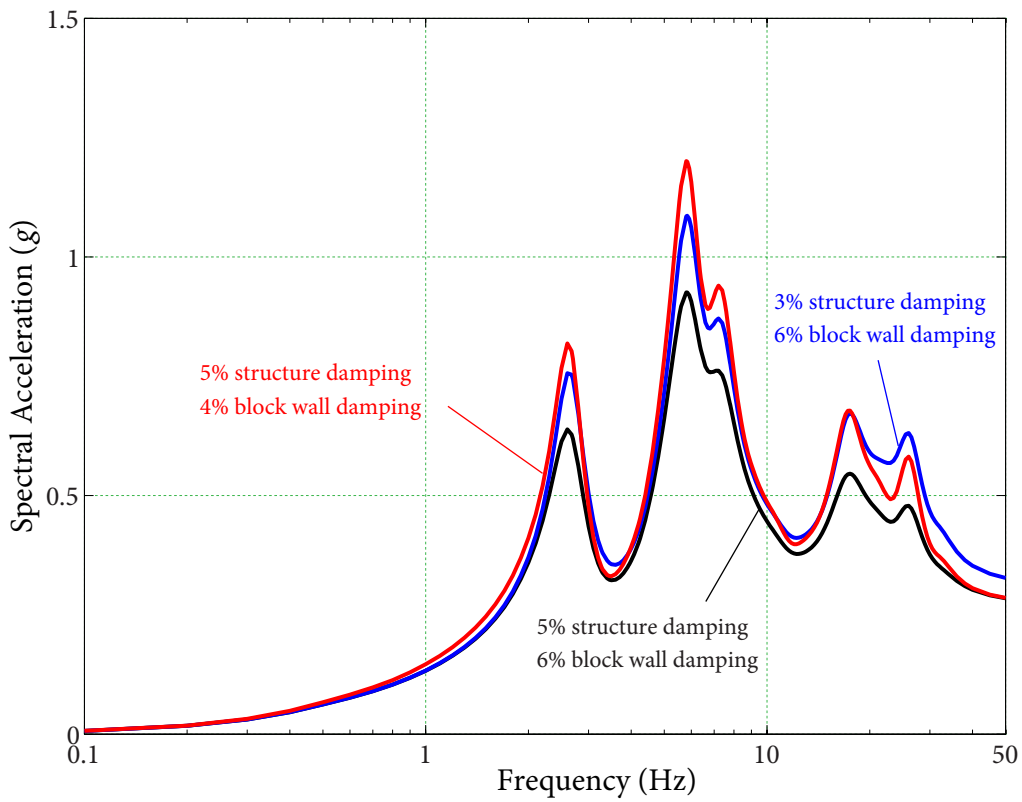


**Figure 5.7** FRS regarding three sets of damping ratios

### Seismic Demand

As in Table 5.4, the fundamental frequency of primary structure is 2.676 Hz. Since it is less than 5 Hz, ground motion incoherence does not need to be considered (EPRI-TR-103959, EPRI, 1994). Therefore, the median elastic demand $\mathcal{S}_D$ of the block wall can be obtained from the FRS $\mathcal{S}_{\mathrm{F}}$ given in Figure 5.7.

As the wall drifts inelastically under earthquake, seismic demand of the wall changes due to two phenomena: (1) the frequency of the wall is lowered due to the inelastic drift, and its value depends on the level of inelastic drift; (2) the damping is increased in accordance with the inelastic drifts. Seismic demand to the wall with lowered frequency and increased damping needs to be checked within the entire permissible inelastic range. Since both seismic capacity and demand are functions of the permissible drift, somewhere between the elastic bound and the inelastic bound, the capacity/demand ratio will produce the maximum strength factor (or margin) that is to be applied to the selected ground motion parameter.

One approach to determining such nonlinear demand is the *equivalent linear elastic procedure* given in Section 3 of EPRI-TR-103959 (1994). This procedure aims at approximating the average reduced stiffness (or frequency) and average increased damping, which occur during the nonlinear response cycles, by using the secant stiffness as the minimum effective stiffness. By applying this procedure, the nonlinear demand can be directly obtained from using the elastic design spectra.

Equation (R-20) in Appendix R of EPRI-NP-6041-SL (1991A) determines the secant frequency as

$$f_{\mathrm{sec}} = \frac{1}{2\pi}\sqrt{\frac{1.5\,\mathcal{S}_C}{\Delta_u}}. \tag{5.4.19}$$

where $\mathcal{S}_C$ is structural capacity of the block given the ultimate nonlinear displacement $\Delta_u$ at the mid-span of the wall.

Because of the distinct hysteretic behavior of centrally reinforced masonry wall under cyclic loading (see Figure 5.3), the formulation in the equivalent linear elastic procedure for shear-wall-type structures is not readily applicable. Time history analyses of similar block

wall models using very severely pinched hysteretic loops, similar to those in Figure 5.3, shows that the seismic demand to such walls could be accurately approximated by treating them as pseudo-elastic with effective frequency $f_{\text{eff}}$ and effective damping $\beta_{\text{eff}}$ (equation (R-21) of EPRI-NP-6041-SL, 1991A)

$$f_{\text{eff}} = f_{\text{sec}}, \quad \beta_{\text{eff}} = 6\%. \tag{5.4.20}$$

Due to the severely pinched hysteretic loop, the effective frequency $f_{\text{eff}}$ drops down to the secant frequency $f_{\text{sec}}$ and the effective damping is small (about 6%). Thus, the effective nonlinear demand is given by

$$\mathcal{S}_D = \mathcal{S}_{\text{F}}(f_{\text{sec}}, 6\%), \tag{5.4.21}$$

which can be obtained from the FRS given in Figure 5.7.

## 5.4.3 Structural Capacity Analysis

For a lightly-reinforced non-load-bearing block wall, there is no factored axial load acting on the wall ($P_u = 0$), and no factored load from tributary floor or roof areas ($P_{uf} = 0$). In the wall analysis, a unit section width $b = 1$ in is used.

### "Best-Estimate" Moment Strength

The theoretical ultimate moment strength according to the established principles is calculated first. To achieve the "best-estimate" moment strength, a factor accounting for the conservatism of the calculated strength against the actual strength measured in test usually needs to be applied.

For median strength $f_y = 55.65$ ksi, the ultimate moment strength $M_u'$ of the centrally reinforced block wall is determined using equations (5.4.13) and (5.4.14) as

$$a = \frac{A_s f_y}{0.80\, f_m'\, b} = \frac{0.0123 \times 55.65}{0.80 \times 2.68 \times 1.0} = 0.320\,\text{in}, \tag{5.4.22}$$

$$M_u' = A_s f_y \left(d - \tfrac{1}{2}a\right) = 0.0123 \times 55.65 \times \left(3.812 - \tfrac{1}{2} \times 0.320\right) = 2.500\,\frac{\text{kip}\cdot\text{in}}{\text{in}}. \tag{5.4.23}$$

In fragility analysis, all factors affecting the median strength must be identified and evaluated, including possible errors in materials, design, and construction. The factors

relevant to materials mainly involve the possible strength variabilities, which are given in Table 5.2. The factor on design considers the potential equation error in predicting the moment strength. The factor regarding construction for the block-wall accounts for mainly the error in rebar placement over the wall section.

### Error in Equation

In order to uncover the conservatism in the calculated strength, test results of measured strength for similar masonry wall members are needed. However, the availability of such test results is quite limited in public domain.

One source that may be used is the report by Hamid *et al.* (1989), in which full-scale reinforced concrete block masonry walls were tested under out-of-plane monotonic and cyclic loads. Based on testing of some prisms that were built along with the walls and tensile testing of reinforcement, the compressive strength $f'_{\mathrm{m}}$, modulus of rupture $f_t$, elastic modulus $E_{\mathrm{m}}$, and steel yield strength $f_y$ were recorded. The calculated moment strengths of the walls were determined using the mean material properties and the strength calculation procedure given in the Appendix of the report. The ratio of measured peak strength to calculated strength of 12 similar masonry walls is listed in Table 5.5, with a median of 1.145 and a logarithmic standard deviation of 0.105.

**Table 5.5** Ratio of Measured Peak Test to Calculated Strength of Twelfth Masonry Walls

| **Test** | 1 | 2 | 3 | 4 | 5 | 6 | 7 | 8 | 9 | 10 | 11 | 12 |
|---|---|---|---|---|---|---|---|---|---|---|---|---|
| $\dfrac{M_u\ (\textbf{Test})}{M_u\ (\textbf{Calculated})}$ | 1.14 | 1.19 | 1.19 | 1.02 | 1.16 | 1.01 | 1.16 | 0.83 | 1.06 | 1.19 | 1.15 | 1.09 |

However, under cyclic loadings at large displacements, the average "elasto-perfectly-plastic" moment capacity tends to be somewhat less than the peak test capacity (Figure 5.8). In addition, the maximum moment capacity reached in subsequent loading cycles might be somewhat less than the previously recorded peak value. Thus, using the peak capacity as the ultimate moment capacity is overly optimistic. As a slightly conservative estimation, the average test capacity will be taken as 90% of the peak test capacity, which results in a median equation factor of $F'_{\mathrm{eqn}} = 1.145 \times 0.90 = 1.031$.

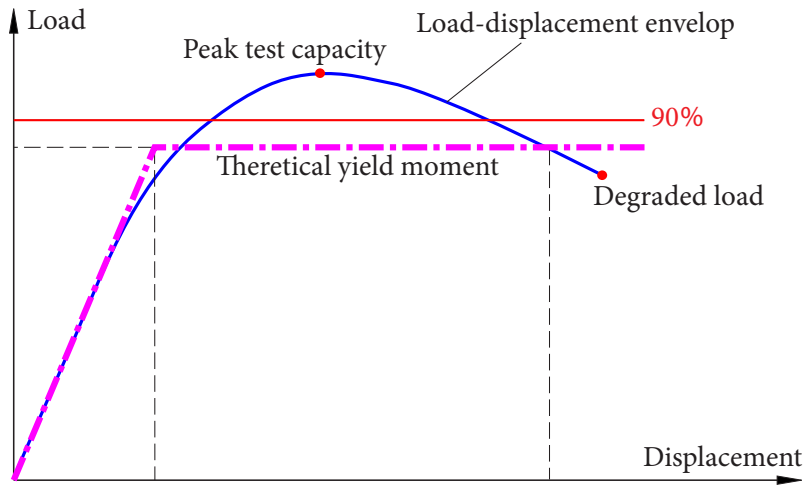


**Figure 5.8** Typical force-displacement relationship

Noting that the above factor represents the conservatism in the calculated moment strength in the report by Hamid *et al.*(1989), obtained using mean (approximately median) material strengths. A conversion must be made to obtain the factor that can be applied to TMS 402-11/ACI 530-11/ASCE 5-11 (2011).

Based on the sample calculation procedure given in Appendix A of the report by Hamid *et al.*(1989), the ultimate moment strength of this example masonry wall can be recalculated as $M_u''$

$$a = \frac{A_s f_y}{0.85\, f_m'\, b} = \frac{0.0123 \times 55.65}{0.85 \times 2.68 \times 1} = 0.300\,\text{in}, \tag{5.4.24}$$

$$M_u'' = A_s f_y \left(d - \tfrac{1}{2} a\right) = 0.0123 \times 55.65 \left(3.812 - \tfrac{1}{2} \times 0.300\right) = 2.507\, \frac{\text{kip} \cdot \text{in}}{\text{in}}, \tag{5.4.25}$$

where the only difference is that the equivalent block stress depth $a$ in masonry block given by equation (5.4.24) is assumed to be 0.85 of the total compressive depth $c$ as opposed to 0.80 used in equation (5.4.12).

By multiplying the median equation factor $F_{\text{eqn}}' = 1.031$ to the ultimate moment strength $M_u''$, the "best-estimate" moment strength is obtained as

$$M_u = F_{\text{eqn}}' \cdot M_u'' = 1.031 \times 2.507 = 2.584\, \frac{\text{kip} \cdot \text{in}}{\text{in}}. \tag{5.4.26}$$

The equation factor that should be applied to TMS 402-11/ACI 530-11/ASCE 5-11 (2011) is then

$$F_{\text{eqn}} = \frac{M_u}{M_u'} = \frac{2.584}{2.500} = 1.034.$$

Hence, the equation factor for the example wall fragility analysis is

$$\begin{aligned} \text{Median:} \quad & F_{\text{eqn}} = 1.034, \\ \text{Logarithmic standard deviation:} \quad & \beta_{\text{eqn}} = 0.105. \end{aligned} \tag{5.4.27}$$

### Error in Rebar Placement

Error in rebar placement in construction can be large and must be considered. From careful inspection, it is estimated that the standard deviation on depth $d$ for a single bar is about 0.5 in. Assuming that the moment capacity over a section is governed by 4 bars, the standard deviation of $d$ for 4 bars is $0.5/\sqrt{4} = 0.25$ in. For a nominal 8-in thick wall, the moment strength due to reduction of one standard deviation of $d$ is

$$M_u' = A_s f_y \left(d - 0.25 - \tfrac{1}{2}a\right) \tag{5.4.28}$$

$$= 0.0123 \times 55.65 \left(3.812 - 0.25 - \tfrac{1}{2} \times 0.320\right) = 2.329 \, \frac{\text{kip} \cdot \text{in}}{\text{in}}, \tag{5.4.29}$$

which is 93.2% of $M_u$ without considering this error, and the logarithmic standard deviation is

$$\beta_{\text{rb}} = \ln \frac{M_u}{M_u'} = \ln \frac{2.500}{2.329} = 0.071.$$

However, any strength reduction due to rebar placement can be assumed to be already lumped into the equation factor $F_{\text{eqn}}$ and is not explicitly considered. Only the variability in the rebar placement factor needs to be provided. This results in a factor accounting for error in rebar given by

$$\begin{aligned} \text{Median:} \quad & F_{\text{rb}} = 1.0, \\ \text{Logarithmic standard deviation:} \quad & \beta_{\text{rb}} = 0.071. \end{aligned} \tag{5.4.30}$$

For material strengths $f_y$ of steel and $f_{\text{m}}'$ of concrete, since median values have been used, no further reduction in median moment strength is possible. With predefined randomness for material strength, no further analysis is necessary for the purpose of fragility analysis.

### "Best-Estimate" of Drift Capability

Under seismic loading, if seismic demand on the wall exceeds the structural moment capacity, the wall will begin to drift inelastically. Such behavior is acceptable as long as the drift stays within a permissible limit. The permissible drift limit can be defined in terms of the ratio of mid-height displacement $\Delta$ and the wall height $L$. The effect of this wall drift is to impose a secondary moment on the wall and hence lower its seismic capacity. In seismic capacity analysis of walls, the drift capability must be incorporated using applicable test results.

Only a limited amount of test data exists for defining permissible drift limits under cyclic loading. Table 5.6 summarizes the cyclic test results on out-of-plane drift capability of seven walls report by Hamid (1989, Table 4.3), in which $\rho = A_s/d$ is the steel ratio, $c = a/0.85$ is the depth from the compressive flanges to the neutral axis, and $\Delta_u$ is the ultimate drift corresponding to the onset of significant strength degradation. All of these walls were simply supported at top and bottom with a span height $L$ of 117.5 in.

**Table 5.6** Displacement Capability Data of Masonry Walls

| Wall | $d$ (in) | $\rho$ (%) | $\frac{c}{d}$ | $\frac{L}{d}$ | $\Delta_u$ (in) | $\frac{\Delta_u}{L}$ | $\frac{\Delta_u}{L} \cdot \frac{c}{d}$ | $\frac{\text{Measured}}{\text{Predicted}^\dagger}$ |
|---|---|---|---|---|---|---|---|---|
| W2 | 2.81 | 0.455 | 0.201 | 41.8 | 5.65 | 0.0481 | 0.0097 | 1.07 |
| W3 | 2.81 | 0.455 | 0.215 | 41.8 | 4.80 | 0.0409 | 0.0088 | 0.98 |
| W5 | 2.81 | 0.291 | 0.136 | 41.8 | 7.94 | 0.0676 | 0.0092 | 1.02 |
| W7 | 2.81 | 0.892 | 0.375 | 41.8 | 3.16 | 0.0269 | 0.0101 | 1.12 |
| W11 | 2.81 | 0.455 | 0.231 | 41.8 | 6.18 | 0.0526 | 0.0122 | 1.35 |
| W13 | 2.26 | 0.362 | 0.227 | 52.0 | 8.35 | 0.0711 | 0.0161 | 1.79 |
| W14 | 3.82 | 0.483 | 0.217 | 30.8 | 4.80 | 0.0409 | 0.0089 | 0.99 |

† The predicted value is obtained from equation (5.4.32).

The drift ratio of ultimate displacement to wall height $\Delta_u/L$ ranges from a low value of 2.7% for wall W7 (with the largest $c/d$ ratio of 0.375) up to 6.8% for wall W5 (with the smallest $c/d$ ratio of 0.136).

Previous studies on concrete beams and slabs showed that the drift ratio $\Delta_u/L$ should be inversely proportional to $c/d$ at least for large $L/d$ ratios. This conclusion also appears to hold for the masonry walls summarized in Table 5.6, for which

$$\frac{\Delta_u}{L} \cdot \frac{c}{d} \geqslant 0.009. \tag{5.4.31}$$

However, equation (5.4.31) should not be extrapolated to $c/d$ ratios substantially lower than the smallest test data ratio of 0.136. The $L/d$ ratios range from 30.8 to 52.0 and show some increase in $\Delta_u/L$ with $L/d$. Likewise, equation (5.4.31) should not be extrapolated to $L/d$ ratios less than about 30, without an $L/d$ correction.

The "best-estimate" out-of-plane drift capability can be approximated by

$$\frac{\Delta_u}{L} = \frac{0.009}{c/d} F_{C(L/d)} \leqslant 0.07, \qquad F_{C(L/d)} = \frac{L/d}{30} \leqslant 1.0. \tag{5.4.32}$$

In Table 5.6, equation (5.4.32) accurately predicts $\Delta_u/L$ for walls W2, W3, W5, W7, and W14 with the ratio of measured to predicted $\Delta_u/L$ ranging from 0.98 to 1.12 for these five walls.

However, it is seen that equation (5.4.32) is very conservative for walls W11 and W13. Wall W13 has the largest $L/d$ ratio, which might indicate some benefit to $\Delta_u/L$ as $L/d$ is much larger than 30, whereas equation (5.4.32) does not provide for this benefit. Wall W11 was only partially grouted (one third of the cells filled), which may indicate increased drift capability for partially grouted walls. All other walls were fully-grouted.

For this example block-wall problem,

$$c = \frac{a}{0.85} = \frac{A_s f_y}{0.85^2 f'_m} = \frac{0.0123 \times 55.65}{0.85^2 \times 2.68} = 0.354. \tag{5.4.33}$$

Since $L/d = 132/3.812 = 34.6 > 30$, equation (5.4.32) becomes

$$\frac{\Delta_u}{L} = \frac{0.009}{c/d} F_{C(L/d)} = \frac{0.009}{0.354/3.812} \times 1.0 = 0.097 > 0.07. \tag{5.4.34}$$

Hence, the drift capability is finally given as

$$\frac{\Delta_u}{L} = 0.07, \quad \text{or} \quad \Delta_u = 0.07L = 0.07 \times 11 \times 12 = 9.24 \text{ in.} \tag{5.4.35}$$

### Static Capacity Considering Permissible Drift

Consider the free body diagrams shown in Figure 5.9, where $w_s$ is the seismic loading intensity per unit width acting perpendicular to the wall, $H_T$ is the horizontal support reaction at the top T, $H_B$ and $R_B$ are support reactions at the bottom B, $P_W = WL$ is the wall weight per unit width, and $\Delta$ is the displacement at mid-span of the wall under seismic loading. In calculating the total moment acting on the wall, the resultant moment due to relative lateral displacement of the wall should be included. Bending moment $M_C$ at the mid-span of the wall can be determined using statics.

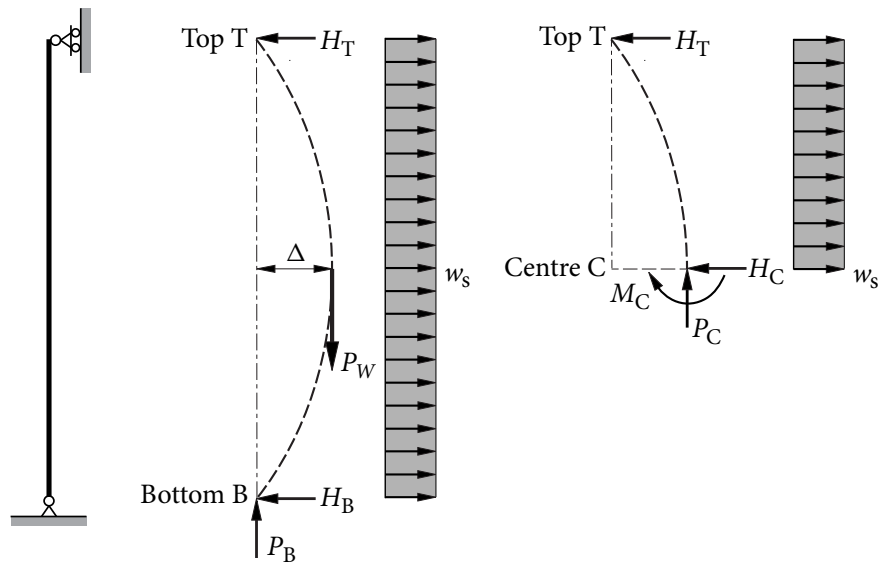


**Figure 5.9** The free-body diagram of block wall

Considering the entire wall, the horizontal force $H_T$ at the top is found by summing moments about B

$$\circlearrowleft + \sum M_B = 0: \quad H_T \cdot L - w_s L \cdot \frac{L}{2} - P_W \cdot \Delta = 0 \implies H_T = \frac{1}{2} w_s L + \frac{P_W \Delta}{L}. \tag{5.4.36}$$

Consider top half of the wall. By summing moments about the wall mid-span C, the mid-span moment $M_C$ can be obtained

$$\circlearrowleft + \sum M_C = 0: \quad H_T \cdot \frac{L}{2} - w_s \frac{L}{2} \cdot \frac{L}{4} - M_C = 0 \implies M_C = \frac{1}{8} w_s L^2 + \frac{1}{2} P_W \Delta. \tag{5.4.37}$$

Note that $w_s = (W/g) \cdot S_a$, where $S_a$ is the spectral acceleration corresponding to the vibration frequency of the wall. Equation (5.4.37) gives the mid-span moment due to seismic loading considering the lateral displacement

$$M_C = \frac{WL^2 S_a}{8g} + \frac{WL}{2}\Delta. \tag{5.4.38}$$

As the displacement $\Delta$ increases, the vibration frequency of the wall and the spectral acceleration $S_a$ acting on the wall will vary. Thus, it is necessary to check the structural capacity within the entire permissible drift limit. According to the strength design method, the bending moment $M_C$ must not exceed the ultimate moment strength $M_u$.

Static capacity of the block wall $\mathcal{S}_C$ can be obtained by equating the maximum bending moment $M_C$ with its "best-estimate" ultimate moment strength $M_u$

$$\frac{WL^2 \mathcal{S}_C}{8g} + \frac{WL}{2}\Delta = M_u \implies \mathcal{S}_C = \left(\frac{8M_u}{WL^2} - 4 \cdot \frac{\Delta}{L}\right) g, \tag{5.4.39}$$

$$\mathcal{S}_C = \left(\frac{8 \times 2.584 \times 10^3}{83.5 \times 11^2} - 4 \cdot \frac{\Delta}{L}\right) g = \left(2.046 - 4 \cdot \frac{\Delta}{L}\right) g. \tag{5.4.40}$$

The structural capacity $\mathcal{S}_C$ decreases from $2.046g$ to $1.766g$ as $\Delta/L$ increases from 0 to the permissible limit 0.07.

### 5.4.4 Median Seismic Capacity

Having obtained the capacity $\mathcal{S}_C$ and seismic demand $\mathcal{S}_D$, the *median* strength factor $F_{S,m}$ can be determined by

$$F_{S,m} = \frac{C - D_{NS}}{D_S + \Delta C_S} = \frac{\mathcal{S}_C}{\mathcal{S}_D}. \tag{5.4.41}$$

Since both $\mathcal{S}_C$ and $\mathcal{S}_D$ are functions of wall drift, a maximum $F_{S,m}$ can be found within the limits of elastic drift and the maximum inelastic drift.

The elastic drift at the mid-span of the wall is given by

$$\Delta = \frac{5WL^4}{384 E_m I_e} = \frac{5 \times 83.5 \times 11^4 \times 12^2}{384 \times 1.755 \times 10^6 \times 22.15} = 0.06 \text{ in}. \tag{5.4.42}$$

Recalling that the maximum inelastic drift at mid-span of the wall is equal to 9.24 in as given by equation (5.4.35), the secant frequency corresponding to the maximum inelastic drift is,

according to the equation (5.4.19)

$$f_{\text{sec}} = \frac{1}{2\pi}\sqrt{\frac{1.5\,\mathcal{S}_C}{\Delta_u}} = \frac{1}{2\times 3.14}\sqrt{\frac{1.5\times(1.766\times 386.4)}{9.24}} = 1.68\,\text{Hz}. \tag{5.4.43}$$

For the example block wall, $\mathcal{S}_C, \mathcal{S}_D$, and the *median* strength factor $F_{S,m}$ are calculated for the elastic frequency and a few secant frequencies corresponding to some discrete drifts $\Delta$; the results are given in Table 5.7.

**Table 5.7** Median Strength Factor as Function of Drift Level for Block Wall

| Drift ratio $\Delta/L$ | $u$ (in) | Frequency (Hz) $f$ | Frequency (Hz) $f_{\text{sec}}$ | Reference demand $\mathcal{S}_D$ $(g)$ | Capacity $\mathcal{S}_C$ $(g)$ | $F_{S,m}$ |
|---|---|---|---|---|---|---|
| Elastic | 0.06 | 14.51 | | 0.422 | 2.046 | 4.855 |
| 0.15% | 0.20 | | 12.30 | 0.378 | 2.040 | 5.403 |
| 0.66% | 0.87 | | 5.84 | 0.926 | 2.020 | 2.183 |
| 1% | 1.32 | | 4.72 | 0.554 | 2.006 | 3.624 |
| 1.79% | 2.36 | | 3.50 | 0.322 | 1.975 | 6.125 |
| 2% | 2.64 | | 3.30 | 0.337 | 1.966 | 5.834 |
| 3% | 3.96 | | 2.68 | 0.628 | 1.926 | 3.066 |
| 5% | 6.60 | | 2.03 | 0.370 | 1.846 | 4.985 |
| 7% | 9.24 | | 1.68 | 0.260 | 1.766 | 6.786 |

It is seen from Table 5.7 that

- As shown in Figure 5.7, the FRS has two main peaks between the elastic frequency 14.51 Hz and the minimum secant frequency 1.68 Hz of the block wall. Seismic demand decreases as the wall starts to become inelastic and then increases rapidly when the secant frequency approaches the second dominant natural frequency 5.84 Hz of the service building (see Table 5.4). Subsequently, the seismic demand decreases again until the secant frequency reaches 3.5 Hz. Afterwards, the seismic demand increases to peak value of $0.628g$ PGA at the first dominant frequency 2.68 Hz. At last, the seismic demand decreases to $0.26g$ PGA at the minimum secant frequency 1.68 Hz.

- Structural capacity decreases monotonically from $2.046g$ to $1.766g$ with increasing drift.
- The minimum *median* strength factor $F_{S,m} = 2.183$ occurs at $(\Delta/L) = 0.66\%$. However, this is not a steady state for defining the wall seismic capacity, since it will drift further inelastically to escape from this large seismic demand.
- The maximum $F_{S,m} = 6.786$ corresponds to $(\Delta_u/L) = 7\%$, which is the maximum credit that the wall can take within the permissible drift limit.

For the block wall, horizontal peak response is unit median (Table 3-3, EPRI TR-103959, EPRI, 1994), foundation-soil interaction is not considered, and direct spectra-to-spectra method is used to generate FRS, hence $F_{RS,m} = 1.0$ (see Section 3.1.2). Therefore, *median factor of safety* $F_m$ is given by

$$F_m = F_\mu \cdot F_{RS,m} \cdot F_{S,m} = 1.0 \times 1.0 \times 6.786 = 6.786. \tag{5.4.44}$$

Finally, the *median* seismic capacity of the block wall is given by

$$A_m = F_m \cdot A_{RLE} = 6.786 \times 0.3g\,\text{PGA} = 2.036g\,\text{PGA}. \tag{5.4.45}$$

## 5.4.5 Logarithmic Standard Deviations

The *approximate second-moment procedure* is applied to calculate the variability of $A$ due to response and capacity variables.

### 5.4.5.1 Basic Variables for Seismic Demand

Logarithmic standard deviations for basic response variables are taken in accordance EPRI-TR-103959 (EPRI, 1994). It is noted that damping and frequency uncertainties need to be converted to be uncertainties on spectral acceleration at secant frequency of the block wall.

#### Structural Damping

Based on FRS in Figure 5.7, $\beta_U$ of seismic demand of the block wall due to structure damping can be calculated by

$$\beta_U = \frac{1}{1} \ln \frac{\mathcal{S}_F(f = 1.68\,\text{Hz},\ \zeta = 3\%)}{\mathcal{S}_F(f = 1.68\,\text{Hz},\ \zeta = 5\%)} = \ln \frac{0.264g}{0.260g} = 0.014. \tag{5.4.46}$$

### Structural Frequency

In this study, an accurate three-dimensional finite element model of the service building is used for generating FRS. It is assumed that it can reasonably represent the realistic case and that the modelling is unbiased. $\beta_U = 0.15$ is used to take account of structure frequency (page 3-18, EPRI, 1994).

Based on the RLE, as shown in Figure 5.5, the logarithmic standard deviation of spectral acceleration at the first natural frequency ($f_1 = 2.676$ Hz) in direction 2 due to structure frequency variability is calculated by

$$\beta_S = \frac{1}{1} \ln \frac{\mathcal{S}_A(f_1 = 2.676 \cdot e^{0.15}\,\text{Hz},\ \zeta = 5\%)}{\mathcal{S}_A(f_1 = 2.676\,\text{Hz},\ \zeta = 5\%)} = \ln \frac{0.327g}{0.294g} = 0.109, \tag{5.4.47}$$

Taking $\mathcal{S}_A(f_1) = 0.294g \cdot e^{0.109} = 0.327g$, one can apply the direct spectra-to-spectra method to generate FRS as shown in Figure 5.10. $\beta_U$ of the seismic demand due to structure frequency is given by

$$\beta_U = \frac{1}{1} \ln \frac{\mathcal{S}_F(f_{sec} = 1.68\,\text{Hz},\ f_1 = 2.676 \cdot e^{0.15}\,\text{Hz})}{\mathcal{S}_F(f_{sec} = 1.68\,\text{Hz},\ f_1 = 2.676\,\text{Hz})} = \ln \frac{0.271g}{0.260g} = 0.04. \tag{5.4.48}$$

### Block Wall Damping

Based on FRS in Figure 5.7, $\beta_U$ value for block wall damping can be calculated as

$$\beta_U = \frac{1}{1} \ln \frac{\mathcal{S}_F(f_{sec} = 1.68\,\text{Hz},\ \zeta = 4\%)}{\mathcal{S}_F(f_{sec} = 1.68\,\text{Hz},\ \zeta = 6\%)} = \frac{1}{1} \ln \frac{0.293g}{0.260g} = 0.12. \tag{5.4.49}$$

### Block Wall Frequency

Based on FRS in Figure 5.7, $\beta_U$ for block wall frequency can be calculated by

$$\beta_U = \frac{1}{1} \ln \frac{\mathcal{S}_F(f_{sec} = 1.68 \cdot e^{0.16}\,\text{Hz},\ \zeta = 6\%)}{\mathcal{S}_F(f_{sec} = 1.68\,\text{Hz},\ \zeta = 6\%)} = \ln \frac{0.348g}{0.260g} = 0.29. \tag{5.4.50}$$

## 5.4.5.2 Basic Variables for Block Wall Capacity

The structural capacity of block wall can be obtained from equation (5.4.39) by setting $\Delta = \Delta_u$

$$\mathcal{S}_C = \left(\frac{8M_u}{WL^2} - 4 \cdot \frac{\Delta_u}{L}\right) g, \tag{5.4.51}$$

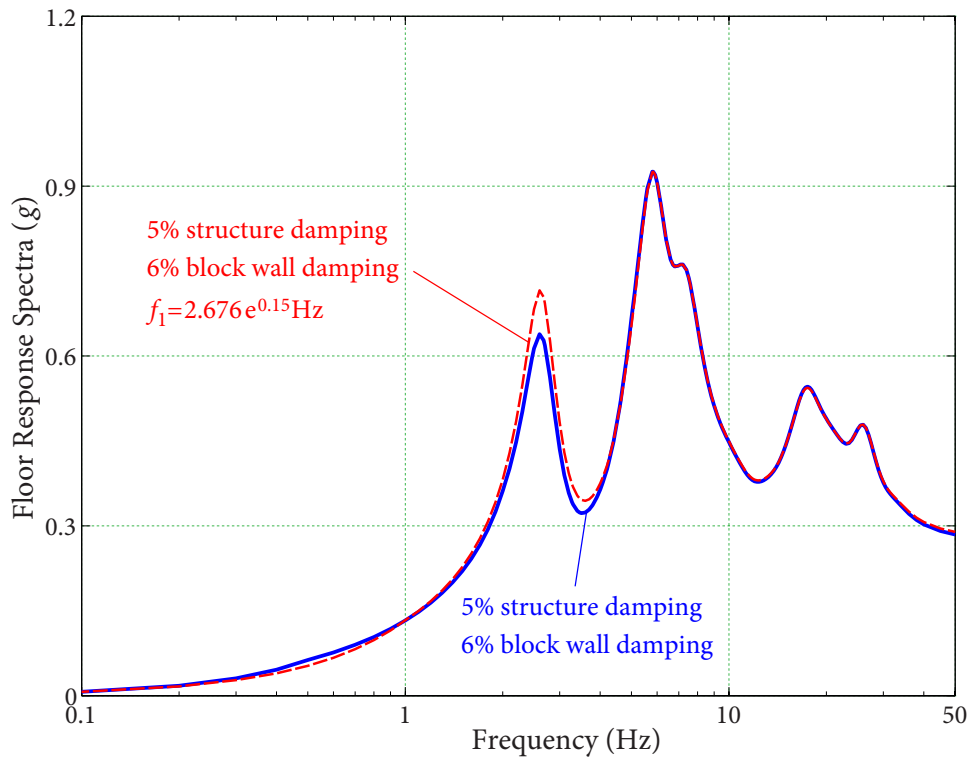


**Figure 5.10** FRS of Node 1 in direction 2 of service building

where $M_u$ is the "best estimate" moment strength given by

$$M_u = F_{\text{eqn}} \cdot F_{\text{rb}} \cdot (A_{\text{s}} f_y)\left(d - \frac{a}{2}\right), \tag{5.4.52}$$

and $a$ is given by equation (5.4.13). Combining these equations gives

$$\mathcal{S}_C = \left[\frac{8}{WL^2} \cdot F_{\text{eqn}} \cdot F_{\text{rb}} \cdot (A_{\text{s}} f_y)\left(d - \frac{A_{\text{s}} f_y}{1.60 f'_{\text{m}} b}\right) - 4 \cdot \frac{\Delta_u}{L}\right] g. \tag{5.4.53}$$

It can be seen that the structural capacity $\mathcal{S}_C$ is a nonlinear function of lognormal random variables $F_{\text{eqn}}$, $F_{\text{rb}}$, $f_y$, and $f'_{\text{m}}$.

### 5.4.5.3 Variability of Factor of Safety

From Table 5.7, corresponding to $\Delta/L = 7\%$, the *median factor of safety* is $F_m = 6.786$. Herein, the variability of $F$ due to equation error is evaluated as an example. Given $\beta_U = 0.105$ of equation error variability, substituting $F_{\text{eqn}} = 1.034 \cdot \text{e}^{-0.105}$ into equation

(5.4.53) gives block wall capacity $\mathcal{S}_C = 1.562g$. Thus the secant frequency of block wall is

$$f_{\text{sec}} = \frac{1}{2\pi}\sqrt{\frac{1.5\,\mathcal{S}_C}{\Delta_u}} = \frac{1}{2\times 3.14}\sqrt{\frac{1.5\times(1.562\times 386.4)}{9.24}} = 1.58\,\text{Hz}. \tag{5.4.54}$$

Based on FRS in Figure 5.7, seismic demand of the block wall is given by

$$\mathcal{S}_D = \mathcal{S}_{\text{F}}(f_{\text{sec}},\, 6\%) = 0.237g. \tag{5.4.55}$$

Hence *median* strength factor $F_{\text{S},m}$ is given by

$$F_{\text{S},m} = \frac{1}{|-1|}\ln\frac{\mathcal{S}_C}{\mathcal{S}_D} = \ln\frac{1.562g}{0.237g} = 6.603. \tag{5.4.56}$$

Having obtained $F_{\text{S},m}$, the *factor of safety* $F_{-1\sigma}$ is given by

$$F_{-1\sigma} = F_\mu \cdot F_{\text{RS},m} \cdot F_{\text{S},m} = 1.0\times 1.0\times 6.603 = 6.603, \tag{5.4.57}$$

The variability of $F$ due to equation error variability is determined by

$$F_{-1\sigma} = \frac{1}{|-1|}\ln\frac{F_m}{F_{-1\sigma}} = \ln\frac{6.786}{6.603} = 0.027. \tag{5.4.58}$$

Table 5.8 enumerates the logarithmic standard deviations for all basic variables.

### 5.4.6 Seismic Fragility Curves

Having obtained seismic fragility parameters, seismic fragility of the heat exchanger, at confidence level $Q = q$, can be determined by

$$p_{\text{F},q}(a) = \mathcal{P}\big\{A < a \,\big|\, \text{GMP} = a,\ Q = q\big\} = \Phi\left[\frac{\ln(a/A_m) + \beta_U\Phi^{-1}(q)}{\beta_R}\right]. \tag{5.4.59}$$

Figure 5.11 shows seismic fragility curves of the block wall. When composite variability is used, a mean seismic fragility curve can be obtained and is shown in Figure 5.11.

In addition, one can obtain HCLPF seismic capacity of the block wall as

$$C_{\text{HCLPF}} = A_m\,\mathrm{e}^{(\beta_R+\beta_U)\,\Phi^{-1}(0.05)} = 2.036\times\mathrm{e}^{-1.6449\,(0.21+0.36)} = 0.809g\ \text{PGA}. \tag{5.4.60}$$

## 5.5 Weighting Seismic Fragility Analysis

In this Section, weighting fragility curves and HCLPF seismic capacities of the block wall are determined. The fragility results based on weighting and current methods are compared.

**Table 5.8** The Variability of $F$ from Response and Capacity Variables

| Case | **Variable** | *Randomness* | *Uncertainty* | $F$ | $\beta$ | |
|---|---|---|---|---|---|---|
| 0 | **Base Case** | Variable at median | | 6.79 | | |
| | **Response Variables** | Variable at median plus $1\sigma$ | | $F_{1\sigma}$ | $\beta_R$ | $\beta_U$ |
| 1 | Horizontal direction peak response | $\mathcal{S}_D\,\mathrm{e}^{0.13}$ | | 5.96 | 0.13 | |
| 2 | Structure frequency | | $\mathcal{S}_D\,\mathrm{e}^{0.04}$ | 6.52 | | 0.04 |
| 3 | Structure damping | | $\mathcal{S}_D\,\mathrm{e}^{0.014}$ | 6.69 | | 0.014 |
| 4 | Structure mode shape | | $\mathcal{S}_D\,\mathrm{e}^{0.15}$ | 5.84 | | 0.15 |
| 5 | Structure mode combination | $\mathcal{S}_D\,\mathrm{e}^{0.15}$ | | 5.84 | 0.15 | |
| 6 | Block wall frequency | | $\mathcal{S}_D\,\mathrm{e}^{0.29}$ | 5.08 | | 0.29 |
| 7 | Block wall damping | | $\mathcal{S}_D\,\mathrm{e}^{0.12}$ | 6.02 | | 0.12 |
| 8 | Block wall mode shape | | $\mathcal{S}_D\,\mathrm{e}^{0.05}$ | 6.45 | | 0.05 |
| 9 | Block wall mode combination | $\mathcal{S}_D\,\mathrm{e}^{0.05}$ | | 6.45 | 0.05 | |
| | **Capacity Variables** | Variable at median minus $1\sigma$ | | $F_{-1\sigma}$ | $\beta_R$ | $\beta_U$ |
| 10 | Equation error $F_{\mathrm{eqn}}$ | | $F_{\mathrm{eqn}}\,\mathrm{e}^{-0.105}$ | 6.60 | | 0.027 |
| 11 | Rebar error $F_{\mathrm{rb}}$ | | $F_{\mathrm{rb}}\,\mathrm{e}^{-0.071}$ | 6.67 | | 0.017 |
| 12 | Masonry strength $f'_{\mathrm{m}}$ | $f'_{\mathrm{m}}\,\mathrm{e}^{-0.05}$ | | 6.79 | 0.00 | |
| 13 | Steel strength $f_y$ | $f_y\,\mathrm{e}^{-0.08}$ | | 6.66 | 0.019 | |
| | **SRSS Combination** | | | | $\beta_R$ | $\beta_U$ |
| | | | | | 0.21 | 0.36 |
| | | | | $\beta_{\mathrm{C}}$ | 0.41 | |

## 5.5.1 Generation of Input Ground Response Spectra

### Vector-valued Ground Motion Parameters

As shown in Table 5.4, the first two dominant frequencies of the service building in direction 2 is 2.676 Hz (denote as $f_1$) and 5.838 Hz (denote as $f_2$), respectively. As shown in Figure

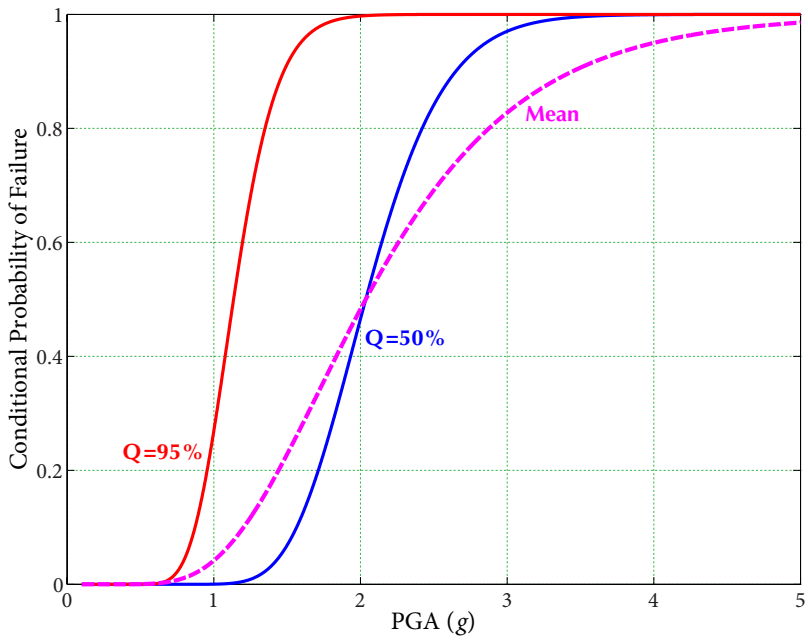


**Figure 5.11** Seismic fragility curves of block wall

5.5, the FRS has two main peaks at $f_1$ and $f_2$. Based on the spectral correlation model developed by Baker and Jayaram (2008), the correlation coefficient between $\ln \mathcal{S}_A(f_1)$ and $\ln \mathrm{PGA}$ is 0.736; whereas the correlation coefficient between $\ln \mathcal{S}_A(f_2)$ and $\ln \mathrm{PGA}$ is 0.902, which is pretty close to 1.0. For other three small peaks, the correlation coefficients among logarithmic spectral accelerations at these peak frequencies and $\ln \mathrm{PGA}$ are much closer to 1.0. Therefore, in this example, two GMPs, i.e., $\mathcal{S}_A(f_1)$ and PGA, are chosen as VGMPs. In the meantime, the correlation coefficients among logarithmic spectral accelerations at remaining natural frequencies of the service building and $\ln \mathrm{PGA}$ are taken as 1.0, i.e., fully correlated.

### Generation of Input Ground Response Spectra

In this example, $\mathcal{S}_A(f_1)$ and PGA are taken as VGMPs, thus a large number of input ground response spectra (GRS) are generated accounting for aleatory randomness in estimating $\mathcal{S}_A(f_1)$. Since spectral accelerations at natural frequencies (exclude $f_1$) of the service building are assumed to be fully correlated with PGA, given a PGA value such as $\mathrm{PGA} = 1.0g$, spectral values at these frequencies can be obtained as follows:

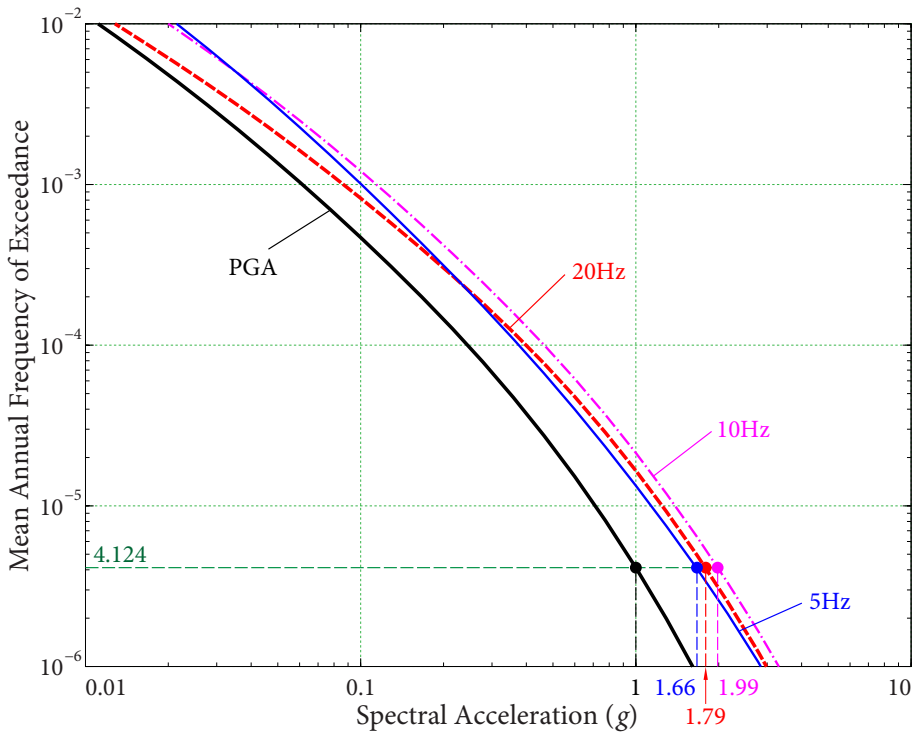


**Figure 5.12** Mean seismic hazard curves for PGA and spectral accelerations at three representative frequencies

1. determine seismic hazard, i.e., mean annual frequency of exceedance, of $4.124 \times 10^{-6}$ with respect to $\text{PGA} = 1.0g$, from mean seismic hazard curve for PGA (see Figure 5.12)

2. calculate spectral values $1.66g$, $1.79g$, and $1.99g$ at three representative frequencies (i.e., 5, 10, and 20 Hz), regarding $4.124 \times 10^{-6}$, based on mean seismic hazard curves at these three frequencies (see Figure 5.12)

3. given an example of $1.2g$ of $\mathcal{S}_{\text{A}}(f_1)$, define the smooth input GRS going through these spectral values as seismic input, as shown in Figure 5.13

4. determine spectral values at natural frequencies of the service building by linearly interpolating the input GRS in logarithmic scale

5. changing spectral values of $\mathcal{S}_{\text{A}}(f_1)$ from lower to upper bounds can generate input GRS accounting for aleatory randomness in $\mathcal{S}_{\text{A}}(f_1)$.

Changing PGA values from lower to upper bounds and repeating above procedure can generate input GRS that take aleatory randomness and ground motion intensity effect into consideration.

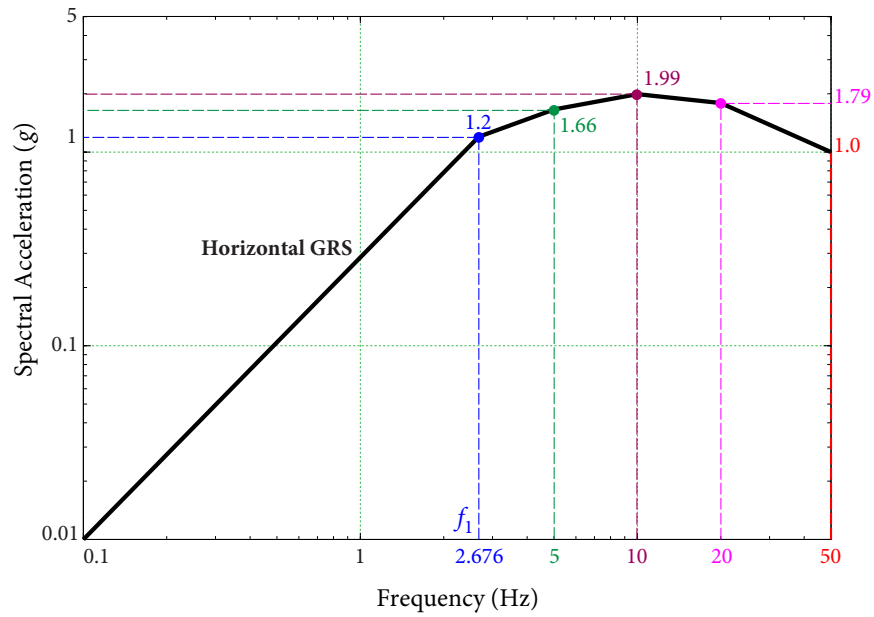


**Figure 5.13** An example of input GRS

## 5.5.2 Weights of Input GRS

As in Chapter 4, vector-valued PSHA (VPSHA) is performed to calculate mean annual rate density of $\mathcal{S}_{\mathrm{A}}(f_1)\,|\,\mathrm{PGA}$. The lower and upper bounds of $\mathcal{S}_{\mathrm{A}}(f_1)$ and PGA are $0.1g$ and $5g$, respectively. Both $\mathcal{S}_{\mathrm{A}}(f_1)$ and PGA are uniformly discretized into 100 intervals in logarithmic scale. Figure 5.14 shows three curves of mean rate density of $\mathcal{S}_{\mathrm{A}}(f_1)$ with respect to three PGA values.

Given a PGA value, the weights of input GRS with spectral value of $\mathcal{S}_{\mathrm{A}}(f_1)$ from an interval can be determined based on mean annual rate density of $\mathcal{S}_{\mathrm{A}}(f_1)$. As shown in Figure 5.15, taking $\mathrm{PGA}=1.0g$ for example, the annual rate of occurrence of $\mathcal{S}_{\mathrm{A}}(f_1)$ in the entire spectral domain $[0.10g, 5g]$ is given by

$$\lambda\left(0.1 \leqslant s_1 \leqslant 5 \,\middle|\, s_0 = 1.0g\right) \approx \sum_{i_1=1}^{100} f'_{\mathcal{S}_{\mathrm{A}}(f_1)\,|\,\mathrm{PGA}}\left(s_1^{(i_1)} \,\middle|\, s_0 = 1.0g\right) \Delta s_1^{(i_1)} = 0.215, \tag{5.5.1}$$

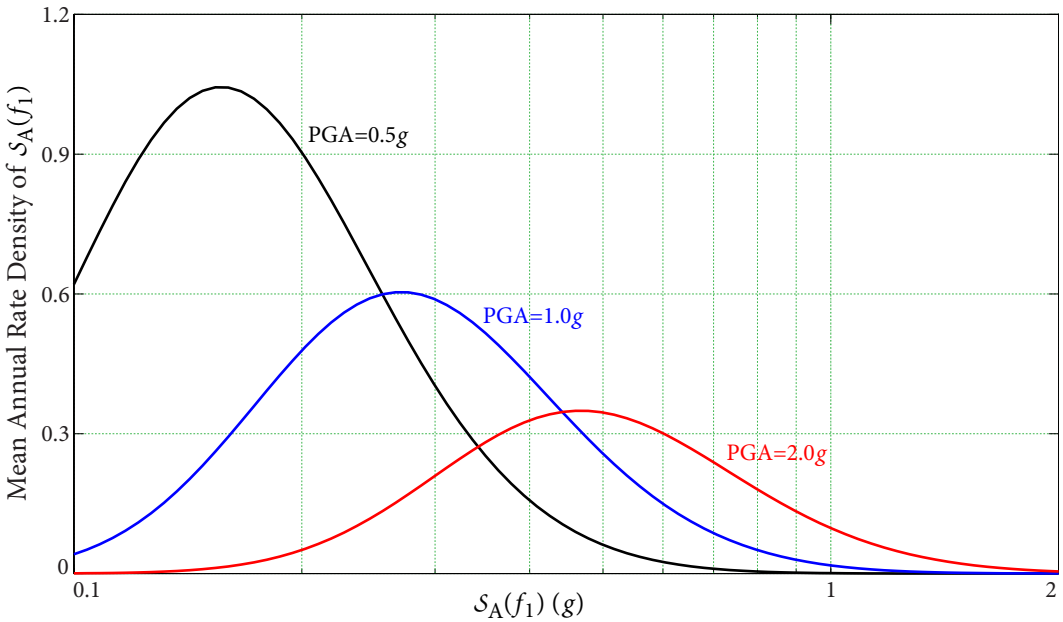


**Figure 5.14** Mean annual rate density of $\mathcal{S}_A(f_1)$ with respect to three PGA values

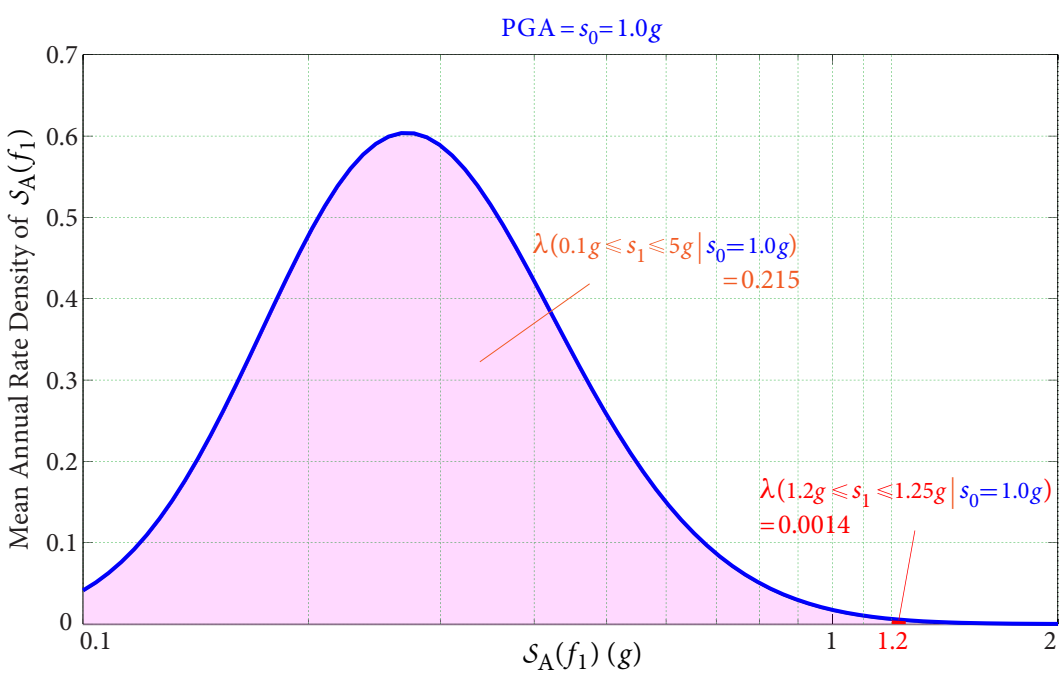


**Figure 5.15** Mean annual rate density of $\mathcal{S}_A(f_1)$ at PGA $= 1.0g$

thus given $s_0 = 1.0g$, the weight of input GRS with spectral value $\mathcal{S}_A(f_1) = s_1^{(i_1)}$ can be determined by

$$w\left(s_1^{(i_1)} \leqslant s_1 < s_1^{(i_1+1)} \,\middle|\, s_0 = 1.0g\right) = \frac{\lambda\left(s_1^{(i_1)} \leqslant s_1 \leqslant s_1^{(i_1+1)} \,\middle|\, s_0 = 1.0g\right)}{\lambda\left(0.1 \leqslant s_1 \leqslant 5 \,\middle|\, s_0 = 1.0g\right)}$$
$$\approx \frac{f'_{\mathcal{S}_A(f_1)\,|\,\mathrm{PGA}}\left(s_1^{(i_1)} \,\middle|\, s_0 = 1.0g\right)\Delta s_1^{(i_1)}}{0.215}. \tag{5.5.2}$$

In Figure 5.15, the blue curve denotes mean annual rate density of $\mathcal{S}_A(f_1)$ at $\mathrm{PGA} = 1.0g$, while the red column area is annual rate of occurrence of $\mathcal{S}_A(f_1)$ in the interval between $1.2g$ and $1.25g$. The weight of input GRS in this interval is determined by

$$w\left(1.2g \leqslant s_2 \leqslant 1.25g \,\middle|\, s_0 = 1.0g\right) = \frac{f'_{\mathcal{S}_A(f_1)\,|\,\mathrm{PGA}}\left(s_2 = 1.2g \,\middle|\, s_0 = 1.0g\right) \cdot 0.05g}{0.215}$$
$$= \frac{0.0014}{0.215} = 0.0065. \tag{5.5.3}$$

Changing spectral values of $\mathcal{S}_A(f_1)$ from lower bound of $0.1g$ to upper bound value of $5g$ can obtain the weights of input GRS given $\mathrm{PGA} = 1.0g$. Afterwards, changing PGA values from lower bound to upper bound results in a two-dimensional numerical distribution for weights of input GRS, as shown in Figure 5.16. The input GRS with the assigned weights would be defined as seismic input in seismic fragility analysis considering VGMPs.

## 5.5.3 Development of Seismic Fragility Surfaces

### 5.5.3.1 Procedure

Structural capacity of the block wall has been calculated in Section 5.4.3; hence structural capacity analysis would not be performed here. Since VGMPs are used, a great number of input GRS are defined as seismic input. A brief procedure for developing seismic fragility surfaces of the block wall is presented as follows:

1. Discretize spectral domain of $\mathcal{S}_A(f_1)$ and PGA into suitable intervals
   (1) Truncate the spectral domain at a reasonable small value and a large value
   (2) Uniformly discretize the spectral domain in logarithmic scale into $100 \times 100$ intervals

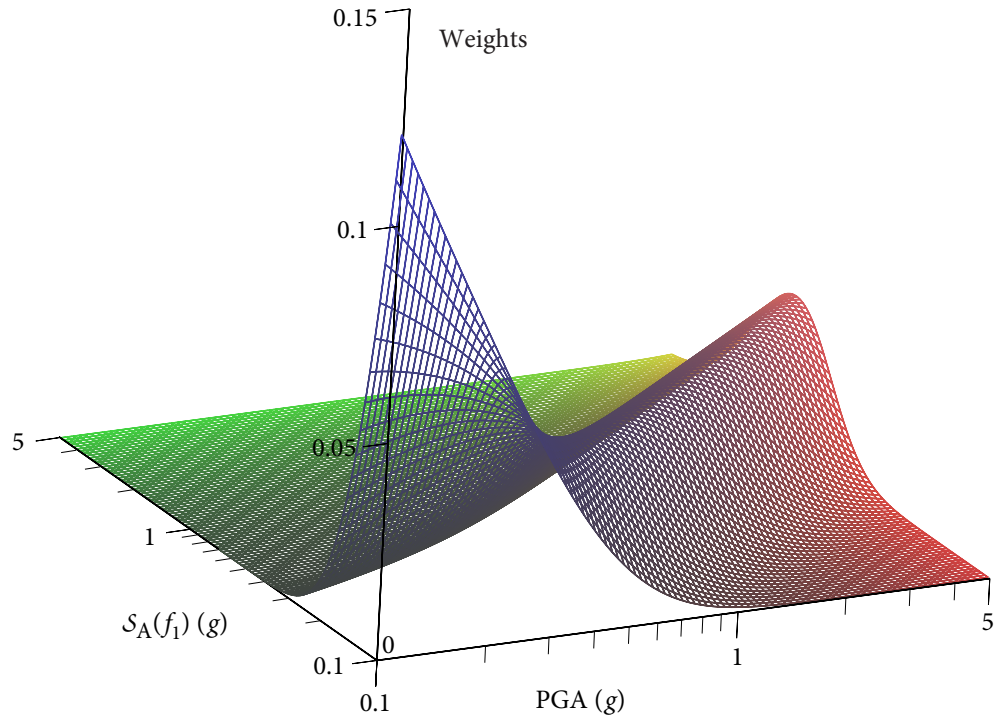


**Figure 5.16** Weights of input GRS

2. Calculate median seismic demand of the block wall
   (1) Define the GRS with spectral values from an interval as seismic input
   (2) Generate the FRS where the block wall is located given the input GRS
   (3) Interpolate the FRS to obtain median seismic demand of the block wall
   (4) Repeat steps (1) to (3) to determine median seismic demand of the block wall given input GRS from other intervals

3. Determine numerical distributions of seismic fragility for the block wall
   (1) Calculate *median ratio factor* $R_m$ given an input GRS
   (2) Calculate logarithmic standard deviations $\beta_R$ and $\beta_U$ given the input GRS
   (3) Determine conditional probability of failure value given the input GRS
   (4) Repeat steps (1) to (3) to calculate conditional probability of failure values from other intervals

(5) Integrate conditional probability of failure values to obtain numerical conditional probability of failure distributions.

As long as the sizes of intervals are reasonable small, seismic fragility surfaces can be well represented by numerical conditional probability of failure distributions.

#### 5.5.3.2 Conditional Probability of Failure Given an Input GRS

To better illustrate above procedure, conditional probability of failure given an example of input GRS is calculated in the following.

**Generation of Input GRS**

Input GRS are needed to be defined as the seismic input for generating FRS. Herein, the input GRS with spectral value $\mathcal{S}_{\mathrm{A}}(f_1)=1.2g$ at $\mathrm{PGA}=1.0g$ is taken for example. Given $\mathrm{PGA}=1.0g$, spectral values at representative frequencies, i.e., 5, 10, 20 Hz, can be determined in accordance with the procedure in Section 5.5.1. Afterwards, a smooth GRS with these spectral values (black curve in Figure 5.17), can be defined as horizontal input GRS. Spectral accelerations at natural frequencies (exclude $f_1$) of the service building are determined by interpolating the horizontal input GRS in logarithmic scale. Changing spectral values of $\mathcal{S}_{\mathrm{A}}(f_1)$ can generate input GRS accounting for aleatory randomness in estimating $\mathcal{S}_{\mathrm{A}}(f_1)$. At last, change PGA values to determine the input GRS accounting for ground motion effect.

Having defined the horizontal input GRS, the vertical input GRS can be obtained using V/H ratios (AMEC, 2009). Assume that horizontal seismic input in longitudinal and transverse directions are equal in magnitude, then seismic input in three directions can be applied simultaneously to calculate FRS at the location of block wall.

**Generation of FRS**

Define the input GRS with spectral value $\mathcal{S}_{\mathrm{A}}(f_1)=1.2g$ at $\mathrm{PGA}=1.0g$ as seismic input. The direct spectra-to-spectra method is used to generate three sets of FRS in direction 2 of Node 1, as shown in Figure 5.18. The median elastic demand $\mathcal{S}_D$ of the block wall can be obtained from the FRS ($\mathcal{S}_{\mathrm{F}}$) given in Figure 5.18. When the wall drifts inelastically under

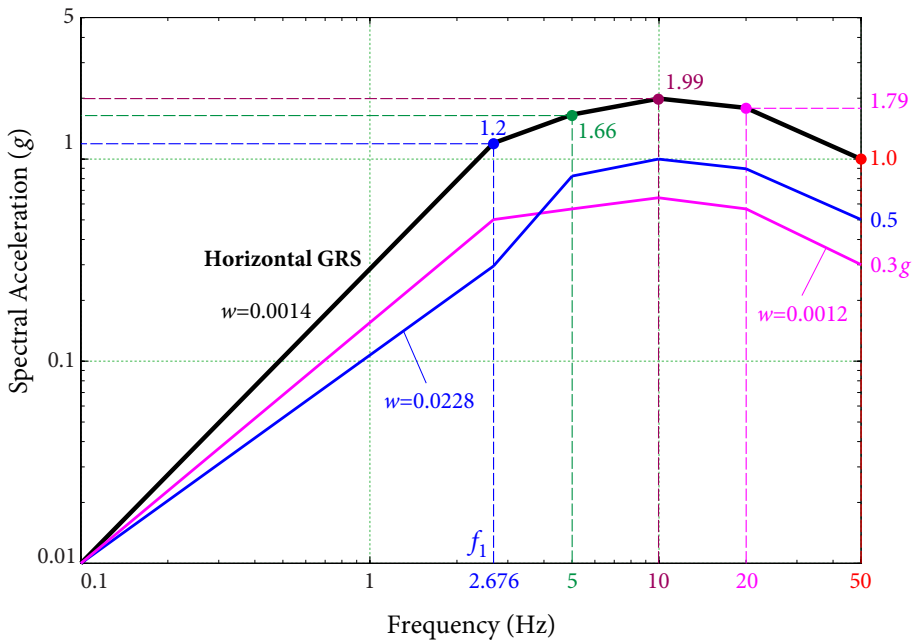


**Figure 5.17** An example of horizontal input GRS

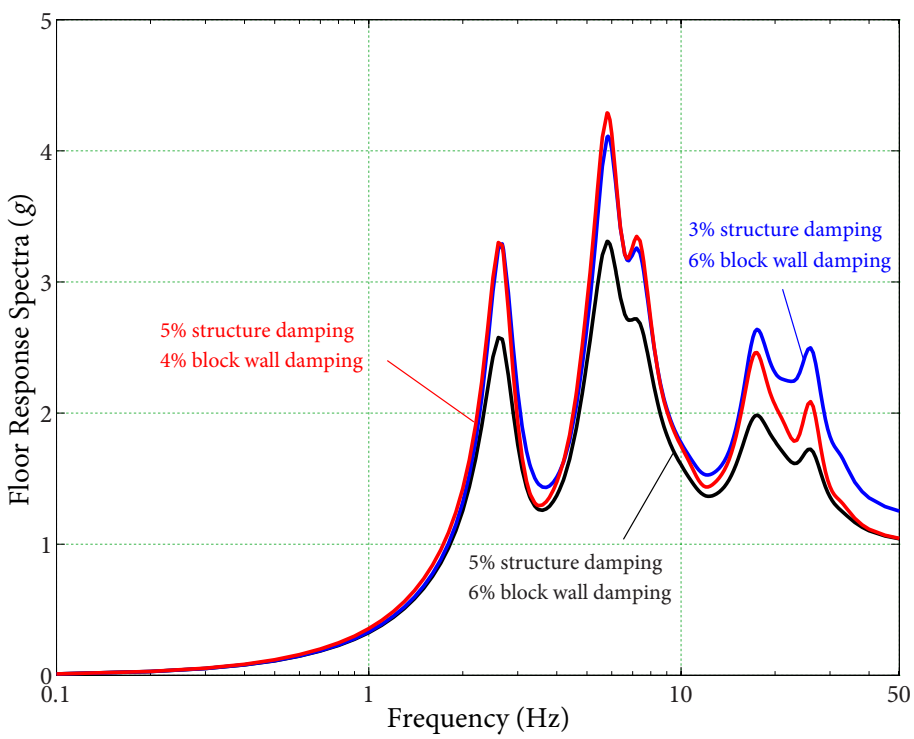


**Figure 5.18** FRS at Darlington NGS site given an input GRS

earthquake, *equivalent linear elastic procedure* is used to determine the nonlinear demand of the block wall by

$$\mathcal{S}_D = \mathcal{S}_{\mathrm{F}}(f_{\mathrm{sec}}, 6\%), \tag{5.5.4}$$

where $\mathcal{S}_{\mathrm{F}}(f_{\mathrm{sec}}, 6\%)$ can be obtained from the FRS given in Figure 5.18.

By changing the input GRS, FRS of the block wall can be generated repeatedly.

### Determination of Median Ratio Factor

Having obtained the capacity $\mathcal{S}_C$ (see Section 5.4.3) and seismic demand $\mathcal{S}_D$, the *median* strength factor $F_{\mathrm{S},m}$ can be determined by equation (5.4.41). Table 5.9 gives *median* strength factor $F_{\mathrm{S},m}$ with respect to wall drift ratios. It can be seen that maximum $F_{\mathrm{S},m} = 2.129$ occurs when $f_{\mathrm{sec}} = 1.68$ Hz.

**Table 5.9** Median Strength Factor as Function of Drift for Block Wall

| Drift ratio $\Delta/L$ | $u$ (in) | Frequency (Hz) $f_{\mathrm{sec}}$ | Reference demand $\mathcal{S}_D$ $(g)$ | Capacity $\mathcal{S}_C$ $(g)$ | $F_{\mathrm{S},m}$ |
|---|---|---|---|---|---|
| 0.15% | 0.20 | 12.20 | 1.365 | 2.040 | 1.494 |
| 0.66% | 0.87 | 5.84 | 3.309 | 2.020 | 0.610 |
| 1% | 1.32 | 4.72 | 2.014 | 2.006 | 0.996 |
| 1.70% | 2.36 | 3.60 | 1.258 | 1.978 | 1.572 |
| 2% | 2.64 | 3.30 | 1.341 | 1.966 | 1.467 |
| 3% | 3.96 | 2.68 | 2.565 | 1.926 | 0.751 |
| 5% | 6.60 | 2.03 | 1.304 | 1.846 | 1.416 |
| 7% | 9.24 | 1.68 | 0.830 | 1.766 | 2.129 |

Having obtained $F_{\mathrm{S},m}$, the *median* ratio factor $R_m$ is given by

$$R_m = F_\mu \cdot F_{\mathrm{RS},m} \cdot F_{\mathrm{S},m} = 1.0 \times 1.0 \times 2.129 = 2.129. \tag{5.5.5}$$

### Determination of Logarithmic Standard Deviations

The *approximate second-moment procedure* is applied to calculate variability of ratio factor $R$. Table 5.10 enumerates the variability of $R$ due to response and capacity variables.

**Table 5.10** The Variability of $R$ from Response and Capacity Variables

| Case | **Variable** | *Randomness* | *Uncertainty* | $R$ | $\beta$ | |
|---|---|---|---|---|---|---|
| 0 | **Base Case** | Variable at median | | 2.129 | | |
| | **Response Variables** | Variable at median plus $1\sigma$ | | $R_{1\sigma}$ | $\beta_R$ | $\beta_U$ |
| 1 | Horizontal direction peak response | $\mathcal{S}_D\,\mathrm{e}^{0.13}$ | | 1.87 | 0.13 | |
| 2 | Structure frequency | | $\mathcal{S}_D\,\mathrm{e}^{0.09}$ | 1.94 | | 0.09 |
| 3 | Structure damping | | $\mathcal{S}_D\,\mathrm{e}^{0.03}$ | 2.06 | | 0.03 |
| 4 | Structure mode shape | | $\mathcal{S}_D\,\mathrm{e}^{0.15}$ | 1.83 | | 0.15 |
| 5 | Structure mode combination | $\mathcal{S}_D\,\mathrm{e}^{0.15}$ | | 1.83 | 0.15 | |
| 6 | Block wall frequency | | $\mathcal{S}_D\,\mathrm{e}^{0.37}$ | 1.47 | | 0.37 |
| 7 | Block wall damping | | $\mathcal{S}_D\,\mathrm{e}^{0.11}$ | 1.91 | | 0.11 |
| 8 | Block wall mode shape | | $\mathcal{S}_D\,\mathrm{e}^{0.05}$ | 2.02 | | 0.05 |
| 9 | Block wall mode combination | $\mathcal{S}_D\,\mathrm{e}^{0.05}$ | | 2.02 | 0.05 | |
| | **Capacity Variables** | Variable at median minus $1\sigma$ | | $R_{-1\sigma}$ | $\beta_R$ | $\beta_U$ |
| 10 | Equation error $F_{\mathrm{eqn}}$ | | $F_{\mathrm{eqn}}\,\mathrm{e}^{-0.105}$ | 2.129 | | 0.0 |
| 11 | Rebar error $F_{\mathrm{rb}}$ | | $F_{\mathrm{rb}}\,\mathrm{e}^{-0.071}$ | 2.129 | | 0.0 |
| 12 | Masonry strength $f'_{\mathrm{m}}$ | $f'_{\mathrm{m}}\,\mathrm{e}^{-0.05}$ | | 2.129 | 0.0 | |
| 13 | Steel strength $f_y$ | $f_y\,\mathrm{e}^{-0.08}$ | | 2.129 | 0.0 | |
| | **SRSS Combination** | | | | $\beta_R$ | $\beta_U$ |
| | | | | | 0.20 | 0.43 |
| | | | | $\beta_{\mathrm{C}}$ | 0.48 | |

It is noted that in the evaluation of capacity variability, the secant frequency of the block wall changes when an capacity variable is set at $-1\sigma$ level, thus seismic demand of the block wall changes as well. As a result, the variability of $R$ due to capacity variability is the combined effects of capacity and seismic demand. The variability of $R$ due to

equation error variability is calculated as an example. Substituting $F_{\text{eqn}} = 1.034 \cdot \mathrm{e}^{-0.105}$ into equation (5.4.53) gives block wall capacity $\mathcal{S}_C = 1.562g$. Thus the secant frequency of block wall is given by

$$f_{\text{sec}} = \frac{1}{2\pi}\sqrt{\frac{1.5\,\mathcal{S}_C}{\Delta_u}} = \frac{1}{2\times 3.14}\sqrt{\frac{1.5\times(1.562\times 386.4)}{9.24}} = 1.58\,\text{Hz}. \tag{5.5.6}$$

Based on FRS in Figure 5.18, when the block wall approaches drift limit, seismic demand of the block wall is given by

$$\mathcal{S}_D = \mathcal{S}_{\text{F}}(f_{\text{sec}},\, 6\%) = 0.732g. \tag{5.5.7}$$

Hence *median* strength factor $F_{\text{S},m}$ is given by

$$F_{\text{S},m} = \frac{1}{|-1|}\ln\frac{\mathcal{S}_C}{\mathcal{S}_D} = \ln\frac{1.562g}{0.732g} = 2.136. \tag{5.5.8}$$

Having obtained $F_{\text{S},m}$, the ratio factor $R_{-1\sigma}$ is given by

$$R_{-1\sigma} = F_\mu \cdot F_{\text{RS},m} \cdot F_{\text{S},m} = 1.0\times 1.0\times 2.136 = 2.136, \tag{5.5.9}$$

It can be seen that $R_{-1\sigma} > R_m$, which indicates median seismic capacity of the block wall increases with the decrease of its structural capacity. Therefore, $\beta$ value of $R$ due to equation error variability should be taken as 0.

### Determination of Seismic Fragility

Having obtained *median* ratio factor $R_m$ and logarithmic standard deviations $\beta_R$ and $\beta_U$, given the input GRS, conditional probability of failure $p_{\text{F},q}\big(1.0, 1.2\big)$, at confidence level $Q = q$, can be determined by

$$p_{\text{F},q}\big(1.0, 1.2 \,\big|\, Q = q\big) = \Phi\left\{\frac{\ln\big(1/R_m\big) + \beta_U\,\Phi^{-1}(q)}{\beta_R}\right\}. \tag{5.5.10}$$

In applications, confidence level $Q$ is usually taken as discrete values. Taking confidence level $Q = 95\%$ for example, $p_{\text{F},q}\big(1.0, 1.2 \,\big|\, Q = 0.95\big)$ is given by

$$p_{\text{F},q}\big(1.0, 1.2 \,\big|\, Q = 0.95\big) = \Phi\left\{\frac{\ln(1/2.129) + 0.43\times\Phi^{-1}(0.95)}{0.20}\right\} = 0.408. \tag{5.5.11}$$

When composite variability is used, a mean seismic fragility $p_{\mathrm{F,C}}(1.0, 1.2)$ is calculated as

$$p_{\mathrm{F,C}}(1.0, 1.2) = \Phi\left\{\frac{\ln(1/R_m)}{\beta_{\mathrm{C}}}\right\} = \Phi\left\{\frac{\ln(1/2.129)}{0.48}\right\} = 0.056. \tag{5.5.12}$$

### Seismic Fragility Surfaces

Defining input GRS with spectral acceleration values at three frequencies from all other intervals of spectral domain, and repeating the procedure for calculating conditional probability of failure values result in a family of seismic fragility surfaces, as shown in Figure 5.19. When composite variability is used, a composite (mean) seismic fragility surface is obtained and is shown in Figure 5.19.

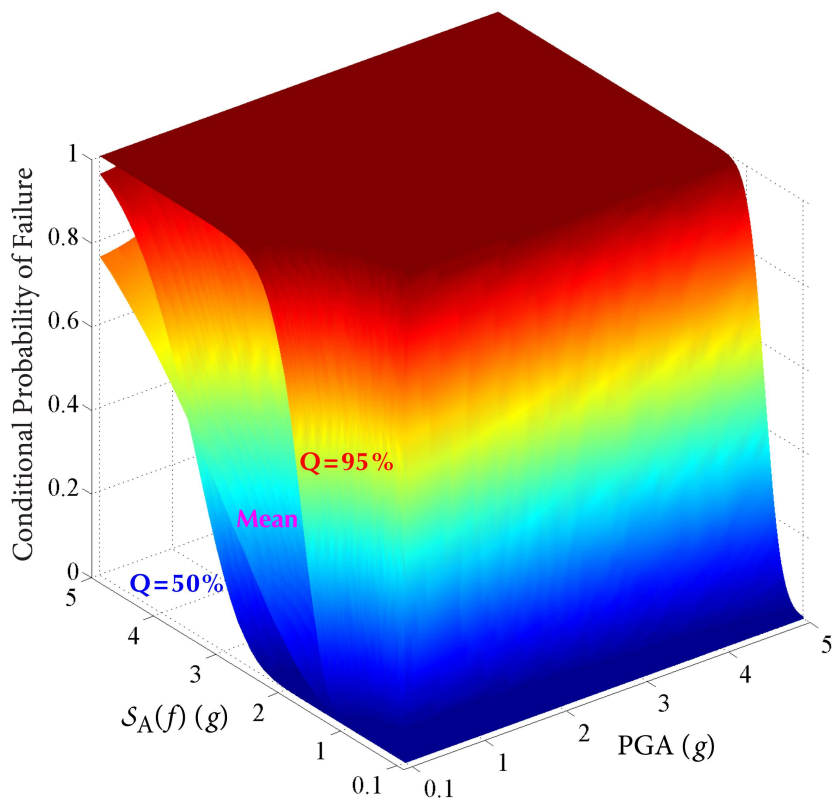


**Figure 5.19** Seismic fragility surfaces of $\mathcal{S}_{\mathrm{A}}(f_1)$ and PGA

It is noted that the secant frequency $f_{\mathrm{sec}}$ of the block wall decreases to 1.68 Hz when the block wall approaches drift limit. Given a small spectral value of $\mathcal{S}_{\mathrm{A}}(f_1)$, FRS would be pretty low in frequency range less than $f_1 = 2.676$ Hz. Therefore, spectral acceleration at

$f_{\text{sec}} = 1.68$ Hz is reasonable small. It would result in pretty small conditional probability of failure even if PGA value is reasonable large, as shown in Figure 5.19.

### 5.5.4 Weighting Seismic Fragility Curves

Having obtained the weights of input GRS (see section 5.5.2) and seismic fragility surfaces (see section 5.5.3), the weighting seismic fragility in terms of PGA, at confidence level $Q = q$ is determined by

$$\bar{p}_{\text{F},q}(s_0) = \sum_{i_1=1}^{100} \left[ p_{\text{F},q}\left(s_1^{(i_1)}, s_0\right) \cdot w\left(s_1^{(i_1)} \leqslant s_1 \leqslant s_1^{(i_1+1)} \,\middle|\, s_0\right) \right], \tag{5.5.13}$$

where $i_1 = 100$ is the number of intervals of $\mathcal{S}_{\text{A}}(f_1)$, $w\left(s_1^{(i_1)} \leqslant s_1 \leqslant s_1^{(i_1+1)} \,\middle|\, s_0\right)$ is the weight of input GRS given by equation (5.5.2), and $p_{\text{F},q}\left(s_1^{(i_1)}, s_0\right)$ is the seismic fragility at $Q = q$ given by equation (5.5.11).

When composite variability is used, a weighting composite (mean) seismic fragility is determined by

$$\bar{p}_{\text{F,C}}(s_0) = \sum_{i_1=1}^{100} \left[ p_{\text{F,C}}\left(s_1^{(i_1)}, s_0\right) \cdot w\left(s_1^{(i_1)} \leqslant s_1 \leqslant s_1^{(i_1+1)} \,\middle|\, s_0\right) \right], \tag{5.5.14}$$

where $p_{\text{F,C}}\left(s_1^{(i_1)}, s_0\right)$ is mean seismic fragility given by equation (5.5.12).

Changing PGA values from lower bound of $0.1g$ to upper bound of $5g$ results in weighting seismic fragility curves, as shown in Figure 5.20.

Conventional seismic fragility curves of the block wall in section 5.4 are plotted together with the weighting curves. It shows that the weighting *median* seismic capacity of the heat exchanger has a significant increase (from $2.036g$ PGA to $> 5g$ PGA). HCLPF seismic capacity of the block wall based on weighting and current seismic fragility analysis methods are calculated and shown in Figure 5.21. It can be seen that the weighting seismic capacity has 42.5% increase (from $0.809g$ PGA to $1.167g$ PGA). Both results indicate that current seismic fragility analysis includes remarkable conservatism in the estimation of *median* and HCLPF seismic capacity of the block wall. Weighting seismic fragility analysis method should be used to acquire more accurate seismic capacity estimates of components on primary structures.

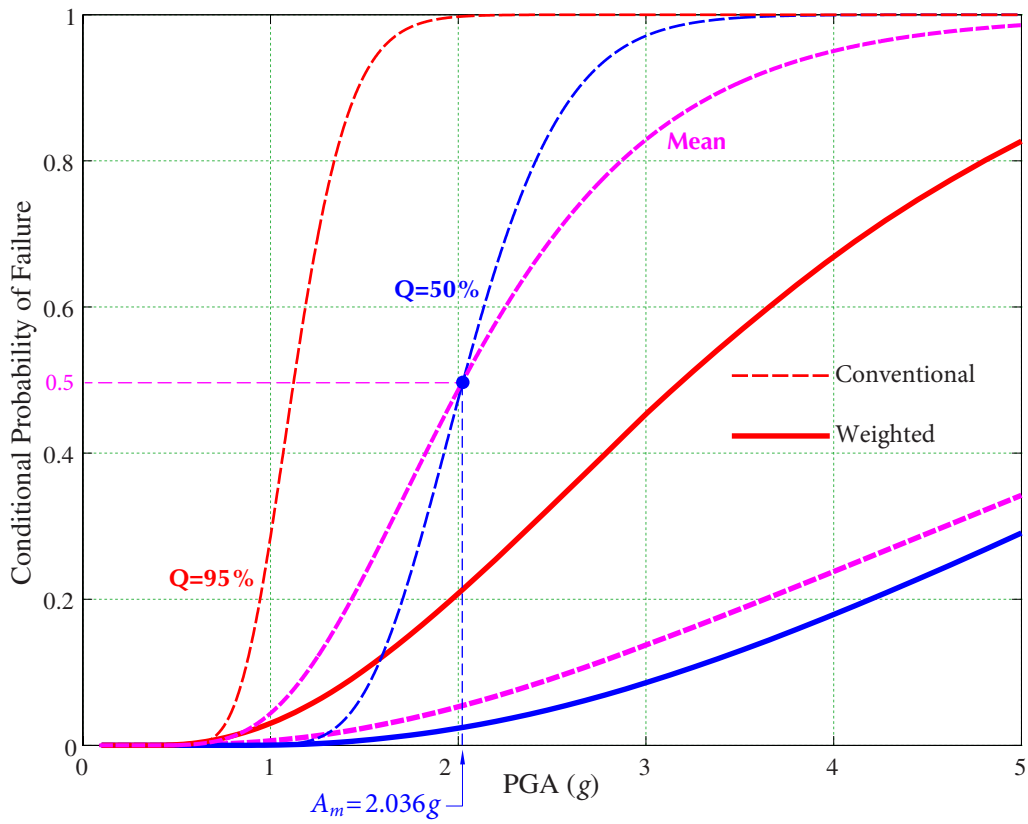


**Figure 5.20** Seismic fragility curves of block wall based on two methods

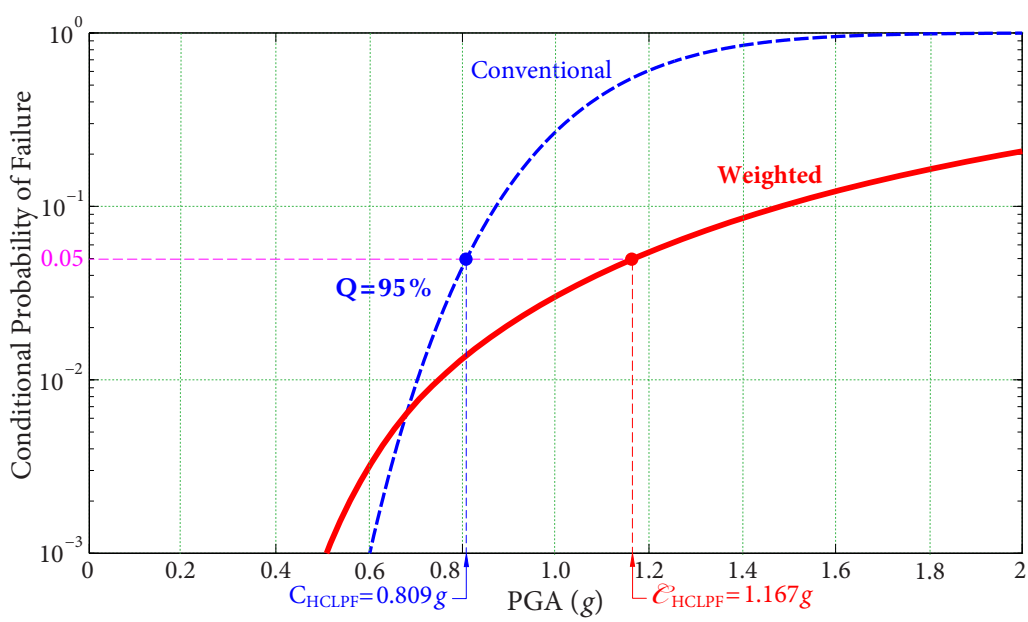


**Figure 5.21** HCLPF seismic capacities of block wall based on two methods

## 5.6 Summary

In this Chapter, weighting seismic fragility analysis for components on primary structures is presented:

- a direct spectra-to-spectra method is introduced to generate FRS with high efficiency and sufficient accuracy, and
- uncertainties in structural responses are efficiently captured.

The proposed method can efficiently develop seismic fragility surfaces and provides more accurate seismic capacity estimates of components.

Numerical example for a block wall located in the service building of Darlington nuclear generating station is performed:

- weighting *median* seismic capacity has over 100% increase, and
- weighting HCLPF seismic capacity has 42.5% increase.

Recall that in Chapter 4, correlation coefficient $\rho$ is 0.905 between vector-valued GMPs (VGMPs). For the block wall in this example, $\rho$ is 0.736 between VGMPs, which is much smaller than 0.905. It indicates that, with smaller correlation coefficient between VGMPs, more increase are found in seismic capacity estimates of structures, systems, and components (SSCs).

Weighing seismic fragility analysis should be performed for SSCs mounted on structures aiming to obtain more accurate seismic capacity estimates.

C H A P T E R 6

# Improved Seismic Margin Assessment

A nuclear power plant consists of a great number of structures, systems, and components (SSCs). Seismic margin assessment (SMA) is widely used to evaluate plant seismic capacity. A general procedure of the SMA is shown in Figure 6.1. High Confidence and Low Probability of Failure (HCLPF) seismic capacities of SSCs, in terms of a single ground-motion parameter such as PGA, are defined as input for performing system analysis by means of event trees and fault trees. Therefore, accurate HCLPF seismic capacities of SSCs are pretty important in the SMA.

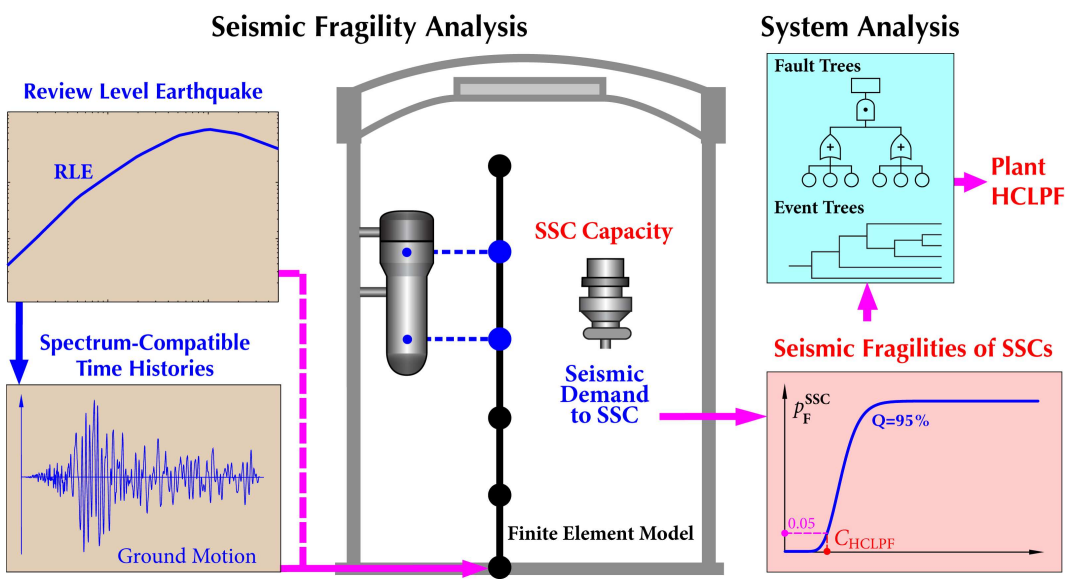


**Figure 6.1** A general procedure of seismic margin assessment

In this Chapter, an improved SMA procedure is proposed:

- weighting seismic fragility analysis is performed for calculating HCLPF seismic capacities of "weak link" SSCs, and
- current seismic fragility analysis is conducted for determining HCLPF seismic capacities of less important SSCs.

This ensures that more accurate plant seismic capacity is obtained while computational cost is acceptable.

Numerical example for an emergency coolant injection (ECI) system is performed to illustrate the procedure and demonstrate its advantages. The results show that the improved SMA procedure effectively increase HCLPF seismic capacity estimate of the ECI system.

## 6.1 System Analysis

Engineering practice has recognized that, the occurrence of an adverse consequence such as core damage accident, probably results from the initiating event (fault) of an SSC. Therefore, system analysis is necessarily performed to propagate basic events to the occurrence of adverse consequence. It mainly includes three key steps: (1) event trees are applied to develop accident sequences (failure paths) of an adverse consequence based on top events following the initiating event; (2) fault trees are developed to determine HCLPF capacities of top events contributed from basic events; (3) HCLPF capacities of top events in accident sequences are propagated to calculate plant damage state HCLPF seismic capacity, thus saves the redesign cost for a electric cabinet.

### 6.1.1 Event Tree Analysis

When an initiating event occurs, an accident sequence is required to be developed to find out all the possible failure paths triggering an adverse consequence, following the initiating failure. In engineering applications, event trees are usually used to establish the accident sequence. As shown in Figure 6.2, one can take core damage (CD) accident for example, an event tree is developed to establish the accident sequence following the large loss of coolant accident (LLOCA). Six top events, LLOCA, EC, LPI, CHR, CV, and LI are addressed in this

accident sequence. "Success" indicates that the top event does not fail due to the failure of preceding top event.

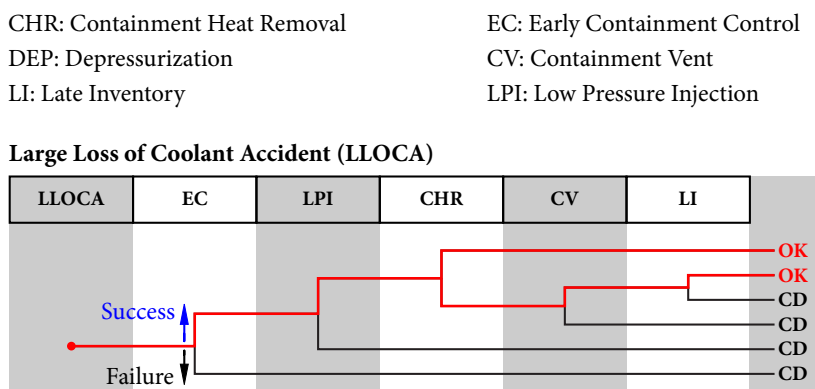


**Figure 6.2** An example of event tree for core damage accident

## 6.1.2 Fault Tree Analysis

For each top event in the accident sequence, as shown in Figure 6.2, a fault tree is developed to decompose it into sub-events until the failures (faults) of the sub-events can be evaluated as single-mode faults. NUREG-0492 (USNRC, 1981) presents more detailed introduction of fault tree analysis.

### Fault Tree Diagram

A *fault tree* diagram essentially decomposes the top event into unions and intersections of sub-events or combination of sub-events. The objective of a fault tree is to identify and model the various faults that can result in the occurrence of the top event. A fault tree diagram is then a graphical decomposition of a top event into the union and/or intersection of sub-events. The alternative faults that could lead to top event are logically related to the top event by "OR" and "AND" gates. Some commonly used symbols of fault trees are listed in Table 6.1. A simple fault tree is shown in Figure 6.3. The top event $E$ is connected to events $E_1$ and $E_2$ through a "OR" gate, which indicates that the top event $E$ is the union of sub-events $E_1$ and $E_2$, i.e., $E$ will occur if at least one of the two events $E_1$ and $E_2$ occurs. Event $E_1$ is the union of $B_1$ and $B_2$. Event $E_2$ is developed further at the transfer-out "1", in which $E_2$ is the intersection of sub-events $E_3$ and $E_4$. Event $E_3$ is the union of $B_1$ and $B_3$,

and event $E_4$ is the intersection of $B_4$ and $B_5$. Mathematically, the events can be expressed as

$$E = E_1 + E_2, \quad E_1 = B_1 + B_2, \quad E_2 = E_3 \cdot E_4 = (B_1 + B_3) \cdot (B_4 \cdot B_5). \tag{6.1.1}$$

**Table 6.1** Common Fault Tree Symbols

| | |
|---|---|
| ○ | **Basic Event**, which is a basic initiating fault |
| ◇ | **Undeveloped Event**, which is not developed further because of insufficient consequence or unavailable information |
| ⬠ | **External Event**, which is not a fault but a normally occurring basic event |
| ▭ | **Intermediate Event**, which occurs because of the occurrence of one or more antecedent events through logic gates |
| + | **"OR" Gate**, in which the output event occurs if at least one of the input events occur |
| • | **"AND" Gate**, in which the output event occurs if all of the input events occur |
| △ | **Transfer-In**, indicating that the tree is developed further at the corresponding Transfer-Out |
| △— | **Transfer-Out**, indicating that this portion of the tree must be attached at the corresponding Transfer-In |

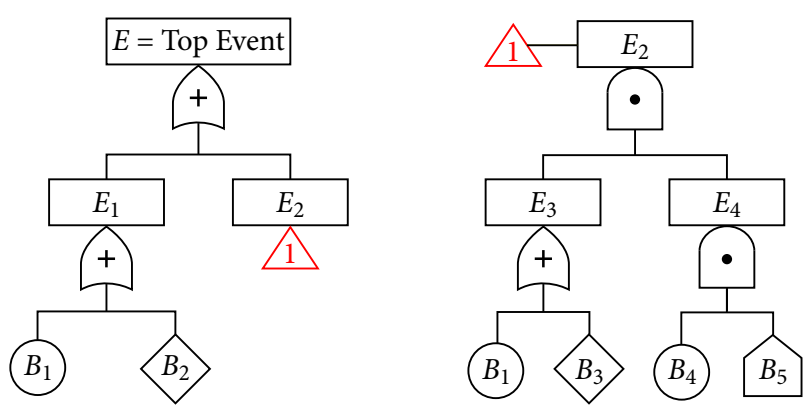


**Figure 6.3** A simple fault tree

## Boolean Algebra

Constructing fault trees is a systematic procedure that permits the analysis of complex systems. However, redundant events in a fault tree will lead to double accounting if they are

not eliminated. The algebra of sets, or more generally the Boolean algebra, can be applied to remove any redundancies of the same event.

A complete list of rules of Boolean algebra is given in NUREG-0492 (USNRC, 1981). Some useful rules are listed in Table 6.2. Considering the fault tree shown in Figure 6.3, the top event $E$ can be written as, using equations (6.1.1) and the rules of Boolean algebra,

$$\begin{aligned} E = E_1 + E_2 &= (B_1 + B_2) + (B_1 + B_3) \cdot (B_4 \cdot B_5) \\ &= B_1 + B_2 + B_1 \cdot B_4 \cdot B_5 + B_3 \cdot B_4 \cdot B_5 \\ &= (B_1 + B_1 \cdot B_4 \cdot B_5) + B_2 + B_3 \cdot B_4 \cdot B_5 \\ &= B_1 + B_2 + B_3 \cdot B_4 \cdot B_5. \end{aligned} \tag{6.1.2}$$

The corresponding reduced fault tree is shown in Figure 6.4.

**Table 6.2** Some Useful Boolean Algebra Rules

| |
|---|
| $X \cdot X = X$ |
| $X + X = X$ |
| $X \cdot (X + Y) = X$ |
| $X + X \cdot Y = X$ |
| $X + \overline{X} = \Omega$ (sample space) |
| $X \cdot \overline{X} = \emptyset$ (empty set) |
| $\overline{X \cdot Y} = \overline{X} + \overline{Y}$ |
| $\overline{X + Y} = \overline{X} \cdot \overline{Y}$ |

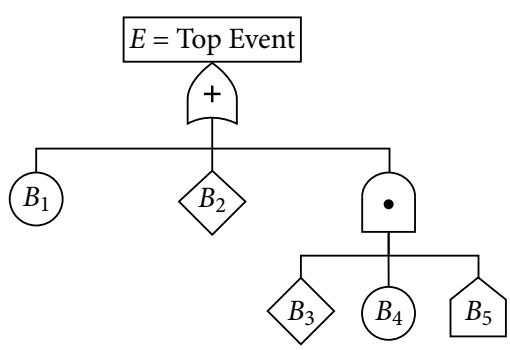


**Figure 6.4** Reduced fault tree

### HCLPF Max/Min Method

Since the top event is related to the sub-events and basic faults at subsequent levels of a fault tree through combinations of "AND" and "OR" logic gates, the top event can be expressed in terms of unions and intersections of sub-events and basic faults. Having simplified the Boolean expression of the top event using Boolean algebra, the HCLPF seismic capacity of the top event can be determined by HCLPF Max/Min method:

- **Sub-events and basic faults are combined with "AND" gate**
  The maximum HCLPF seismic capacity among the faults under "AND" gate is taken as HCLPF seismic capacity of the intersection.
- **Sub-events and basic faults are combined with "OR" gate**
  The minimum HCLPF seismic capacity among the faults under "OR" gate is taken as HCLPF seismic capacity of the union.

As shown in Figure 6.4, $B_3$, $B_4$, and $B_5$ are combined with "AND" gate, the HCLPF seismic capacity for this intersection (denote as $B_6$) is taken as the maximum one among these three events. Afterwards, events $B_1$, $B_2$, and $B_6$ are combined with "OR" gate. Thus the HCLPF seismic capacity of the top event $E$ is taken as the minimum HCLPF seismic capacity among these three events.

## 6.2 Numerical Example for Emergency Coolant Injection System

### 6.2.1 Basic Configuration of ECI System

The ECI system is shown in Figure 6.5. The system consists of a water tank T, a manual valve V that is normally open, two pumps P1 and P2, two check valves CV1 and CV2, and three motor-operated valves MV1, MV2, and MV3 that are normally closed. When the ECI system is activated, the ECI injection signal is delivered to operate pumps P1 and P2, and to open the motor-operated valves MV1, MV2, and MV3. The success criterion is that water flow is delivered from at least one pump through at least one motor-operated valve.

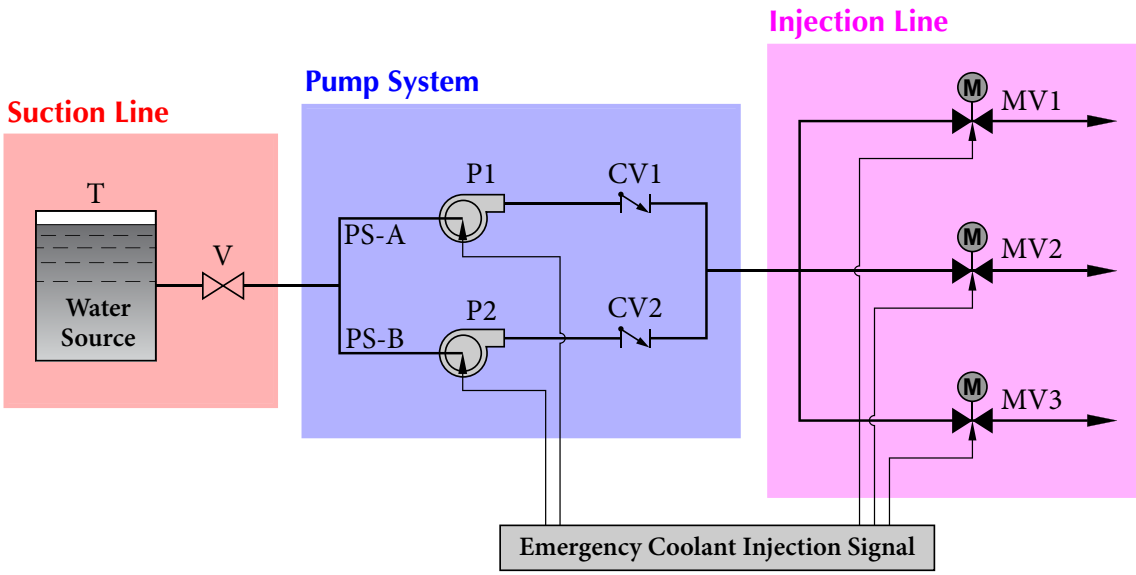


**Figure 6.5** A simplified ECI system

### Fault Tree Analysis

The ECI system can be divided into three subsystems: Suction Line, Pump System, and Injection Line, as shown in Figure 6.5. The Suction Line consists of a water tank T and a manual valve V. It fails when the tank fails (no water supply) or the manual valves fails (not able to remain open). The Pump system has two flow routes PS-A and PS-B connected in parallel. Each flow route consists of a pump and a check valve connected in series, which fails if no ECI Signal is delivered to operate the pump, or the pump fails to operate, or the check valve is not open. This subsystem fails when both flow routes fail. The Injection Line consists of three motor-operated valves connected in parallel, which fails when all three injection lines fail. An injection line fails if no ECI Signal is delivered or the valve fails to open. The fault tree of the ECI system is shown in Figure 6.6. Define the following events:

$E =$ ECI system fails (ECI fails to deliver at least one pump of flow),

$W =$ Suction Line fails,

$P =$ Pump system fails,

$I =$ Injection Line fails,

$T =$ Water Tank T fails,

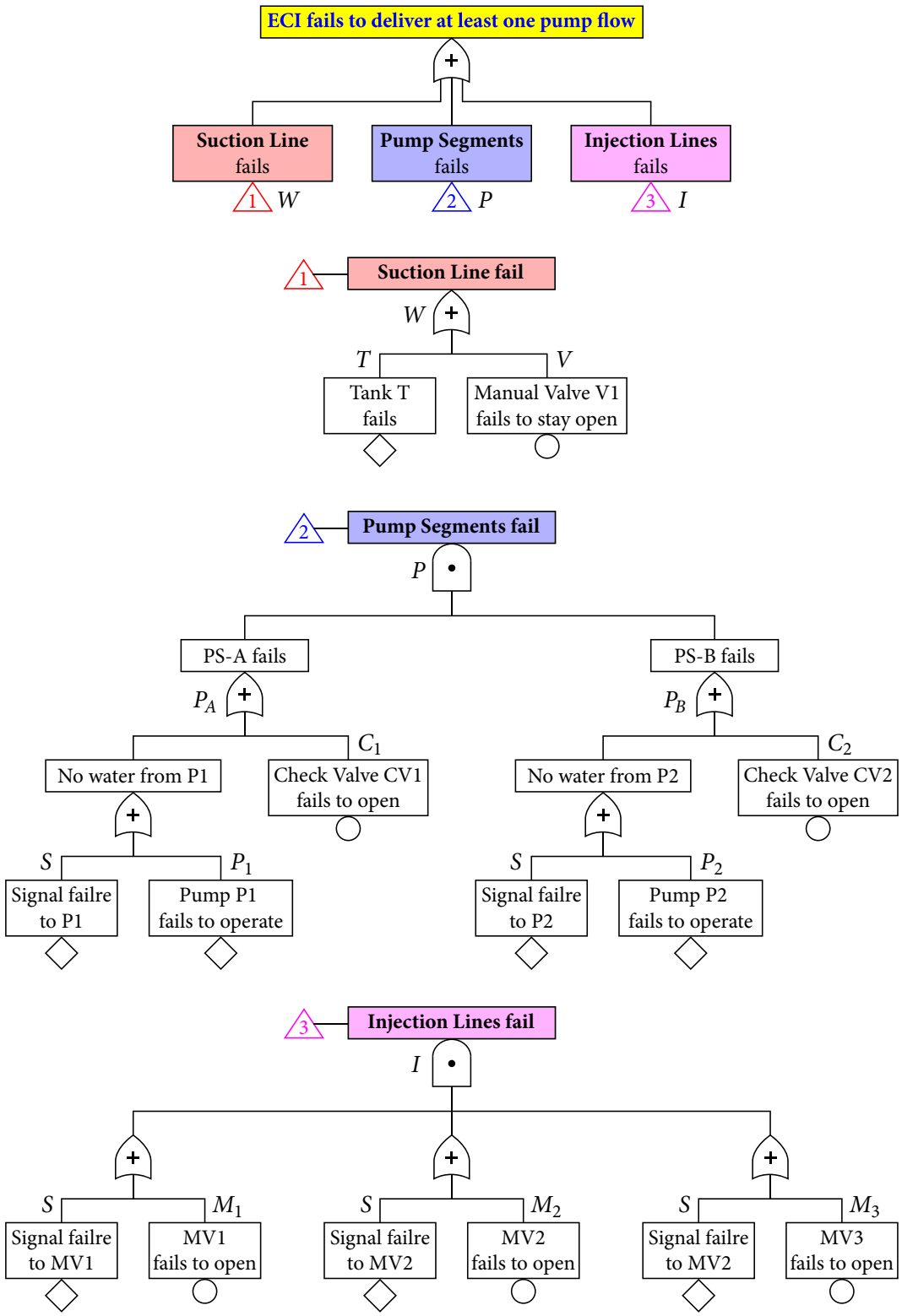


**Figure 6.6** Fault tree of the ECI system

$$
\begin{aligned}
V &= \text{Manual valve V fails,}\\
P_i &= \text{Pump P}i,\ i=1,2,\text{ fails,}\\
C_i &= \text{Check Valve C}i,\ i=1,2,\text{ fails,}\\
M_i &= \text{Motor-operated valve MV}i,\ i=1,2,3,\text{ fails,}\\
S &= \text{No ECI Signal delivered.}
\end{aligned}
$$

Hence, performing Boolean algebra on the events results in

$$
\begin{aligned}
W &= T + V,\\
P &= P_A \cdot P_B = [(S + P_1) + C_1] \cdot [(S + P_2) + C_2]\\
&= S \cdot S + S \cdot (P_1 + P_2 + C_1 + C_2) + P_1 \cdot P_2 + P_1 \cdot C_2 + P_2 \cdot C_1 + C_1 \cdot C_2\\
&= S + (P_1 + C_1) \cdot (P_2 + C_2)\\
I &= (S + M_1) \cdot (S + M_2) \cdot (S + M_3)\\
&= S \cdot S \cdot S + S \cdot S \cdot (M_1 + M_2 + M_3) + S \cdot (M_1 \cdot M_2 + M_2 \cdot M_3 + M_1 \cdot M_3) + M_1 \cdot M_2 \cdot M_3\\
&= S + M_1 \cdot M_2 \cdot M_3\\
E &= W + P + I = (T + V) + [S + (P_1 + C_1) \cdot (P_2 + C_2)] + (S + M_1) \cdot (S + M_2) \cdot (S + M_3)\\
&= T + V + S + (P_1 + C_1) \cdot (P_2 + C_2) + M_1 \cdot M_2 \cdot M_3. \qquad (6.2.1)
\end{aligned}
$$

The Boolean expression (6.2.1) can be used to draw the reduced fault tree in Figure 6.7. It is noted that, the ECI signal control in located in an electric cabinet. The ECI signal fails to deliver when the cabinet falls down due to earthquake excitations.

### Screening Table

In order to be cost-efficient, the SMA should incorporate a step where SSCs are quickly screened from further review. In applications, a screening table is used based upon experience. The advantage of screening out SSCs from further review is that a great amount of unnecessary HCLPF capacity computations are eliminated for SSCs whose HCLPF capacities clearly exceed the screening level $A_{\text{RLE}}$, so that efforts can be quickly concentrated on those SSCs for which there is a legitimate concern about seismic ruggedness. After screening process, detailed seismic fragility analysis is performed for the SSCs that are

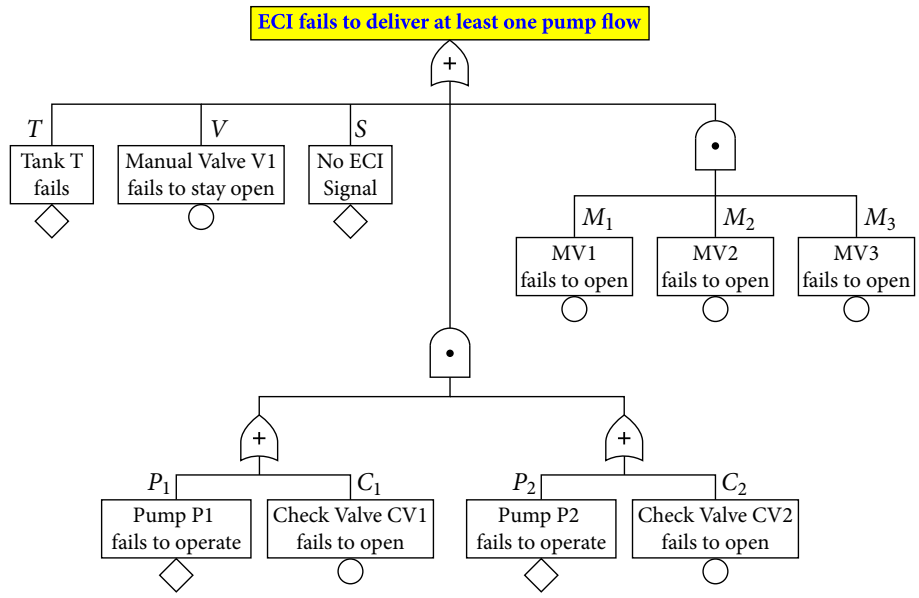


**Figure 6.7** The reduced fault tree of ECI system

not screened out. The outputs of seismic fragility analysis are HCLPF seismic capacities. HCLPF Max/Min method is used to determine plant HCLPF seismic capacity.

Suppose that the ECI system is used in the reactor building of Darlington nuclear generating station (NGS). Since the NGS is located in eastern North America, the screening table can be set at $A_{\mathrm{RLE}} = 0.3g$ PGA (EPRI-NP-6041-SL, EPRI, 1991A). For illustration, assume that manual valve V, pumps P$i$, check valves CV$i$, and motor-operated valve MV$i$ are screened out. The water tank T and electric cabinet are identified as "weak link" components, hence detailed seismic fragility analysis needs to be performed for these two components.

## 6.2.2 Current Seismic Fragility Analysis for Water Tank

In this Section, current seismic fragility analysis is performed for determining HCLPF seismic capacitiy of the water tank.

### 6.2.2.1 Basic Configuration of Water Tank

Water tank in Section 7 of EPRI TR-103959 (EPRI, 1994) is used in this example. Geometry information of the water tank is shown in Figure 6.8. The tank radius $R$ is 20 feet, while the water height $H$ is 37 feet when it is full. The overall tank height to the top of its dome

roof is 43.4 feet, which is about twice as high as its radius. This tank was built with only a minimal number of hold-down anchor bolts consisting of eight 2-inch diameter A307 bolts around its circumference (8 @45°). These bolts provide hold-down forces to the tank shell through the top plate of well-designed bolt chairs at a height $h_c$ of 24.75 inches above the tank bottom. The bolts are anchored into the concrete foundation through an anchor plate at a depth $h_a$ of 28.5 inches. The bolt chairs, their attachment to the tank, and the bolt anchorage are sufficient to develop the full capacity of the bolts. The tanks shell is SA240-Type 304 stainless steel. Detailed properties of the water tank are listed in Table 6.1.

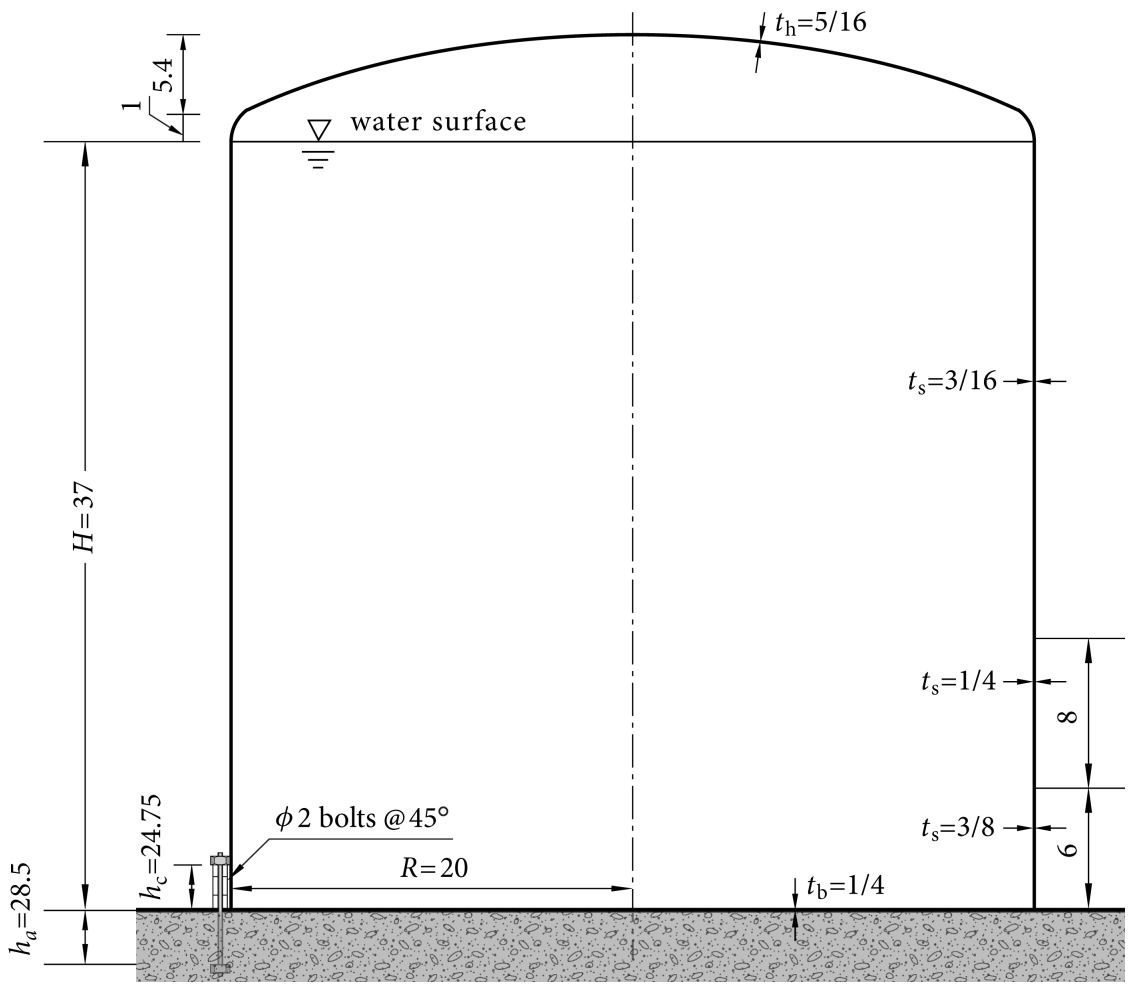


**Figure 6.8** Basic configuration of the water tank

**Table 6.1** Deterministic Properties of Water Tank

| Property | Parameter | Value |
|---|---|---|
| **Water Tank** | | |
| Radius | $R$ | 20 ft |
| Height of bottom to water surface (when full) | $H$ | 37 ft |
| Height of bottom to roof | $H_r$ | 43.4 ft |
| Shell thickness (varies with height) | $t_s$ | |
| Bottom to 6 ft | | 3/8 in |
| 6 ft to 14 ft | | 1/4 in |
| 14 ft to 37 ft | | 1/4 in |
| Roof thickness | $t_r$ | 5/16 in |
| Bottom plate thickness | $t_b$ | 1/4 in |
| Tank weight | | |
| Bottom plate | $W_b$ | 12.8 kips |
| Shell (bottom to 37 ft) | $W_s$ | 44.9 kips |
| Roof | $W_r$ | 17.2 kips |
| Water weight | $W_w$ | 2900 kips |
| Height of bottom to center of gravity | | |
| Bottom plate | $H_{cr,b}$ | 0 |
| Shell | $H_{cg,s}$ | 16.4 ft |
| Roof | $H_{cg,r}$ | 42 ft |
| Water (when full) | $H_{cg,w}$ | 18.5 ft |
| **A307 Bolt** | | |
| Bolt diameter | $d$ | 2 in |
| Number of bolts around tank circumference | $N$ | 8 |
| Bolt chair height | $h_c$ | 24.75 in |
| Embedment length | $h_a$ | 28.5 in |

### Potential Failure Mode

For this water tank, only one potential failure mode, i.e., overturning moment induced rupture of the water tank near its connection to its base, due to a combination of excessive tank wall buckling, bolt stretching, and excessive baseplate uplift, is considered (EPRI TR-103959, EPRI, 1994). This failure mode has been selected for review because:

- it generally controls the seismic capacity of a minimally anchored tank,
- it is the controlling failure mode for the Conservative Deterministic Failure of Margin capacity of the water tank (see Figure 6.8) as was shown in Appendix H of EPRI NP-6041 (EPRI, 1991A), and
- it is one of the more complex and controversial failure modes to evaluate.

### Modal Information

EPRI NP-6041 (EPRI, 1991A) gives the best estimate natural frequency $f = 6$ Hz for the horizontal fundamental impulsive mode. This is the only significant mode which influences the overturning moment response (EPRI NP-6041-SL, EPRI, 1991A). The best estimate (median) and plus/median one logarithmic standard deviation estimate ($\pm 1\beta$) parameter values for this mode are given in Table 6.2. The uncertainties in frequency and damping can be calculated given a specified Review Level Earthquake (RLE).

**Table 6.2** Horizontal Impulsive Mode Variability (Table 7-2, EPRI, 1994)

| **Parameter** | $-1\beta$ | Median | $+1\beta$ |
|---|---|---|---|
| Frequency (Hz) | 4.8 | 6.0 | 6.6 |
| Damping | 3% | 5% | 7% |

## 6.2.2.2 Review Level Earthquake

Assume the water tank is located on ground floor of a reactor building in Darlington nuclear generating station (NGS). A generic ground response spectrum (GRS) such as NUREG/CR-0098 median response spectrum (abbreviated as NUREG spectrum) or a site-specific uniform hazard spectrum (UHS), can be defined as RLE.

In this example, spectral acceleration at 50 Hz is taken as PGA. PGA is chosen as GMP in determining HCLPF seismic capacity of the water tank. Since Darlington NGS is located in eastern North America, screening level can be taken as $A_{\mathrm{RLE}} = 0.3g$ PGA. Figure 6.9 gives NUREG spectrum and site-specific UHS anchoring to PGA at $A_{\mathrm{RLE}} = 0.3g$. In the following, NUREG spectrum and site-specific UHS are chosen as RLE separately to perform seismic fragility analysis for the water tank.

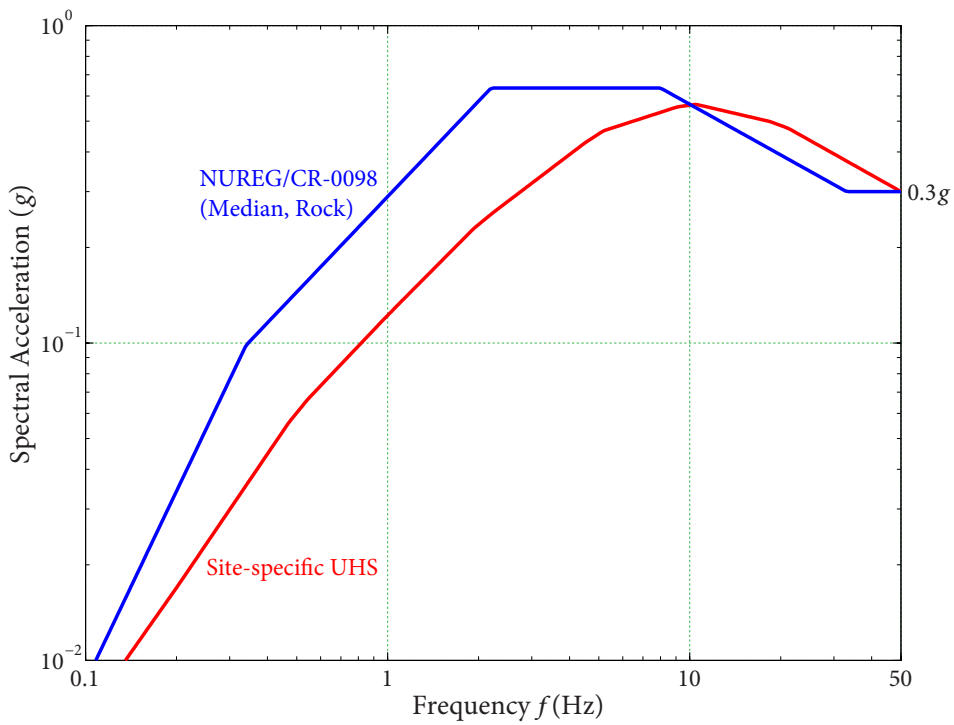


**Figure 6.9** NUREG spectrum and site-specific UHS anchoring to PGA at $0.3g$

### 6.2.2.3 Current Seismic Fragility Analysis - NUREG Spectrum is RLE

NUREG spectrum anchoring to PGA at screening level $0.3g$ is defined as RLE. The vertical GRS is assumed to be 2/3 of the horizontal input over the entire frequency range. The water tank is subjected to earthquake excitations in three directions.

#### Median Seismic Demand

For this water tank, only the horizontal fundamental impulsive mode at $f = 6$ Hz is considered. Based on NUREG spectrum in Figure 6.9, spectral acceleration $\mathcal{S}_{\mathrm{A}}(f = 6\,\mathrm{Hz})$ is equal

to $0.636g$. The overturning moment response is given by (EPRI NP-6041-SL, EPRI, 1991A)

$$M_{\mathrm{R}} = \mathcal{S}_{\mathrm{A}}(f)\left[W_{\mathrm{r}} \cdot H_{\mathrm{cg,r}} + W_{\mathrm{s}} \cdot H_{\mathrm{cg,s}} + W_{\mathrm{b}} \cdot H_{\mathrm{cg,b}} + W_{\mathrm{I}} \cdot H_{\mathrm{cg,I}}\right], \tag{6.2.2}$$

where $W_{\mathrm{r}}$, $W_{\mathrm{s}}$, $W_{\mathrm{b}}$, $H_{\mathrm{cg,r}}$, $H_{\mathrm{cg,s}}$, and $H_{\mathrm{cg,b}}$ are given in Table 6.1. $W_{\mathrm{I}}$ is the effective impulsive weight of contained fluid and $H_{\mathrm{cg,I}}$ is the effective height of bottom to its center of gravity.

When $H/R > 1.5$, $W_{\mathrm{I}}$ and $H_{\mathrm{cg,I}}$ can be determined by (EPRI NP-6041-SL, EPRI, 1991A)

$$\frac{W_{\mathrm{I}}}{W_{\mathrm{w}}} = 1.0 - 0.436(R/H), \tag{6.2.3a}$$

$$\frac{H_{\mathrm{cg,I}}}{H} = 0.5 - 0.188(R/H), \tag{6.2.3b}$$

where $W_{\mathrm{w}}$ is the weight of water and $H$ is the height of bottom to the water surface.

For this water tank, $H/R = 1.85 > 1.5$. Substituting $H/R = 1.85$ into equations (6.2.3a) and (6.2.3b) gives

$$W_{\mathrm{I}} = 0.764\,W_{\mathrm{w}}, \quad H_{\mathrm{cg,I}} = 0.398\,H, \tag{6.2.4}$$

where $W_{\mathrm{w}}$ and $H$ are given in Table 6.1.

Substituting weight and height of center of gravity values into equation (6.2.2) gives

$$M_{\mathrm{R}} = 0.636\,[17.2 \times 42 + 44.9 \times 16.4 + 12.8 \times 0 + 0.764\,(2900) \times 0.398\,(37)] = 21678\,\mathrm{kip{\cdot}ft}. \tag{6.2.5}$$

It is recognized that seismic capacity of the water tank is mildly influenced by seismic induced hydrodynamic pressure, it is necessary to scale the RLE to an estimate of *median* seismic capacity $\hat{A}_m$ (EPRI TR-103959, EPRI, 1994). This estimate does not have to be very precise since the seismic response influence on capacity is only mild. However, the estimate $\hat{A}_m$ should generally be within 30% of the ultimately computed $A_m$. So long as $\hat{A}_m$ is within 30% of $A_m$, the error in computing $A_m$ resulting from using scaled seismic response is less than 5% (EPRI TR-103959, EPRI, 1994).

In this example, $\hat{A}_m$ is taken as $0.54g$ PGA, which is consistent with Section 7 of EPRI TR-103959 (EPRI, 1994). Therefore, the scale factor SF is given by

$$\mathrm{SF} = \frac{0.54g}{A_{\mathrm{RLE}}} = \frac{0.54g\ \mathrm{PGA}}{0.3g\ \mathrm{PGA}} = 1.8. \tag{6.2.6}$$

For $\hat{A}_m$, the estimate *median* largest horizontal overturning moment is given by

$$M_{\mathrm{SR},m} = (\mathrm{SF})\, M_{\mathrm{R}} = 1.8 \times 21678 = 39020\,\mathrm{kip{\cdot}ft}. \tag{6.2.7}$$

### Median Structural Capacity

In this example, overturning moment rupture of the water tank near its connection to its base is considered. Section 7 of EPRI TR-103959 (EPRI, 1994) provides the *median* overturning moment capacity:

$$M_{\mathrm{C},m} = 26800\,\mathrm{kip{\cdot}ft}. \tag{6.2.8}$$

### Median Inelastic Energy Absorption Factor

For this water tank, inelastic energy absorption factor should be considered. Section 7 of EPRI TR-103959 (EPRI, 1994) gives the *median* inelastic energy absorption factor by

$$F_{\mu,m} = 1.54. \tag{6.2.9}$$

### Median Seismic Capacity

Having obtained *median* overturning moment response and capacity, *median* strength factor $F_{\mathrm{S},m}$ is given by

$$F_{\mathrm{S},m} = \frac{M_{\mathrm{C},m}}{M_{\mathrm{SR},m}} = \frac{26800\,\mathrm{kip{\cdot}ft}}{39020\,\mathrm{kip{\cdot}ft}} = 0.687. \tag{6.2.10}$$

For this water tank, horizontal peak response is equal to 1.09 (Table 3-3, EPRI TR-103959 EPRI, 1994). In this example, foundation-soil interaction effect is not considered, and response spectrum analysis method is used to calculate overturning moment response, hence *median* response factor $F_{\mathrm{RS},m}$ is given by

$$F_{\mathrm{RS},m} = \frac{1}{1.09} = 0.92. \tag{6.2.11}$$

Therefore, *median factor of safety* $F_m$ is calculated as

$$F_m = F_{\mu,m} F_{\mathrm{S},m} F_{\mathrm{RS},m} = 1.54 \times 0.687 \times 0.917 = 0.97. \tag{6.2.12}$$

Finally, the *median* seismic capacity $A_m$ is determined by

$$A_m = F_m \cdot \hat{A}_m = 0.97 \times 0.54g\,\mathrm{PGA} = 0.52g\,\mathrm{PGA}, \tag{6.2.13}$$

which is pretty close to the estimate of *median* seismic capacity $\hat{A}_m$ so that iteration is unnecessary.

### Logarithmic Standard Deviations

Logarithmic standard deviations for basic response and capacity variables and taken in accordance Sections 3 and 7 of EPRI-TR-103959 (EPRI, 1994). It is noted that horizontal impulsive mode frequency ($f = 6\,\text{Hz}$) is on the plateau of NUREG spectrum, thus no frequency uncertainty in $\mathcal{S}_\text{A}(f)$. Since only one mode is considered in the evaluation of overturning moment response, there is no mode combination uncertainty. In addition, vertical earthquake component has no contribution on overturning moment response, hence vertical earthquake component variability is not considered in response evaluation.

It is noted that damping uncertainty needs to be converted to be uncertainty $\mathcal{S}_\text{A}(f)$. This uncertainty is obtained from the ground response spectra with $\zeta = 5\%$ and 3% damping values, i.e.,

$$\beta_U = \frac{1}{|-1|} \ln \frac{\mathcal{S}_\text{A}(f = 6\,\text{Hz},\ \zeta = 3\%)}{\mathcal{S}_\text{A}(f = 6\,\text{Hz},\ \zeta = 5\%)} = \ln \frac{0.739g}{0.636g} = 0.15. \tag{6.2.14}$$

The *approximate second-moment procedure* is applied to calculate variability of $F$ due to basic variables. Table 6.3 enumerates the logarithmic standard deviations of $F$ due to response and capacity variables.

### HCLPF Seismic Capacity

Having obtained *median* seismic capacity $A_m$ and its variability, HCLPF seismic capacity of the heat exchanger is calculated as

$$C_\text{HCLPF} = A_m\, \mathrm{e}^{(\beta_R + \beta_U)\,\Phi^{-1}(0.05)} = 0.52 \times \mathrm{e}^{-1.6449\,(0.229 + 0.244)} = 0.24g\ \text{PGA}. \tag{6.2.15}$$

## 6.2.2.4 Current Seismic Fragility Analysis - UHS is RLE

Site-specific UHS anchoring to $0.3g$ PGA (see Figure 6.9) is chosen as RLE and defined as horizontal seismic input. The vertical seismic input can be obtained using V/H ratios given in Table 3.8 (AMEC, 2009). The water tank is subjected to earthquake excitations in three directions.

**Table 6.3** The Variability of $F$ due to Response and Capacity Variables

| Case | **Variable** | *Randomness* | *Uncertainty* | $F$ | $\beta$ | |
|---|---|---|---|---|---|---|
| 0 | **Base Case** | Variable at median | | 0.97 | | |
| | **Response Variables** | Variable at median plus $1\sigma$ | | $F_{1\sigma}$ | $\beta_R$ | $\beta_U$ |
| 1 | Earthquake response spectrum shape | $\mathcal{S}_A(f)\,e^{0.20}$ | $\mathcal{S}_A(f)\,e^{0.20}$ | 0.79 | 0.20 | 0.20 |
| 2 | Water tank damping | | $\mathcal{S}_A(f)\,e^{0.15}$ | 0.83 | | 0.15 |
| 3 | Water tank modelling | | $\mathcal{S}_A(f)\,e^{0.07}$ | 0.90 | | 0.07 |
| | **Capacity Variables** | Variable at median minus $1\sigma$ | | $F_{-1\sigma}$ | $\beta_R$ | $\beta_U$ |
| 4 | Inelastic energy absorption | $M_{C,m}\,e^{-0.03}$ | $M_{C,m}\,e^{-0.08}$ | 0.94 | 0.03 | 0.08 |
| 5 | Buckling capacity | | $M_{C,m}\,e^{-0.02}$ | 0.95 | | 0.02 |
| 6 | Anchor bolt tension capacity | | $M_{C,m}\,e^{-0.08}$ | 0.90 | | 0.08 |
| 7 | Fluid pressure | $M_{C,m}\,e^{-0.04}$ | $M_{C,m}\,e^{-0.03}$ | 0.93 | 0.04 | 0.03 |
| 8 | Fluid pressure | $M_{C,m}\,e^{-0.04}$ | $M_{C,m}\,e^{-0.03}$ | 0.93 | 0.04 | 0.03 |
| 9 | Water tank uplift | $M_{C,m}\,e^{-0.04}$ | $M_{C,m}\,e^{-0.08}$ | 0.93 | 0.04 | 0.08 |
| 10 | Equation error | | $M_{C,m}\,e^{-0.10}$ | 0.88 | | 0.10 |
| | **SRSS Combination** | | | | $\beta_R$ | $\beta_U$ |
| | | | | | 0.229 | 0.244 |
| | | | | $\beta_C$ | 0.335 | |

## Median Seismic Demand

Based on site-specific UHS, spectral acceleration $\mathcal{S}_A(f = 6\,\text{Hz})$ at horizontal impulsive mode is equal to $0.488g$. Thus the overturning moment response is determined by equation (6.2.2), i.e.,

$$M_R = 0.488\,[17.2 \times 42 + 44.9 \times 16.4 + 12.8 \times 0 + 0.764\,(2900) \times 0.398\,(37)] = 16634\,\text{kip·ft}. \tag{6.2.16}$$

### Median Seismic Capacity

In Section 6.2.2.3, *median* seismic capacity is equal to $0.52g$ PGA. Recall that ratio of $\mathcal{S}_A(f)$ to PGA is equal to 2.12 from NUREG spectrum. Therefore, given PGA $= 0.52g$, $\mathcal{S}_A(f)$ is calculated as

$$\mathcal{S}_A(f) = 2.12 \times 0.52g = 1.10g. \tag{6.2.17}$$

From equation (6.2.2), given $\mathcal{S}_A(f) = 1.10g$, overturning moment response is calculated as

$$M_{R,m} = 1.10\,[17.2 \times 42 + 44.9 \times 16.4 + 12.8 \times 0 + 0.764\,(2900) \times 0.398\,(37)] = 37494\,\text{kip·ft}. \tag{6.2.18}$$

Therefore, scale factor SF that converts screening level $A_{RLE}$ of $0.3g$ PGA to *median* seismic capacity is determined by

$$\text{SF} = \frac{M_{R,m}}{M_R} = \frac{37494\,\text{kip·ft}}{16634\,\text{kip·ft}} = 2.254. \tag{6.2.19}$$

Therefore, *median* seismic capacity of water tank is given by

$$A_m = (\text{SF})\,A_{RLE} = 2.254 \times 0.3g\,\text{PGA} = 0.676g\,\text{PGA}. \tag{6.2.20}$$

Comparing to $A_m$ of $0.52g$ PGA in equation (6.2.13), there is 30% increase in *median* seismic capacity estimate.

### Logarithmic Standard Deviations

Logarithmic standard deviations for basic response and capacity variables and taken in accordance Sections 3 and 7 of EPRI-TR-103959 (EPRI, 1994). Since site-specific UHS is defined as RLE, there is no earthquake response spectrum shape variability.

It is noted that uncertainties in frequency and damping need to be converted to be uncertainties in $\mathcal{S}_A(f)$:

- **Damping**

  The uncertainty $\beta_U$ in $\mathcal{S}_A(f)$ due to damping uncertainty is obtained from the site-specific UHS with $\zeta = 5\%$ and 3% damping values:

$$\beta_U = \frac{1}{|-1|} \ln \frac{\mathcal{S}_A(f = 6\,\text{Hz},\ \zeta = 3\%)}{\mathcal{S}_A(f = 6\,\text{Hz},\ \zeta = 5\%)} = \ln \frac{0.585g}{0.488g} = 0.18. \tag{6.2.21}$$

- **Frequency**

  The uncertainty $\beta_U$ in $\mathcal{S}_{\mathrm{A}}(f)$ due to frequency uncertainty is obtained from the site-specific UHS at frequencies 6 and 6.6 Hz $(+1\beta)$ :

$$\beta_U = \frac{1}{1}\ln\frac{\mathcal{S}_{\mathrm{A}}(f=6.6\,\mathrm{Hz},\ \zeta=5\%)}{\mathcal{S}_{\mathrm{A}}(f=6\,\mathrm{Hz},\ \zeta=5\%)} = \ln\frac{0.502g}{0.488g} = 0.03. \tag{6.2.22}$$

The *approximate second-moment procedure* is applied to calculate variability of $F$ due to basic variables. Table 6.4 enumerates the logarithmic standard deviations of $F$ due to response and capacity variables.

### HCLPF Seismic Capacity

Having obtained *median* seismic capacity $A_m$ and its variability, HCLPF seismic capacity of the heat exchanger is calculated as

$$C_{\mathrm{HCLPF}} = A_m\,\mathrm{e}^{(\beta_R+\beta_U)\,\Phi^{-1}(0.05)} = 0.676\times\mathrm{e}^{-1.6449\,(0.076+0.264)} = 0.386g\ \mathrm{PGA}. \tag{6.2.23}$$

Comparing to $0.24g$ PGA in equation (6.2.15), there is 60% increase in HCLPF seismic capacity estimate.

## 6.2.2.5 Discussion of HCLPF Seismic Capacity

Comparing to using NUREG spectrum as RLE, using site-specific UHS as RLE leads to a significant increase in HCLPF seismic capacity. Two sources contribute to this change:

1. NUREG spectrum is much higher at $f=6$ Hz, which leads to overestimation of *median* seismic demand thus underestimation of $A_m$, i.e., $0.52g$ PGA (obtained from NUREG spectrum) compared to $0.676g$ PGA (based on UHS).
2. There is no earthquake response spectrum shape variability in site-specific UHS. As a result, $\beta_{\mathrm{C}}$ of composite variability is significantly reduced, i.e., 0.274 (obtained from UHS) compared to 0.335 (based on NUREG spectrum).

By using site-specific UHS as RLE, HCLPF seismic capacity is greater than screening level $A_{\mathrm{RLE}}$ of $0.3g$ PGA. Therefore, water tank actually satisfies the seismic margin requirement. It is unnecessary to redesign the water tank for increasing its overturning moment capacity.

**Table 6.4** The Variability of $F$ due to Response and Capacity Variables

| Case | **Variable** | *Randomness* | *Uncertainty* | $F$ | $\beta$ | |
|---|---|---|---|---|---|---|
| 0 | **Base Case** | Variable at median | | 1 | | |
| | **Response Variables** | Variable at median plus $1\sigma$ | | $F_{1\sigma}$ | $\beta_R$ | $\beta_U$ |
| 1 | Water tank frequency | | $\mathcal{S}_{\mathrm{A}}(f)\,\mathrm{e}^{0.03}$ | 0.97 | | 0.03 |
| 2 | Water tank damping | | $\mathcal{S}_{\mathrm{A}}(f)\,\mathrm{e}^{0.18}$ | 0.84 | | 0.18 |
| 3 | Water tank modelling | | $\mathcal{S}_{\mathrm{A}}(f)\,\mathrm{e}^{0.07}$ | 0.93 | | 0.07 |
| | **Capacity Variables** | Variable at median minus $1\sigma$ | | $F_{-1\sigma}$ | $\beta_R$ | $\beta_U$ |
| 4 | Inelastic energy absorption | $M_{\mathrm{C},m}\,\mathrm{e}^{-0.03}$ | $M_{\mathrm{C},m}\,\mathrm{e}^{-0.08}$ | 0.97 | 0.03 | 0.08 |
| 5 | Buckling capacity | | $M_{\mathrm{C},m}\,\mathrm{e}^{-0.02}$ | 0.98 | | 0.02 |
| 6 | Anchor bolt tension capacity | | $M_{\mathrm{C},m}\,\mathrm{e}^{-0.08}$ | 0.92 | | 0.08 |
| 7 | Fluid pressure | $M_{\mathrm{C},m}\,\mathrm{e}^{-0.04}$ | $M_{\mathrm{C},m}\,\mathrm{e}^{-0.03}$ | 0.96 | 0.04 | 0.03 |
| 8 | Fluid pressure | $M_{\mathrm{C},m}\,\mathrm{e}^{-0.04}$ | $M_{\mathrm{C},m}\,\mathrm{e}^{-0.03}$ | 0.96 | 0.04 | 0.03 |
| 9 | Water tank uplift | $M_{\mathrm{C},m}\,\mathrm{e}^{-0.04}$ | $M_{\mathrm{C},m}\,\mathrm{e}^{-0.08}$ | 0.96 | 0.04 | 0.08 |
| 10 | Equation error | | $M_{\mathrm{C},m}\,\mathrm{e}^{-0.10}$ | 0.90 | | 0.10 |
| | **SRSS Combination** | | | | $\beta_R$ | $\beta_U$ |
| | | | | | 0.076 | 0.264 |
| | | | | $\beta_{\mathrm{C}}$ | 0.274 | |

## 6.2.3 Current Seismic Fragility Analysis for Electric Cabinet

### 6.2.3.1 Basic Configuration of Electric Cabinet

The electric cabinet in section 9 of EPRI-TR-103959 (EPRI, 1994) is used in the ECI system. Details of the cabinet is shown in Figure 6.10 and properties are listed in Table 6.5. It has a height $H$, width $B$, and length $L$ of 96 inches, 30 inches and 48 inches, respectively. It is anchored by four 0.5 inch diameter WEJ-IT expansion bolts as shown in Figure 6.10. The base of the cabinet has a strong, stiff frame through which the bolts are attached near each

corner of the cabinet so that the anchorage capacity is controlled by the bolts and not by the cabinet base. The concrete floor on which the cabinet locates contains an 18-inch by 36-inch cutout for passage of electrical cables into the cabinet. The cabinet is estimated to weight about 3500 pounds (3.5 kip) and is located at the ground floor of the reactor building. The cabinet center of gravity is estimated to be at mid-height (48 inches above the base).

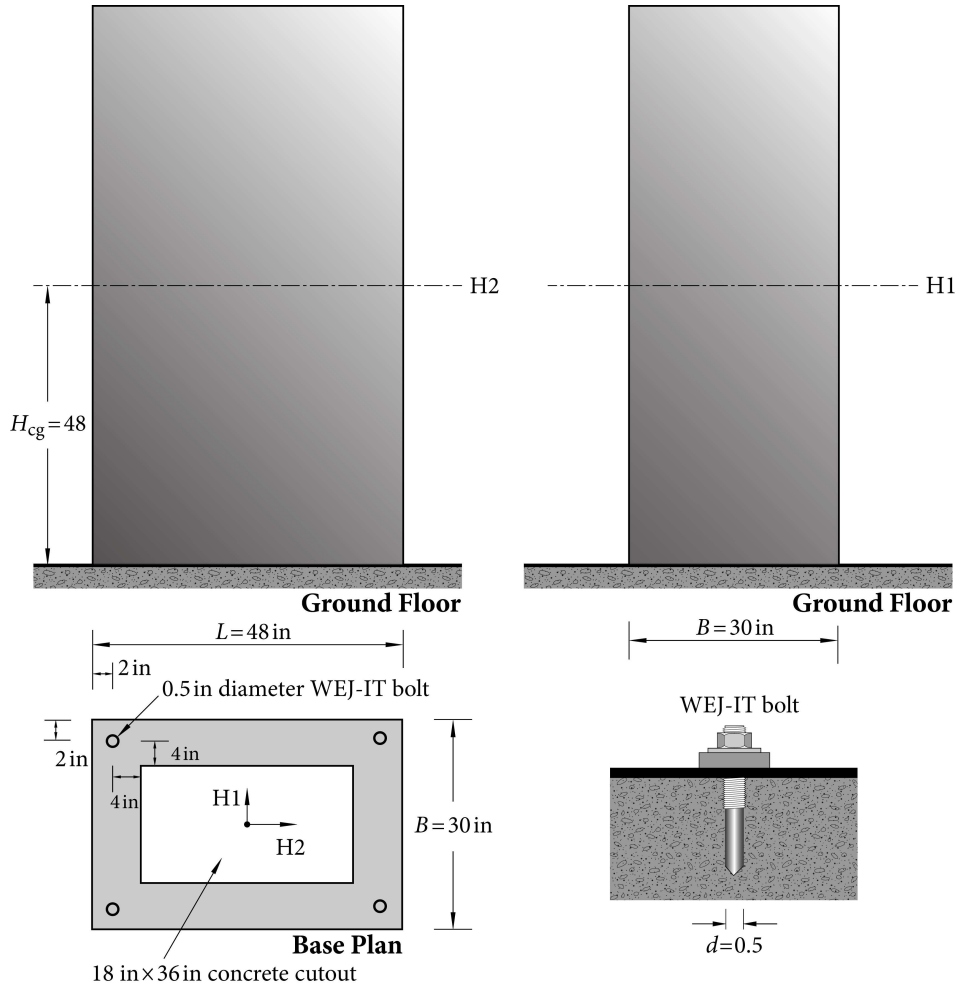


**Figure 6.10** The geometry information of electric cabinet

### 6.2.3.2 Seismic Demand Analysis

The electric cabinet is subjected to earthquake excitations from three directions. The fundamental frequencies of the electric cabinet in two horizontal directions are both estimated

**Table 6.5** Deterministic Properties of Electric Cabinet

| Property | Parameter | Value |
|---|---|---|
| **Electric Cabinet** | | |
| Length | $L$ | 48 in |
| Width | $B$ | 30 in |
| Height to center of gravity | $H_{cg}$ | 48 in |
| Weight | $W$ | 3500 lb |
| **WEJ-IT Expansion Bolt** | | |
| Bolt diameter | $d$ | 1/2 in |
| Number of bolts in H1 direction | $N_1$ | 2 |
| Number of bolts in H2 direction | $N_2$ | 2 |
| Distance between anchor bolts in H1 direction | $D_1$ | 26 in |
| Distance between anchor bolts in H2 direction | $D_2$ | 44 in |

to be $f_H = 8$ Hz. Since the cabinet is seismically robust in vertical direction, fundamental frequency in this direction is taken as $f_V = 50$ Hz.

### Definition of RLE

Seismic fragility analysis for the water tank shows that using site-specific UHS as RLE more accurately estimates its seismic capacity. Therefore, for the cabinet, site-specific UHS (see Figure 6.9) is chosen as RLE and defined as seismic input in two horizontal directions. The vertical seismic input can be determined using V/H ratios (AMEC, 2009).

Based on horizontal and vertical seismic inputs, spectral accelerations are determined and presented in Table 6.6. Response spectrum analysis method is used to calculate seismic demand of the cabinet.

### Median Seismic Demand in H1 Direction

In the H1 direction, under seismic excitation, the tank is subjected to an inertia force equal to the product of its weight $W$ and the spectral acceleration $a_H = 0.53g$, as shown in Figure 6.11. The inertia force is then transferred to the supports, exerting tension and shear

**Table 6.6** Spectral Values at Frequencies in Three Directions

| Direction | Frequency (Hz) | $\mathcal{S}_A\ (g)$ |
|---|---|---|
| H1 | 8 | 0.53 |
| H2 | 8 | 0.53 |
| Vertical | 50 | $0.865 \times 0.3 = 0.259$ |

force on anchor bolts. Assume that all anchor bolts are in elastic tension and shear during earthquake excitations. The geometric information of the cabinet is given in Table 6.5.

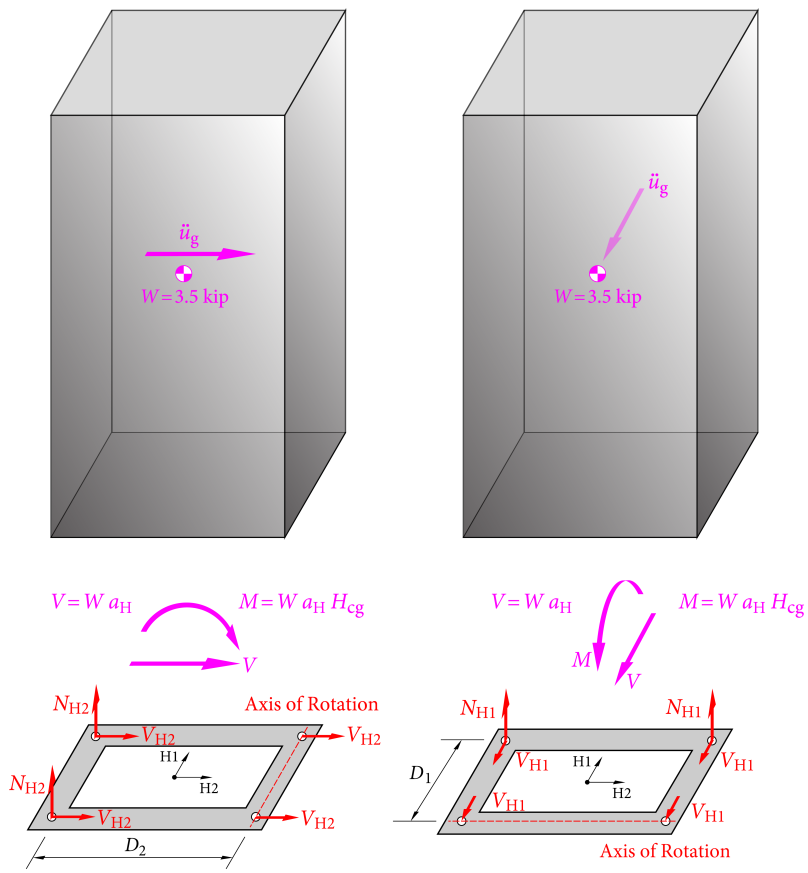


**Figure 6.11** Forces due to earthquake excitations in two horizontal directions

Shear force is induced in all the anchor bolts in all the supports evenly. For a single bolt, the shear force is

$$V_{H1} = \frac{W \cdot a_H}{N_1 \cdot N_2} = \frac{3.5 \times 0.53}{2 \times 2} = 0.464 \text{ kips.} \tag{6.2.24}$$

Tension forces in the support are due to the moment $W \cdot a_{\mathrm{H}} \cdot H_{\mathrm{cg}}$, as shown in Figure 6.11. For the critical anchor bolts, the tension force is given by

$$N_{\mathrm{H1}} = \frac{W \cdot a_{\mathrm{H}} \cdot H_{\mathrm{cg}}}{N_2 \cdot D_1} = \frac{3.5 \times 0.53 \times 48}{2 \times 26} = 1.712 \text{ kips.} \tag{6.2.25}$$

### Median Seismic Demand in H2 Direction

In the transverse direction, under seismic excitation, the seismic loading due to transverse excitation is also transferred to the supports, exerting tension and shear forces in the anchor bolts, as shown in Figure 6.11. Shear force is induced in all the anchor bolts in all the supports evenly. For a single bolt, the shear force is

$$V_{\mathrm{H2}} = \frac{W \cdot a_{\mathrm{H}}}{N_1 \cdot N_2} = \frac{3.5 \times 0.53}{2 \times 2} = 0.464 \text{ kips.} \tag{6.2.26}$$

The moment induces tension forces in the anchor bolts at 2 locations, as shown in Figure 6.11. For the critical anchor bolts, the tension is

$$N_{\mathrm{H2}} = \frac{W \cdot a_{\mathrm{H}} \cdot H_{\mathrm{cg}}}{N_1 \cdot D_2} = \frac{3.5 \times 0.53 \times 48}{2 \times 44} = 1.012 \text{ kips.} \tag{6.2.27}$$

### Median Demand in Vertical Direction

In the vertical direction, under seismic excitation, the inertial force of the tank due to vertical acceleration $a_{\mathrm{V}} = 0.259g$ is transferred to the support as pure tension force, without shear force. All anchor bolts share the seismic load evenly so that the tension force is

$$N_{\mathrm{V}} = \frac{W \cdot a_{\mathrm{V}}}{N_1 \cdot N_2} = \frac{3.5 \times 0.259}{2 \times 2} = 0.227 \text{ kips.} \tag{6.2.28}$$

When the bolts are in tension, the dead load of the electric cabinet also exerts forces in the anchor bolts. All the bolts share the dead load evenly as

$$N_{\mathrm{DL}} = \frac{-W}{N_1 \cdot N_2} = \frac{-3.5}{2 \times 2} = -0.875 \text{ kips.} \tag{6.2.29}$$

### Combination of Seismic Demand from Three Directions

100-40-40 percent combination rule is used to combine the maximum responses from the three earthquake components calculated separately (USNRC, 2006). To combine the effect of the three earthquake components on the critical anchor bolt, first assuming that the H1

direction controls and then assuming that the H2 direction controls. It is obvious that the vertical direction will not control; thus this case is not considered further.

1. **H1 direction controls**

   - Tension force in the critical anchor bolt is

$$\begin{aligned} N_{\mathrm{H1}} &= N_{\mathrm{H1}} + 0.4\,N_{\mathrm{H2}} + 0.4\,N_{\mathrm{V}} \\ &= 1.0 \times 1.712 + 0.4 \times 1.012 + 0.4 \times 0.227 = 2.208 \text{ kips.} \end{aligned} \tag{6.2.30}$$

   - Shear force in the critical anchor bolt is

$$V_{\mathrm{H1}} = \sqrt{(V_{\mathrm{H1}})^2 + (0.4\,V_{\mathrm{H2}})^2} = \sqrt{0.464^2 + (0.4 \times 0.464)^2} = 0.50 \text{ kips.} \tag{6.2.31}$$

2. **H2 direction controls**

   - Tension force in the critical anchor bolt is

$$\begin{aligned} N_{\mathrm{H2}} &= N_{\mathrm{H2}} + 0.4\,_{\mathrm{H1}} + 0.4\,N_{\mathrm{V}} \\ &= 1.0 \times 1.012 + 0.4 \times 1.712 + 0.4 \times 0.227 = 1.787 \text{ kips.} \end{aligned} \tag{6.2.32}$$

   - Shear force in the critical anchor bolt is

$$V_{\mathrm{H2}} = \sqrt{(V_{\mathrm{H2}})^2 + (0.4\,V_{\mathrm{H1}})^2} = \sqrt{0.464^2 + (0.4 \times 0.464)^2} = 0.50 \text{ kips.} \tag{6.2.33}$$

The tension and shear demand of the electric cabinet are summarized in Table 6.7. It is easily to find that the H1 direction is the controlling direction.

**Table 6.7** Median Tension and Shear Demand of Electric Cabinet

| Controlling Direction | Shear Force (kips) | Tension Force (kips) |
|---|---|---|
| **H1** | **0.50** | **2.208** |
| H2 | 0.50 | 1.787 |

### 6.2.3.3 Structural Capacity Analysis

It is assumed that the cabinet itself was designed to be seismically robust. As in Section 6.2.3.1, anchorage capacity is controlled by the bolts and not by the cabinet base. According

to EPRI-NP-6041-SL (EPRI, 1991A) and ACI 349-06 (ACI, 2007), median shear and tension capacities of an anchor bolt are obtained as

$$V_{ST} = 0.65 \times 1.0 \times 7.14 = 4.64 \text{ kips},$$
$$N_{ST} = 0.75 \times 0.95 \times 6.87 = 4.89 \text{ kips}. \tag{6.2.34}$$

#### 6.2.3.4 Median Seismic Capacity

Since anchor bolts are subjected to tension and shear simultaneously, a tension-shear interaction relationship, as shown in Figure 6.12, is used (EPRI, 1991B).

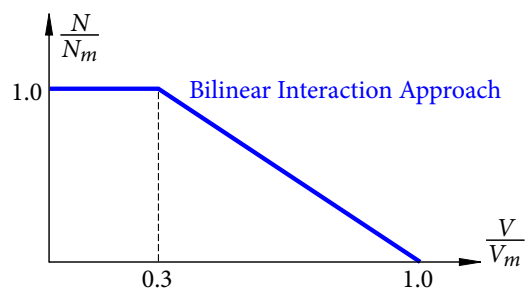


**Figure 6.12** Interaction relationship of tension and shear

To determine the *median* strength factor, two regions in Figure 6.12, i.e., pure tension region and shear/tension region are considered.

- Pure tension region

  The *median* strength factor is given by

$$F_{S1,m} = \frac{C - D_{NS}}{D_S + \Delta C_S} = \frac{N_{ST} - N_{DL}}{N_{H1}} = \frac{4.89 - (-0.875)}{2.208} = 2.61. \tag{6.2.35}$$

- Shear/Tension region

  The *median* strength factor is given by

$$F_{S2,m} = \frac{C - D_{NS}}{D_S + \Delta C_S} = \frac{V_{ST} - 0.7\,\dfrac{V_{ST}}{N_{ST}}\,N_{DL}}{V_{H1} + 0.7\,\dfrac{V_{ST}}{N_{ST}}\,N_{H1}} = \frac{4.64 - 0.7 \times \frac{4.64}{4.89} \times (-0.875)}{0.50 + 0.7 \times \frac{4.64}{4.89} \times 2.208} = 2.66. \tag{6.2.36}$$

It shows that, the controlling failure mode is pure tension failure of the critical anchor bolt in H1 direction. Hence *median* strength factor $F_{S,m}$ is equal to 2.61.

In this example, foundation-soil interaction effect is not considered. Recall that fundamental frequencies in two horizontal directions are the same, thus horizontal direction peak response variability does not need to be considered. In addition, response spectrum analysis method is applied to calculate structural response of the cabinet. Therefore, *median* response factor $F_{RS,m}$ is equal to 1. Neglecting inelastic energy absorption effects, i.e., $F_\mu = 1.0$, *median factor of safety* $F_m$ is thus given by

$$F_m = F_\mu \cdot F_{RS,m} \cdot F_{S,m} = 1.0 \times 1.0 \times 2.61 = 2.61. \tag{6.2.37}$$

Finally, *median* seismic capacity of the electric cabinet in terms of PGA is

$$A_m = F_m \cdot A_{RLE} = 2.61 \times 0.30g \text{ PGA} = 0.783g \text{ PGA}. \tag{6.2.38}$$

### 6.2.3.5 Logarithmic Standard Deviations

Logarithmic standard deviations for basic response and capacity variables and taken in accordance EPRI-TR-103959 (EPRI, 1994). It is noted that damping and frequency uncertainties need to be converted to be uncertainties on spectral accelerations in horizontal and vertical directions.

- **Damping**

  Assume the median damping for the electric cabinet is 5% and the damping at the $-1\sigma$ level is 3%. The uncertainty $\beta_U$ in ground response spectrum due to uncertainty in damping is obtained from the ground response spectra with $\zeta = 5\%$ and 3% damping values.

  - In horizontal direction:

$$\beta_U = \frac{1}{|-1|} \ln \frac{\mathcal{S}_A(f = 8\,\text{Hz},\ \zeta = 3\%)}{\mathcal{S}_A(f = 8\,\text{Hz},\ \zeta = 5\%)} = \ln \frac{0.632g}{0.533g} = 0.17. \tag{6.2.39}$$

  - In vertical direction:

    Since $\mathcal{S}_A(f_V)$ returns to PGA, damping uncertainty in vertical direction has no effects on the response spectral acceleration value.

- **Frequency**

  - In horizontal direction:
    Since $f_{\mathrm{H}} = 8\,\mathrm{Hz}$ in two horizontal directions, the uncertainty $\beta_U$ in modal frequency is 0.10 for simple equipment models, according to EPRI-TR-103959 (EPRI, 1994). Around 8 Hz, spectral acceleration increases when frequency increases. Hence, at the $1\sigma$ level, the frequency is $8 \cdot \mathrm{e}^{0.10} = 8.84\,\mathrm{Hz}$. Therefore, the uncertainty $\beta_U$ in spectral acceleration in the horizontal direction due to modal frequency variation is

$$\beta_U = \frac{1}{1} \ln \frac{\mathcal{S}_{\mathrm{A}}(f = 8.84\,\mathrm{Hz},\ \zeta = 5\%)}{\mathcal{S}_{\mathrm{A}}(f = 8\,\mathrm{Hz},\ \zeta = 5\%)} = \ln \frac{0.55g}{0.53g} = 0.03. \tag{6.2.40}$$

  - In vertical direction:
    Since spectral acceleration around $f_{\mathrm{V}} = 50\,\mathrm{Hz}$ returns to PGA, frequency uncertainty in vertical direction has no effects on $\mathcal{S}_{\mathrm{A}}(f_{\mathrm{V}})$.

Table 6.11 (the third and fourth columns) enumerates the logarithmic standard deviations for all basic variables. The *approximate second-moment procedure* is applied to calculate variability of $F$ due to basic variables, as shown in Table 6.11 (the sixth and seventh columns).

### 6.2.3.6 Seismic Fragility Curves and HCLPF Seismic Capacity

Seismic fragility curves of the cabinet are shown in Figure 6.13. In addition, one can obtain HCLPF seismic capacity of the cabinet as

$$C_{\mathrm{HCLPF}} = A_m\, \mathrm{e}^{(\beta_R + \beta_U)\,\Phi^{-1}(0.05)} = 0.782 \times \mathrm{e}^{-1.6449\,(0.19+0.43)} = 0.283g\ \mathrm{PGA}. \tag{6.2.41}$$

It can be seen that, HCLPF seismic capacity of the cabinet is smaller than $A_{\mathrm{RLE}} = 0.3g$ PGA even if site-specific UHS is chosen as RLE. Based on HCLPF Max/Min method, HCLPF seismic capacity of the ECI system is equal to HCLPF seismic capacity of the cabinet, which does not satisfy seismic margin requirement.

To more accurately estimate seismic capacity of the cabinet, weighting seismic fragility analysis has to be performed.

**Table 6.8** The Variability of $F$ due to Response and Capacity Variables

| Case | **Variable** | *Randomness* | *Uncertainty* | $F$ | $\beta$ | |
|---|---|---|---|---|---|---|
| 0 | **Base Case** | Variable at median | | 2.61 | | |
| | **Response Variables** | Variable at median plus $1\sigma$ | | $F_{1\sigma}$ | $\beta_R$ | $\beta_U$ |
| 1 | Vertical component response | | $\mathcal{S}_A(f_V)\,e^{0.34}$ | 2.57 | | 0.015 |
| 2 | Cabinet frequency | | $\mathcal{S}_A(f_H)\,e^{0.03}$ | 2.53 | | 0.03 |
| 3 | Cabinet damping | | $\mathcal{S}_A(f_H)\,e^{0.17}$ | 2.20 | | 0.17 |
| 4 | Cabinet mode shape | | $\mathcal{S}_A(f_H)\,e^{0.10}$ | 2.37 | | 0.10 |
| 5 | Cabinet mode combination | $\mathcal{S}_A(f_H)\,e^{0.10}$ | | 2.37 | 0.10 | |
| 6 | Earthquake component combination | Abs. Sum at $2.3\sigma$ | | 2.22 | 0.16 | |
| | **Capacity Variables** | Variable at median minus $1\sigma$ | | $F_{-1\sigma}$ | $\beta_R$ | $\beta_U$ |
| 7 | Anchor bolts | | $V_{ST}\,e^{-0.34}$ $N_{ST}\,e^{-0.47}$ | 1.78 | | 0.38 |
| | **SRSS Combination** | | | | $\beta_R$ | $\beta_U$ |
| | | | | | 0.19 | 0.43 |
| | | | | $\beta_C$ | 0.47 | |

## 6.2.4 Weighting Seismic Fragility Analysis for Electrical Cabinet

In this Section, weighting seismic fragility curves of the cabinet are developed based on vector-valued PSHA (VPSHA) and seismic fragility analysis considering vector-valued GMPs (VGMPs).

### 6.2.4.1 Weights of Input GRS

Since the fundamental frequencies of the cabinet in two horizontal directions are both equal to $f_H = 8$ Hz, two GMPs, i.e., $\mathcal{S}_A(f_H)$ and PGA, are chosen as VGMPs. VPSHA is performed to calculate mean annual rate density of $\mathcal{S}_A(f_H) \,|\, \text{PGA}$. The lower and upper

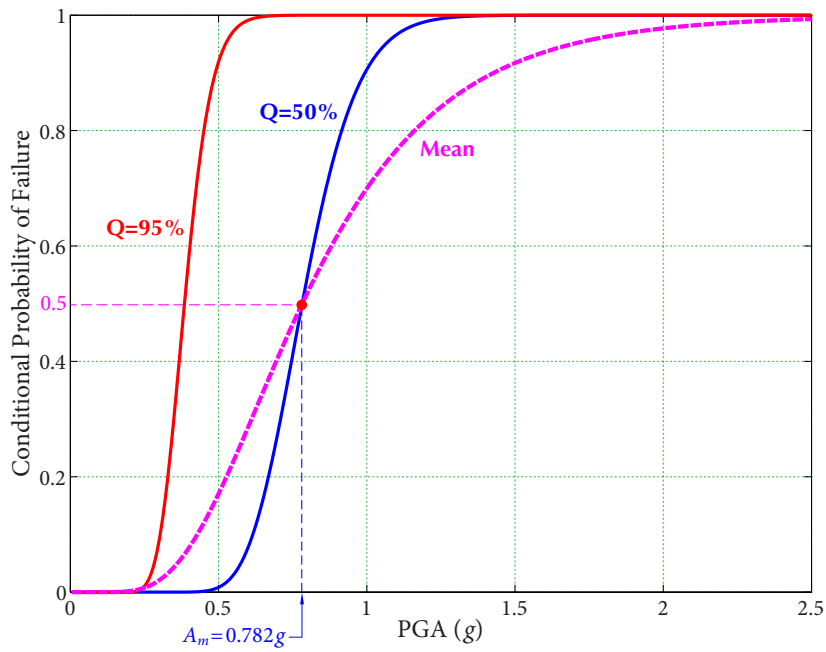


**Figure 6.13** Seismic fragility curves of the electric cabinet

bound values are $0.05g$ and $2.5g$ for PGA, and $0.1g$ and $5g$ for $\mathcal{S}_A(f_H)$. Both PGA and $\mathcal{S}_A(f_H)$ are uniformly discretized into 100 intervals in logarithmic scale.

Mean annual rate density of $\mathcal{S}_A(f_H)\,|\,\text{PGA}$ at three PGA values are shown in Figure 6.14. Given a PGA value, the weights of input GRS with spectral values of $\mathcal{S}_A(f_H)$ can be determined by equations in Chapter 4. Changing the spectral value of $\mathcal{S}_A(f_H)$ from $0.1g$ to $5g$, the weights for all input GRS intervals can be obtained, as shown in Figure 6.15.

### 6.2.4.2 Seismic Fragility Analysis considering VGMPs

Since two GMPs are used, a great number of input GRS are needed to be defined as input GRS (see Figure 6.16). In the following, conditional probability of failure of the cabinet given an input GRS, as shown in Figure 6.16, is calculated for example.

#### Seismic Demand Analysis

Table 6.9 summarizes spectral accelerations at frequencies in three directions. Median tension and shear demand of the cabinet are determined and summarized in Table 6.10. It is easy to find that H1 direction is the controlling direction.

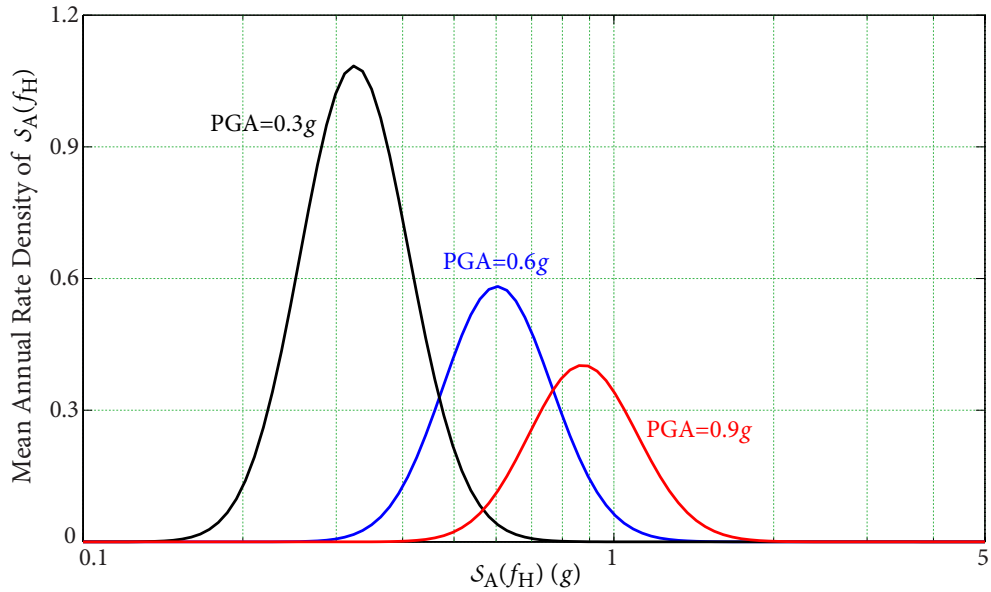


**Figure 6.14** Mean derivative of conditional AFE of $\mathcal{S}_A(f_H) \mid \text{PGA}$

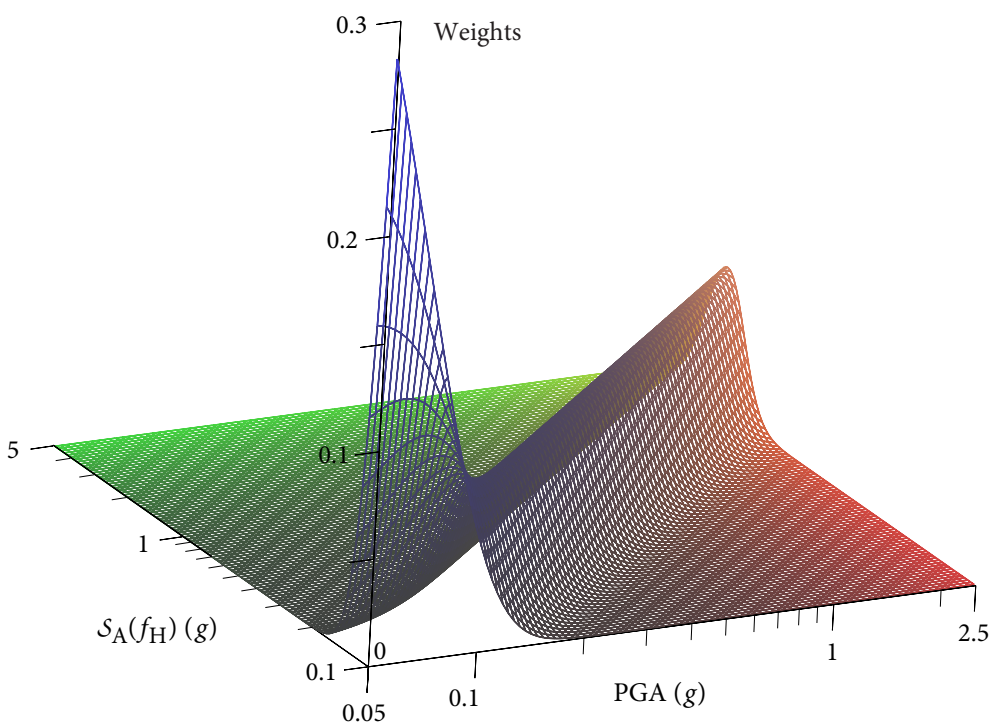


**Figure 6.15** Weights of input GRS

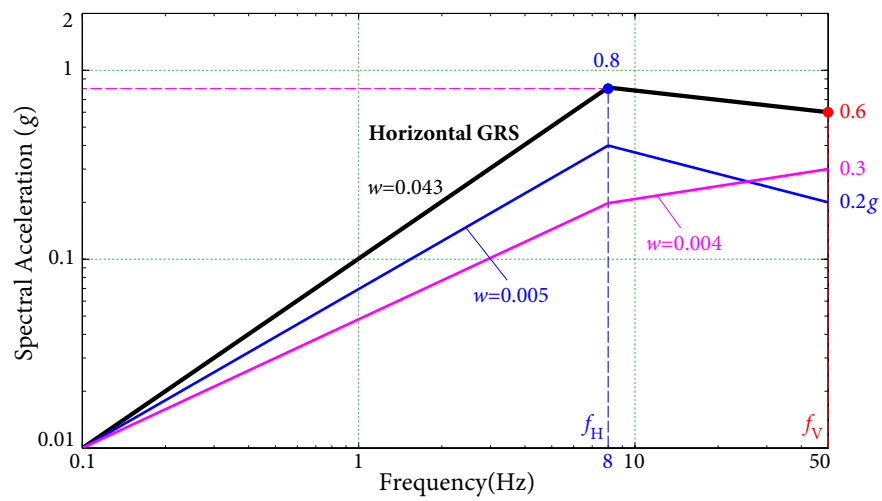


**Figure 6.16** An example of horizontal input GRS

**Table 6.9** Spectral Values at Frequencies in Three Directions

| Direction | Frequency (Hz) | $\mathcal{S}_A$ $(g)$ |
|---|---|---|
| H1 | 8 | 0.8 |
| H2 | 8 | 0.8 |
| Vertical | 50 | $0.865 \times 0.6 = 0.519$ |

**Table 6.10** Median Tension and Shear Demand of Electric Cabinet

| Controlling Direction | Shear Force (kips) | Tension Force (kips) |
|---|---|---|
| **H1** | **0.754** | **3.377** |
| H2 | 0.754 | 2.743 |

## Median Ratio Factor

To determine the median strength factor given the input GRS, two regions, i.e., pure tension region and shear/tension region are considered.

- Pure tension region

  The median strength factor is given by

$$F_{S1,m} = \frac{C - D_{NS}}{D_S + \Delta C_S} = \frac{N_{ST} - N_{DL}}{N_{H1}} = \frac{4.89 - (-0.875)}{3.377} = 1.71. \tag{6.2.42}$$

- Shear/Tension region

  The median strength factor is given by

$$F_{\mathrm{S2},m} = \frac{C - D_{\mathrm{NS}}}{D_{\mathrm{S}} + \Delta C_{\mathrm{S}}} = \frac{V_{\mathrm{ST}} - 0.7\,\dfrac{V_{\mathrm{ST}}}{N_{\mathrm{ST}}}\,N_{\mathrm{DL}}}{V_{\mathrm{H1}} + 0.7\,\dfrac{V_{\mathrm{ST}}}{N_{\mathrm{ST}}}\,N_{\mathrm{H1}}} = \frac{4.64 - 0.7 \times \frac{4.64}{4.89} \times (-0.875)}{0.754 + 0.7 \times \frac{4.64}{4.89} \times 3.377} = 1.74. \tag{6.2.43}$$

It shows that, the controlling failure mode is pure tension failure of the critical anchor bolt in H1 direction. Having obtained *median* strength factor $F_{\mathrm{S},m} = 1.71$, *median ratio factor* $R_m(0.6, 0.8)$ given the input GRS can be determined by

$$R_m(0.6, 0.8) = F_\mu \cdot F_{\mathrm{RS},m} \cdot F_{\mathrm{S},m} = 1.0 \times 1.0 \times 1.71 = 1.71. \tag{6.2.44}$$

### Logarithmic Standard Deviations

The *approximate second-moment procedure* is applied to calculate variability of ratio factor $R$ due to basic variables. The variability from basic variables are enumerated in Table 6.11.

### Determination of Seismic Fragility

Having obtained *median* ratio factor $R_m$ and logarithmic standard deviations $\beta_R$ and $\beta_U$, given the input GRS, conditional probability of failure $p_{\mathrm{F},q}\big(0.6, 0.8\big)$, at confidence level $Q = q$, can be determined by

$$p_{\mathrm{F},q}\big(0.6, 0.8 \,\big|\, Q = q\big) = \Phi\left\{\frac{\ln\big(1/R_m\big) + \beta_U\,\Phi^{-1}(q)}{\beta_R}\right\}. \tag{6.2.45}$$

In applications, confidence level $Q$ is usually taken as discrete values. Taking confidence level $Q = 95\%$ for example, $p_{\mathrm{F},q}\big(0.6, 0.8 \,\big|\, Q = 0.95\big)$ is given by

$$p_{\mathrm{F},q}\big(0.6, 0.8 \,\big|\, Q = 0.95\big) = \Phi\left\{\frac{\ln(1/1.71) + 0.43 \times \Phi^{-1}(0.95)}{0.19}\right\} = 0.821. \tag{6.2.46}$$

When composite variability is used, composite (mean) seismic fragility $p_{\mathrm{F,C}}\big(0.6, 0.8\big)$ is calculated as

$$p_{\mathrm{F,C}}\big(0.6, 0.8\big) = \Phi\left\{\frac{\ln\big(1/R_m\big)}{\beta_{\mathrm{C}}}\right\} = \Phi\left\{\frac{\ln(1/1.71)}{0.47}\right\} = 0.128. \tag{6.2.47}$$

**Table 6.11** The variability of $R$ due to Response and Capacity Variables

| Case | **Variable** | *Randomness* | *Uncertainty* | $R$ | $\beta$ | |
|---|---|---|---|---|---|---|
| 0 | **Base Case** | Variable at median | | 1.71 | | |
| | **Response Variables** | Variable at median plus $1\sigma$ | | $R_{1\sigma}$ | $\beta_R$ | $\beta_U$ |
| 1 | Vertical component response | | $\mathcal{S}_A(f_V)\,e^{0.34}$ | 1.67 | | 0.02 |
| 2 | Cabinet frequency | | $\mathcal{S}_A(f_H)\,e^{0.03}$ | 1.66 | | 0.03 |
| 3 | Cabinet damping | | $\mathcal{S}_A(f_H)\,e^{0.17}$ | 1.44 | | 0.17 |
| 4 | Cabinet mode shape | | $\mathcal{S}_A(f_H)\,e^{0.10}$ | 1.55 | | 0.10 |
| 5 | Cabinet mode combination | $\mathcal{S}_A(f_H)\,e^{0.10}$ | | 1.55 | 0.10 | |
| 6 | Earthquake component combination | Abs. Sum at $2.3\sigma$ | | 1.45 | 0.16 | |
| | **Capacity Variables** | Variable at median minus $1\sigma$ | | $R_{-1\sigma}$ | $\beta_R$ | $\beta_U$ |
| 7 | Anchor bolts | | $V_{ST}\,e^{-0.34}$ $N_{ST}\,e^{-0.47}$ | 1.16 | | 0.38 |
| | **SRSS Combination** | | | | $\beta_R$ | $\beta_U$ |
| | | | | | 0.19 | 0.43 |
| | | | | $\beta_C$ | 0.47 | |

### Development of Seismic Fragility Surfaces

Defining input GRS with spectral acceleration values at three frequencies from other intervals of spectral domain, and repeating the procedure for calculating conditional probability of failure values result in a family of seismic fragility surfaces, as shown in Figure 6.17.

## 6.2.4.3 Weighting Seismic Fragility Curves

Having obtained the weights of input GRS and seismic fragility surfaces, the weighting seismic fragility in terms of PGA, at confidence level $Q=q$ is determined by

$$\bar{p}_{F,q}(s_0) = \sum_{i_1=1}^{100} \left[ p_{F,q}\left(s_1^{(i_1)}, s_0\right) \cdot w\left(s_1^{(i_1)} \leqslant s_1 \leqslant s_1^{(i_1+1)} \,\middle|\, s_0\right) \right], \tag{6.2.48}$$

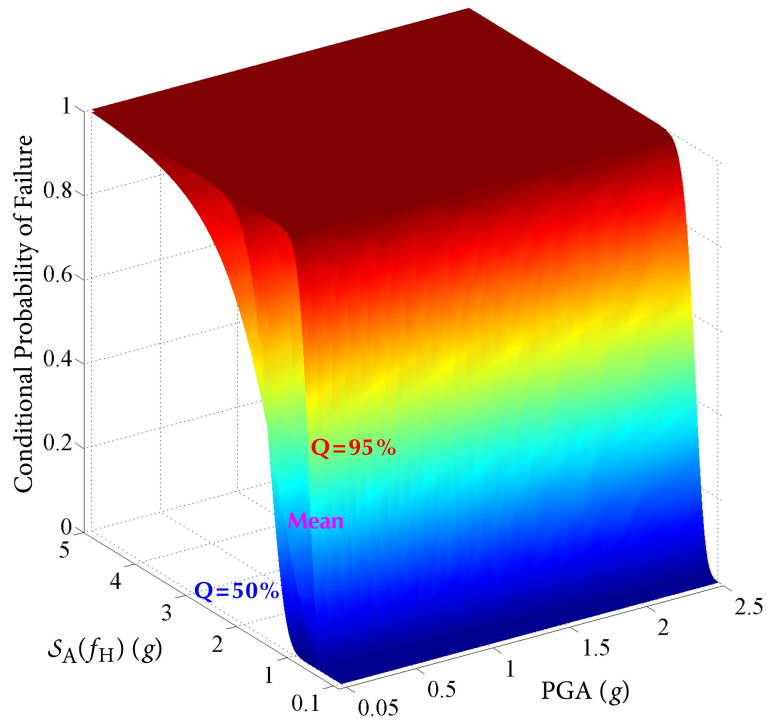


**Figure 6.17** Seismic fragility surfaces of $\mathcal{S}_A(f_H)$ and PGA

where $i_1 = 100$ is the number of intervals of $\mathcal{S}_A(f_H)$.

When composite variability is used, weighting mean seismic fragility is calculated as

$$\bar{p}_{F,C}(s_0) = \sum_{i_1=1}^{100} \left[ p_{F,C}\left(s_1^{(i_1)}, s_0\right) \cdot w\left(s_1^{(i_1)} \leqslant s_1 \leqslant s_1^{(i_1+1)} \,\middle|\, s_0\right) \right], \tag{6.2.49}$$

where $p_{F,C}\left(s_1^{(i_1)}, s_0\right)$ is mean seismic fragility given the input GRS.

Changing PGA values from lower bound of $0.05g$ to upper bound of $2.5g$ results in weighting seismic fragility curves, as shown in Figure 6.18. The conventional seismic fragility curves of the cabinet in Section 6.2.3 are plotted together with the weighting curves. It shows that the weighting *median* seismic capacity of the cabinet has 76.2% increase, i.e., from $0.782g$ PGA to $1.378g$ PGA. In addition, HCLPF seismic capacity of the cabinet, as shown in Figure 6.19, has 31.5% increase (from $0.283g$ PGA to $0.372g$ PGA). Both results indicate that weighting seismic fragility analysis method can more accurately estimate *median* and HCLPF seismic capacity of the cabinet.

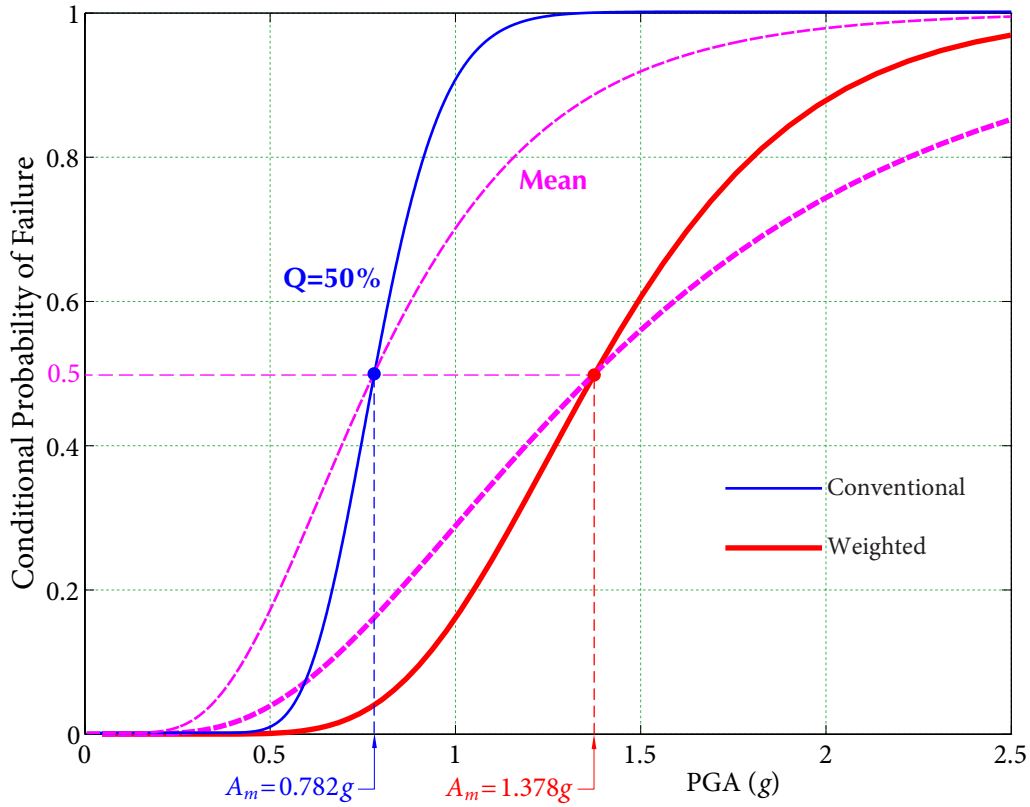


**Figure 6.18** Seismic fragility curves of the electric cabinet based on two methods

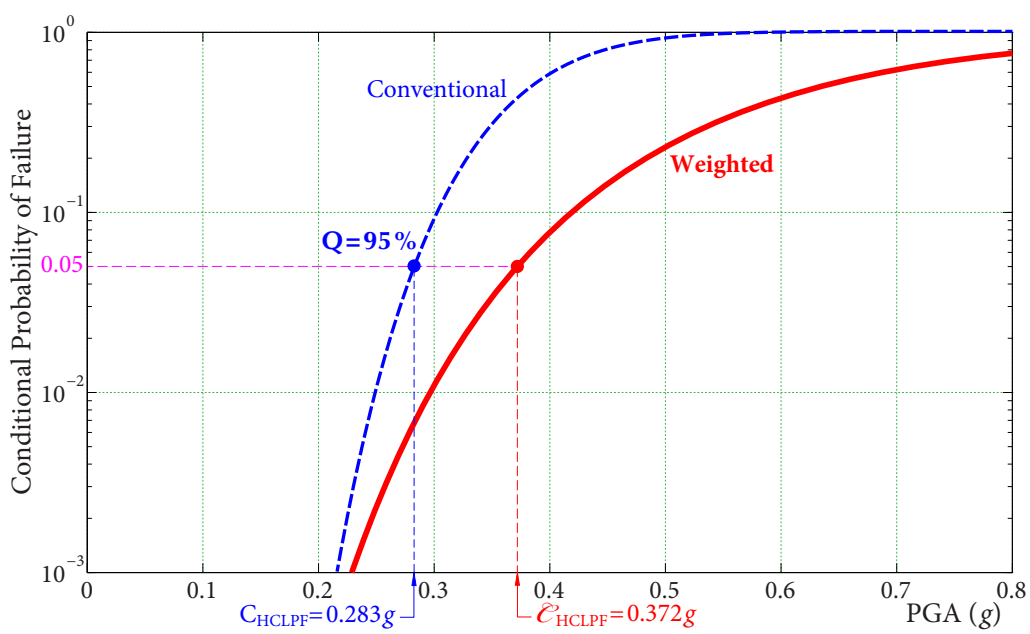


**Figure 6.19** HCLPF seismic capacity of the electric cabinet based on two methods

### 6.2.5 HCLPF Seismic Capacity of ECI System

As in Section 6.2.1, manual valve V, pump system and injection line are screened out. From the reduced fault tree in Figure 6.7, water tank T and electric cabinet S are connected by a "OR" gate. Based on HCLPF Max/Min method, the smaller one of HCLPF capacities of these two components is taken as HCLPF seismic capacity of the ECI system.

Detailed seismic fragility analysis is performed for calculating HCLPF seismic capacities of these two components. The results are presented as follows:

- **Current seismic fragility analysis is performed**
  - NUREG spectrum is chosen as RLE
    HCLPF seismic capacity of water tank is less than screening level $A_{\mathrm{RLE}}$ of $0.3g$ PGA. Therefore, ECI system does not meet seismic margin requirement.
  - Site-specific UHS is chosen as RLE
    HCLPF seismic capacity of water tank exceeds $0.3g$ PGA, while HCLPF seismic capacity of electric cabinet is less than $0.3g$ PGA. Hence ECI system does not meet the seismic margin requirement.

  It shows that the ECI system cannot meet seismic margin requirement based on current method.
- **Current and weighting seismic fragility analysis are performed**
  - Current seismic fragility analysis (site-specific UHS is chosen as RLE) is performed to calculate HCLPF seismic capacity of the water tank, and
  - weighting seismic fragility analysis is conducted to determine that of the electric cabinet.

  The results show that HCLPF seismic capacities of the water tank and cabinet both exceed $0.3g$ PGA, thus the ECI system finally meets requirement.

It can be seen that combining current and weighting seismic fragility analysis methods can more accurately estimate HCLPF seismic capacity of the ECI system so that get rid of unnecessary redesign cost of the cabinet.

## 6.3 Summary

In this Chapter, Seismic Margin Assessment (SMA) is introduced first. In current SMA, HCLPF seismic capacities of these SSCs are defined as input in analysis. HCLPF Max/Min method is then applied to determine plant HCLPF seismic capacity.

Accurate HCLPF seismic capacity estimates of "weak link" structures, systems, and components (SSCs) are crucial in evaluating plant HCLPF seismic capacity. An improved SMA procedure is firstly proposed for this purpose:

- weighting seismic fragility analysis is performed for "weak link" SSCs, and
- current seismic fragility analysis is conducted for less important SSCs.

This ensures that more accurate plant seismic capacity is obtained while computational cost is acceptable.

HCLPF seismic capacity of a simplified emergency coolant injection (ECI) system is evaluated as an example. Water tank and electric cabinet are assumed to be "weak link" SSCs. Current and improved SMA procedures are conducted separately for the ECI system:

1. **Current SMA procedure is performed**

   Current seismic fragility analysis is performed to determine HCLPF seismic capacities of the water tank and cabinet. The results show that HCLPF seismic capacity of the water tank exceeds screening level of $A_{\mathrm{RLE}} = 0.3g$ PGA, while HCLPF seismic capacity of the cabinet is less than $0.3g$ PGA. As a result, the ECI system does not satisfy seismic margin requirement.

2. **Improved SMA procedure is performed**

   Weighting seismic fragility analysis method is conducted for the cabinet, while current seismic fragility analysis is performed for the water tank. The results show that HCLPF seismic capacities of the water tank and cabinet are both greater than $0.3g$ PGA, thus the ECI system meets seismic margin requirement. The improved procedure effectively gets rid of unnecessary redesign cost for the cabinet.

The improved SMA procedure should be used to more accurately estimate plant HCLPF seismic capacity so that redesign cost for "weak link" SSCs is effectively reduced.

C H A P T E R 7

# Conclusions and Future Research

Seismic fragility analysis has been widely used to evaluate seismic capacities of structures, systems, and components (SSCs) in nuclear power plants (NPPs). The seismic capacity is represented by seismic fragility curves or a High Confidence and Low Probability of Failure (HCLPF) seismic capacity, in terms of a single ground-motion parameter (GMP) such as peak ground acceleration (PGA). Due to the use a single GMP, problems are observed in engineering applications. This study aims to develop weighting seismic fragility analysis method that overcomes the problems in current method thus achieves more accurate plant seismic capacity and seismic risk estimates. Major contributions for this purpose and future research are presented.

## 7.1 Mean Annual Rate Density Distribution

Seismic hazard represented by a Review Level Earthquake (RLE) is defined as seismic input in seismic fragility analysis. In current engineering practice, site-specific uniform hazard spectrum (UHS) is recommended to be defined as RLE. This study investigates the problems due to the use of UHS as RLE:

1. In the generation of UHS, logarithmic spectral accelerations at any two frequencies are fully correlated, thus the aleatory randomness in earthquake response spectra is not properly captured.

2. Spectral shape of UHS at a specified seismic hazard is chosen as spectral shape of RLE, hence ground motion intensity effect is not considered.

Vector-valued GMPs (VGMPs) are introduced to resolve above problems. The correlations among VGMPs are properly considered in characterizing earthquake response spectra. In two-dimensional case, for example, $\mathcal{S}_A(f=5\text{ Hz})$ and PGA are chosen as VGMPs. Vector-valued PSHA (VPSHA) is firstly used to calculate mean annual rate density distribution, which is represented by a set of curves given PGA values. The advantages of using mean annual rate density distribution are presented:

1. **Aleatory randomness in earthquake response spectra is properly captured**

   For a given PGA value, spectral values of $\mathcal{S}_A(f)$ yields a distribution instead of a unique spectral value from UHS, accounting for aleatory randomness in $\mathcal{S}_A(f)$.

2. **Ground motion intensity effect is considered**

   By taking PGA values from lower bound (e.g. $0.05g$) to upper bound (e.g. $5g$) values, distributions of $\mathcal{S}_A(f)$ are calculated accounting for ground motion intensity effect.

3. **Conservatism in the generation of UHS is effectively reduced**

   By introducing correlation coefficient between $\ln\mathcal{S}_A(f)$ and $\ln\text{PGA}$, conservatism in predicting spectral value of $\mathcal{S}_A(f)$ for a given PGA value is reduced .

## 7.2 Investigation of Problems in Seismic Fragility Analysis

This study quantitatively investigates the influences of spectral shape of RLE and the use of GMP on seismic capacity estimate of a horizontal heat exchanger. The results show that both factors have noticeable effect on estimating HCLPF seismic capacity of the heat exchanger:

1. **Spectral shape influence**

   HCLPF seismic capacity (site-specific UHS is RLE) has 41.9% increase comparing to that using NUREG/CR-0098 median rock response spectrum as RLE.

2. **Use of GMP**

   HCLPF seismic capacity (average spectral acceleration $\bar{\mathcal{S}}_A$ between 5 and 10 Hz is GMP) has 14.6% increase comparing to that using PGA as GMP.

When performing current seismic fragility analysis for safety-related SSCs in NPPs that are located in eastern North America, two recommendations are provided:

1. Site-specific UHS should be defined as RLE.
2. When a generic ground response spectrum (GRS) is chosen as RLE, average spectral acceleration $\bar{S}_A$ between 5 and 10 Hz should be taken as GMP.

## 7.3 Seismic Fragility Analysis considering VGMPs

This study firstly proposes seismic fragility analysis considering VGMPs method for achieving more accurate seismic capacity estimates of safety-related SSCs. The advantages of the proposed method include that

- generate a large number of input GRS accounting for aleatory randomness in earthquake response spectra;
- efficiently generate floor response spectra using direct spectra-to-spectra method;
- efficiently calculate seismic demand by means of response spectrum analysis method;
- take account of multiple potential controlling failure modes in the development of seismic fragility surfaces.

However, the results of seismic fragility analysis considering VGMPs are seismic fragility surfaces in terms of VGMPs, which can not be directly used in Seismic Probabilistic Risk Analysis (SPRA) and Seismic Margin Assessment (SMA).

## 7.4 Weighting Seismic Fragility Analysis

This study firstly proposes weighting seismic fragility analysis method for developing weighting seismic fragility curves and HCLPF seismic capacities of safety-related SSCs in terms of a single GMP. The key steps of the proposed method are presented as follows:

1. weights of input GRS are determined by mean annual rate density distribution;
2. seismic fragility in terms of VGMPs is obtained from seismic fragility analysis considering VGMPs;

3. weighting process is performed for calculating weighting seismic fragility in terms of a single GMP.

As a result, weighting seismic fragility curves and HCLPF seismic capacities of SSCs are readily incorporated into SPRA and SMA.

## 7.5 Seismic Probabilistic Risk Analysis considering VGMPs

This study further proposes SPRA considering VGMPs procedure for acquiring more accurate seismic risk estimates of NPPs. The key elements of the proposed procedure include

- performing scalar PSHA to obtain seismic hazard curves for a specified GMP such as PGA,
- conducting weighting seismic fragility analysis method to determine seismic fragilities of safety-related SSCs in terms of the chosen GMP, and
- convolving seismic hazard and weighting seismic fragility to calculate annual frequency of occurrence of an adverse consequence such as core damage accident.

In engineering applications, engineers can combine the use of current and weighting seismic fragility analysis methods for calculating seismic capacities of SSCs in NPPs, i.e.,

- weighting seismic fragility analysis is performed for "weak link" SSCs, and
- current seismic fragility analysis is conducted for less important SSCs.

This can make sure that more accurate seismic risk estimates of NPPs are obtained while computational cost is acceptable.

## 7.6 Improved Seismic Margin Assessment

In current SMA, HCLPF seismic capacities of SSCs are defined as input in subsequent system analysis. HCLPF Max/Min method is applied to propagate these HCLPF seismic capacities to determine the plant seismic capacity. It is recognized that, the plant seismic capacity is contributed most from HCLPF seismic capacities of "weak link" SSCs.

This study firstly proposes an improved SMA procedure for determining more accurate plant seismic capacity. The procedure includes that

- weighting seismic fragility analysis is performed for "weak link" SSCs, and
- current seismic fragility analysis is conducted for less important SSCs.

This ensures that more accurate plant seismic capacity is obtained while computational cost is acceptable, so that the unnecessary redesign cost for "weak link" SSCs is saved.

## 7.7 Future Research

It is recognized that, reactor buildings are usually designed to locate on rock sites. For some reasons, reactor buildings probably locate on soil sites. For this case, soil-structure interaction (SSI) effect need to be addressed, because they would significantly influence the seismic input at foundation level of these reactor buildings. In the proposed weighting seismic fragility analysis method, however, SSI effect is not taken into account. In future research, a direct spectra-to-spectra method considering SSI effect should be developed to calculate ground response spectra for equivalent fixed-base structural model.

# Bibliography

ACI, 2007. *Code Requirements for Nuclear Safety-Related Concrete Structures and Commentary*, **ACI 349-06**. American Concrete Institute (ACI).

ACI, 2008. *Building Code Requirements for Structural Concrete and Commentary*, **ACI 318-08**. American Concrete Institute (ACI).

AMEC, 2009. *Site Evaluation of the OPG New Nuclear at Darlington-Probabilistic Seismic Hazard Assessment*. AMEC Geomatrix, Toronto, Ontario.

ASCE, 1998. *Seismic Analysis of Safety-Related Nuclear Structures and Commentary*, **ASCE 4-98**. American Society of Civil Engineers (ASCE).

Atkinson, G.M. and Boore, D.M., 1995. Ground-motion relations for eastern North America. *Bulletin of the Seismological Society of America*, **85**(1): 17–30.

Atkinson, G.M. and Boore, D.M., 2006. Earthquake ground-motion prediction equations for eastern North America. *Bulletin of the Seismological Society of America*, **96**(6): 2181–2205.

Atkinson, G.M. and Elgohary, M., 2007. Typical uniform hazard spectra for eastern North American sites at low probability levels. *Canadian Journal of Civil Engineering*, **34**(1): 12–18.

Atkinson, G. M. and Goda, K., 2011. Effects of seismicity models and new ground-motion prediction equations on seismic hazard assessment. *Bulletin of Seismological Society of America*, **101**(1): 176–189.

Baker, J.W. and Jayaram, N., 2008. Correlation of spectral acceleration values from NGA ground motion models. *Earthquake Spectra*, **24**(1): 299–317.

Baker, J.W., 2008. *An Introduction to Probabilistic Seismic Hazard Analysis (PSHA)*. U.S. Nuclear Regulatory Commission.

Bazzurro, P., 1998. *Probabilistic Seismic Demand Analysis*. PhD thesis, Stanford University, California,USA.

Boore, D.M. and Atkinson, G.M., 2008. Ground-motion prediction equations for the average horizontal component of PGA, PGV, and 5%-damped PSA at spectral periods between 0.01 s and 10.0 s. *Earthquake Spectra*, **24**(1): 99–138.

Cai, Z., Ni, S.-H., Xie, W.-C., Pandey, M. D., Liu, W., and Han, M., 2015. Seismic fragility analysis for structures, systems, and components of nuclear power plants: Part ii - use of multiple ground-motion parameters. In *Transactions of 23th International Conferences on Structural Mechanics in Reactor Technology (SMiRT-23)*, Manchester, United Kingdom.

Cameron, W. I. and Green, R. A., 2007. Damping correction factors for horizontal ground-motion response spectra. *Bulletin of the Seismological Society of America*, **97**(3): 934–960.

Chen, W.F. and Lui, E.M., 2006. *Earthquake Engineering for Structural Design*. CRC Press LLC, Boca Raton, Florida.

Cornell, C.A., 1968. Engineering seismic risk analysis. *Bulletin of the Seismological Society of America*, **58**(5): 1583–1606.

CSA, 2010. *Design Procedures for Seismic Qualification of CANDU Nuclear Power Plants*, **CSA/CAN3 N289.3**. Canadian Standard Association (CSA), Mississauga, Ontario.

Ellingwood, B. R., 1994. *Validation of Seismic Probabilistic Risk Assessments of Nuclear Power Plants*, **NUREG/CR-0008**. U.S. Nuclear Regulatory Commission.

EPRI, 1991A. *A Methodology for Assessment of Nuclear Power Plant Seismic Margin*, **EPRI-NP-6041-SL**. Electric Power Research Institute, California.

EPRI, 1991B. *Seismic Verification of Nuclear Plant Equipment Anchorage (Revision 1), Volume 1: Development of Anchorage Guidelines*, **EPRI-NP-5228-SL**. Electric Power Research Institute, California.

EPRI, 1994. *Methodology for Developing Seismic Fragilities*, **EPRI-TR-103959**. Electric Power Research Institute, California.

EPRI, 2000. *Individual Plant Examination for External Events (IPEEE) Seismic Insights: Revision to EPRI Report TR-112932*, **EPRI-TR-1000895**. Electric Power Research Institute, California.

EPRI, 2009. *Seismic Fragility Application Guide Update*, **EPRI 1019200**. Electric Power Research Institute, California.

EPRI, 2011. *Advanced Methods for Determination of Seismic Fragilities: Seismic Fragilities Using Scenario Earthquakes*, **EPRI 1022995**. Electric Power Research Institute, California.

EPRI, 2013. *Seismic Probabilistic Risk Assessment Implementation Guide*. Electric Power Research Institute, California.

Halchuk, S., Allen, T. I., Adams, J., and Rogers, G. C., 2014. *Fifth Generation Seismic Hazard Model Input Files as Proposed to Produce Values for the 2015 National Building Code of Canada, Open File 7576*. Geological Survey of Canada.

Hamid, A., Abboud, B., Farah, M., Hatem, M., and Harris, H., 1989. *Response of Reinforced Block Masonry Walls to Out-of-plane Static Loads. Report No. 3.2(a)*. U.S.-Japan Coordinated Program for Masonry Building Research, Philadelphia, PA.

Huang, Y.-N., Whittaker, A. S., and Luco, N., 2011. A probabilistic seismic risk assessment procedure for nuclear power plants: (i) methodology. *Nuclear Engineering and Design*, **241**(9): 3996–4003.

Jayaram, N. and Baker, J.W., 2008. Statistical tests of the joint distribution of spectral acceleration values. *Bulletin of the Seismological Society of America*, **98**(5): 2231–2243.

Jiang, W., Li, B., Xie, W.-C., and Pandey, M. D., 2015. Generate floor response spectra, part 1: Direct spectra-to-spectra method. *Nuclear Engineering and Design*, **293**: 525–546.

Kaplan, S., Perla, H. F., and Bley, D. C., 1983. A methodology for seismic risk analysis of nuclear power plants. *Risk Analysis*, **3**(3).

Kennedy, R.P., Cornell, C.A., Campbell, R.D., Kaplan, S., and Perla, H.F., 1980. Probabilistic seismic safety study of an existing nuclear power plant. *Nuclear Engineering and Design*, **59**: 315–338.

Kennedy, R.P. and Ravindra, M.K., 1984. Seismic fragilities for nuclear power plant studies. *Nuclear Engineering and Design*, **79**: 47–68.

Li, B., Jiang, W., Xie, W.-C., and Pandey, M. D., 2015. Generate floor response spectra, part 2: Response spectra for equipment-structure resonance. *Nuclear Engineering and Design*, **293**: 547–560.

Mandal, T. K., Ghosh, S., and Pujari, N. N., 2016. Vector fragility surfaces for reinforced concrete frames in europe. *Structural Safety*, **22**: 11–19.

McGuire, R., 2004. *Seismic Hazard and Risk Analysis*. Earthquake Engineering Research Institute, Oakland.

MSJC, 2011. *Building Code Requirements and Specification for Masonry Structures*. Masonry Standards Joint Committee.

NCMA, 2007. *Section Properties Of Concrete Masonry Walls, 14-1B*. National Concrete Masonry Association, Herndon, VA.

Ni, S.-H., Cai, Z., Xie, W.-C., Pandey, M. D., Liu, W., and Han, M., 2015. Seismic fragility analysis for structures, systems, and components of nuclear power plants: Part i - issues identified in engineering practice. In *Transactions of 23th International Conferences on Structural Mechanics in Reactor Technology (SMiRT-23)*, Manchester, United Kingdom.

NUREG, 1981. *Fault Tree Handbook*, **NUREG-0492**. U.S. Nuclear Regulatory Commission.

NUREG, 1997. *Recommendations for Probabilistic Seismic Hazard Analysis:Guidance on Uncertainty and Use of Experts*, **NUREG-6372**. U.S. Nuclear Regulatory Commission.

Pezeshk, S., Zandieh, A., and Tavakoli, B., 2011. Hybrid empirical ground-motion prediction equations for eastern north america using nga models and updated seismological parameters. *Bulletin of Seismological Society of America*, **101**: 1859–1870.

Pisharady, A. S. and Basu, P. C., 2010. Methods to derive seismic fragility of npp components: A summary. *Nuclear Engineering and Design*, **240**(11): 3878–3887.

Rezaeian, S., Bozorgnia, Y., Idriss, I. M., Campbell, K., Abrahamson, N., and Silva, W., 2012. *Spectral Damping Scaling Factors for Shallow Crustal Earthquakes in Active Tectonic Regions*. Pacific Earthquake Engineering Research Center.

Richter, C.F., 1958. *Elementary Seismology*. W. H. Freeman and Co., San Francisco.

Silva, W. J., Gregor, N. J., and Darragh, R., 2002. Development of regional hard rock attenuation relations for central and eastern north america, technical report. *Canadian Journal of Civil Engineering*.

USNRC, 1975. *Reactor Safety Study: An Assessment of Accident Risks in U.S. Commercial Nuclear Power Plants*, **NUREG-75/014**. U.S. Nuclear Regulatory Commission.

USNRC, 1978. *Development of Criteria for Seismic Review of Selected Nuclear Power Plants*, **NUREG/CR-0098**. U.S. Nuclear Regulatory Commission.

USNRC, 2006. *Combining Modal Responses and Spatial Components in Seismic Response Analysis*, **R.G. 1.92**. U.S. Nuclear Regulatory Commission.

USNRC, 2014A. *Design Response Spectra for Seismic Design of Nuclear Power Plants*, **R.G. 1.60**. U.S. Nuclear Regulatory Commission.

USNRC, 2014B. *Standard Review Plan-Seismic Design Parameters*, **SRP 3.7.1**. U.S. Nuclear Regulatory Commission.